TWO-PHASE FLOW IN HORIZONTAL IMPACTING TEE JUNCTIONS: CURRENT STATE OF THE ART

by

Ahmed M. F. El-Shaboury

A Thesis
Submitted to the Faculty of Graduate Studies
in Partial Fulfillment of the
Requirements for the Degree of

Master of Science
in
Mechanical Engineering

Department of Mechanical and Industrial Engineering
University of Manitoba
Winnipeg, Manitoba

THE UNIVERSITY OF MANITOBA

FACULTY OF GRADUATE STUDIES

*****

COPYRIGHT PERMISSION PAGE

Two-Phase Flow in Horizontal Impacting Tee Junctions: Current State of the Art

BY

Ahmed M.F. El-Shaboury

A Thesis/Practicum submitted to the Faculty of Graduate Studies of The University of Manitoba in partial fulfillment of the requirements of the degree of M.Sc.

ABSTRACT

The present investigation presents a summary of the state of the art in our understanding of the phase distribution in horizontal impacting tee junctions during two-phase flow. The currently existing data base was reviewed and the effects of different parameters on the phase distribution were investigated. These parameters include J_{Ll}, J_{Gl}, P_l, x_l, inlet flow regime, and inlet momentum-flux ratio. It was found that there is a serious lack of pressure-drop data and high-inlet-quality phase-distribution data.

The effect of J_{Ll} was such that as J_{Ll} increases with J_{Gl} fixed, the line, or curve that represents the data rotates in a clockwise direction around the point of (0.5,0.5) on coordinates of F_{BG} vs. F_{BL}. The effect of J_{Gl} was such that as J_{Gl} increases with J_{Ll} fixed, the line, or curve that represents the data rotates in an anti-clockwise direction around the point of (0.5,0.5) on coordinates of F_{BG} vs. F_{BL}. The effect of P_l was found to be similar to the effect of J_{Gl}. The effect of x_l at constant W_l was also found to be similar to the effect of J_{Gl}. The effect of the inlet flow regime was investigated among data of the same x_l and P_l, which limited this investigation to very few data sets. It was found that the inlet flow regime has no effect on phase-distribution data as long as x_l and P_l are fixed. The effect of the inlet momentum-flux ratio (gas to liquid) was such that as it increases, the line, or curve that represents the data rotates in an anti-clockwise direction around the point of (0.5,0.5) on coordinates of F_{BG} vs. F_{BL}. Also, for the same inlet momentum-flux ratio and inlet flow regime, the data points nearly collapsed on coordinates of F_{BG} vs. F_{BL}.

The available analytical models and correlations were examined qualitatively and quantitatively against the data base. It is demonstrated that none of the available models/

correlations can provide accurate predictions of magnitude and trend for all inlet conditions.

It was found that the Hong and Griston (1995) correlation does not satisfy mass balance and does not work for small values of F_{BG}. Also, it is not capable of good predictions for the bubbly, plug, and slug flow regimes. The Chien and Rubel (1992) correlation was found to be insensitive to x_1. The correlation is also limited in the applicable range of P_1, namely from 28.6 to 42.4 bar, given by the authors of the correlation. However, the correlation was found to give the best available predictions for high-inlet-pressure steam-water data. The Ottens et al. (1995) model is applicable to all the flow regimes and it was found to give reasonable agreement with the data of air and water, and it was recommended as the best available prediction tool for air-water data with annular, plug, and slug flow regimes. The Hwang (1986) model was not applied to the slug flow regime because of lack of accurate information on the void fraction for this flow regime. However, it was recommended as the best available prediction tool for air-water data with bubbly and wavy flow regimes.

The design of a test facility that is capable of generating phase-distribution and pressure-drop data for low-pressure, air-water two-phase flow through an impacting tee junction is given. The test facility incorporates a horizontal impacting tee junction with the three sides having equal diameters (37.6-mm I.D.), and was designed for the following operating conditions : pressure of about 150 kPa (abs) at the junction, near ambient temperature, inlet superficial gas velocities, J_{G1}, ranging between 2.7 and 40 m/sec, inlet superficial liquid velocities, J_{L1}, ranging between 0.002 and 0.2 m/sec, and extraction ratios, W_3/W_1, between 0 and 1. These operating conditions were selected to cover previously untested conditions.

ACKNOWLEDGEMENTS

I would like to sincerely thank Dr. Hassan Soliman and Dr. Grant Sims for their great insight, encouragement, and guidance. Their support was extremely helpful in completing my thesis.

Mr. John Finken and Mr. Irwin Penner were very important and helpful in constructing the test facility.

Also, I would like to thank my parents who gave me a lot of support, financially and spiritually, that helped me to be here and finish my thesis.

My father- and mother-in-law gave me great assistance throughout the course of this study.

Last, but definitely not least, I would like to thank my wife and my little daughter who supported me through the most difficult times and encouraged me when I was badly in need for encouragement.

TABLE OF CONTENTS

LIST OF FIGURES

LIST OF TABLES

NOMENCLATURE

Symbol	Description	Units
a	Empirical coefficient in Chien and Rubel (1992) and Hong and Griston (1995) correlations	-
b	Empirical coefficient in Chien and Rubel (1992) and Hong and Griston (1995) correlations	-
b_G	Parameter defining the location of the gas dividing streamline from the point of impact, as in Figure 3.1	m
b_L	Parameter defining the location of the liquid dividing streamline from the point of impact, as in Figure 3.1	m
D_1	Diameter of the inlet	m
D_2	Diameter of outlet 2	m
D_3	Diameter of outlet 3	m
F	Parameter in the Hong and Griston (1995) correlation; see Equation (3.9)	m/s
F_{BG}	Fraction of inlet gas exiting through outlet 3, = W_{G3}/W_{G1}	-
F_{BL}	Fraction of inlet liquid exiting through outlet 3, = W_{L3}/W_{L1}	-
F_{DG}	Drag force acting on gas, as in Figure 3.2	N
F_{DL}	Drag force acting on liquid, as in Figure 3.2	N
g	Gravitational acceleration	m/s^2
J_{G1}	Superficial inlet-gas velocity	m/s
J_{G3}	Superficial gas velocity in outlet 3	m/s
J_{L1}	Superficial inlet-liquid velocity	m/s
J_{L3}	Superficial liquid velocity in outlet3	m/s
k_{12}	Friction loss coefficient between the inlet and outlet 2	-

k_{13}	Friction loss coefficient between the inlet and outlet 3	-
m_G	Coefficient related to the shape of the gas dividing streamline in the Hwang (1986) model	-
m_L	Coefficient related to the shape of the liquid dividing streamline in the Hwang (1986) model	-
$\dot{M}_R$	Inlet momentum-flux ratio; see Equation (2.1)	-
N	Empirical coefficient in Hwang (1986) model	-
P_1	Inlet pressure	bar
Re_{G1}	Inlet-gas Reynolds number	-
Re_{L1}	Inlet-liquid Reynolds number	-
Re_{SL1}	Inlet-liquid superficial Reynolds number	-
R_G	Radius of curvature of a gas streamline	m
R_L	Radius of curvature of a liquid streamline	m
S	Slip ratio = V_{G1} / V_{L1}	-
V_{G1}	Average inlet gas velocity	m/s
V_{L1}	Average inlet liquid velocity	m/s
W_1	Total inlet mass flow rate	kg/s
W_2	Total mass flow rate exiting through outlet 2	kg/s
W_3	Total mass flow rate exiting through outlet 3	kg/s
W_{G1}	Inlet-gas mass flow rate	kg/s
W_{G2}	Mass flow rate of gas exiting through outlet 2	kg/s
W_{G3}	Mass flow rate of gas exiting through outlet 3	kg/s
W_{L1}	Inlet-liquid mass flow rate	kg/s
W_{L2}	Mass flow rate of liquid exiting through outlet 2	kg/s

W_{L3}	Mass flow rate of liquid exiting through outlet 3	kg/s
x_1	Inlet quality = W_{G1} / W_1	-
x_2	Quality in outlet 2 = W_{G2} / W_2	-
x_3	Quality in outlet 3 = W_{G3} / W_3	-

Greek Symbols

α_1	Void fraction in the inlet	-
β	Angle between gas and liquid streamlines when crossing, as in Figure 3.2	rad
β_G	Constant in Ottens et al. (1995) model	-
β_L	Constant in Ottens et al. (1995) model	-
δ_G	Parameter defining the location of the gas dividing streamline in the inlet pipe, as in Figure 3.1	m
δ_L	Parameter defining the location of the liquid dividing streamline in the inlet pipe, as in Figure 3.1	m
ε_1	Liquid hold-up in the inlet	-
γ	Angle between the centrifugal and drag forces acting on gas, as in Figure 3.2	rad
κ	Ratio of kinetic energies per unit volume of gas and liquid in the inlet; See Equation (3.23)	-
λ_0	Junction energy dissipation factor; see Equation (3.24)	-
μ_G	Gas viscosity	Pa.s
μ_L	Liquid viscosity	Pa.s
ρ_G	Gas density	kg/m^3
ρ_L	Liquid density	kg/m^3
θ_{L1}	Fraction of the inlet pipe wetted by the liquid	-

Chapter 1

INTRODUCTION

Two-phase flow commonly occurs in many systems in the power and process industries, such as conventional steam power plants, evaporators and condensers, boiling-water and pressurized-water nuclear reactors, and a wide variety of chemical and petroleum applications. Quite often, the complex piping networks in these systems require the two-phase flow to pass through impacting tees. When two-phase flow passes through an impacting tee, maldistribution of the phases may occur; i.e., the qualities of the mixtures in both outlets downstream from the junction are not equal to the inlet quality. Certain inlet conditions can lead to single-phase gas flowing in one of the outlets, while other conditions can lead to single-phase liquid flowing in one of the outlets. This severe maldistribution of the phases can have a significant effect on the operation and efficiency of components downstream from the junction. Therefore, it is very important to be able to predict the manner by which the two phases distribute themselves at impacting tees for different operating conditions. Another consideration is the pressure drop that occurs at the junction. Experimental evidence has shown that the pressure drop during two-phase flow can be much greater than that during a comparable single-phase flow.

Figure 1.1 shows a schematic diagram of an impacting tee junction. The relevant flow parameters are as follows: the inlet, and the two outlet mass flow rates (W_1, W_2, and W_3, respectively); the inlet, and the two outlet average pressures (P_1, P_2, and P_3, respectively); and the inlet, and the two outlet qualities (x_1, x_2, and x_3, respectively).

Relevant geometric parameters are the inlet, and the two outlets diameters (D_1, D_2, and D_3, respectively). Other important parameters are the thermophysical and transport properties of the two-phase mixture. The two phases may belong to the same fluid component, such as steam and water, or two distinct components, such as air and water. The extraction ratio, given by W_3/W_1, is the fraction of the total inlet flow that is withdrawn through outlet 3. In a typical application, the geometrical parameters (D_1, D_2, and D_3), the inlet conditions (W_1, P_1, and x_1), one outlet flow rate (e.g., W_3), and the fluid properties will be known. For these given parameters, it will be required to determine W_2 , x_2 , x_3 , P_2 , and P_3 .

Figure 1.2(a) illustrates one method that has been used to present the phase-distribution data. The ordinate in this figure is the ratio of one of the outlet qualities to the inlet quality (x_3/x_1), and the abscissa is the extraction ratio W_3/W_1. Line **AB** represents the limiting case where only gas is diverted into outlet 3 ($x_3 = 1$) and all of the liquid and some gas flow into outlet 2. Curve **BC** represents another limiting case where only single-phase liquid flows into outlet 2 ($x_2 = 0$) and all of the gas and some liquid are diverted into outlet 3. A mass balance on the gaseous phase yields the following equation for this curve: $x_3/x_1 = W_1/W_3$. At point **B**, single-phase liquid is flowing in outlet 2 and single-phase gas is flowing in outlet 3. Thus, at point **B** the junction acts as a perfect separator. No data can exist above curve **ABC**. Curve **ABC** will be referred to as the total-phase-separation curve. Line **CD** is the even-phase-distribution line where the outlet qualities are equal to the inlet quality ($x_3 = x_2 = x_1$). Point **E** has a quality ratio of 1 and an extraction ratio of 0.5. Because of the geometric symmetry of the outlets of an impacting tee, all the curves representing the data should pass through point **E**.

Another method used to present the phase-distribution data is shown in Figure1.2(b). In this figure, the ordinate F_{BL} is the fraction of inlet liquid flowing in outlet 3 ($F_{BL} = W_{L3}/W_{L1}$) and the abscissa F_{BG} is the fraction of inlet gas flowing in the same outlet ($F_{BG} = W_{G3}/W_{G1}$). The points labeled **A, B, C, D,** and **E** correspond to the same points given in Figure 1.2(a). Again, due to geometric symmetry, all the curves representing the phase-distribution data should pass through point **E** that has an F_{BG} of 0.5 and an F_{BL} of 0.5. Also, in order to satisfy mass balance, the two parts of the curve before and after point **E** should be the inverted mirror image of each other. Therefore, F_{BL} at a given value of F_{BG} should be equal to $1-F_{BL}$ at $(1-F_{BG})$. An example of data that satisfy mass balance is shown in Figure 1.2(c) with two selected values of F_{BG} and F_{BL} illustrated. For simplicity, the term "point of 0.5" will be used throughout this study to refer to point **E** in the three parts of Figure 1.2. Also, the term "symmetry of the data" (or "symmetry of prediction" in case of model and correlation predictions) will be used to refer to a data curve of two parts that are the inverted mirror image of each other and pass through the "point of 0.5", or in other words to indicate that the data satisfy mass balance. In the present study, phase-distribution data, or prediction, will be presented on coordinates of F_{BG} vs. F_{BL}.

A review of the currently existing data (Chapter 2) indicates that limited work has been done on horizontal impacting tee junctions. Few phase-distribution data sets and even fewer pressure-drop data sets have been published. The phase-distribution data cover small ranges of the inlet mass flow rates and qualities. Some models have been developed to predict the phase-distribution and pressure-drop data. Some of these models are claimed to be general , i.e. flow-regime independent, while others are not.

A general model should be able to predict the phase-distribution and pressure-drop data for any combination of inlet mass flow rate, inlet quality, fluid properties, junction geometry, and extraction ratio. The literature review indicates that such a model does not exist yet. Also, the physics on which these models were based are extremely different. This is probably because of lack of understanding of the associated phenomena.

A fundamental prerequisite to the development of a mathematical model capable of predicting the phase distribution and pressure drop, is a full understanding of the physical phenomena associated with the existing data. Also, the availability of a wide range of experimental data against which any proposed model can be tested will help significantly in the development of a successful model. The purpose of this study, therefore, is to enhance the current state of knowledge on two-phase flow in impacting tee junctions.

The following is a list of the specific objectives of the present study :

1- To examine the available data in order to identify the most important factors that affect the phenomenon of phase distribution for two-phase flows through horizontal impacting tee junctions.

2- To test all the available models and correlations against the existing data in order to determine the most promising one(s) and, if possible, to modify it to improve its performance.

3- To design and construct a two-phase flow experimental apparatus capable of generating phase-distribution and pressure-drop data for air-water mixtures through a horizontal impacting tee junction, with equal outlet diameters (37.6-mm I.D.).

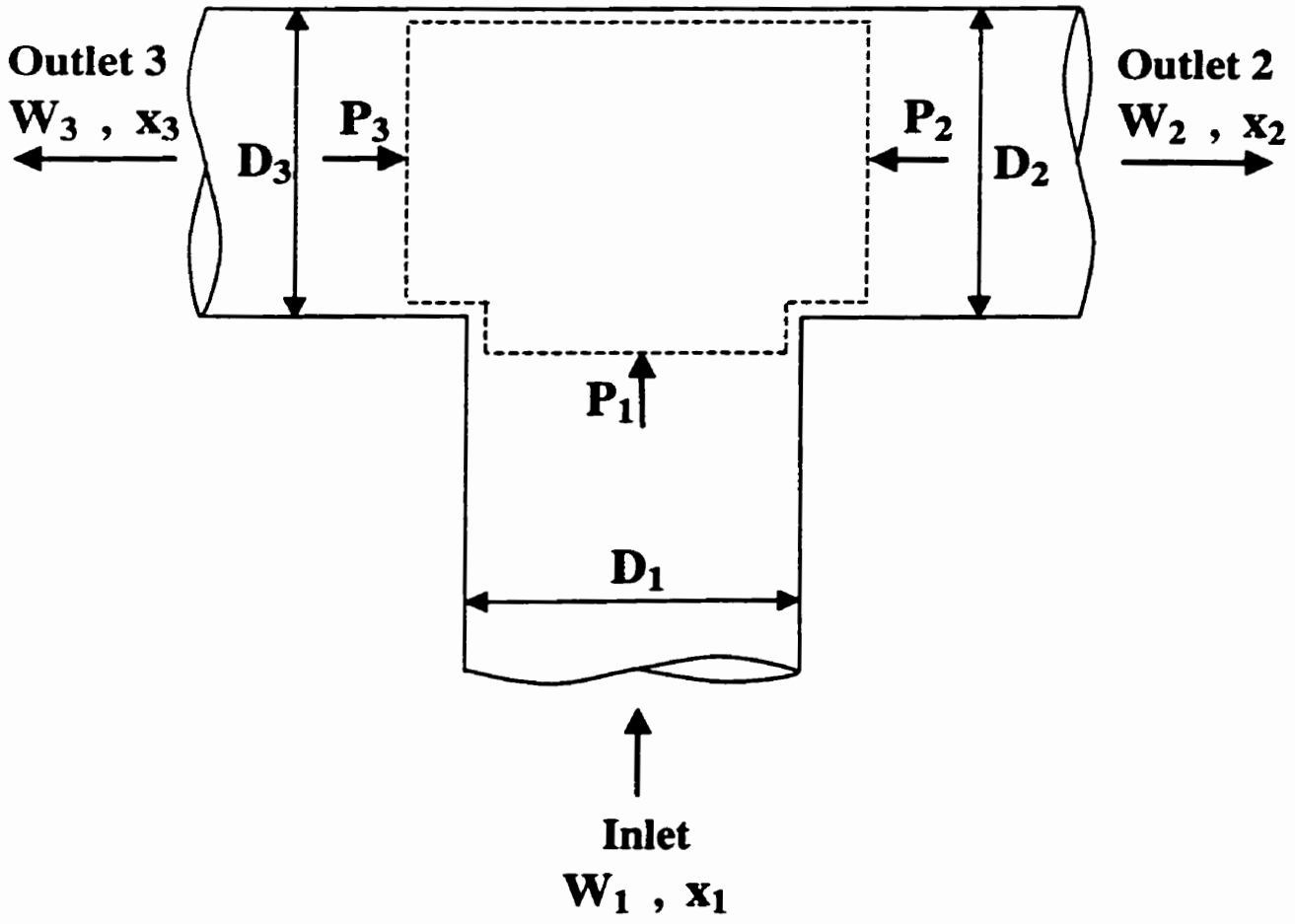

Figure 1.1 Relevant parameters for two-phase flow in an impacting tee junction.

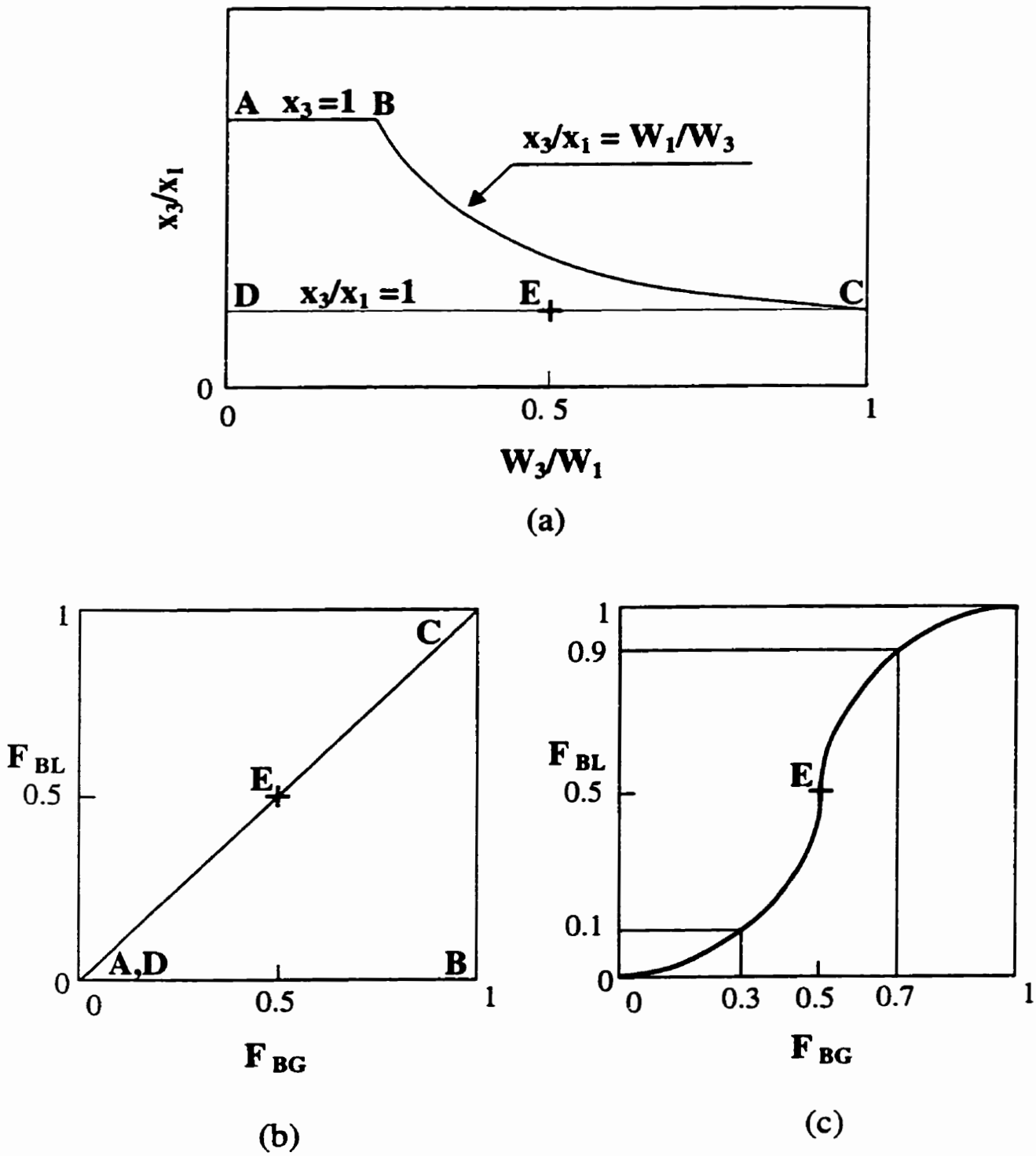

Figure 1.2 Schematic representation of two different ways to present the phase-distribution data.

Chapter 2

CRITICAL REVIEW OF EXISTING DATA

2.1 Overview

Table 2.1 gives a summary of all the previously published work on two-phase flow through impacting junctions. Most of the previous work has been done for air-water flows at low pressure; however, some work has been done for wet-steam and R-11 two-phase flows. Table 2.1 includes the previous work for all the inlet orientations and junction geometries. This table indicates a serious lack in pressure-drop data for two-phase flow in impacting junctions with only one reference (Hwang,1986) reporting such data for bubbly and bubbly-stratified inlet flow regimes. Both the phase distribution and pressure drop are expected to be dependent on the inlet flow regime and therefore, it is mandatory to cover as wide a region as possible of the flow regime map. The rest of this chapter focuses on two-phase flow through horizontal impacting tee junctions.

2.2 Phase-Distribution and Pressure-Drop Data for Horizontal Impacting Tee Junctions

Hong (1978) presented data for phase distribution through a horizontal impacting tee junction. The experiment was conducted with air-water flow in a 9.5-mm I.D. tee with an inlet mass flux of 73.5 ($kg/m^2.s$) and a quality of 0.68. The data indicated that over a wide range of W_3/W_1 (0.15 to 0.85), even phase split was obtained; i.e. the outlet flows had the same quality as the inlet flow. Data were obtained for one set of inlet conditions only. The trend of Hong's data is quite different from that obtained by later researchers. It was suggested by other researchers that Hong's data may have been

Author(s)	Junction Geometry and Orientation			D_1 (mm)	$D_2=D_3$ (mm)	Test Fluids	P_1 (bar)	J_{G1} (m/s)	J_{L1} (m/s)	W_3/W_1	Inlet Flow Regime	Inlet flow regimes are specified based on	Phase Dist.	Press. Drop
	Angle Between Inlet and Outlets	Inlet Orientation	Outlets Orientation											
Hong (1978)	90°	Horizontal	Horizontal	9.5	9.5	Air - Water	1.22	27.4	0.023	0.0 - 1.0	An	Barnea et al. (1983)	Yes	No
Hwang (1986)	45° 90°	Horizontal	Horizontal	38	38	Air - Water	1.3-1.9	1.5 - 6.5	1.35 - 2.539	0.02-0.95	Bub Bub-St	Visual observation	Yes	Yes
Lightstone et al. (1991)	90° *	Horizontal	Horizontal	20	20	Air - Water		0.1- 0.18	0.01 – 0.18		An , Pl Sl , St St-W	Visual observation	**	***
Chien and Rubel (1992)	90°	Horizontal	Horizontal	49.3	49.3	Steam - Water	28.6 - 42.4	12 - 40		0.2-0.5	An An-Mt	Visual observation	Yes	No
Ottens et al. (1995)	90°	Horizontal	Horizontal	29.5	29.5	Air - Water	1	15.8	0.00063-0.03	0.0 - 1.0	W	Mandhane et al. (1974)	Yes	No
Hong and Griston (1995)	90°	Horizontal	Horizontal	19 (50) (100)	19 (50) (100)	Air – Water (Steam-Water)	1	4.6 - 22.86	0.045-1.35	0.05-0.95	An-Mt St	Visual observation	Yes	No
Fujii et al. (1995)	90°	Horizontal	Horizontal	10	10	Nitrogen - Water	1	0.03 - 12	0.05 - 0.5	0.0 - 1.0	An , Pl Sl , St W	Visual observation	Yes	No
Fujii et al. (1996)	30° 60° 90°	Horizontal	Horizontal	10.5	10.5	Air - Water	1	0.1-7	0.05 - 0.5	0.0 - 1.0	An , Pl	Visual observation	Yes	****
Asano et al. (1997)	30° 60° 90°	Horizontal	Horizontal	10	10	R-11 (Saturated mixture)	1				Pl, Sl	Visual observation	Yes	No
Azzopardi et al. (1986)	90°	Vertical (Upward)	Horizontal	31.8	31.8	Air - Water	1.7	10.0 - 22.06	0.032-0.079	0.0-1.0	An	Visual observation	Yes	No
Azzopardi et al. (1986)	90°	Vertical (Upward)	Horizontal	31.8	31.8	Air - Water	1.7	1.62 - 4.05	0.08 - 0.8	0.0-1.0	Ch	Visual observation	Yes	No

An=Annular, **An-Mt**=Annular-Mist, **Bub**=Bubbly, **Bub-St**=Bubbly-Stratified, **Ch**=Churn, **Pl**=Plug, **Sl**=Slug, **St**=Stratified, **St-W**=Stratified-Wavy, **W**=Wavy.

* They also tested symmetric Y- junctions with angles 60°, 90°, and 120° between the outlets.

** They provided data on the distribution of void fraction upstream and downstream of the junction.

*** They reported limited data on the pressure distribution including two locations both upstream and downstream of the junction.

**** They provided data on the total rate of mechanical energy loss due to the junction.

Table 2.1 Summary of the previous work for impacting junctions

affected by strong surface tension forces due to the small tube diameter and the hydrostatic head of the fluid in the pipes leading to the phase separators (Hwang et al., 1989).

Hwang (1986) presented data for phase distribution and pressure drop through horizontal impacting tees. Measurements were taken for air-water flow through a 38-mm I.D. tee at various inlet conditions. The system pressure ranged between 0.13 and 0.19 MPa. Three inlet mass fluxes (1350, 2050, and 2700 $kg/m^2.s$) with three different qualities (0.2, 0.3, and 0.4 %) were considered. These inlet conditions resulted in bubbly and bubbly-stratified inlet flow regimes. The extraction ratio was varied over a range of 0.02 to 0.96. The data indicated that over the whole range of the extraction ratio, there were three distinct zones. The first one started from $W_3/W_1 = 0.02$ up to a value between 0.3 and 0.4 in which only liquid was diverted into outlet 3. The second went up to a value of W_3/W_1 between 0.6 and 0.7 in which both gas and liquid were diverted into outlet 3. The last one went to the end of the extraction-ratio range in which all the gas was diverted into outlet 3.

Lightstone et al. (1991) reported data for the average void fraction and pressure drop for horizontal air-water two-phase flow through impacting junctions. The experiments were conducted using 20-mm I.D. tubes. Observations of the flow-regime transitions were also reported. Flow regime maps were developed at four different locations along the test tubes. Two of these locations were upstream of the junction at 37 and 14 pipe diameters. The other two were downstream at 2 and 25 pipe diameters. The maps were drawn in terms of the superficial gas velocity and the superficial liquid velocity. A method for predicting the time-averaged pressure drop and the void fraction

based on a two-fluid separated flow model was proposed. Results of this method were compared against the experimental results. Comparisons based on their own data revealed that the method was reliable. Numerical and experimental results indicated that a large increase in void fraction occurs just downstream of the junction due to the splitting of the fluid mass flow rate. It was also reported that an impacting tee junction always produces pressure loss contrary to impacting wyes which may produce pressure recovery.

Chien and Rubel (1992) investigated the phase distribution of wet steam through horizontal impacting tee junctions. The tee junction diameter was 49.3 mm. The inlet pressure range was 28.6 to 42.4 bars, inlet steam quality range was 0.2 to 0.8, and the vapor extraction ratio ranged from 0.2 to 0.8. The inlet superficial vapor velocity ranged from 12 to 40 m/s which gave annular and annular-mist inlet flow regimes. The data showed that the outlet steam qualities were always different from the inlet quality if the vapor extraction ratio was not 0.5. The difference between the inlet and outlet-3 qualities increased as the vapor extraction ratio deviated from 0.5. The difference was reduced as the inlet quality increased. For a given inlet quality, outlet-3 quality decreased slightly with increasing inlet vapor velocity. Inlet steam pressure was not found to have a significant effect on the data.

Ottens et al. (1995) reported an experimental and analytical investigation for two-phase flow through impacting junctions. Phase distribution data of air-water flow for four sets of inlet conditions were reported. A superficial gas velocity of 15.8 m/s with four superficial liquid velocities of 0.00063 , 0.00302 , 0.012 , and 0.3 m/s represent the four sets. The inlet quality range was approximately 0.38 to 0.97. The data indicated

that at high qualities, no liquid was diverted into outlet 3 up to a certain gas extraction ratio (F_{BG} of around 0.4). At F_{BG} = 0.5 the qualities at the inlet and both outlets were equal, as expected . For gas extraction ratios above a certain value (around 0.6), all the liquid was diverted into outlet 3. At low qualities, no gas was diverted into outlet 3 up to a certain liquid extraction ratio (F_{BL} of around 0.2). Again, the three qualities were equal at the point of F_{BL} = 0.5. For liquid extraction ratios above a certain value (around 0.8), all the gas was diverted into outlet 3. This trend of data at low qualities agrees with the trend obtained by Hwang et al. (1989).

Hong and Griston (1995) reported phase-distribution data for laboratory air-water and field wet-steam flows through horizontal impacting junctions. They also developed an empirical method for predicting phase splitting. They also tested different types of insert devices in order to determine the one that increases the extraction-ratio range over which even phase splitting can be obtained. Laboratory experiments were conducted using 19.-mm I.D. tee with superficial gas velocities between 4.6 and 22.86 m/s and liquid volume fractions of 0.01, 0.02, 0.04, and 0.06. The pressure at the junction was atmospheric. The four liquid volume fractions tested correspond to inlet qualities of 0.1, 0.05, 0.027, and 0.018, respectively. These are low qualities and one would expect the trend of the data to be similar to that obtained by Hwang (1986) and Ottens et al. (1995). Indeed, this was the case and the only differences were the values of F_{BL} up to which F_{BG} was equal to zero and the value of F_{BL} beyond which F_{BG} reaches 1. The data showed that, at low gas superficial velocity (e.g., 4.6 m/s) and low liquid volume fraction (e.g., 0.01), equal phase splitting occurred over the entire range of the extraction ratio. Also, as the liquid volume fraction increased (or the quality

decreased) the data points approach a horizontal line passing through the "point of 0.5". A horizontal line would mean a constant F_{BL} over the whole range of F_{BG}. It may be noted that the data obtained by Ottens et al. (1995) showed that as the quality increased the data points approached a vertical line passing through the "point of 0.5". A vertical line would mean a constant F_{BG} over the whole range of F_{BL}. Data for tees modified with insert devices showed that the mixer stratifier does not improve phase splitting, the preseparator vane slightly improves phase splitting, and the nozzle reducer greatly improves phase splitting so that liquid and gas phases split evenly over the entire range of extraction ratio.

Fujii et al. (1995) investigated the effect of the inlet flow regime on phase splitting of nitrogen-water flow through horizontal impacting junctions. The possibility of using the junction as a separator was the main objective. A 10-mm I.D. tee was used with liquid superficial velocities of 0.05 to 0.5 m/s and gas superficial velocities of 0.03 to 12 m/s. These inlet flow conditions correspond to plug, slug, annular, stratified, and wavy flow regimes. For plug, slug, and annular flows, the data followed the same trend obtained by Hwang (1986) , Ottens et al. (1995) , and Hong and Griston (1995). No gas was diverted into outlet 3 up to a certain value of the extraction ratio W_3/W_1. This value was called the "gas take-off point". On increasing the extraction ratio, gas started to divert into outlet 3 and data points passed through the "point of 0.5" up to a certain value where all the gas was diverted into outlet 3. The only exception to the above-mentioned trend was for liquid superficial velocities less than 0.15 m/s with annular flow, where gas and liquid always appeared in outlet 3 no matter what was the value of the extraction ratio. For stratified and wavy flows, the data did not follow the same

trend. Instead, gas and liquid were diverted into the two outlets for all values of the extraction ratio. The conclusion was that the phase separation is strongly affected by the inlet flow regime and somewhat affected by the liquid superficial velocity. Experiments were also conducted under microgravity in order to investigate the reliability of an impacting tee junction as a phase separator for two-phase flow thermal control systems in space application. These two-phase systems have been proposed to replace the single-phase systems used already in space ships because of their compactness and reduced weight .

Fujii et al. (1996) reported phase distribution and pressure drop data for air-water flow through horizontal impacting tees. Experiments were conducted using a 10.5-mm I.D. tee with liquid superficial velocities of 0.05 to 0.5 m/s and gas superficial velocities of 0.1 to 7.0 m/s. It was reported that these flow conditions correspond to annular and plug flow regimes. The data obtained follow the same trend obtained by Hwang (1986) , Ottens et al. (1995) , Hong and Griston (1995), and Fujii et al. (1995). No gas was diverted into outlet 3 up to a certain extraction ratio (below 0.5) . Increasing the extraction ratio, the data points passed through the "point of 0.5". For extraction ratios above a certain value (higher than 0.5) , all the gas was diverted into outlet 3.

Asano et al. (1997) reported phase distribution data for two-phase one-component flow through horizontal impacting tee junction. The inlet mass flux ranged from 63.7 to 828 $kg/m^2.s$ and the quality ranged from 0.001 to 0.3. Refrigerant R-11 was used as the working fluid through a 10-mm I.D. tee. At low qualities, the results followed the same trend obtained by Hwang (1986), Ottens et al. (1995), Hong and Griston (1995),

and Fujii et al. (1995). This was the case with differences in values of the "gas take-off point" which is the value of W_3/W_1 at which gas starts to be diverted into outlet 3. For the same inlet conditions, the value of the "gas take-off point" for R-11 was lower than that for air-water.

2.3 Effect of J_{Ll} on the Phase Distribution

2.3.1 Within Data Sets of the Same Researcher

The effect of varying J_{Ll}, with constant J_{Gl}, on the phase distribution within data sets of the same researcher was investigated in this study. Figure 2.1 shows the data of Ottens et al. (1995) using J_{Gl} = 15.8 m/s and J_{Ll} from 0.00063 to 0.03 m/s. It can be seen that in the range of F_{BG} from 0 to 0.5, increasing J_{Ll} resulted in increasing the preference of the liquid to flow into outlet 3, while in the range of F_{BG} from 0.5 to 1.0, increasing J_{Ll} resulted in increasing the preference of the gas to flow into the same outlet. This trend can also be observed in Figures 2.2 to 2.6, which show the data of Hong and Griston (1995). Each figure corresponds to a fixed value of J_{Gl} with variable J_{Ll}. Values of J_{Gl} tested were 4.57, 9.14, 13.7, 18.3 and 22.9 m/s, respectively. This trend is also followed by the data of Fujii et al. (1995) using J_{Gl} = 12.0 m/s and J_{Ll} from 0.05 to 0.5 m/s. This is shown in Figure 2.7. Figures 2.8 to 2.12 show the data of Chien and Rubel (1992) following the same trend except for Figures 2.10 and 2.12, where the data are somewhat scattered rather than having a trend. Values of J_{Gl} tested were 12.2, 15.2, 18.3, 24.4, and 33.5 m/s, respectively. It should be noted that, for the case of Hong and Griston (1995), as the value of J_{Gl} increased, the effect of varying J_{Ll} was reduced. From all the above-mentioned figures the effect of varying J_{Ll}, with constant J_{Gl}, on the phase-separation data can be summarized as follows:

- Increasing J_{Ll} results in turning the line, or curve that connects the data points in a clockwise direction around the "point of 0.5" on an F_{BG} vs. F_{BL} graph.
- As the value of J_{Gl} increases, the effect of varying J_{Ll} becomes smaller.

2.3.2 Among Data Sets of Different Researchers

The effect of varying J_{Ll}, with constant J_{Gl}, on the phase distribution among data sets of different researchers was also investigated in this study. Figure 2.13 shows the data of Ottens et al. (1995) and the data of Hong and Griston (1995). The value of J_{Gl} for the former data set was 15.8 m/s with J_{Ll} varied from 0.00063 to 0.03 m/s while for the latter data set the value of J_{Gl} was 13.7 m/s with J_{Ll} varied from 0.139 to 0.876 m/s. Both data sets follow a similar trend. That is, increasing J_{Ll} rotated the data line, on an F_{BG} vs. F_{BL} graph, in a clockwise direction around the "point of 0.5". Also, the data of Hong and Griston (1995) appear to continue the trend in the data of Ottens et al. (1995) in terms of the J_{Ll} effect. In Figures 2.14 and 2.15, different data sets taken at approximately the same value of J_{Gl} over a range of J_{Ll} were compared against each other. In Figure 2.14, the effect of varying J_{Ll} on the data of Hong and Griston (1995) is similar to the trend that was seen in Figure 2.13, while for the Hwang (1986) data the effect of varying J_{Ll} is not clear because of the small range of J_{Ll} tested. In Figure 2.15, the effect of J_{Ll} on the data can be seen as we move from Fujii et al. (1995) data set to Hwang (1986) first data set, while within the data sets of Hwang (1986) the effect of J_{Ll} is not clear because of the small range of J_{Ll} tested. Figure 2.16 is very similar to Figure 2.13 except that the data of Chien and Rubel (1992) using J_{Gl}=15.2 m/s and J_{Ll} values of 0.1 and 1.60 m/s are added to the data sets that were already plotted in Figure 2.13. It can be seen that, the data of Chien and Rubel (1992) follow the expected trend

within themselves; however, they are slightly shifted from the region corresponding to their value of J_{Ll} with respect to the other data sets. This might be attributed to the fact that the data of Chien and Rubel (1992) were taken for different fluids, steam and water, and at very high pressures compared with the other data sets. That observation from Figure 2.16 can also be seen in Figures 2.17 to 2.19, where data sets of Chien and Rubel (1992) were compared against the data of Fujii et al. (1995), and Hong and Griston (1995).

2.4 Effect of J_{Gl} on the Phase Distribution

2.4.1 With Constant J_{Ll}

Figure 2.20 shows the data of Hong and Griston (1995) with $J_{Ll} = 0.19$ m/s and J_{Gl} varied from 4.57 to 18.3 m/s. It can be seen that in the range of F_{BG} from 0 to 0.5, increasing J_{Gl} resulted in decreasing the preference of the liquid to flow into outlet 3, while in the range of F_{BG} from 0.5 to 1.0, increasing J_{Gl} resulted in decreasing the preference of the gas to flow into the same outlet. It can be noted that this trend is exactly the same as that obtained for decreasing J_{Ll} at a constant J_{Gl}. It can also be seen that the change in the data in Figure 2.20 is not significant. This may be attributed to the small range of J_{Gl} tested. In Figure 2.21 another value for J_{Ll} was used to investigate the effect of varying J_{Gl} within the Hong and Griston (1995) data. The value of J_{Ll} was 0.5 m/s on average while J_{Gl} varied from 9.14 to 22.9 m/s. The trend observed in Figure 2.20 applies even though it is not as clear as in Figure 2.20, but it may be concluded that varying J_{Gl} at a constant J_{Ll} has an effect on the phase separation. Figures 2.22 to 2.24 show the data of Hwang (1986). Each figure corresponds to a constant value for J_{Ll} and variable J_{Gl}. The three values of J_{Ll}

examined were 1.35, 2.04 and 2.5 m/s, respectively. For each figure, increasing J_{GI} has almost no effect on the data. This may be attributed to the small ranges of J_{GI} tested in each figure. The same observation can be made regarding Figures 2.25 and 2.26 for the Fujii et al. (1995) data using J_{LI} = 0.2 and 0.5 m/s, respectively. The fact that J_{GI} has almost no effect on the phase distribution in the data of Fujii et al. (1995) may be attributed to the scattering of the data which makes it difficult to discern any trends in their data. From all the above-mentioned figures the effect of varying J_{GI}, with constant J_{LI}, on the phase-separation data can be summarized as follows:

- In principle, increasing J_{GI} with constant J_{LI} results in turning the line, or curve that connects the data points in an anti-clockwise direction around the "point of 0.5" on an F_{BG} vs. F_{BL} graph.
- The observed effect of J_{GI} on the phase distribution is not as significant as that of J_{LI} and this may be attributed to the small ranges of J_{GI} tested.

2.4.2 With Constant x_I

Figure 2.27 shows the data of Hong and Griston (1995) for a quality x_I = 0.105 and J_{GI} range of 4.57 to 22.9 m/s. Similar graphs are shown in Figures 2.28 to 2.30 with x_I = 0.055, 0.028, and 0.018, respectively. In these data, J_{LI} increases as J_{GI} increases in order to keep the quality x_I constant. The figures show that as J_{GI} increases at constant x_I, the preference of the liquid to flow into outlet 3 increases in the range of F_{BG} of 0 to 0.5, while the preference of the gas to flow into the same outlet increases in the range of F_{BG} of 0.5 to 1. This trend is similar to the trend observed for increasing J_{LI} at constant J_{GI} while it is opposite to the trend observed for increasing J_{GI} at constant J_{LI} which means that the effect of increasing J_{LI} overcame the effect of increasing J_{GI}. This

is consistent with the fact that J_{Ll} has a more significant effect on the phase distribution than J_{Gl}, which was observed in Section 2.4.1. From the same figures, it can also be seen that as the quality x_l decreases, the data points were getting closer. For the same range of gas velocities, the lower the quality, the less significant is the effect of J_{Gl}. Figures 2.31 to 2.34 show the data of Chien and Rubel (1992) for x_l = 0.2, 0.4, 0.6, and 0.8, respectively. In Figures 2.31 and 2.34, the trend observed in the data is similar to the trend observed in the data of Hong and Griston (1995) even though it is not as clear as in Figures 2.27 and 2.28. In Figures 2.32 and 2.33 the data show a small effect for J_{Gl}. It should be observed that the range of J_{Gl} covered by Hong and Griston (1995) is wider than the range of J_{Gl} covered by Chien and Rubel (1992). Therefore, it might be concluded that the effect of varying J_{Gl}, with constant quality x_l, is as follows:

- Increasing J_{Gl} with constant x_l results in turning the line, or curve that connects the data points in a clockwise direction around the "point of 0.5" on an F_{BG} vs. F_{BL} graph.

2.5 Effect of Inlet Pressure on the Phase Distribution

Most of the work on phase distribution in horizontal impacting tee junctions was done at or near atmospheric pressure with only one exception: the work of Chien and Rubel (1992), which was done at pressures of 28.6 and 42.4 bar. The data of Chien and Rubel (1992) were compared against other data that were obtained at the atmospheric pressure to investigate the effect of inlet pressure on the phase distribution. Figure 2.35 shows the data of Chien and Rubel (1992) at a pressure of 28.6 bar, J_{Gl} of 18.3 m/s, and J_{Ll} of 1.18 m/s against the data of Hong and Griston (1995) at atmospheric pressure, J_{Gl} of 18.3 m/s, and J_{Ll} of 1.17 m/s. It was taken into consideration that the

data sets would have the same, or as close as possible, J_{GI} and J_{LI} in order to eliminate their effects. The flow regime for both data sets was annular. It can be seen that increasing the pressure results in decreasing the preference of the liquid to flow into outlet 3 in the range of F_{BG} from 0 to 0.5. The data of Chien and Rubel (1992) did not go beyond the value of 0.5 for F_{BG}. However, it is very probable that the trend in the range of F_{BG} from 0.5 to 1 would be consistent with the trend observed in the range of F_{BG} from 0 to 0.5. In other words, increasing the pressure would probably result in decreasing the preference of the gas to flow into outlet 3 in the range of F_{BG} from 0.5 to 1. This trend observed in Figure 2.35 can also be seen in Figure 2.36, where the data of Chien and Rubel (1992) at a pressure of 28.6 bar, J_{GI} of 12.2 m/s, and J_{LI} of 0.158 m/s are plotted with the data of Fujii et al. (1995) at atmospheric pressure, J_{GI} of 12.0 m/s, and J_{LI} of 0.15 m/s. The same trend can also be seen in Figure 2.37 where data of Chien and Rubel (1992) at a pressure of 28.6 bar, J_{GI} of 12.2 m/s, and J_{LI} of 0.328 m/s are plotted with the data of Fujii et al. (1995) at the atmospheric pressure, J_{GI} of 12.0 m/s, and J_{LI} of 0.3 m/s. It can be noted that the effect of increasing the inlet pressure is similar to the effect of increasing J_{GI} at a constant J_{LI}. When J_{GI} increases at a constant J_{LI}, the gas momentum increases while the liquid momentum would probably remain the same. Also, when the inlet pressure increases, the gas density increases and consequently the gas momentum increases while the liquid density and momentum would be almost unchanged. In the case of Chien and Rubel (1992) data at a pressure of 28.6 bar, the gas density was 14.2 kg/m^3 while the liquid density was 825 kg/m^3. For the atmospheric-pressure data, the gas density was 1.2 kg/m^3 while the liquid density was 1000 kg/m^3. That is, for Chien and Rubel (1992) data, the gas density increases by

a factor of 11.8 while the liquid density decreases by a factor of 1.21. So, increasing the inlet pressure and increasing J_{GI} at constant J_{LI} have the same effect on the gas momentum and this might be a reason that both have the same effect on the phase distribution. It should be mentioned that Chien and Rubel (1992) used steam and water, Hong and Griston (1995) used air and water, and Fujii et al. (1995) used nitrogen and water. So, the effect that appears in Figures 2.35 to 2.37 is not solely the effect of the inlet pressure as the difference in the fluid properties might have played a roll in giving that effect. However, the huge difference in the inlet pressure from 1 to 28.6 bar must have had an effect in these figures. That effect of the inlet pressure on the phase distribution can be summarized as follows:

- Increasing the inlet pressure at constant J_{GI} and J_{LI} results in turning the line, or curve that connects the data points in an anti-clockwise direction around the "point of 0.5" on an F_{BG} vs. F_{BL} graph.

2.6 Effect of Inlet Quality on the Phase Distribution

The effect of inlet quality on the phase distribution was investigated using data sets with the same inlet mass flow rate, W_I, and different inlet qualities. Figure 2.38 shows the data of Ottens et al. (1995) using $W_I = 0.013$ kg/s and $x_I = 0.968$ against the data of Fujii et al. (1995) using $W_I = 0.013$ kg/s and $x_I = 0.085$. It is very clear that increasing the quality decreases the preference of the liquid to flow into outlet 3 in the range of F_{BG} from 0 to 0.5 and decreases the preference of the gas to flow into the same outlet in the range of F_{BG} from 0.5 to 1. This is the expected effect because increasing x_I at the same W_I results in increasing J_{GI} and decreasing J_{LI}. As shown earlier, increasing J_{GI} or decreasing J_{LI} produced trends in the phase-distribution data

similar to those shown in Figure 2.38. Figures 2.39 to 2.42 show different data sets taken at approximately the same inlet mass flow rate, W_I, and different inlet qualities, x_I. The same trend that was observed in Figure 2.38 still applies. So, it may be concluded that the effect of inlet quality, x_I, on the phase distribution can summarized as follows:

- Increasing the inlet quality, x_I, at constant W_I results in turning the line, or curve that connects the data points in an anti-clockwise direction around the "point of 0.5" on an F_{BG} vs. F_{BL} graph.

2.7 Effect of Inlet Flow Regime on the Phase Distribution

To investigate the effect of the inlet flow regime on the phase distribution, different data sets with different inlet flow regimes and similar x_I (as close as possible) were compared against each other. It was also taken into consideration that the inlet pressure would be the same. Figure 2.43 shows the data of Fujii et al. (1995) at x_I of 0.003, J_{GI} of 1.25 m/s, and J_{LI} of 0.5 m/s against the data of Hwang (1986) at x_I of 0.003, J_{GI} of 2.27 m/s, and J_{LI} of 1.35 m/s. The flow regime changed from slug to bubbly as we go from the former data set to the latter. The figure indicates that changing the flow regime with the same inlet quality has no effect on the phase distribution. Similar results are shown in Figure 2.44. It can be concluded that, within the present test range, the inlet flow regime had no effect on the phase distribution as long as x_I remained the same. The data in Figures 2.43 and 2.44 correspond to the same x_I but different W_I. This can be achieved by increasing (or decreasing) both J_{GI} and J_{LI}. Since J_{GI} and J_{LI} have opposite effects on the phase distribution, the net effect seen in Figures 2.43 and 2.44 is not surprising.

2.8 Effect of Inlet Momentum-Flux Ratio on the Phase Distribution

The inlet momentum-flux ratio is given by

$$\dot{M}_R = \rho_{GI} V^2_{GI} / (\rho_{LI} V^2_{LI}) \quad (2.1)$$

where, ρ_{GI} is the inlet gas density, ρ_{LI} is the inlet liquid density, and V_{GI} and V_{LI} are the average velocities of gas and liquid, respectively, in the inlet pipe. In order to calculate the average velocity of each phase, the void fraction α or the slip ratio S must be known. The void fraction is defined as

$$\alpha_I = A_{GI} / A_I \quad (2.2)$$

where, A_{GI} is the area occupied by the gas in the inlet pipe, and

A_I is the whole cross-sectional area of the inlet pipe.

After calculating the void fraction, α, the average velocities of the gas and liquid in the inlet can be calculated from the inlet superficial velocities using the following relations:

$$V_{GI} = W_{GI} / (\rho_{GI} A_{GI}) = W_{GI} / (\rho_{GI} A_I \alpha_I) = J_{GI}/\alpha_I \quad (2.3)$$

and

$$V_{LI} = W_{LI} / (\rho_{LI} A_{LI}) = W_{LI} / (\rho_{LI} A_I (1-\alpha_I)) = J_{LI}/(1-\alpha_I) \quad (2.4)$$

The slip ratio is defined as follows:

$$S_I = V_{GI} / V_{LI} = J_{GI} (1-\alpha_I) / (J_{LI} \alpha_I) \quad (2.5)$$

Therefore, knowledge of S_I and the inlet superficial velocities is sufficient for determining α_I, V_{GI}, and V_{LI}. The procedure by which the void fraction or the slip ratio were calculated was dependent on the inlet flow regime. For bubbly and plug flow regimes, the drift-flux model given in Hwang (1986) was used to calculate the slip ratio in the inlet. For wavy and annular flow regimes, the geometrical and physical models

given in Shoham et al. (1987) were used to calculate the void fraction in the inlet for each individual flow regime. The previously mentioned models are given in details in Appendix A. It should be mentioned that for the annular-mist flow regime, the inlet void fraction was calculated in the same way as for the annular flow regime. Also, for the bubbly-stratified flow regime, the inlet void fraction was calculated in the same way as for the bubbly flow regime. There are no available physical or geometrical models for calculating the slip ratio or the void fraction for the slug flow regime. Therefore, the effect of the inlet momentum-flux ratio was not investigated for this flow regime.

It was found that, for data sets that correspond to the bubbly and plug flow regimes, the value of the inlet momentum-flux ratio does not change significantly with the change of J_{GI} or J_{LI}. This might be attributed to the fact that the drift-flux model that was used to calculate the slip ratio for these flow regimes is dependent only on two parameters. These parameters are the gas-liquid density ratio, ρ_G / ρ_L, and the inlet quality, x_I. The density ratio is almost constant and the inlet quality, x_I, for bubbly and plug flow regimes is usually very small. This causes the slip ratio calculated by the drift-flux model to be almost unchanged for bubbly and plug flow regimes. So, the effect of the inlet momentum-flux ratio on the phase distribution was only investigated among data sets that correspond to wavy, annular, and annular-mist flow regimes.

Figure 2.45 shows the data of Ottens et al. (1995) with J_{GI} = 15.8 m/s and J_{LI} varied from 0.00063 to 0.03 m/s. Values of the inlet momentum-flux ratio are given in the figure with the flow regimes based on which they were calculated. These flow regimes were determined from the Mandhane et al. (1974) flow-regime map. It can be seen that, within the same flow regime, decreasing the inlet momentum-flux ratio

results in increasing the preference of the liquid to flow into outlet 3 in the range of F_{BG} from 0 to 0.5 and decreasing the preference of the liquid to flow into the same outlet in the range of F_{BG} from 0.5 to 1.0. This effect is similar to the effect of decreasing J_{Ll} which was discussed in Section 2.3. This is not surprising because decreasing J_{Ll} would result in increasing the inlet momentum-flux ratio as long as the flow regime is the same. Figures 2.46 to 2.50 show the data of Hong and Griston (1995) with values of the inlet momentum-flux ratio indicated. The flow regimes based on which the momentum-flux ratios were calculated were determined from the Mandhane et al. (1974) flow-regime map. Each figure corresponds to a constant value of J_{Gl} and variable J_{Ll}. It can be seen that, as the inlet momentum-flux ratio decreases, the preference of the liquid to flow into outlet 3 increases in the range of F_{BG} from 0 to 0.5 and decreases in the range of F_{BG} from 0.5 to 1. These trends in the Hong and Griston (1995) data are similar to the trends observed in the Ottens et al. (1995) data in Figure 2.45. Similar trends were observed in the data of Chien and Rubel (1992) and Fujii et al. (1995).

In order to get a better understanding of the effect of the inlet momentum-flux ratio on the phase distribution, the data sets that have the same inlet momentum-flux ratio and inlet flow regime with different values for J_{Gl} and J_{Ll} were compared against each other. This was done using data sets of the same researchers and different researchers. Figure 2.51 shows the data of Hong and Griston (1995) for a value of 0.155 for the inlet momentum-flux ratio, annular flow regime, atmospheric inlet pressure, and an inlet quality of 0.105. Values of J_{Gl} varied from 13.7 to 22.9 m/s and in order to keep the same inlet quality, J_{Ll} varied as well. It can be seen that, for the same inlet flow regime and inlet momentum-flux ratio, the data points are very close even with different values

for J_{GI} and J_{LI}. Similar graphs are shown in Figures 2.52 to 2.54 for the data of Hong and Griston (1995) and Figures 2.55 to 2.58 for the data of Chien and Rubel (1992). The same trend that was observed in Figure 2.51 can be noted in Figures 2.52 to 2.58. Figure 2.59 shows the data of Fujii et al. (1996) for inlet momentum-flux ratio = 0.036, annular flow regime, atmospheric inlet pressure, and J_{GI} = 7.0 m/s against the data of Hong and Griston (1995) for inlet momentum-flux ratio = 0.039, annular flow regime, atmospheric inlet pressure, and an inlet quality of 0.018. The same trend that was observed in Figures 2.51 to 2.58 when comparing data of the same researchers can be observed in Figure 2.59. That is, for the same inlet flow regime and inlet momentum-flux, the data points are more or less collapsed. Figure 2.60 shows the data of Fujii et al. (1995) against the data of Hong and Griston (1995). The same trend observed in Figures 2.51 to 2.59 is applicable. Figure 2.61 shows the data of Ottens et al. (1995), who tested air and water at atmospheric inlet pressure, against the data of Chien and Rubel (1992) who tested wet steam at an inlet pressure = 28.6 bar. The flow regime was annular for both data sets and the values of the inlet momentum-flux ratios were close. It can be noted that the lines, or the curves, that connect the data points for both data sets have slightly different slopes. However, the data points are still reasonably close even with different fluids tested and the huge difference in the inlet pressure. Figure 2.62 shows the data of Hong and Griston (1995) for air and water and atmospheric inlet pressure against the data of Chien and Rubel (1992) for wet steam and an inlet pressure = 28.6 bar. Figure 2.63 shows the data of Fujii et al. (1995) for air and water and atmospheric inlet pressure against the data of Chien and Rubel (1992) for wet steam

and an inlet pressure = 42.4 bar. The same trend observed in Figure 2.61 can be observed in Figures 2.62 and 2.63.

The trends observed in Figures 2.45 to 2.63 imply that the effect of the inlet momentum-flux ratio on the phase distribution can be summarized as follows:

- Increasing the inlet momentum-flux ratio results in turning the line, or curve that connects the data points in an anti-clockwise direction around the "point of 0.5" on an F_{BG} vs. F_{BL} graph.
- For the same inlet momentum-flux ratio and inlet flow regime, the data points on an F_{BG} vs. F_{BL} graph are reasonably close at any fixed F_{BG} even if the values of J_{GI}, J_{LI}, and P_I are substantially different.

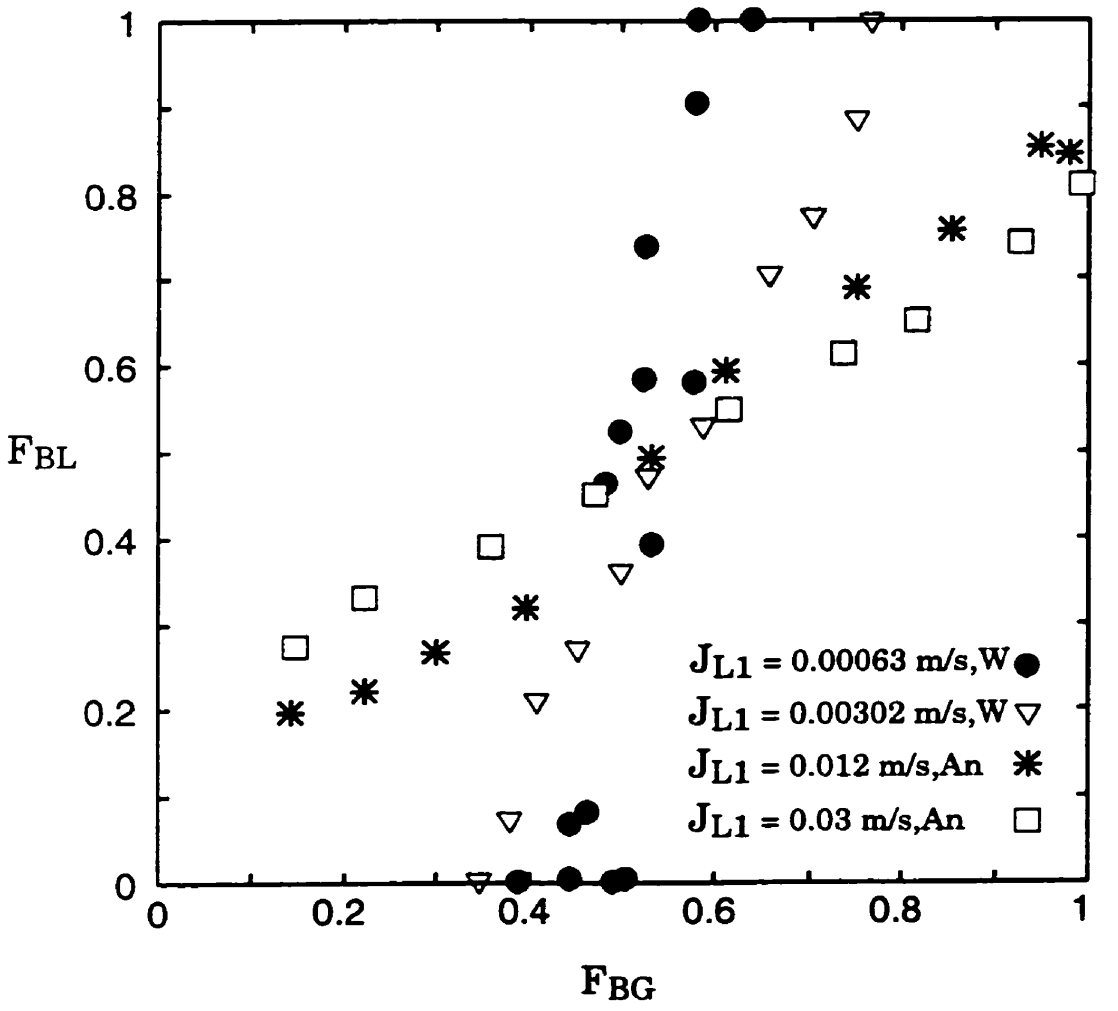

Figure 2.1 Effect of J_{L1} on the phase distribution in the data of Ottens et al. (1995) for J_{G1} =15.8 m/s, (W:Wavy, An:Annular).

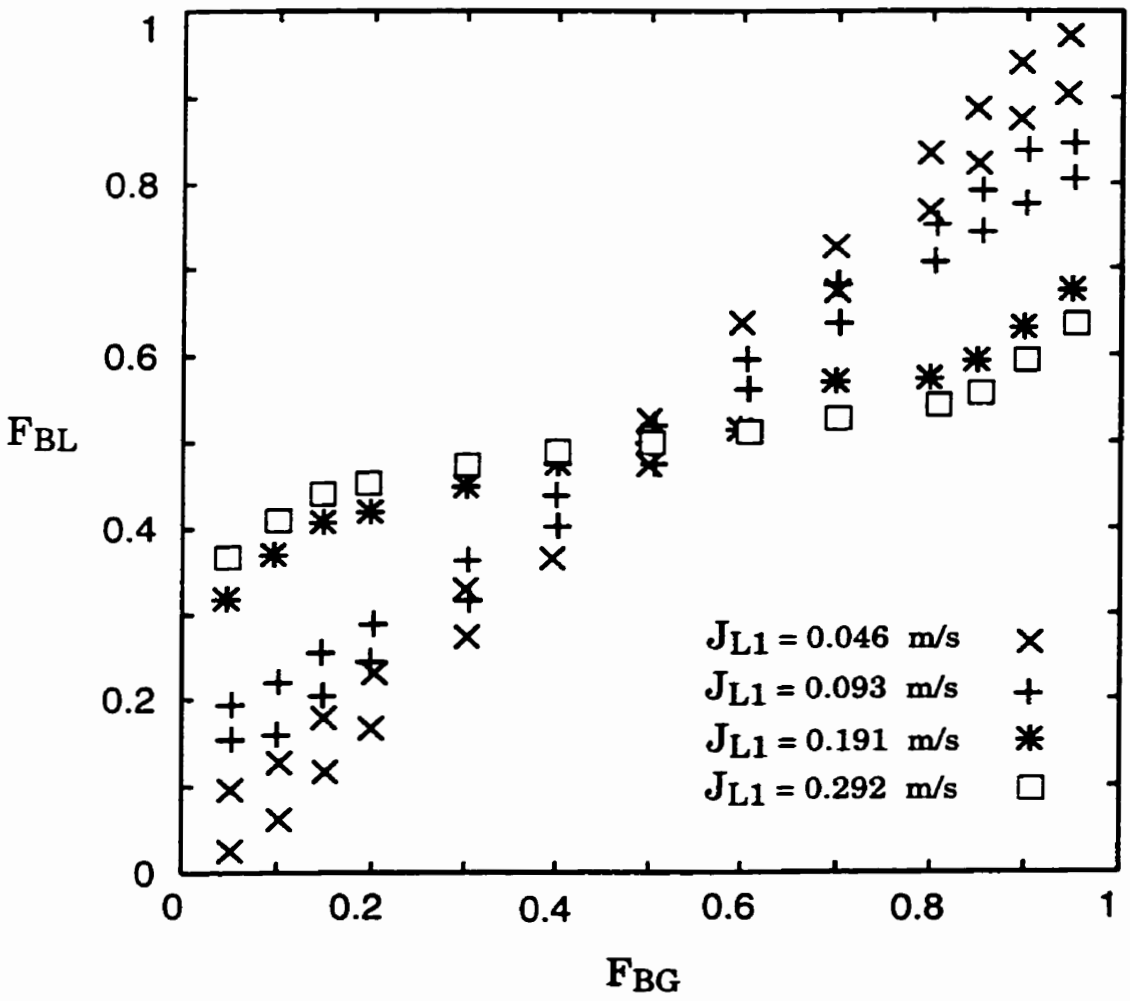

Figure 2.2 Effect of J_{L1} on the phase distribution in the data of Hong and Griston (1995) for J_{G1} = 4.57 m/s.

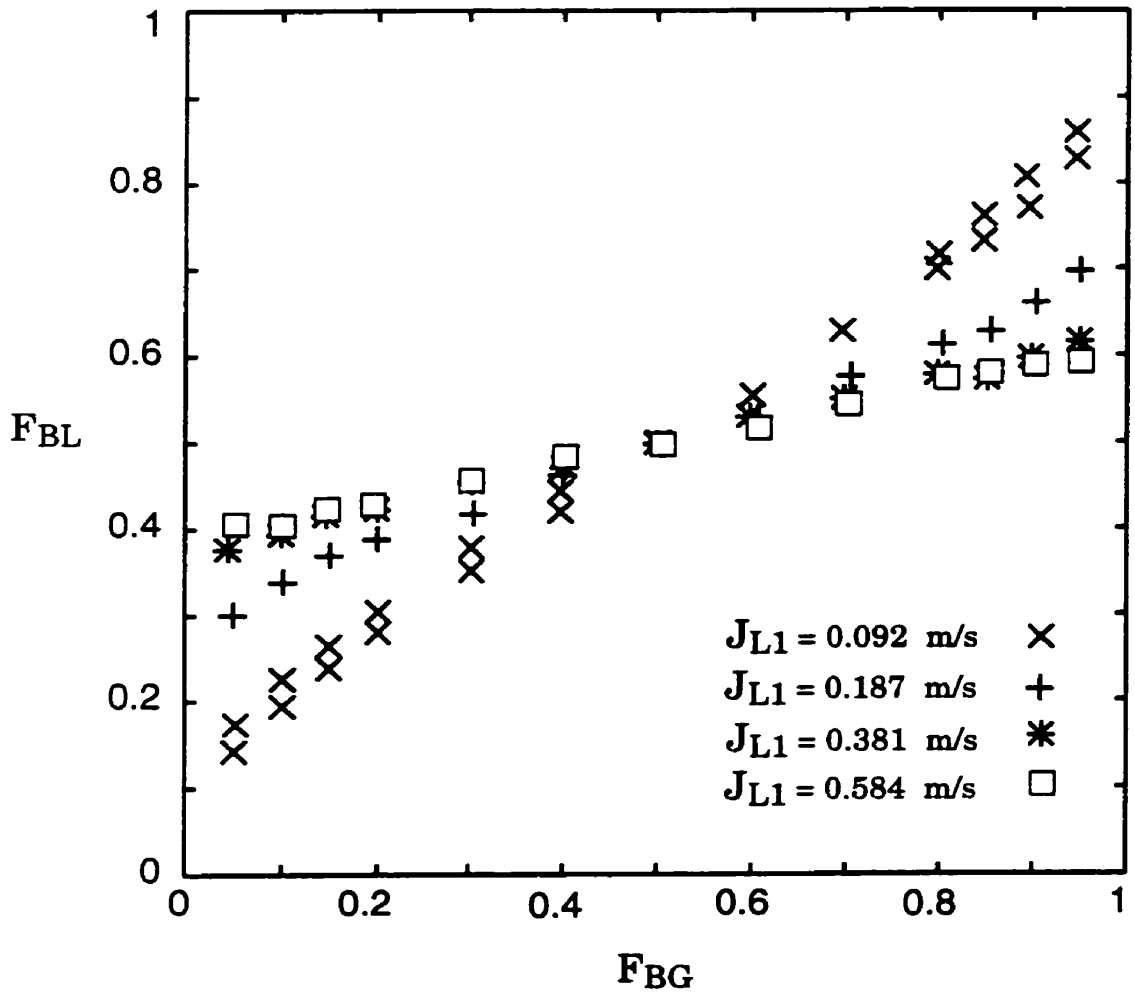

Figure 2.3 Effect of J_{L1} on the phase distribution in the data of Hong and Griston (1995) for J_{G1} = 9.14 m/s.

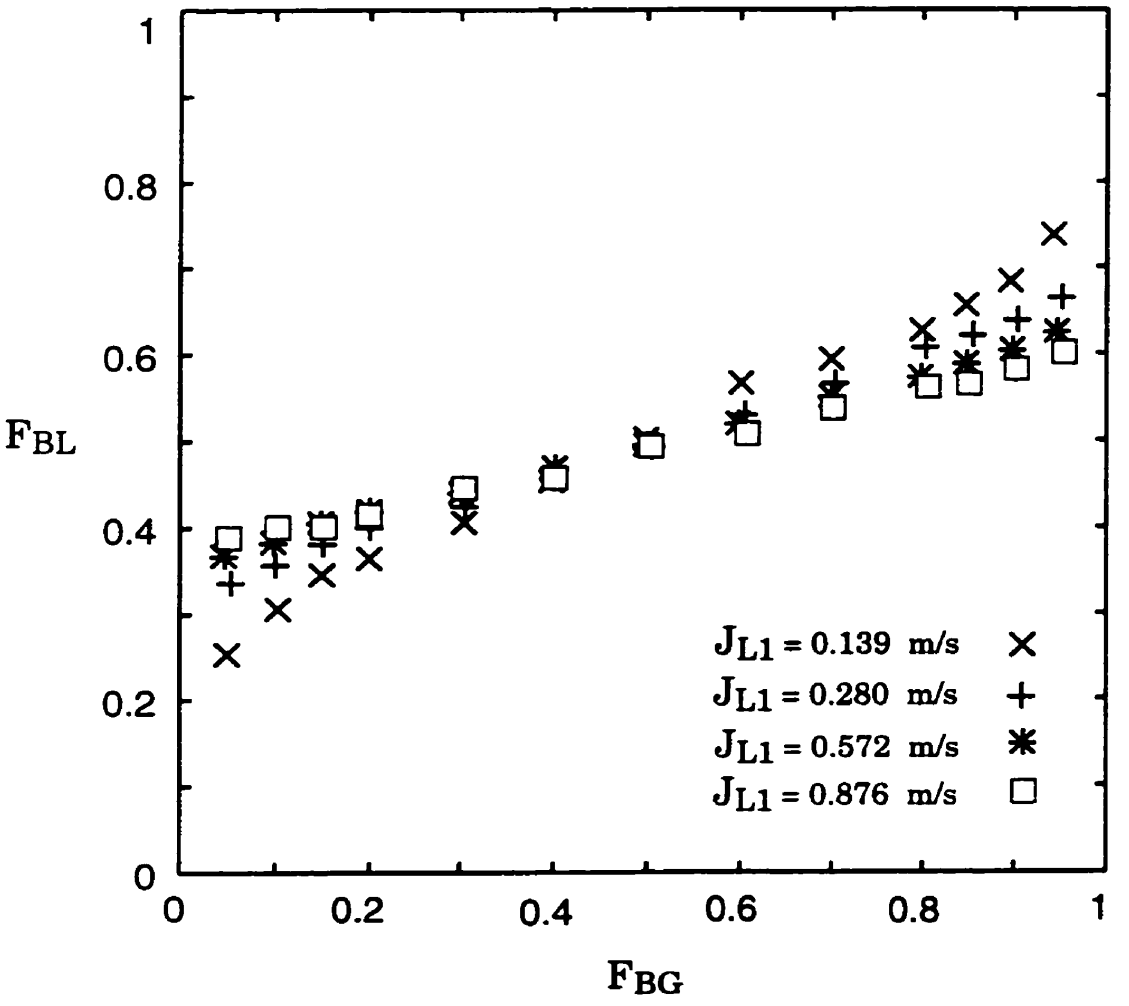

Figure 2.4 Effect of J_{L1} on the phase distribution in the data of Hong and Griston (1995) for J_{G1} = 13.7 m/s.

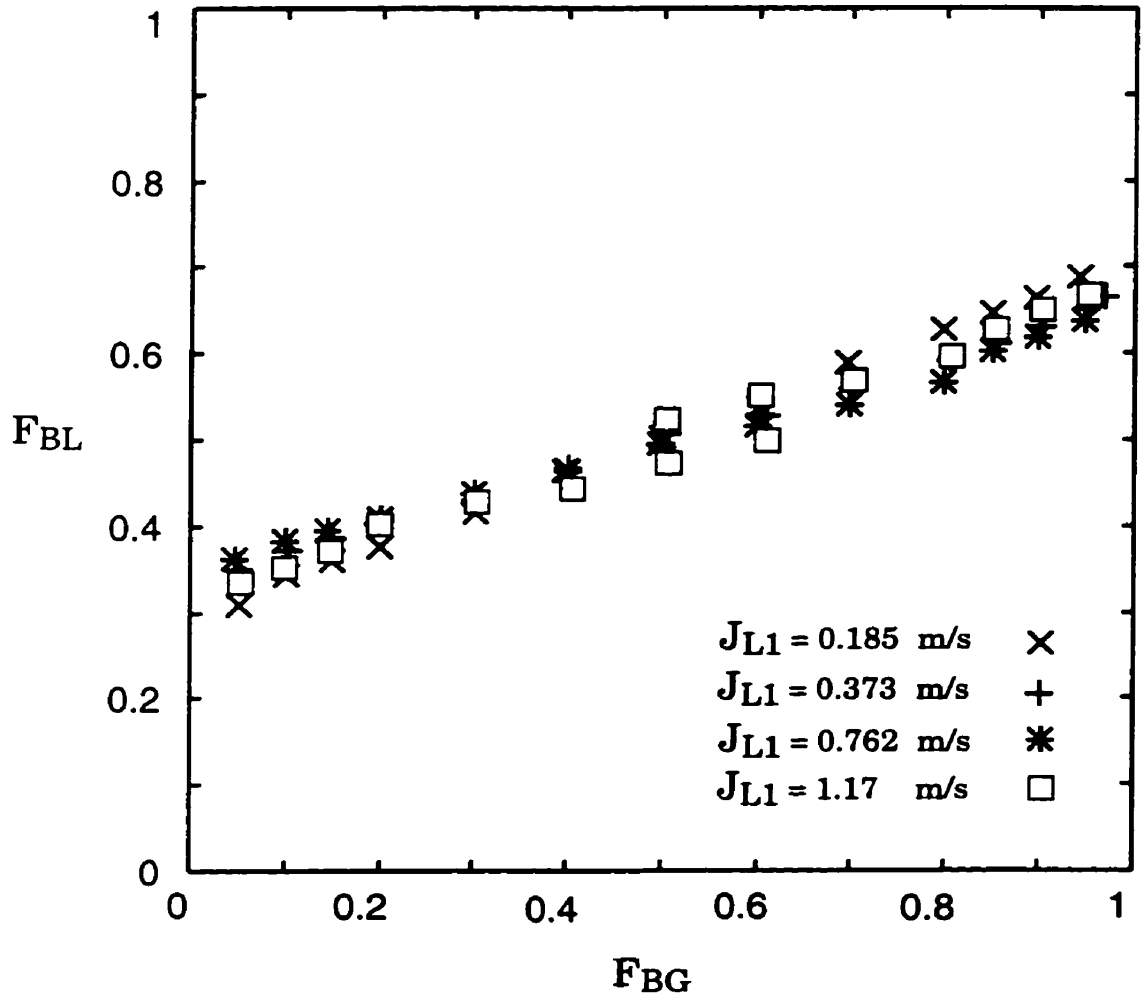

Figure 2.5 Effect of J_{L1} on the phase distribution in the data of Hong and Griston (1995) for J_{G1} = 18.3 m/s.

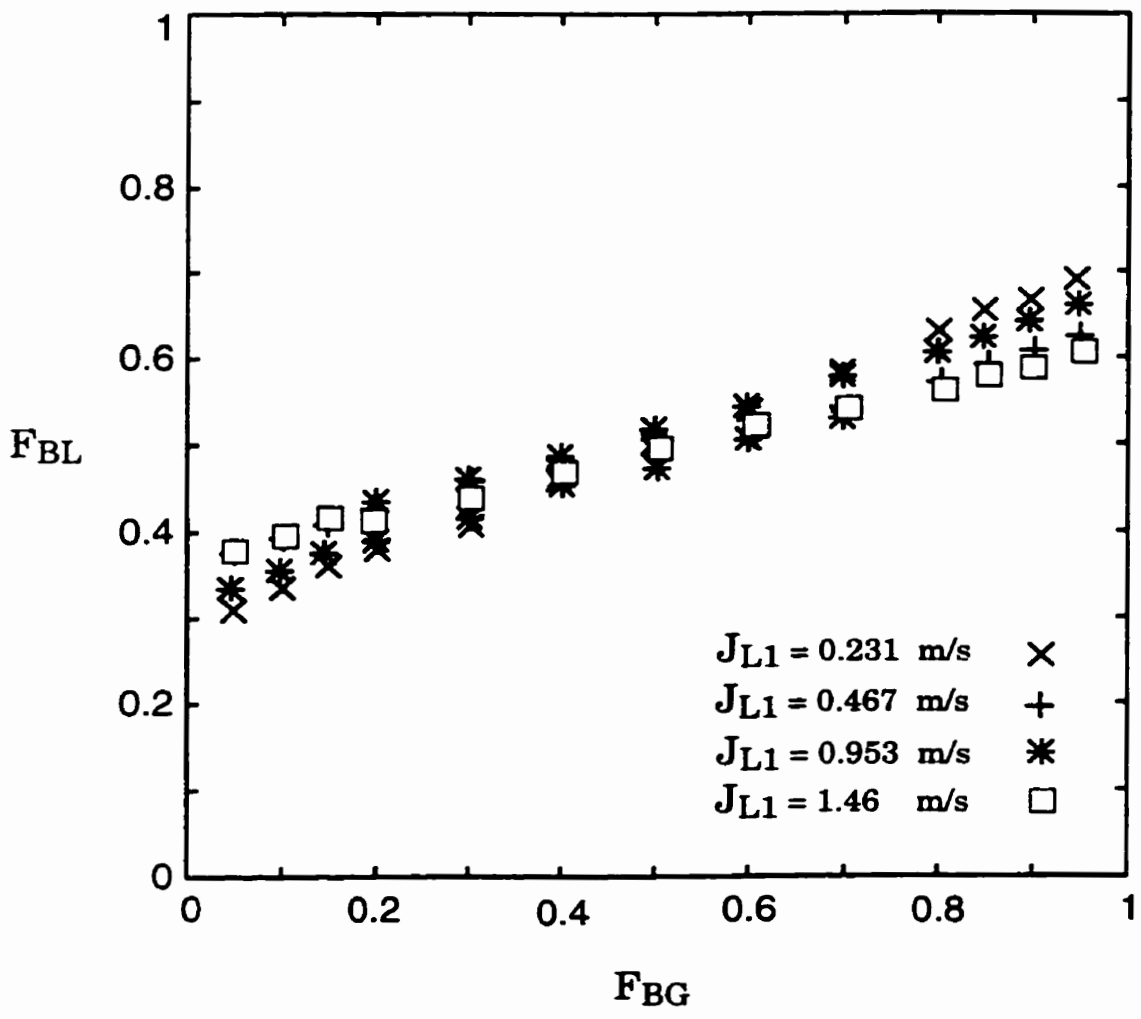

Figure 2.6 Effect of J_{L1} on the phase distribution in the data of Hong and Griston (1995) for J_{G1} = 22.9 m/s.

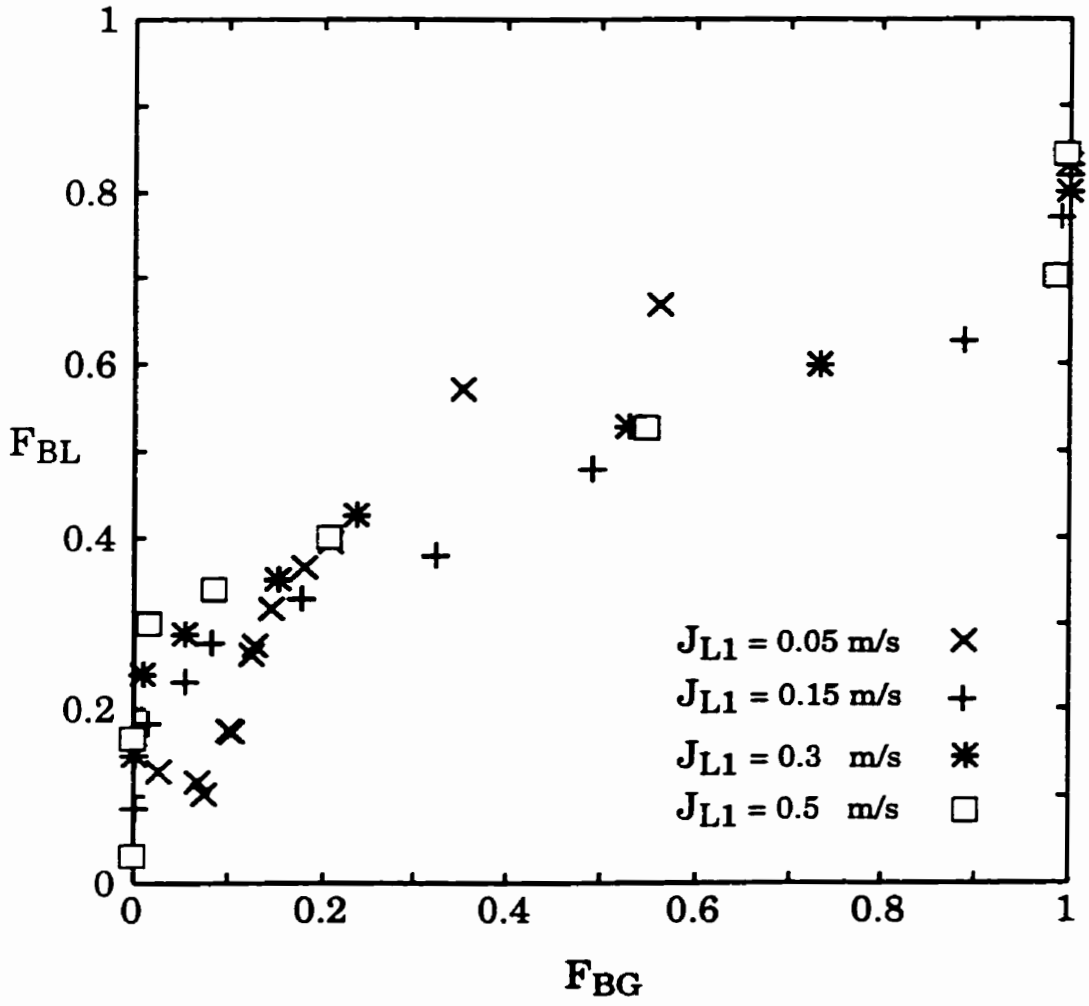

Figure 2.7 **Effect of J_{L1} on the phase distribution in the data of Fujii et al. (1995) for J_{G1} = 12.0 m/s and annular flow.**

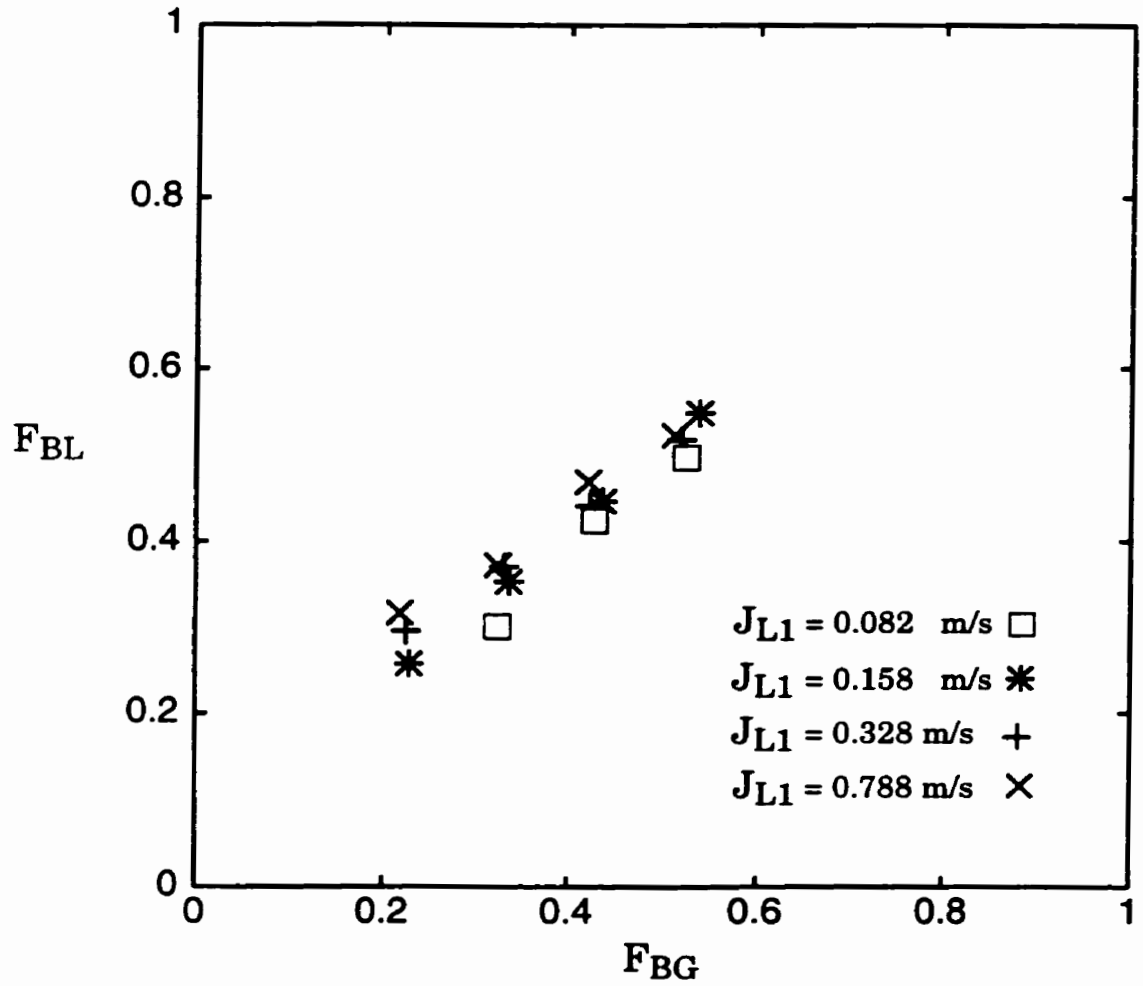

Figure 2.8 Effect of J_{L1} on the phase distribution in the data of Chien and Rubel (1992) for J_{G1} = 12.2 m/s and annular flow.

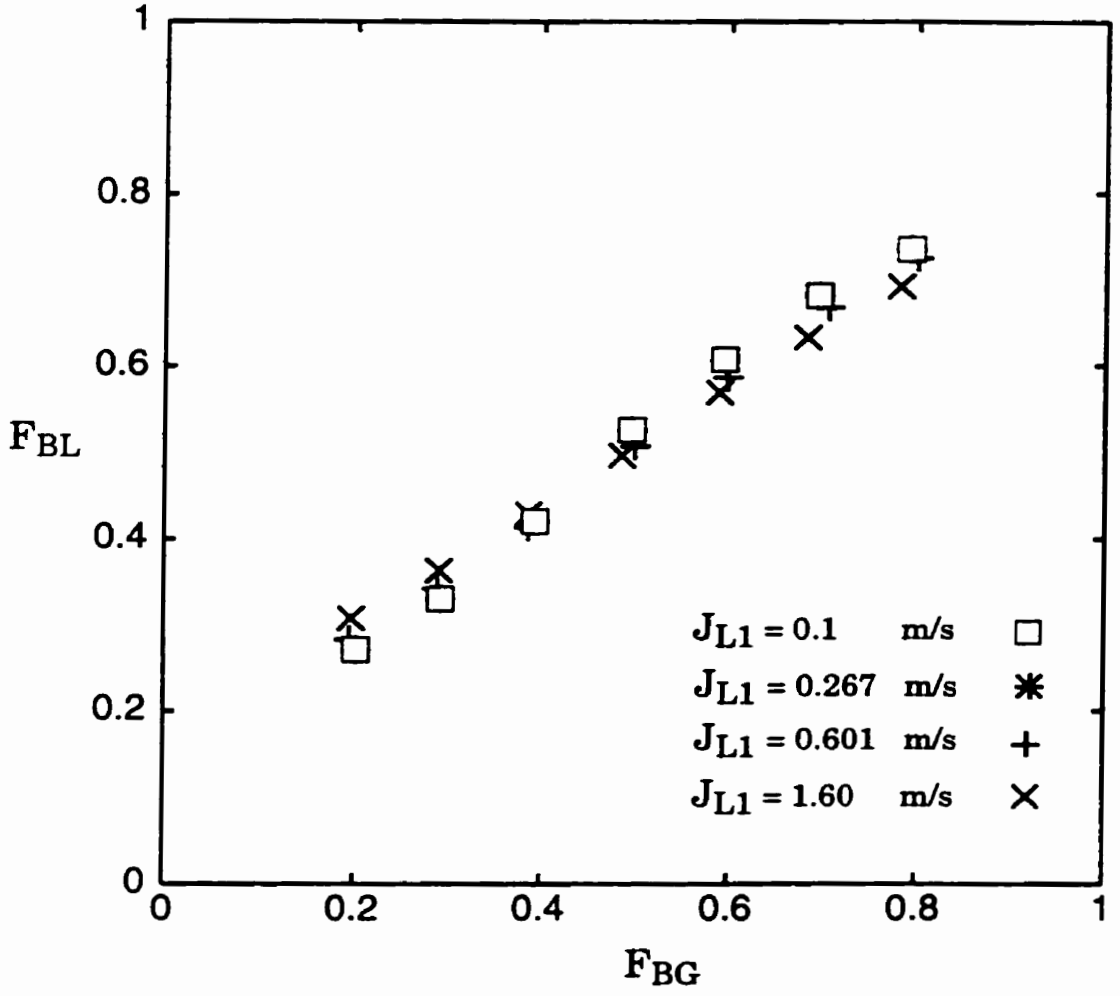

Figure 2.9 Effect of J_{L1} on the phase distribution in the data of Chien and Rubel (1992) for J_{G1} = 15.2 m/s and annular flow.

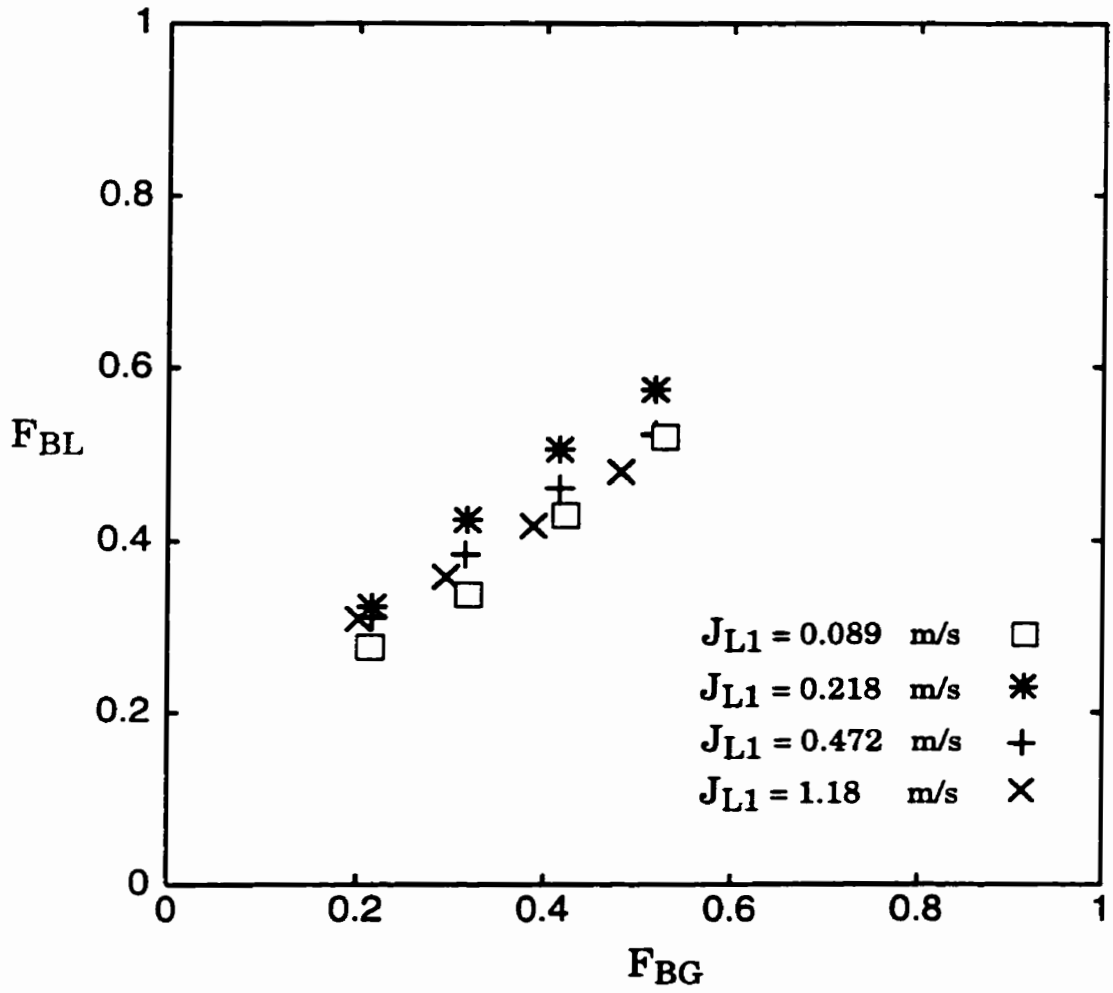

Figure 2.10 Effect of J_{L1} on the phase distribution in the data of Chien and Rubel (1992) for J_{G1} = 18.3 m/s and annular flow.

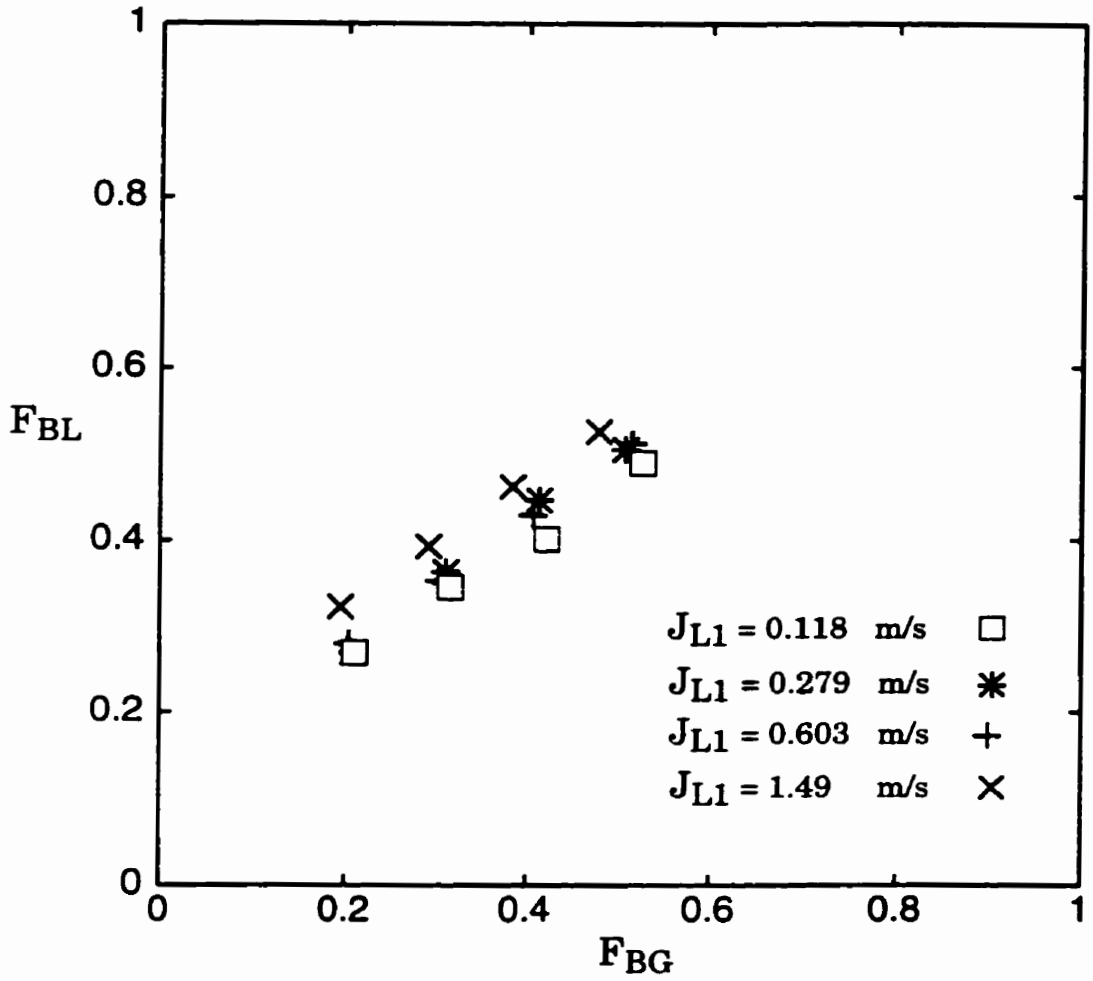

Figure 2.11 Effect of J_{L1} on the phase distribution in the data of Chien and Rubel (1992) for J_{G1} = 24.4 m/s and annular flow.

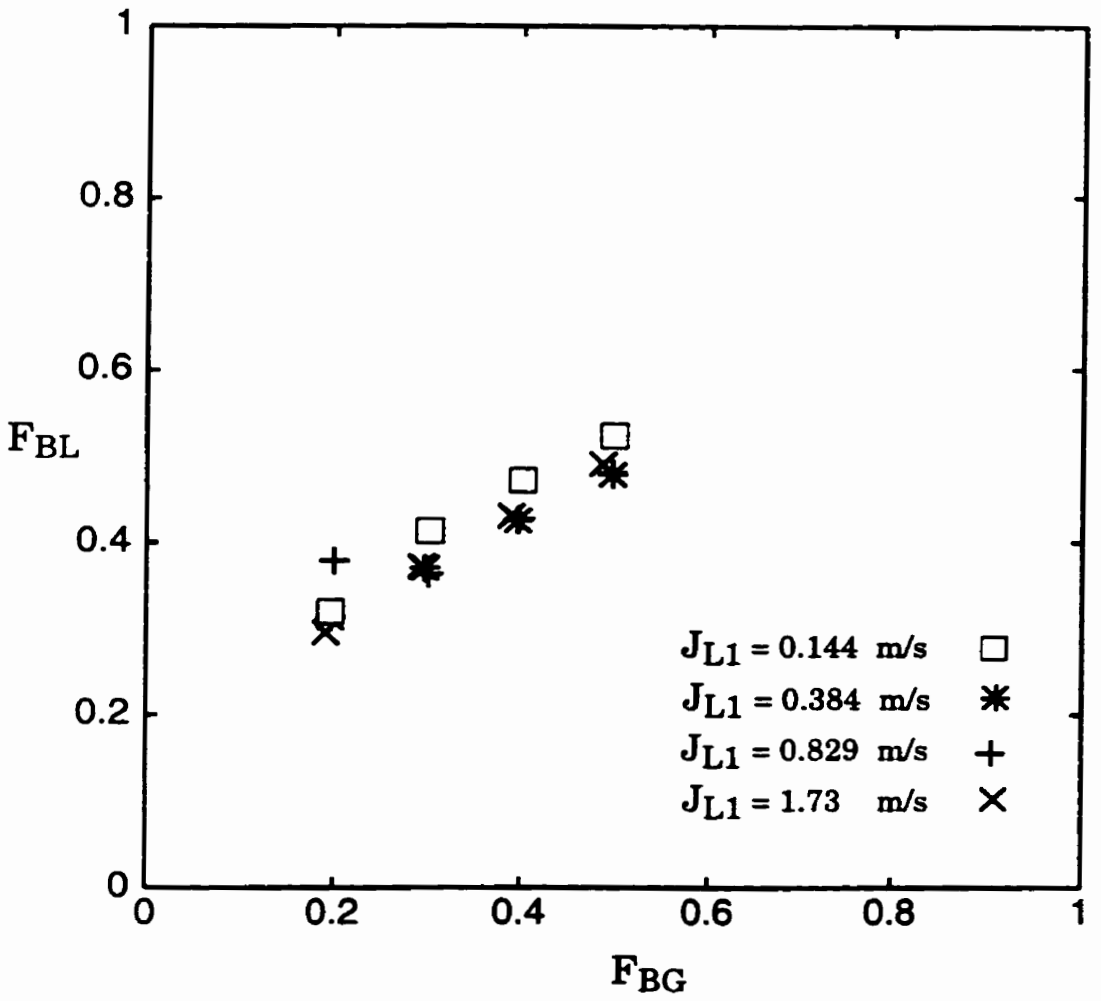

Figure 2.12 Effect of J_{L1} on the phase distribution in the data of Chien and Rubel (1992) for J_{G1} = 33.5 m/s and annular flow.

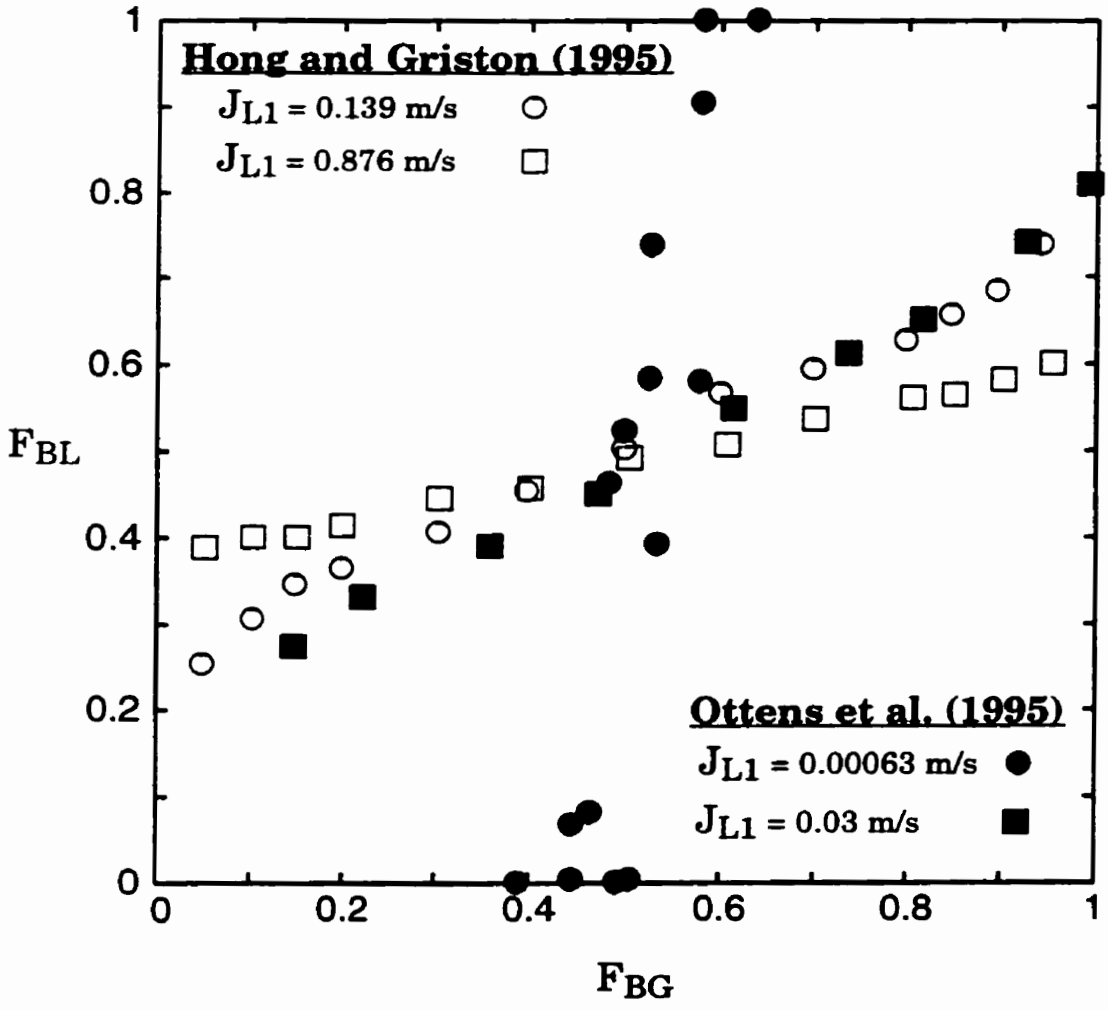

Figure 2.13 Effect of J_{L1} on the phase distribution in the data of Ottens et al. (1995) for J_{G1} =15.8 m/s and the data of Hong and Griston (1995) for J_{G1} = 13.7 m/s.

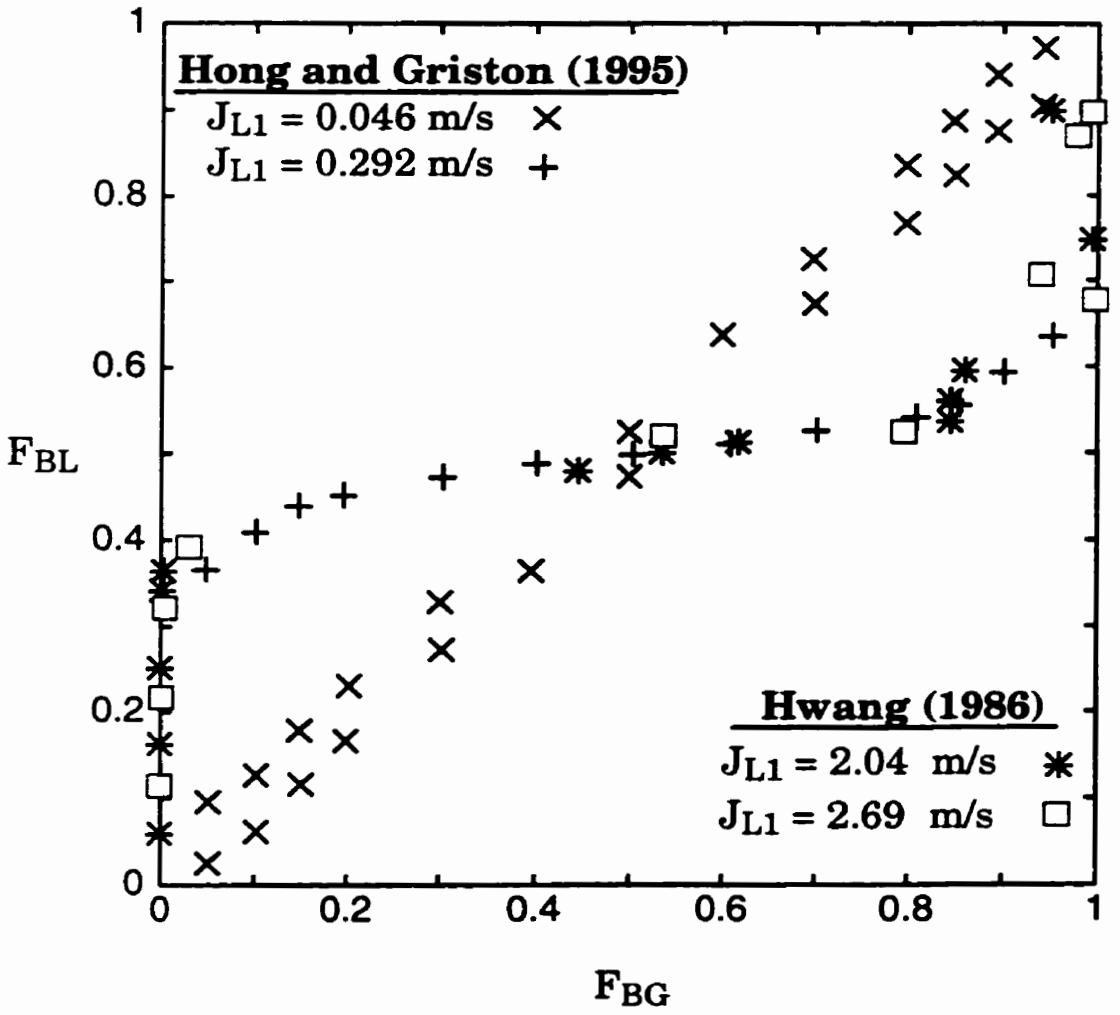

Figure 2.14 Effect of J_{L1} on the phase distribution in the data of Hong and Griston (1995) for J_{G1} = 4.57 m/s, and the data of Hwang (1986) for a nominal J_{G1}=4.75 m/s.

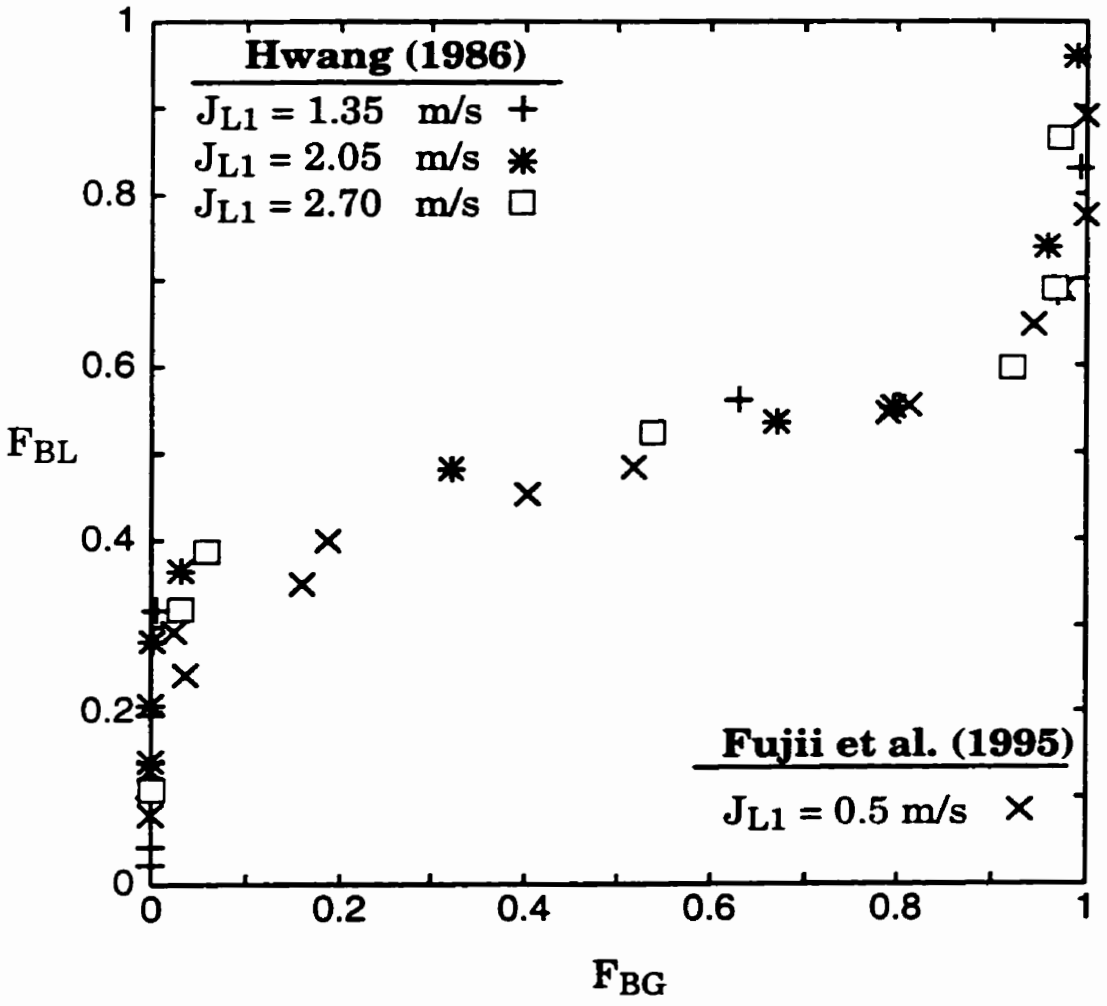

Figure 2.15 Effect of J_{L1} on the phase distribution in the data of Hwang (1986) for a nominal J_{G1} = 2.42 m/s, and the data of Fujii et al. (1995) for J_{G1}=2.34 m/s.

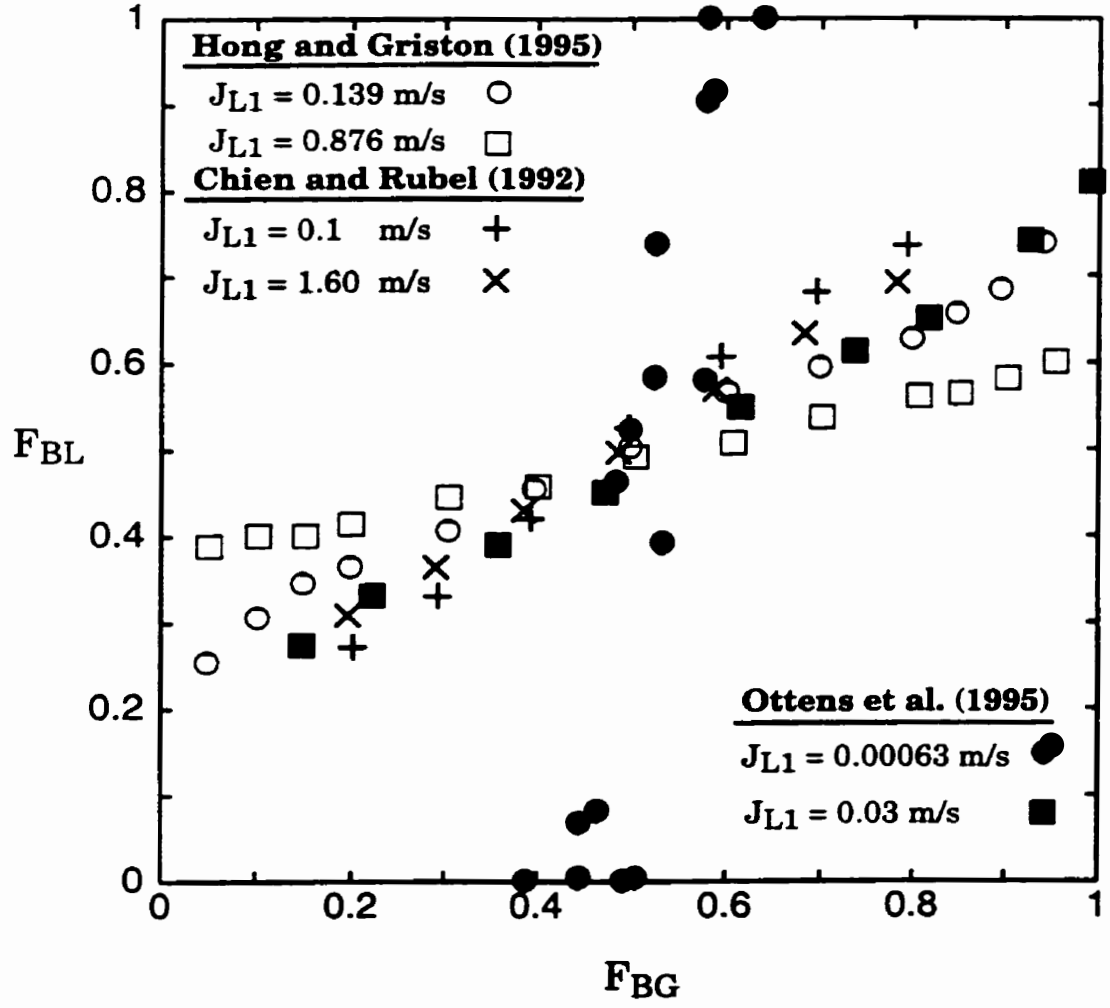

Figure 2.16 Effect of J_{L1} on the phase distribution in the data of Ottens et al. (1995) for J_{G1} =15.8 m/s, Hong and Griston (1995) for J_{G1} = 13.7 m/s, and Chien and Rubel (1992) for J_{G1}=15.2 m/s.

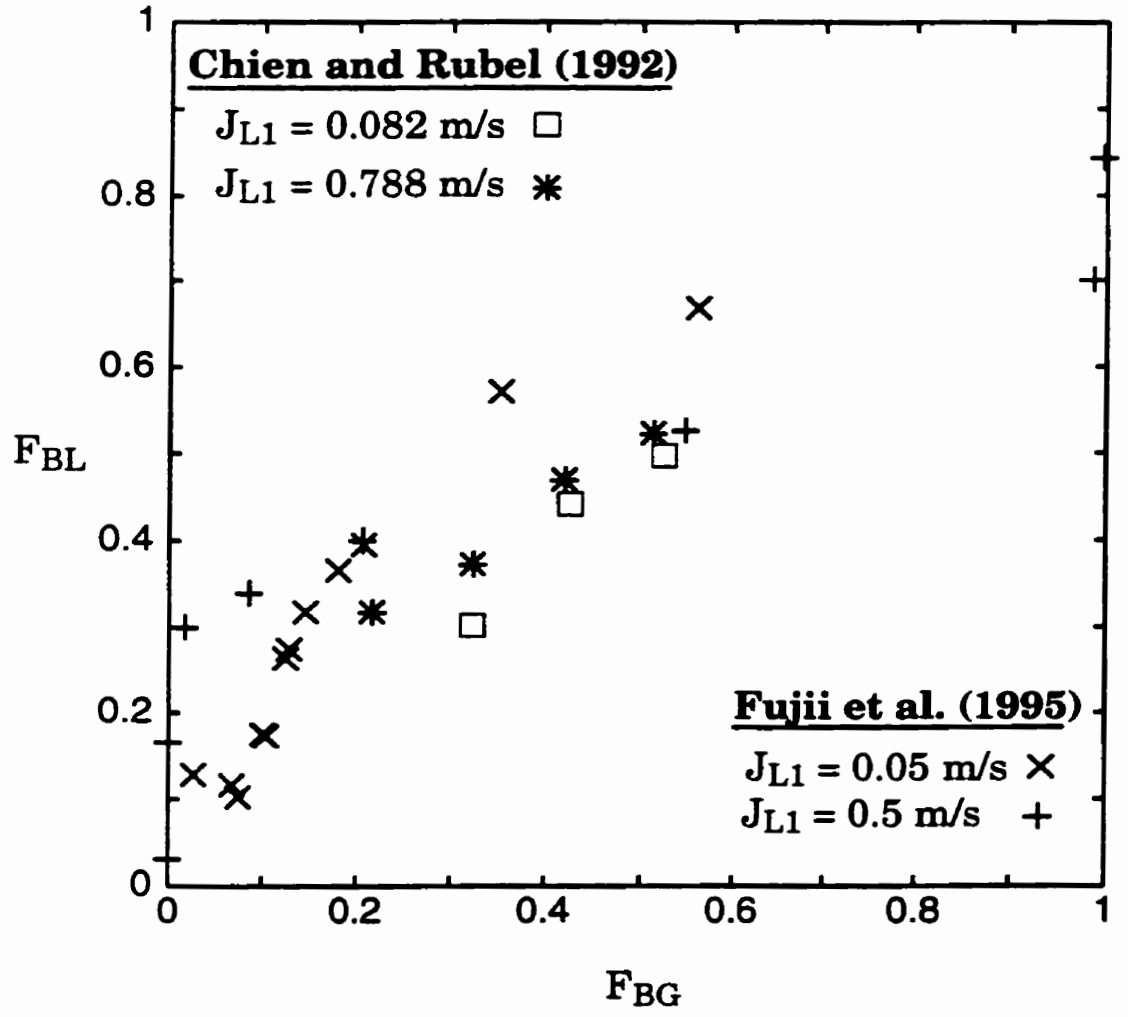

Figure 2.17 Effect of J_{L1} on the phase distribution in the data of Fujii et al. (1995) for J_{G1} =12.0 m/s, and the data of Chien and Rubel (1992) for J_{G1} = 12.2 m/s.

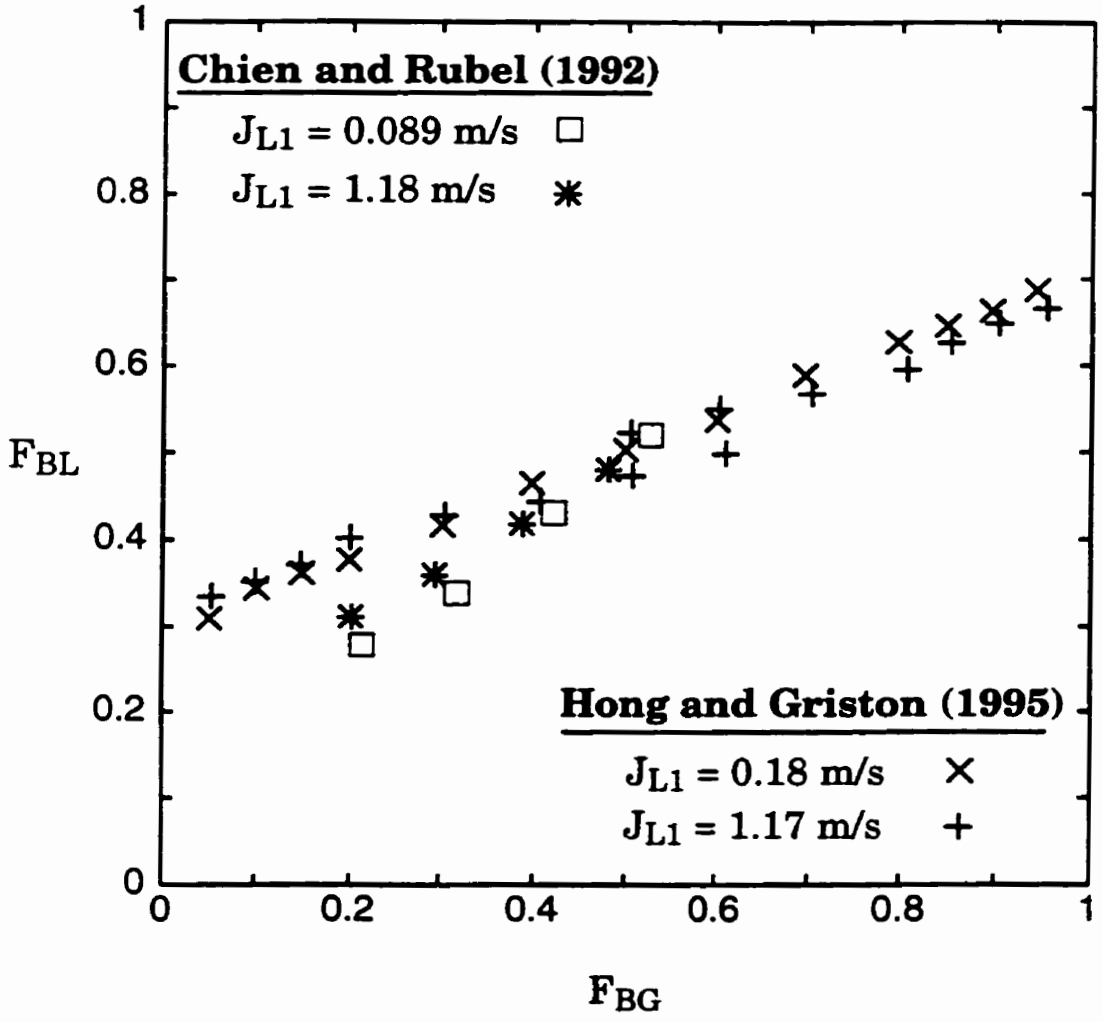

Figure 2.18 Effect of J_{L1} on the phase distribution in the data of Hong and Griston (1995) for J_{G1} = 18.3 m/s, and the data of Chien and Rubel (1992) for J_{G1} = 18.3 m/s.

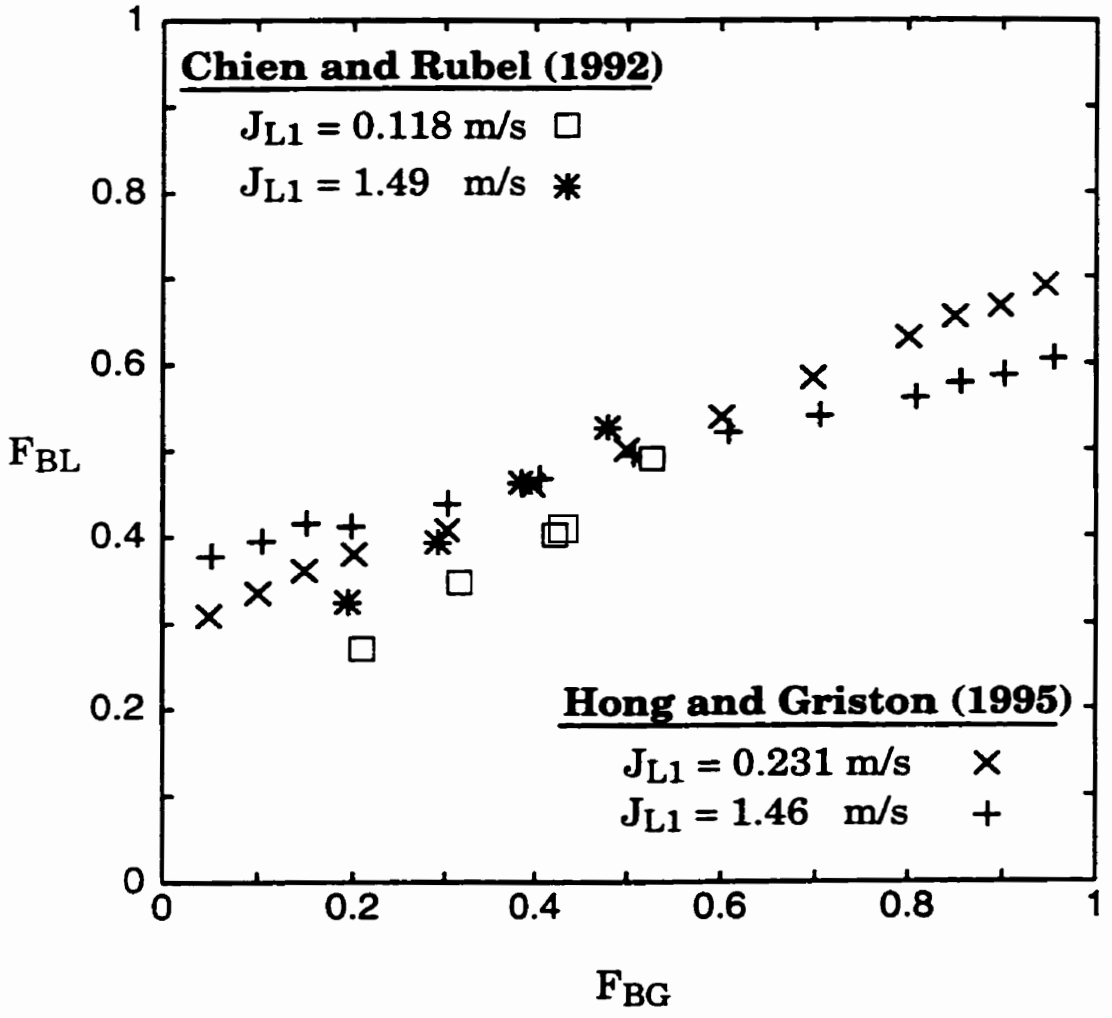

Figure 2.19 Effect of J_{L1} on the phase distribution in the data of Hong and Griston (1995) for J_{G1} =22.9 m/s, and the data of Chien and Rubel (1992) for J_{G1} = 24.4 m/s.

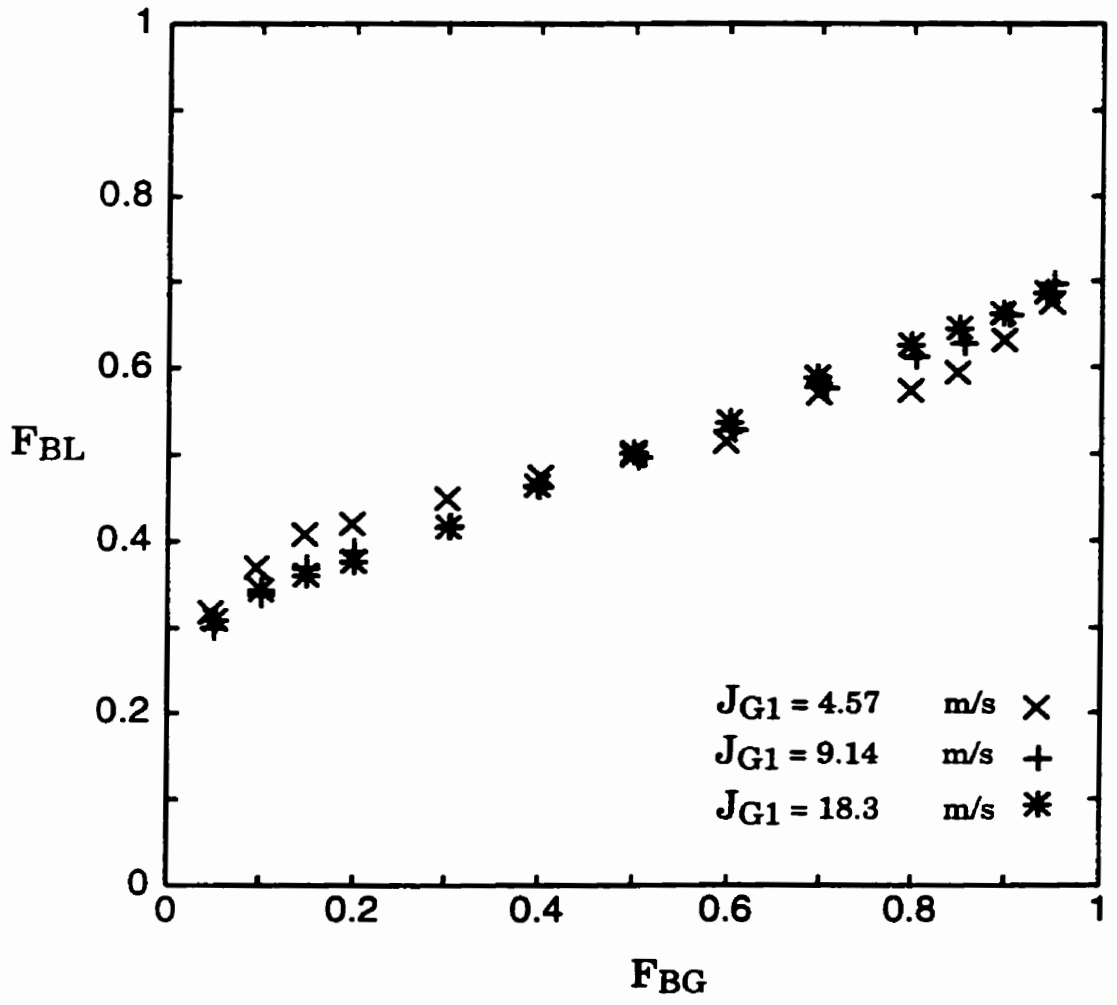

Figure 2.20 Effect of J_{G1} on the phase distribution in the data of Hong and Griston (1995) for a nominal J_{L1}=0.19 m/s.

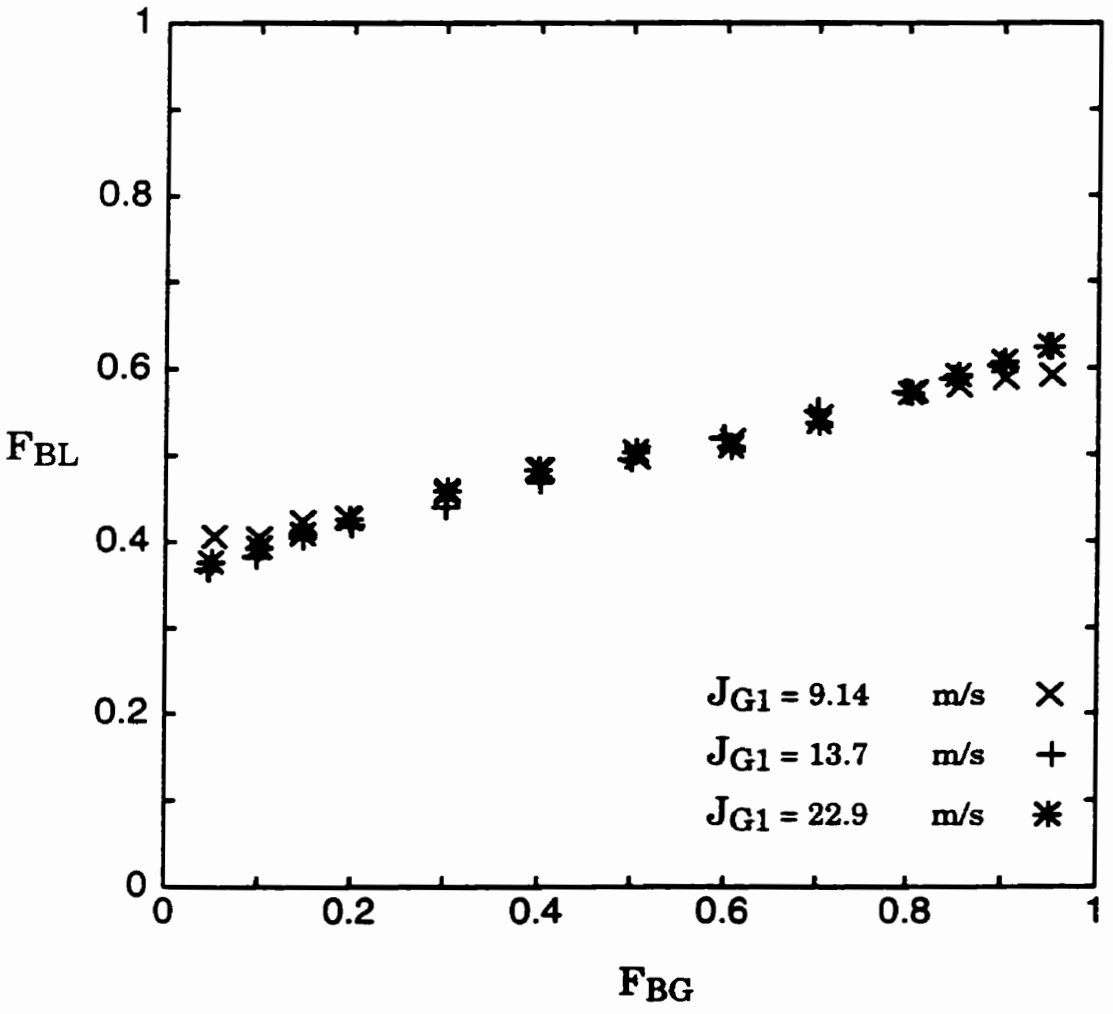

Figure 2.21 Effect of J_{G1} on the phase distribution in the data of Hong and Griston (1995) for a nominal J_{L1} =0.5 m/s.

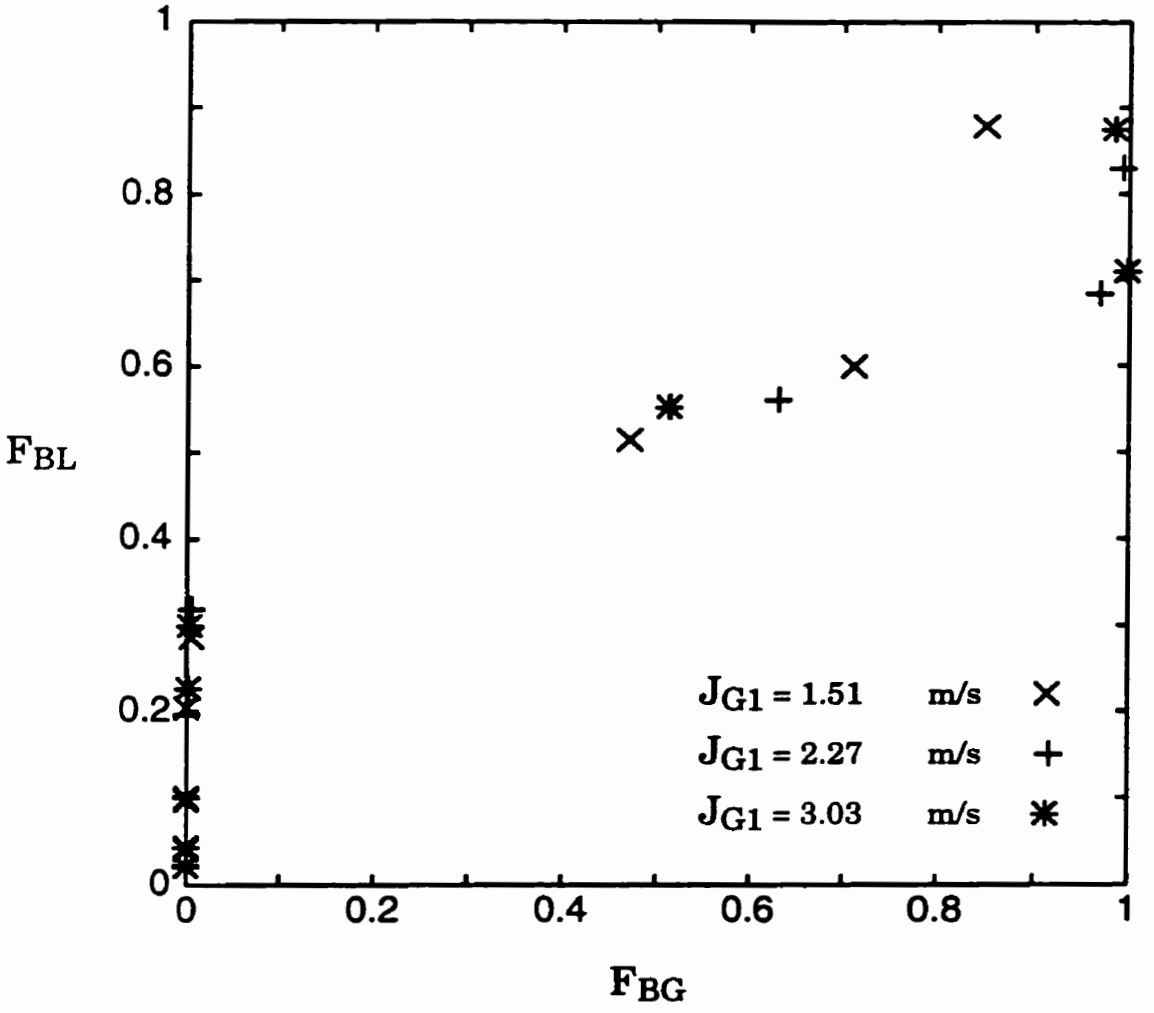

Figure 2.22 **Effect of J_{G1} on the phase distribution in the data of Hwang (1986) for a nominal J_{L1} = 1.35 m/s and bubbly flow.**

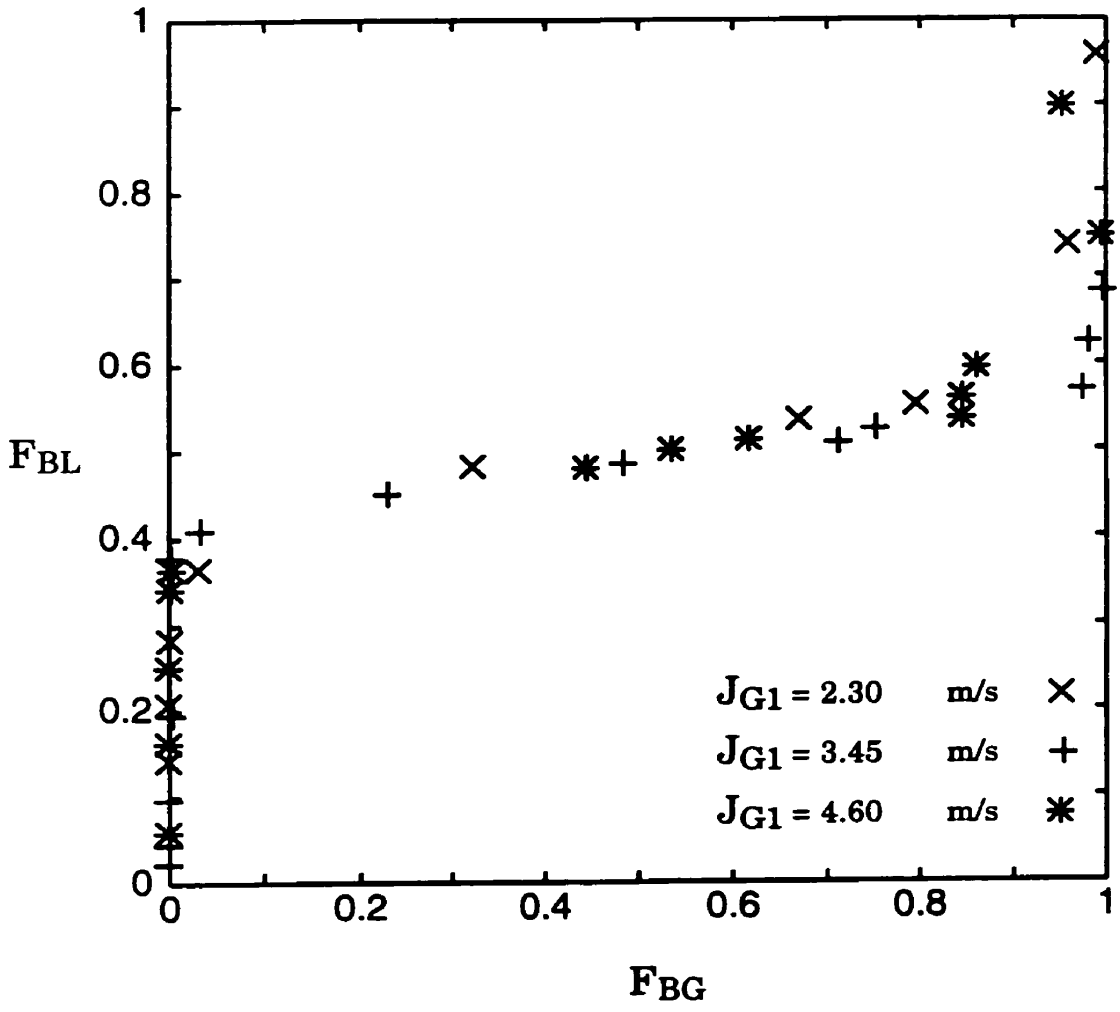

Figure 2.23 **Effect of J_{G1} on the phase distribution in the data of Hwang (1986) for a nominal J_{L1} = 2.04 m/s and bubbly flow.**

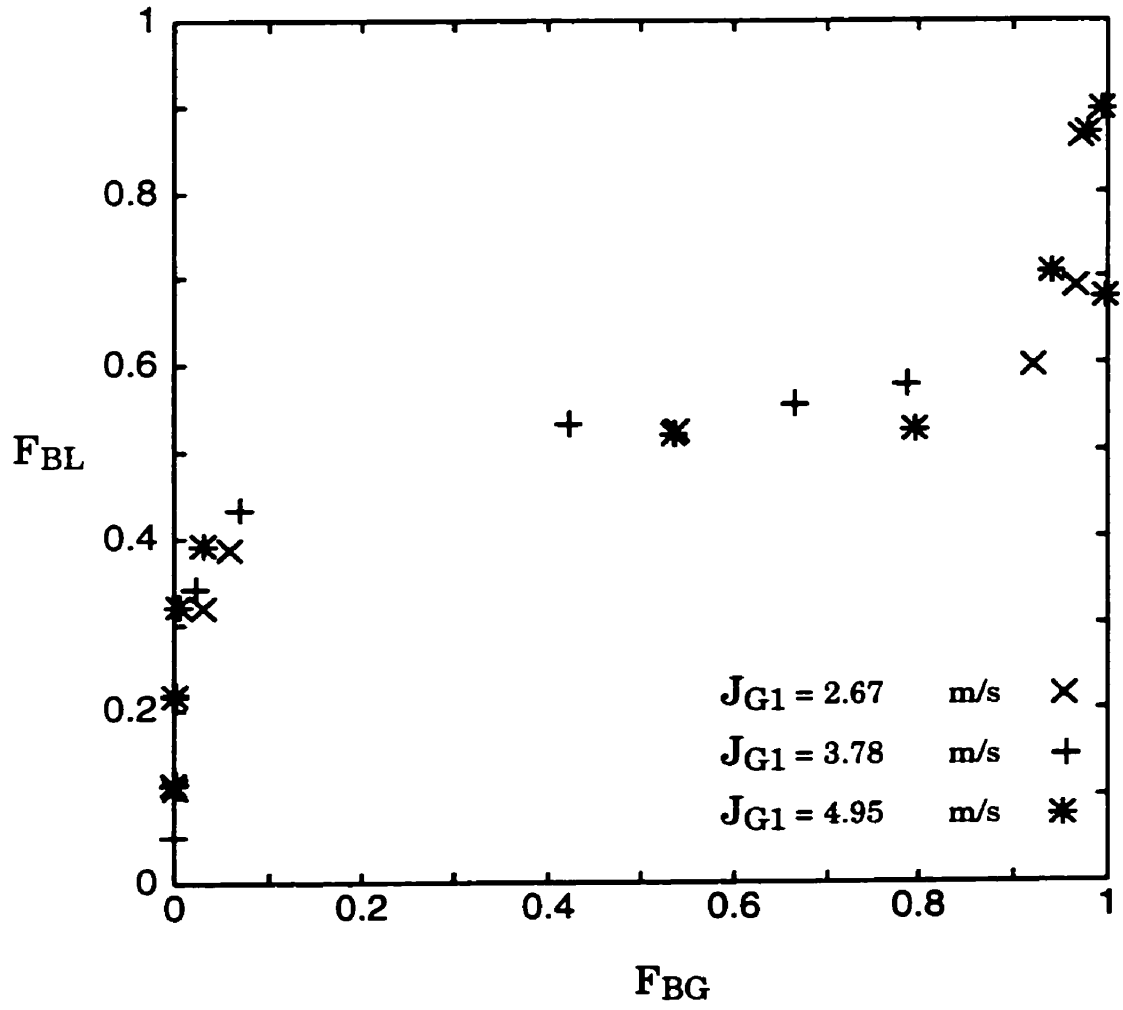

Figure 2.24 Effect of J_{G1} on the phase distribution in the data of Hwang (1986) for a nominal J_{L1} = 2.5 m/s and bubbly flow.

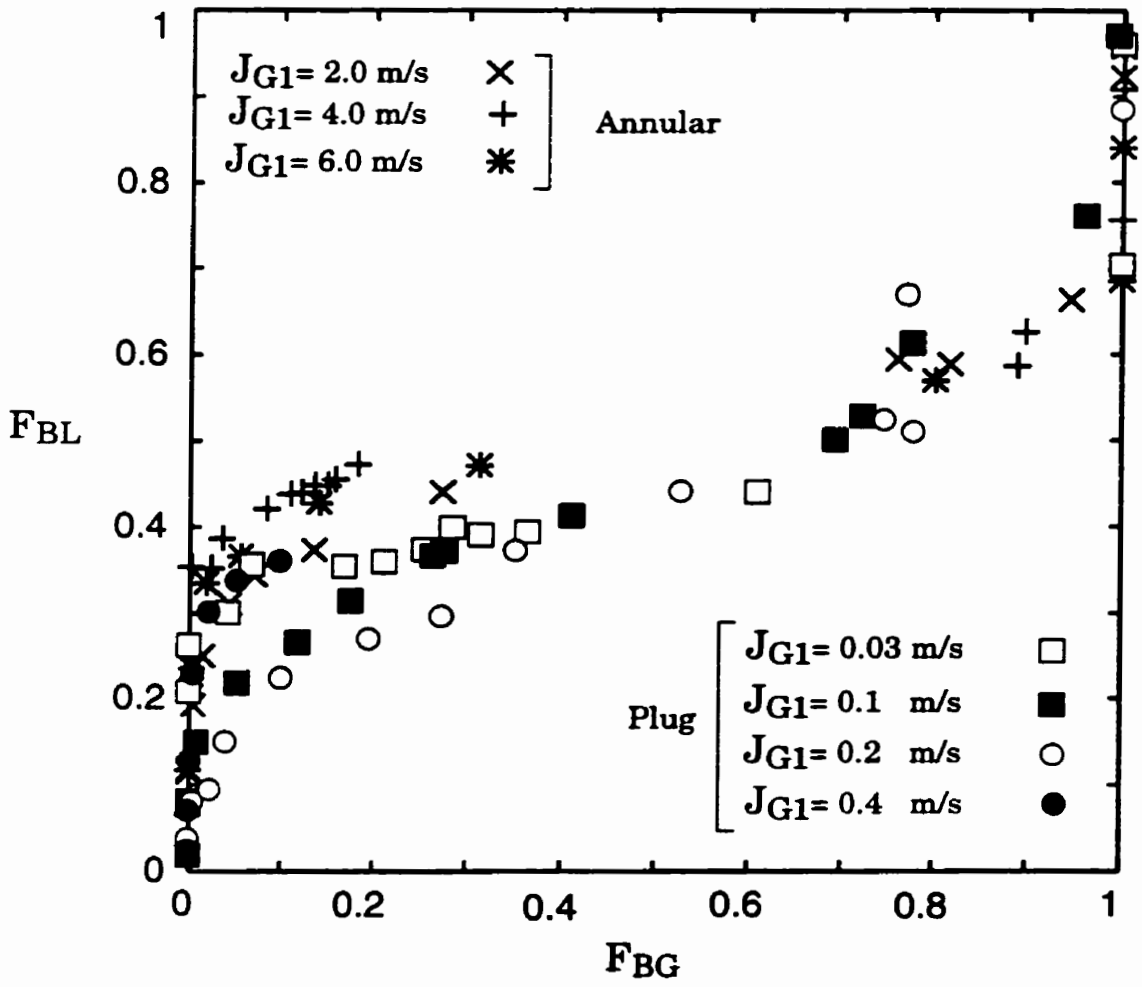

Figure 2.25 Effect of J_{G1} on the phase distribution in the data of Fujii et al. (1995) for J_{L1} = 0.2 m/s.

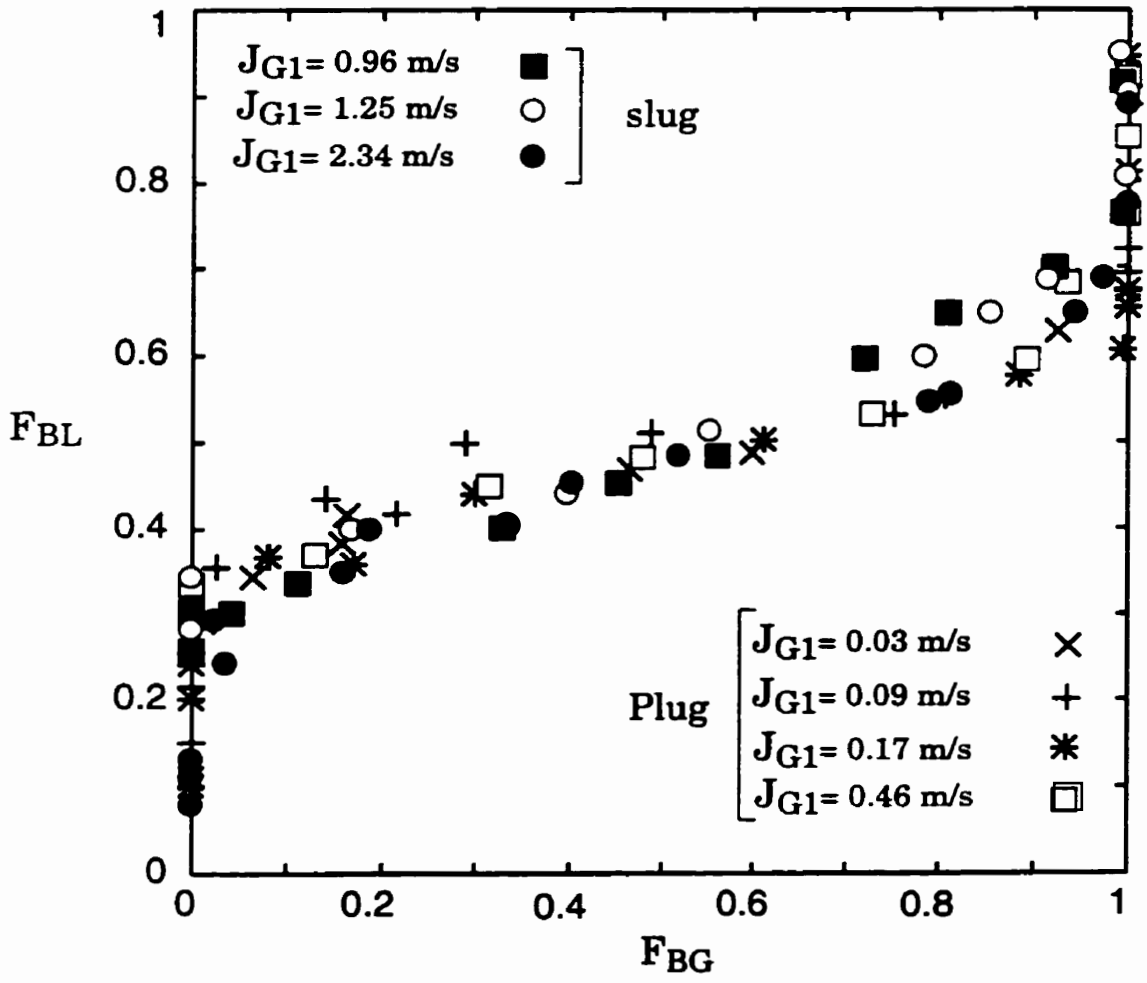

Figure 2.26 Effect of J_{G1} on the phase distribution in the data of Fujii et al. (1995) for J_{L1} = 0.5 m/s.

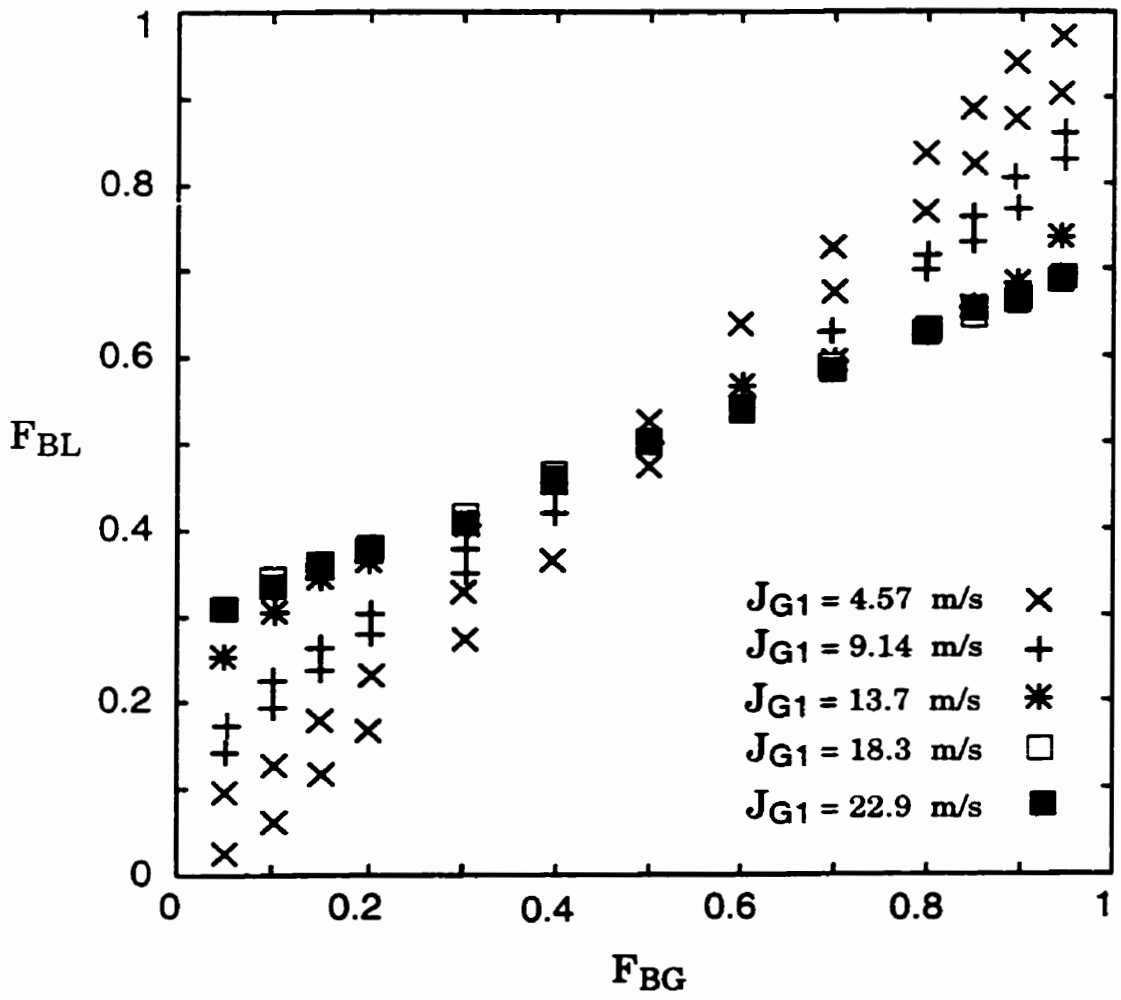

Figure 2.27 **Effect of J_{G1} on the phase distribution in the data of Hong and Griston (1995) for x_1= 0.105.**

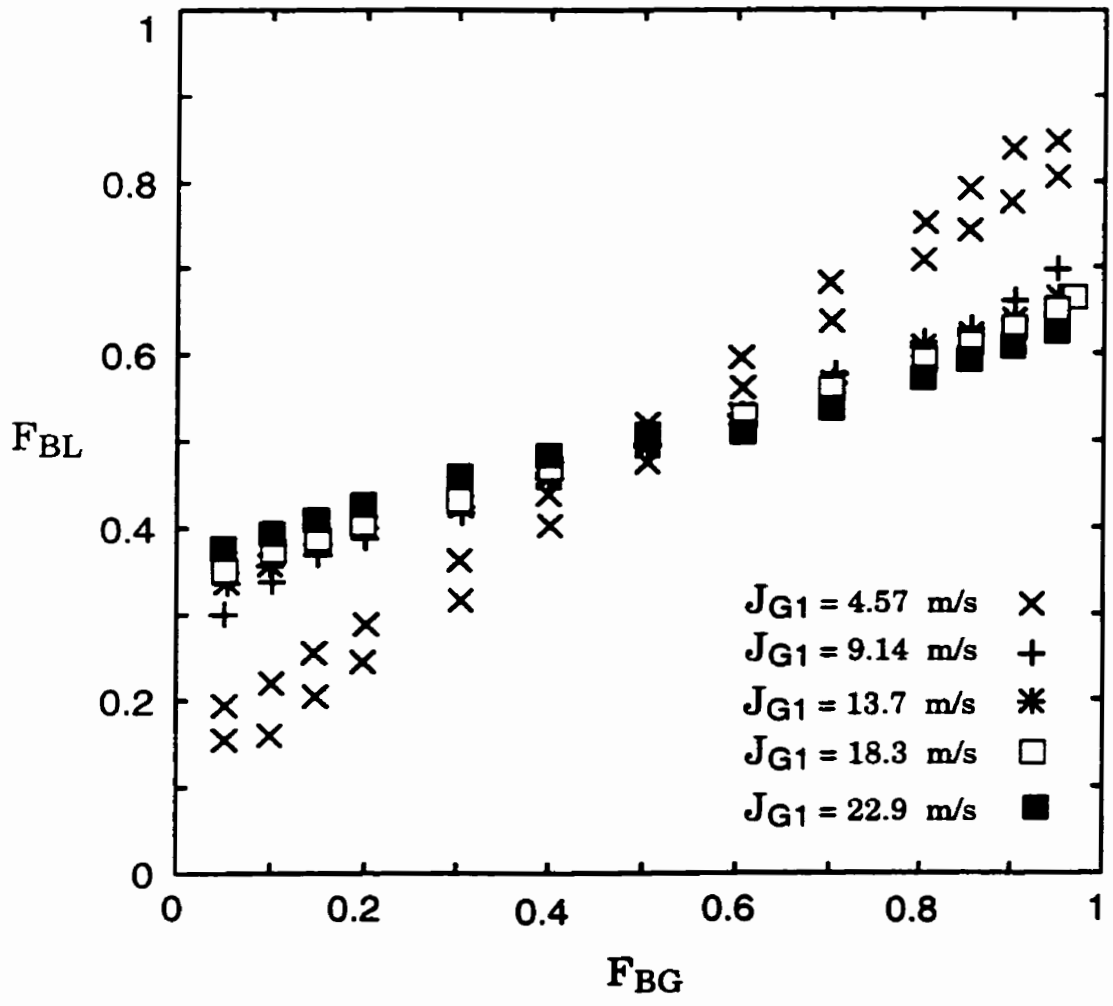

Figure 2.28 **Effect of J_{G1} on the phase distribution in the data of Hong and Griston (1995) for x_1= 0.055.**

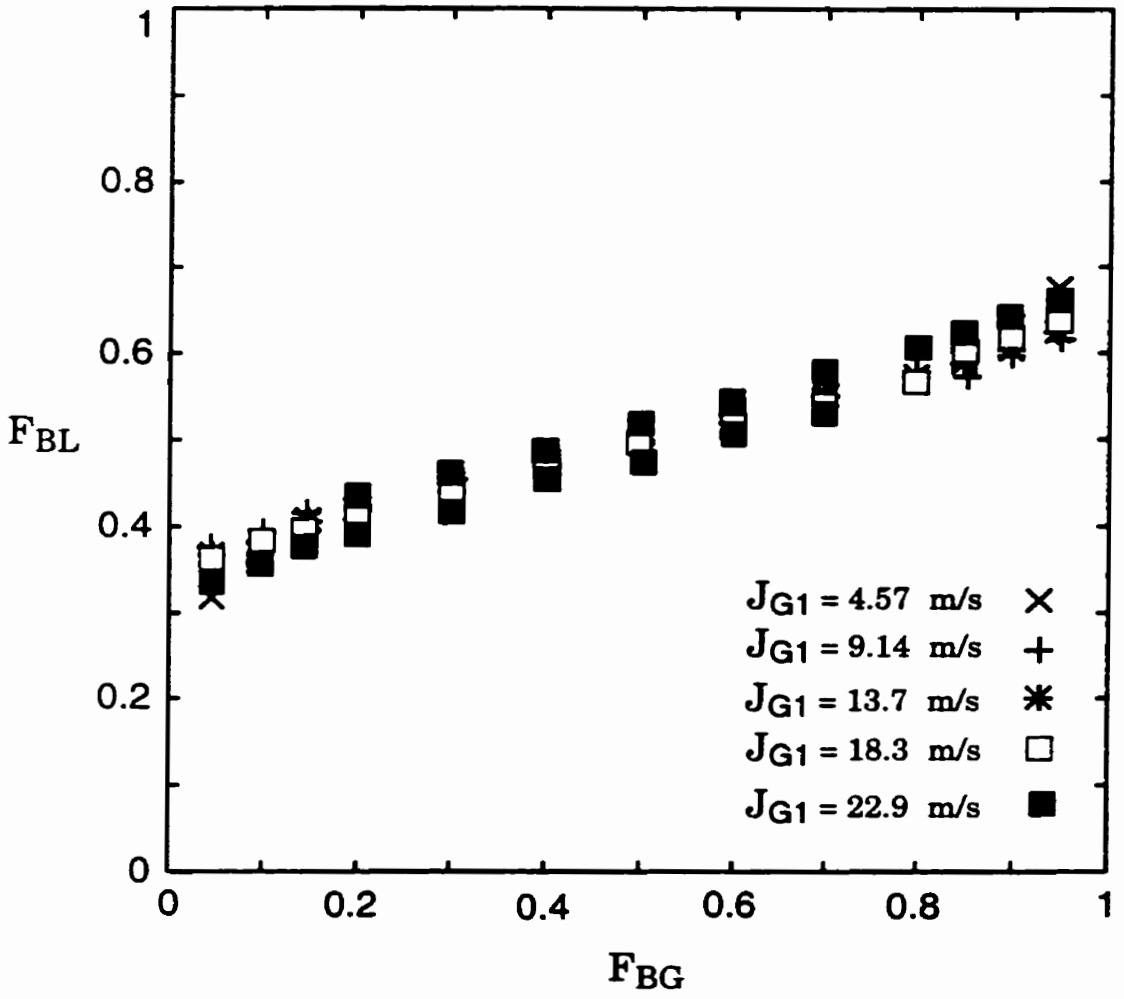

Figure 2.29 Effect of J_{G1} on the phase distribution in the data of Hong and Griston (1995) for x_1= 0.028.

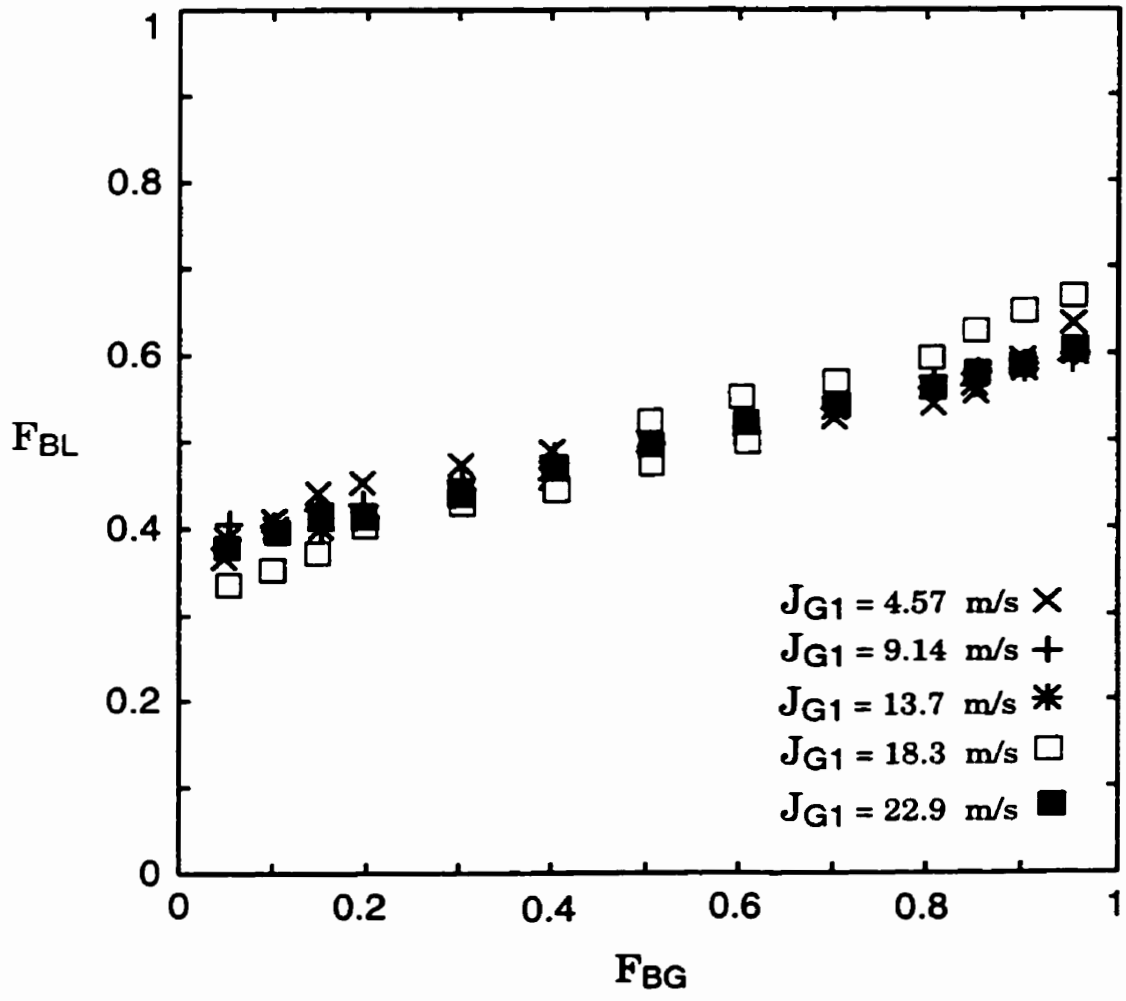

Figure 2.30 Effect of J_{G1} on the phase distribution in the data of Hong and Griston (1995) for x_1= 0.018.

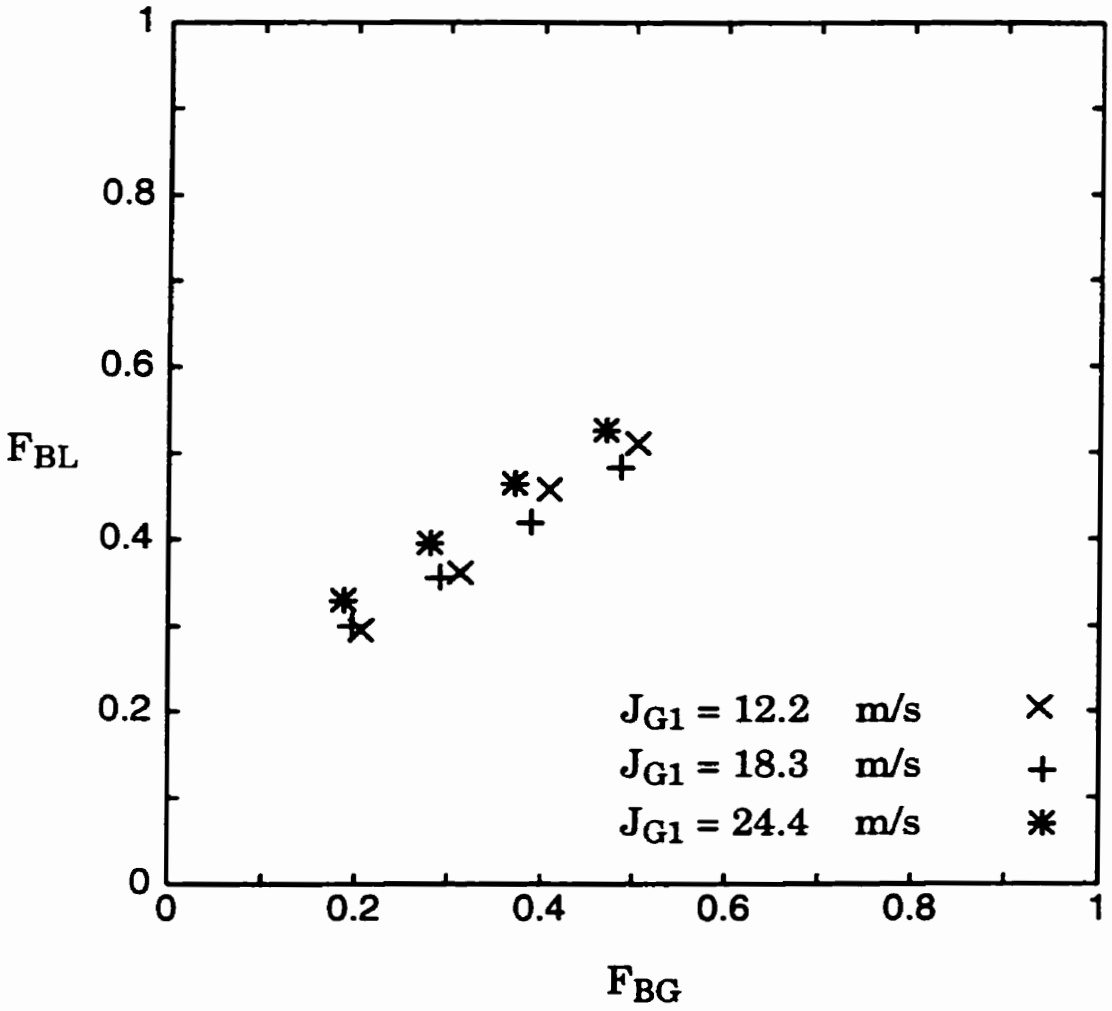

Figure 2.31 Effect of J_{G1} on the phase distribution in the data of Chien and Rubel (1992) for a nominal x_1=0.2.

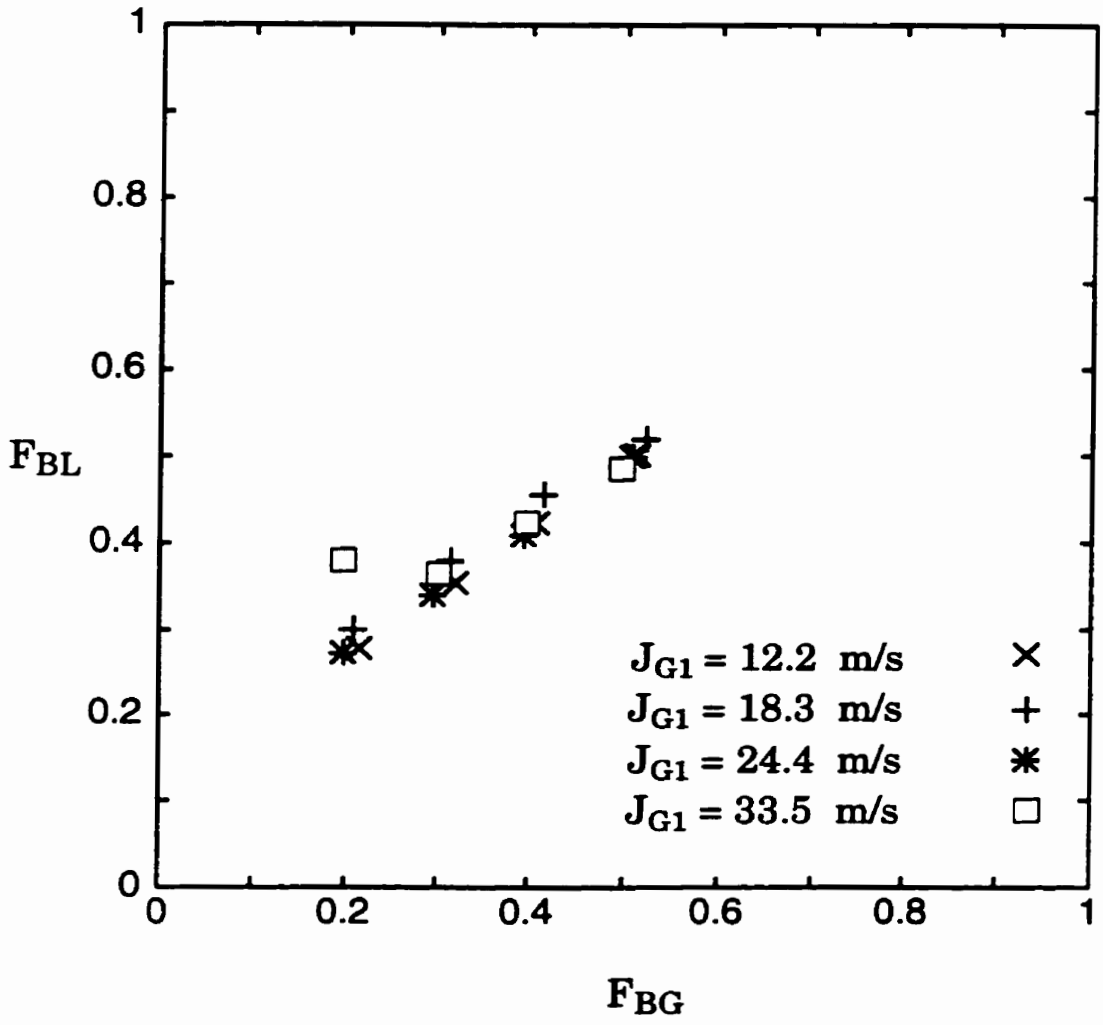

Figure 2.32 Effect of J_{G1} on the phase distribution in the data of Chien and Rubel (1992) for a nominal x_1=0.4.

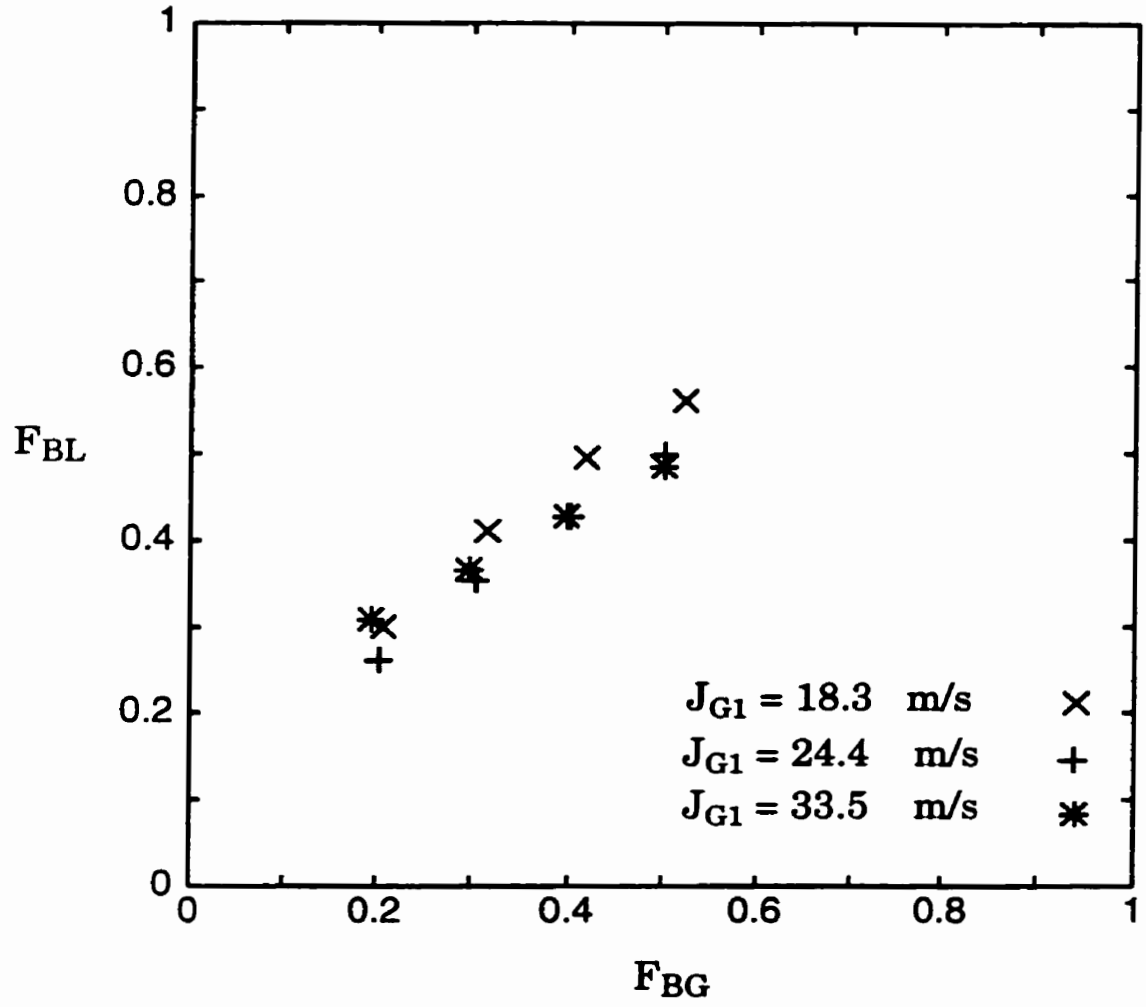

Figure 2.33 Effect of J_{G1} on the phase distribution in the data of Chien and Rubel (1992) for a nominal x_1=0.6.

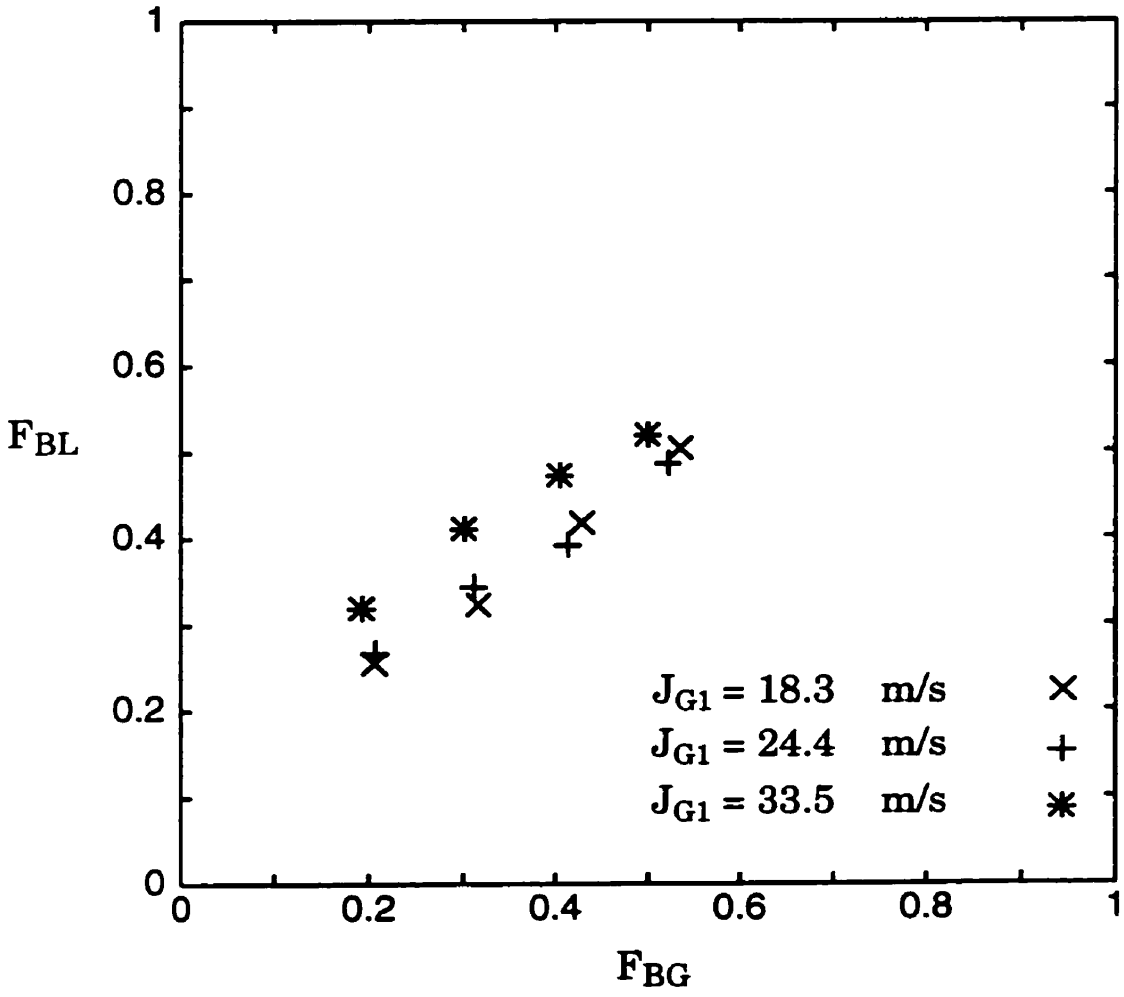

Figure 2.34 **Effect of J_{G1} on the phase distribution in the data of Chien and Rubel (1992) for a nominal x_1=0.8.**

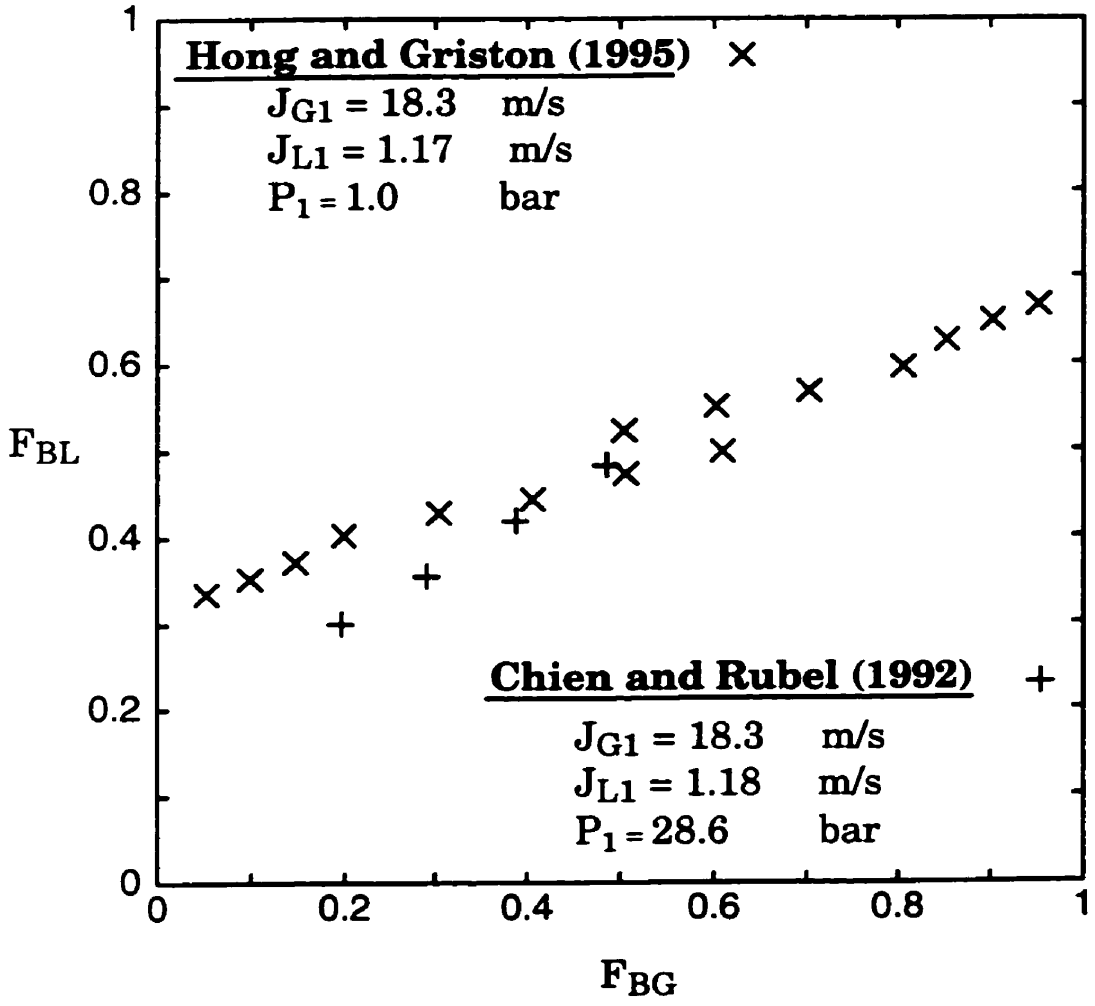

Figure 2.35 Effect of inlet pressure on the phase distribution in the data of Hong and Griston (1995) and the data of Chien and Rubel (1992) at P_1 = 28.6 bar.

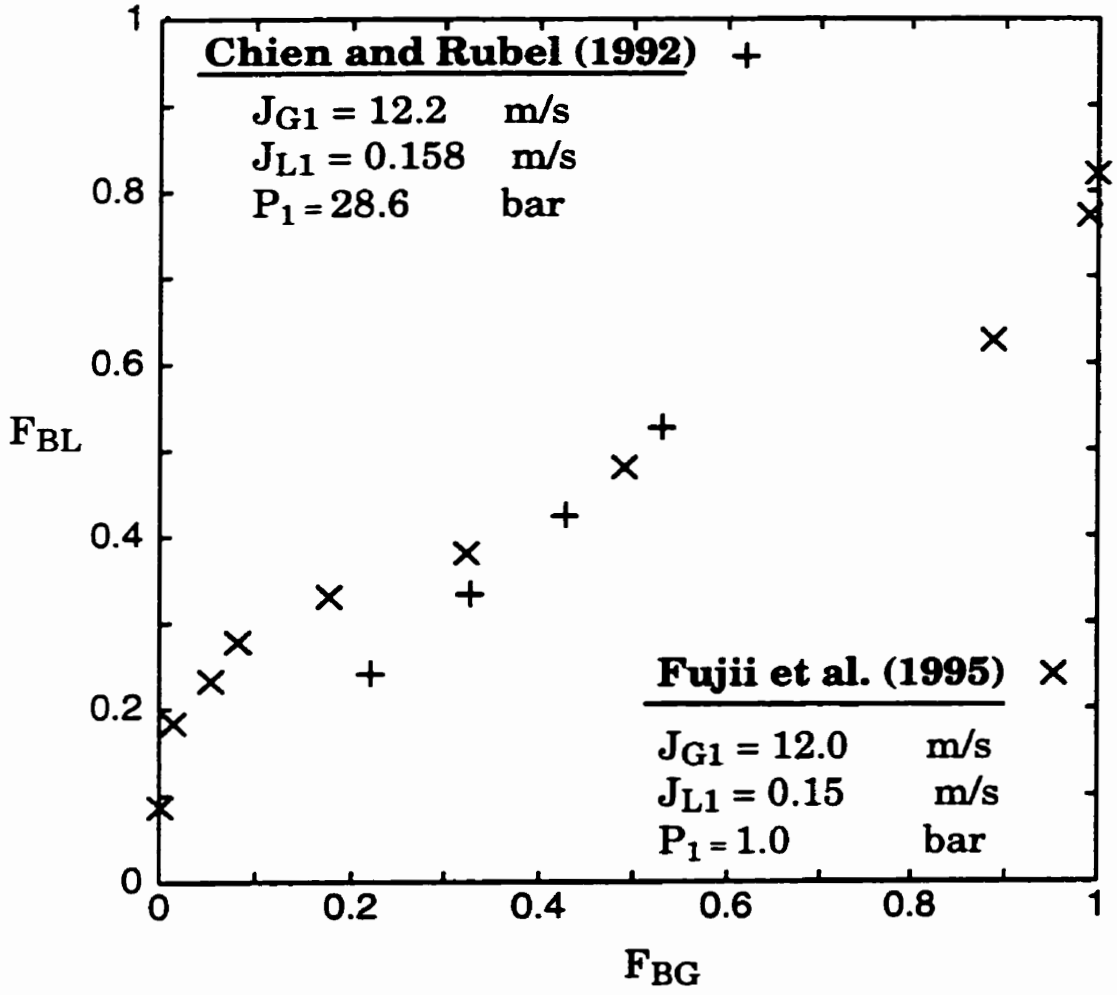

Figure 2.36 Effect of inlet pressure on the phase distribution in the data of Fujii et al. (1995) and the data of Chien and Rubel (1992) at P_1=28.6 bar.

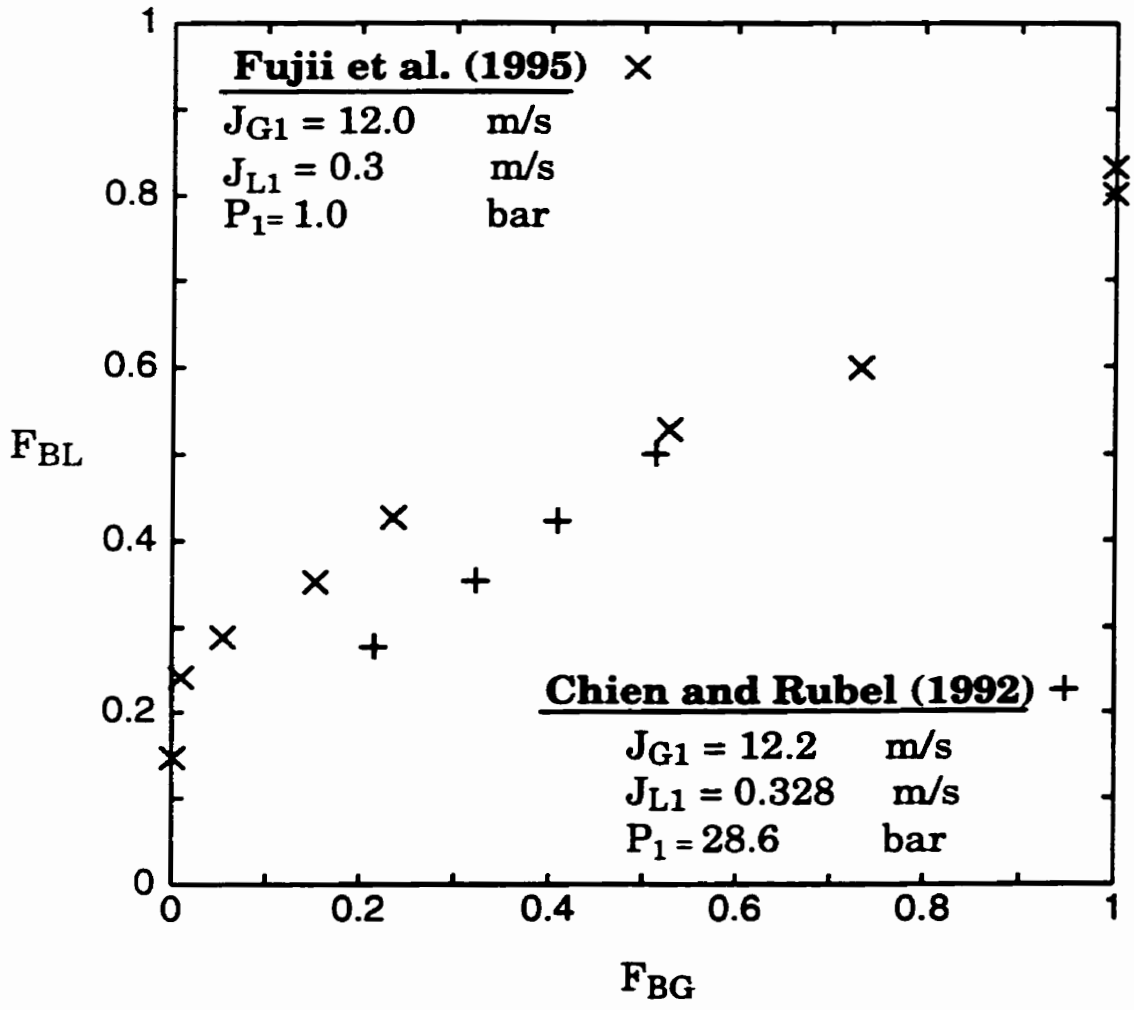

Figure 2.37 Effect of inlet pressure on the phase distribution in the data of Fujii et al. (1995) and the data of Chien and Rubel (1992) at P_1=28.6 bar.

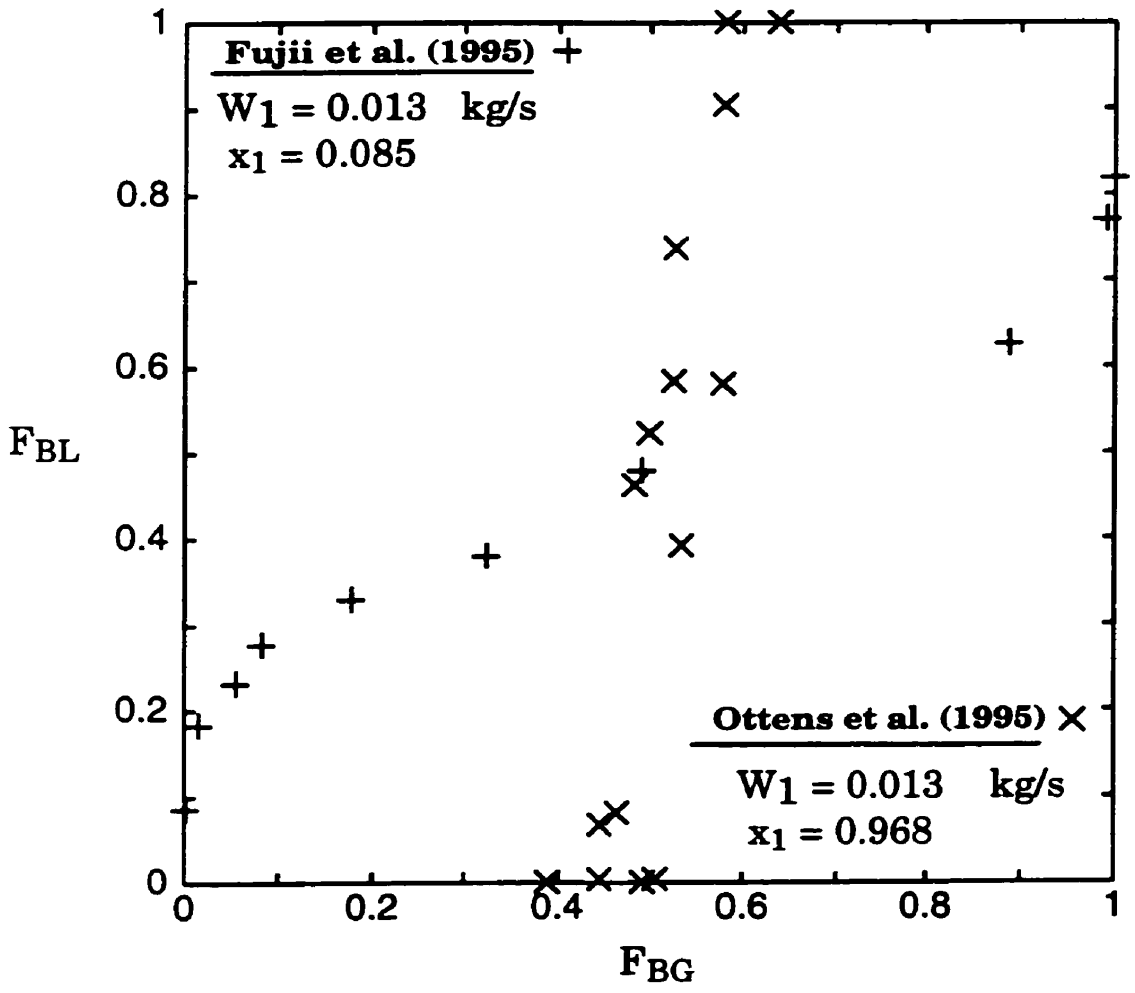

Figure 2.38 Effect of inlet quality (x_1) on the phase distribution in the data of Ottens et al. (1995) and the data of Fujii et al. (1995), at W_1 = 0.013 kg/s.

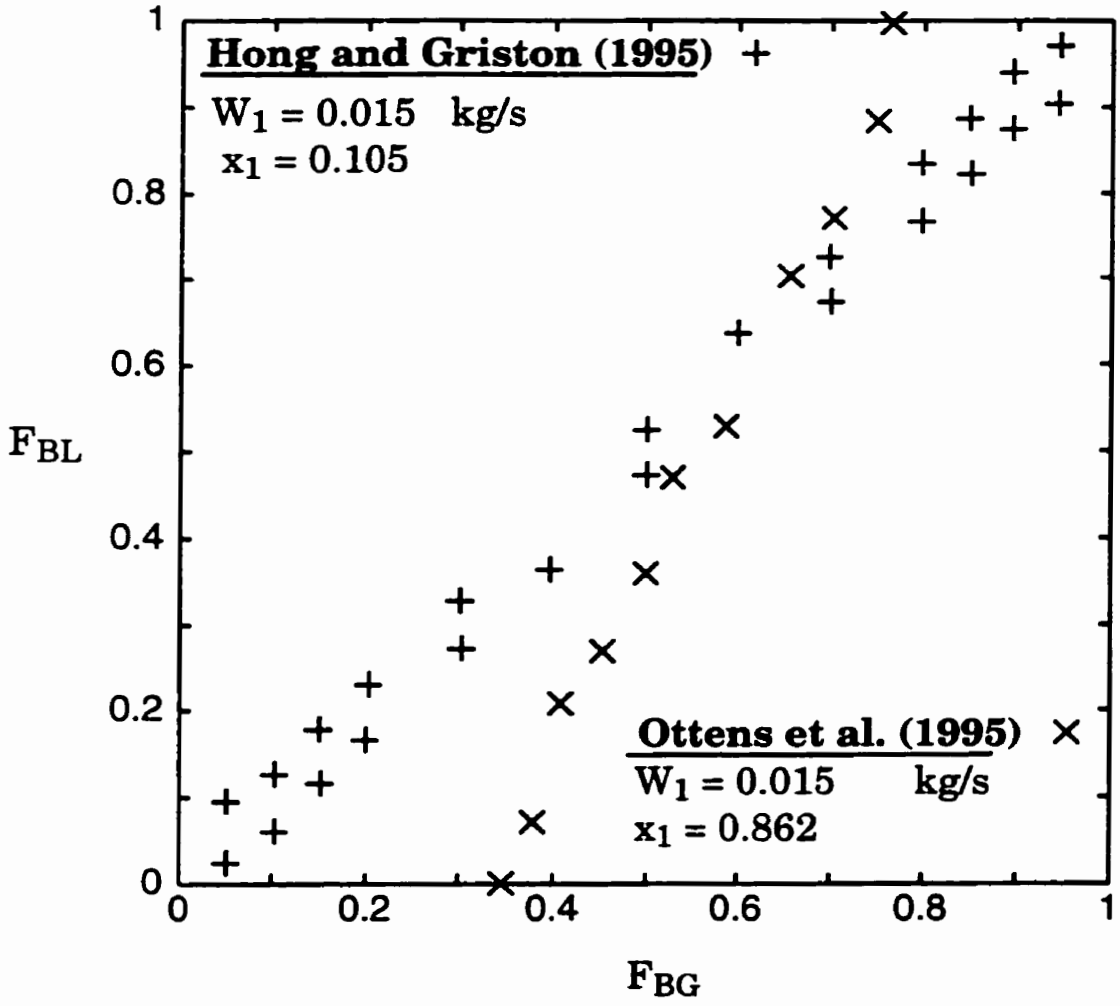

Figure 2.39 Effect of inlet quality (x_1) on the phase distribution in the data of Ottens et al. (1995) and the data of Hong and Griston (1995), at W_1 = 0.015 kg/s.

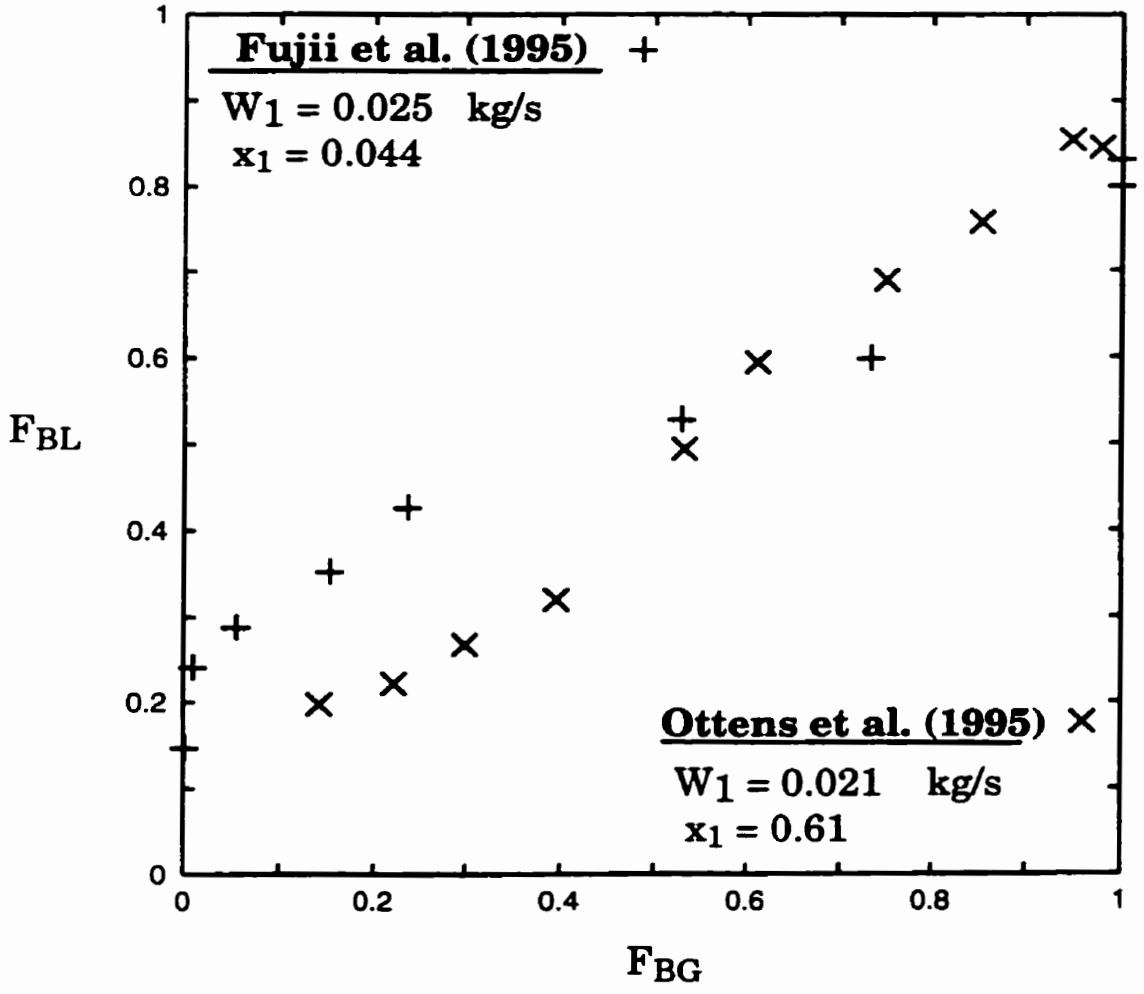

Figure 2.40 Effect of inlet quality (x_1) on the phase distribution in the data of Ottens et al. (1995) and the data of Fujii et al. (1995), at $W_1 \equiv 0.023$ kg/s.

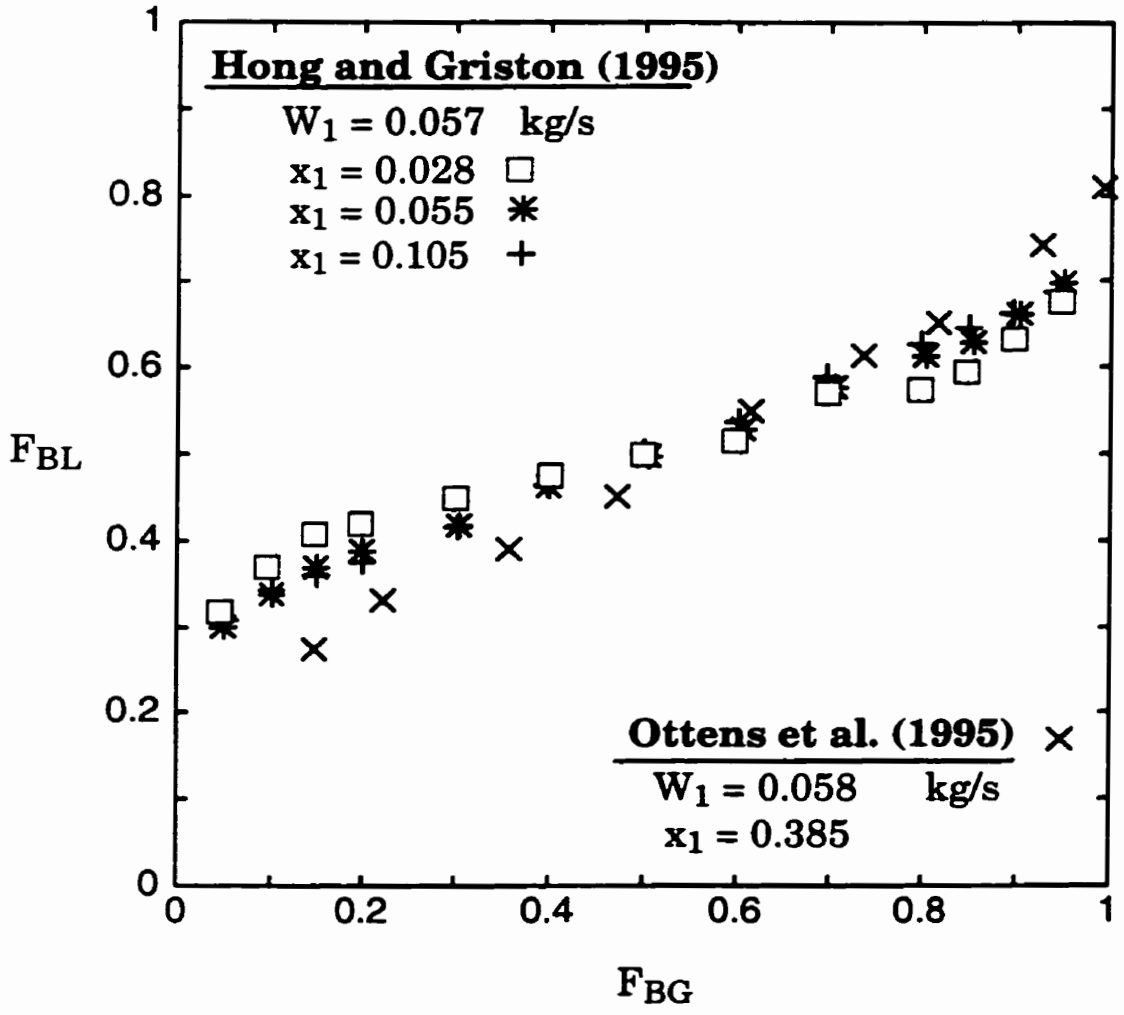

Figure 2.41 Effect of inlet quality (x_1) on the phase distribution in the data of Ottens et al. (1995) and the data of Hong and Griston (1995), at $W_1 \cong 0.058$ kg/s.

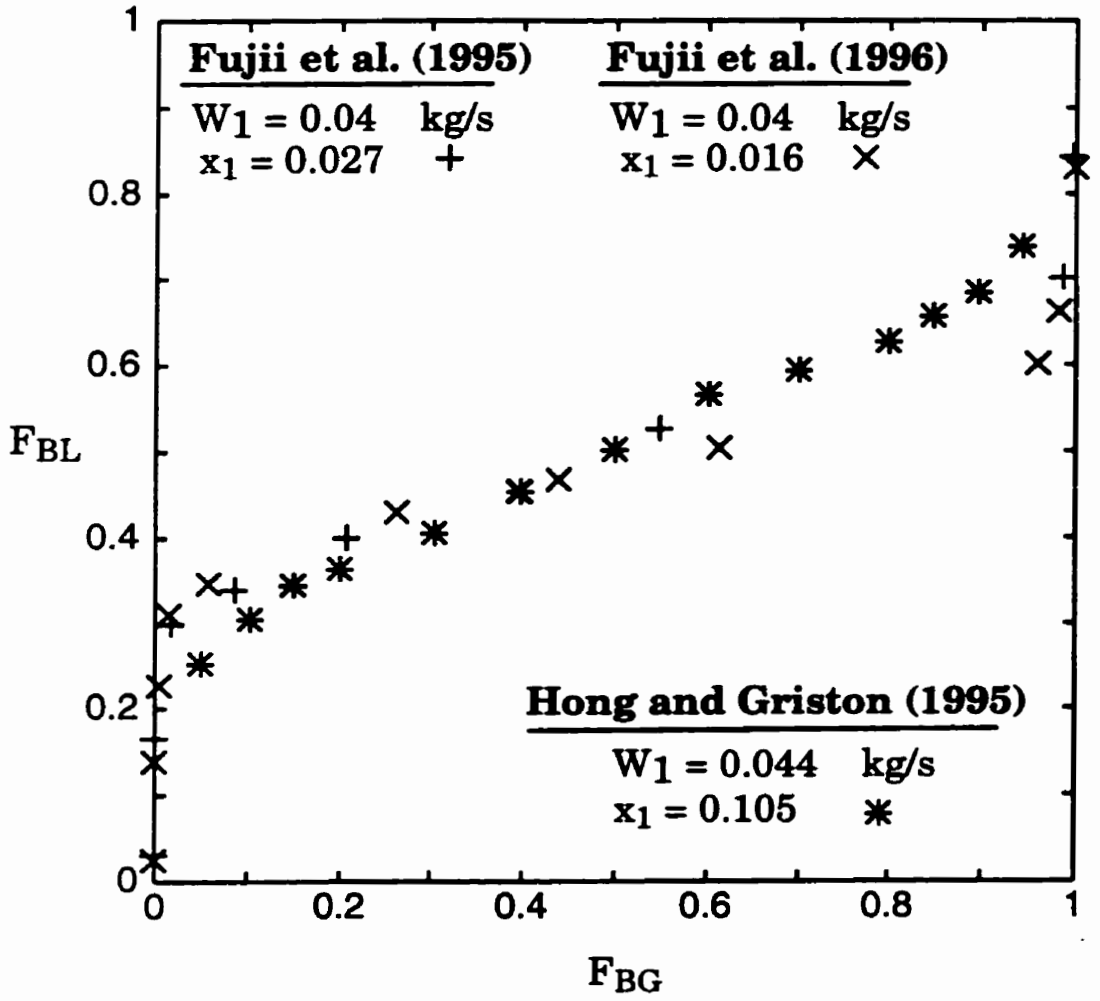

Figure 2.42 Effect of inlet quality (x_1) on the phase distribution in the data of Fujii et al. (1995) and the data of Hong and Griston (1995), at $W_1 \cong 0.042$ kg/s.

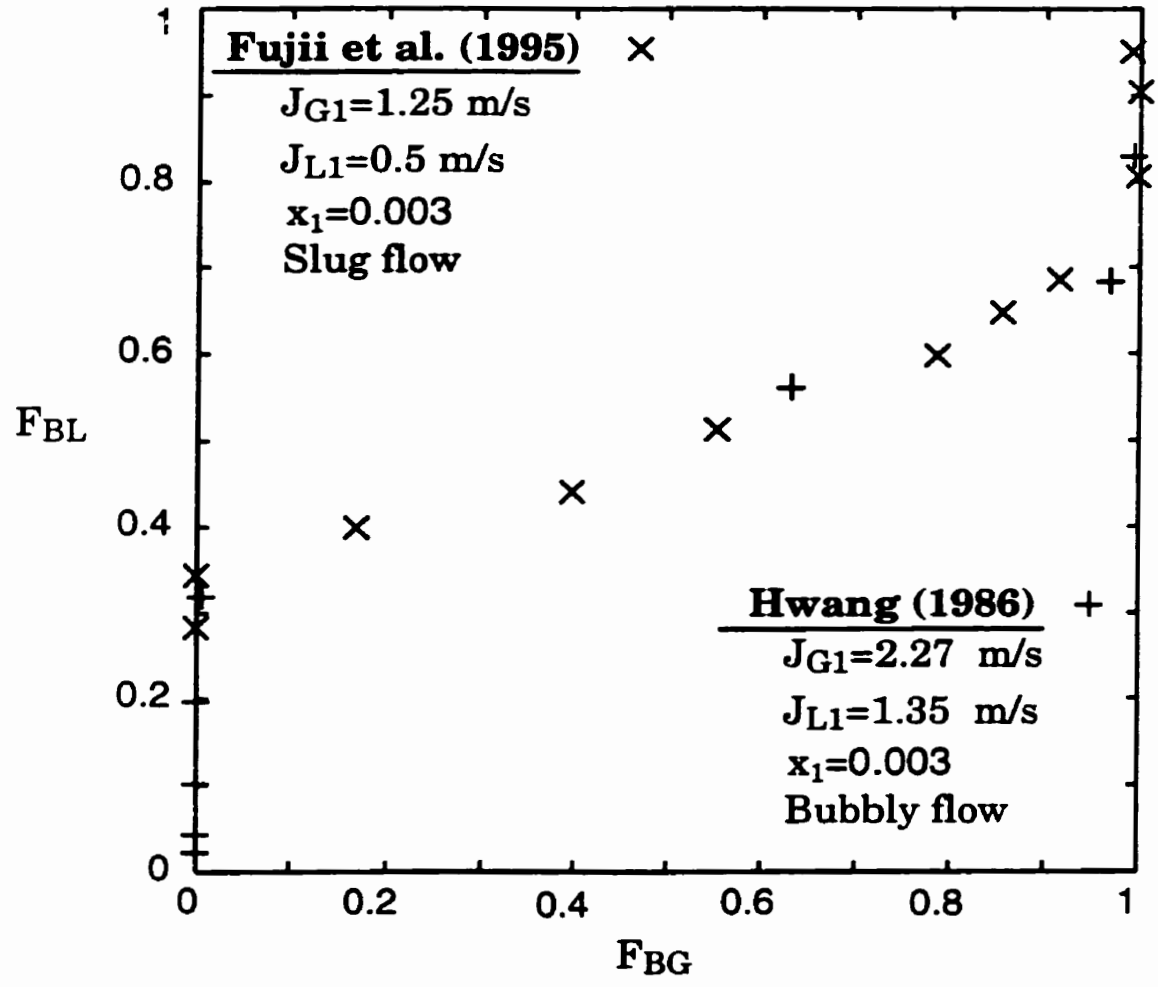

Figure 2.43 Effect of inlet flow regime on the phase distribution in the data of Fujii et al. (1995) for slug flow and the data of Hwang (1986) for bubbly flow.

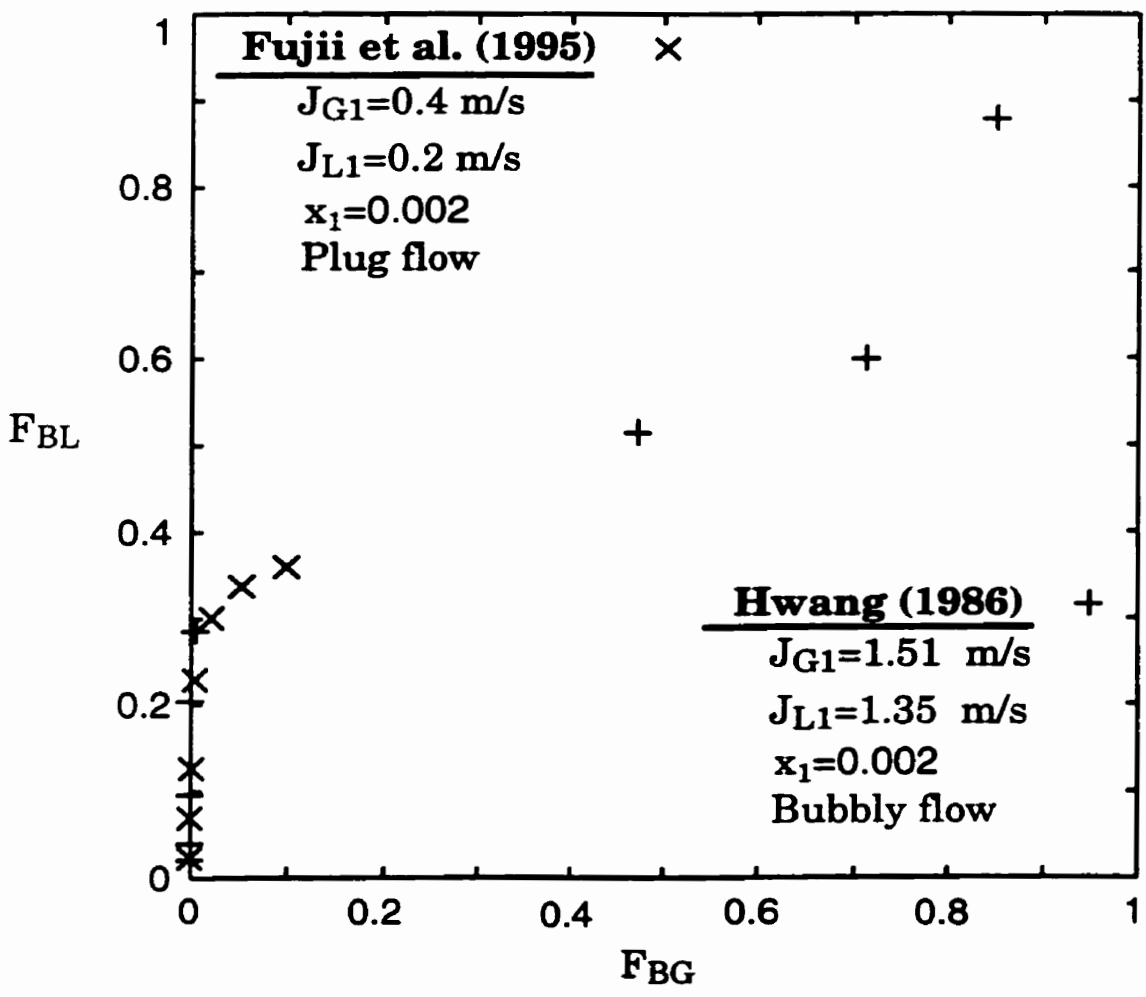

Figure 2.44 Effect of inlet flow regime on the phase distribution in the data of Fujii et al. (1995) for plug flow and the data of Hwang (1986) for bubbly flow.

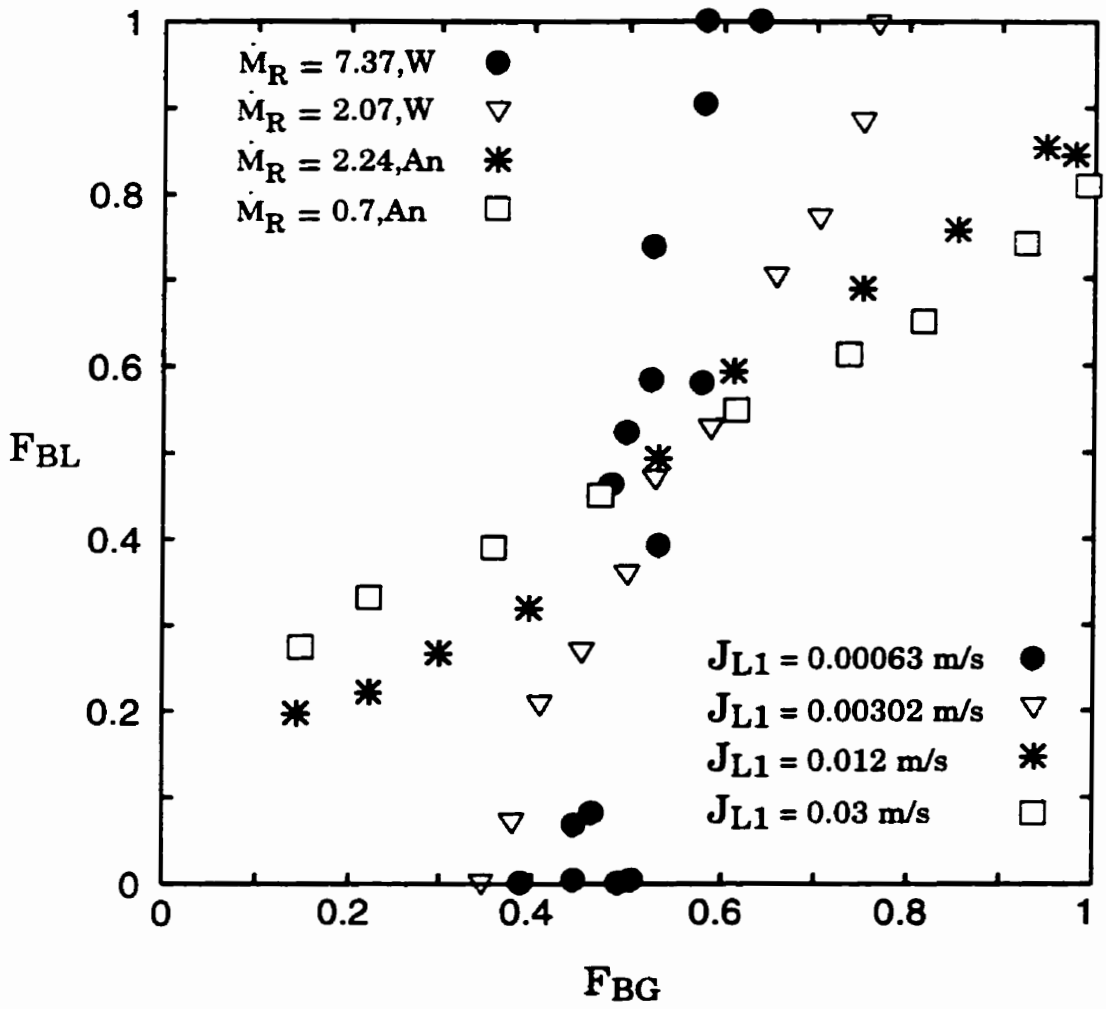

Figure 2.45 Effect of inlet momentum-flux ratio on the phase distribution in the data of Ottens et al. (1995) for J_{G1}=15.8 m/s, (W:Wavy, An:Annular).

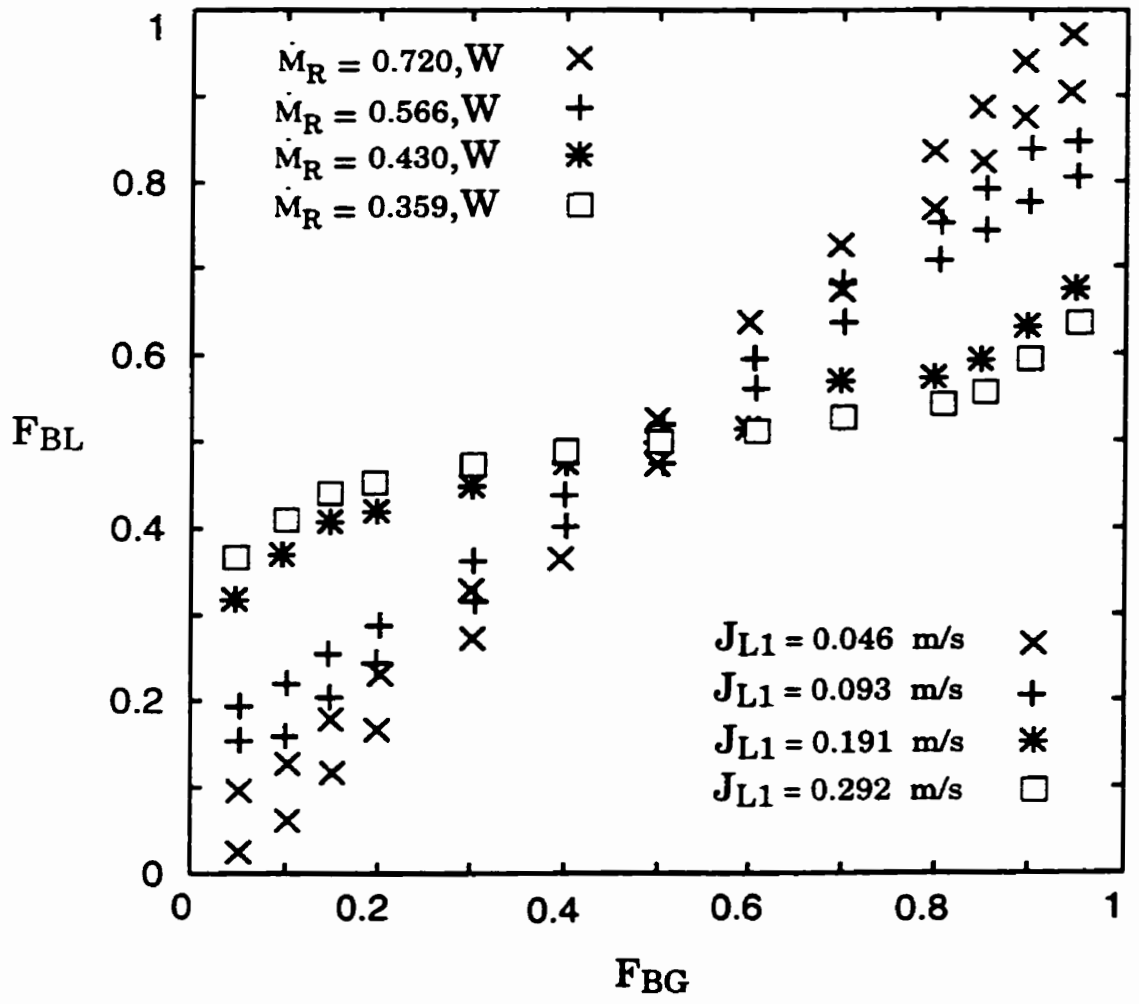

Figure 2.46 Effect of inlet momentum-flux ratio on the phase distribution in the data of Hong and Griston (1995) for J_{G1} = 4.57 m/s, (W:Wavy).

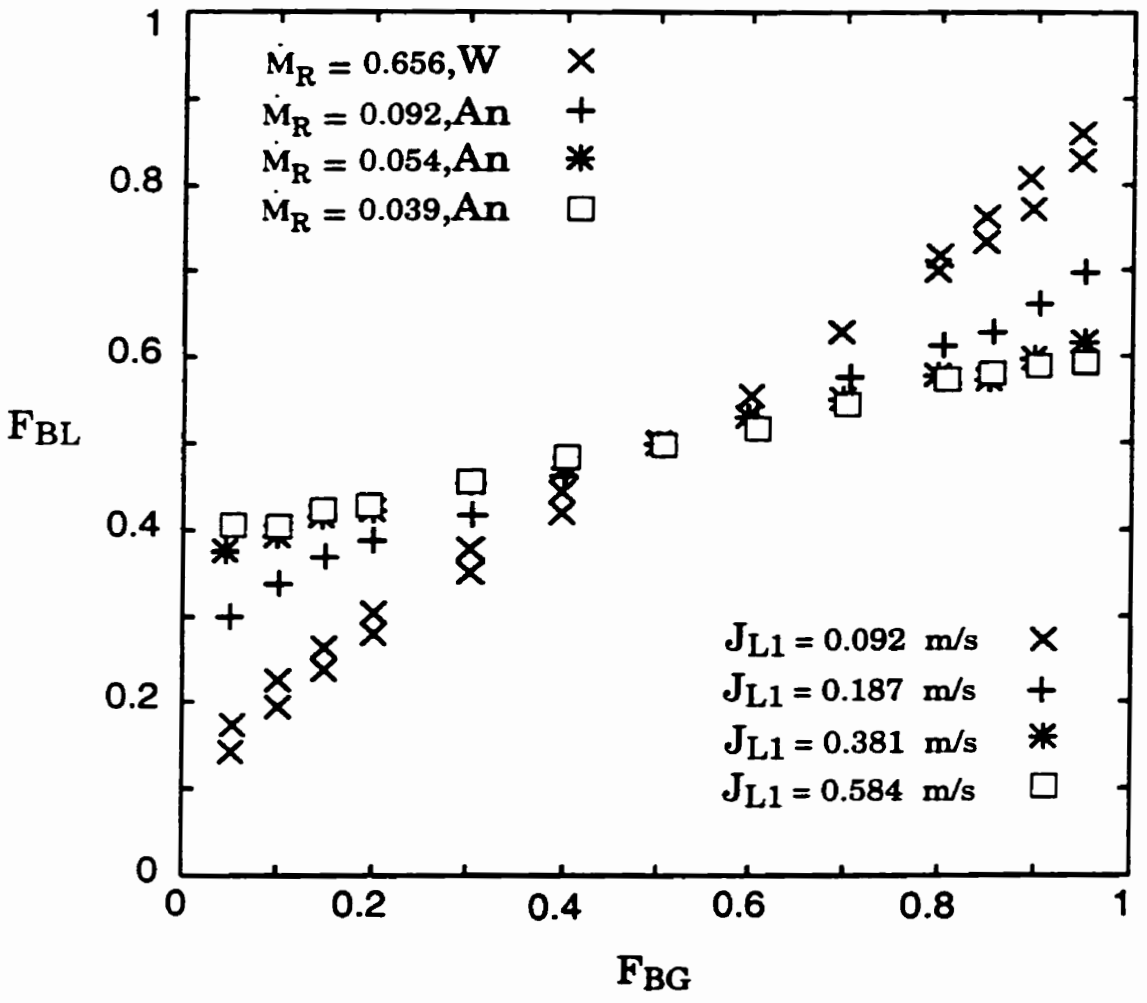

Figure 2.47 **Effect of inlet momentum-flux ratio on the phase distribution in the data of Hong and Griston (1995) for J_{G1} = 9.14 m/s, (W:Wavy, An:Annular).**

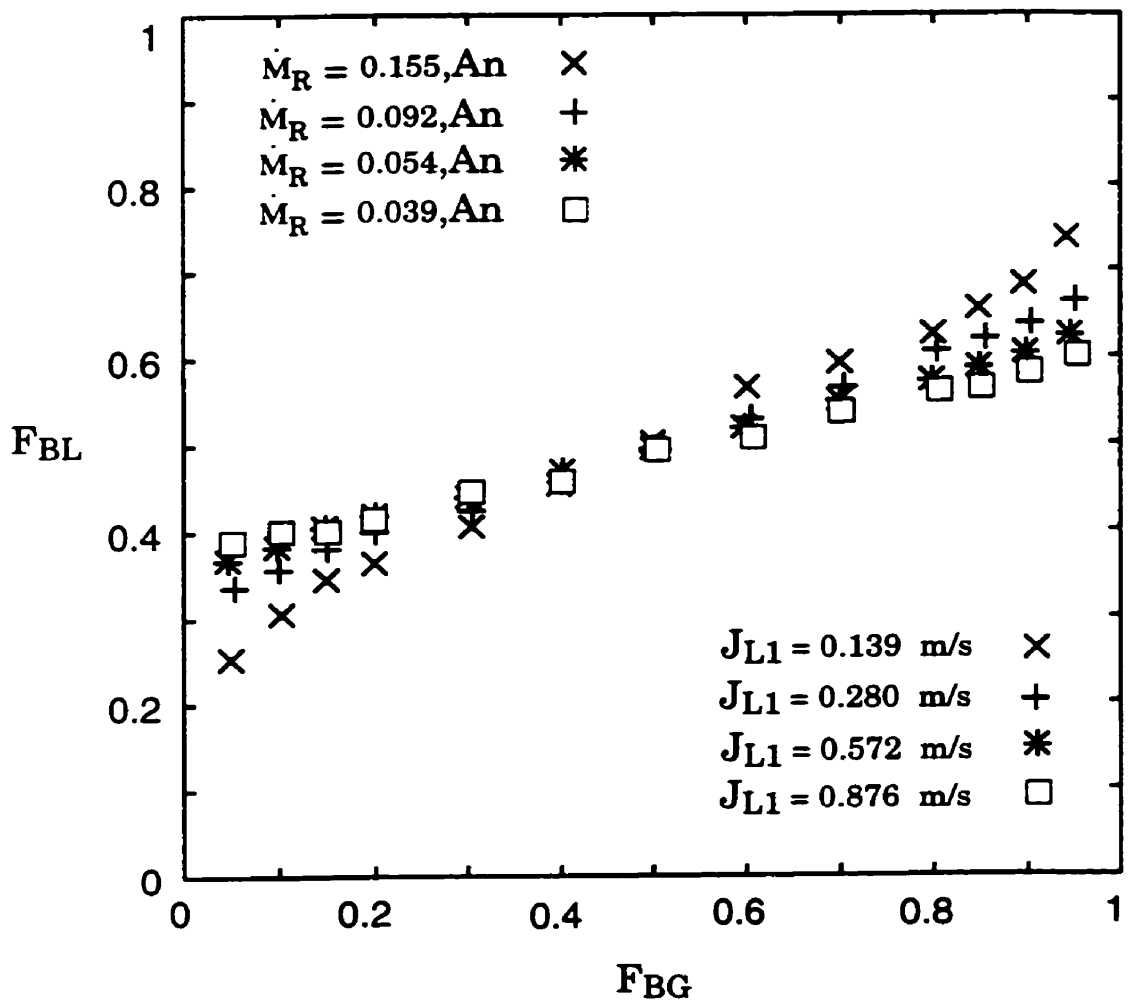

Figure 2.48 Effect of inlet momentum-flux ratio on the phase distribution in the data of Hong and Griston (1995) for J_{G1} = 13.7 m/s, (An:Annular).

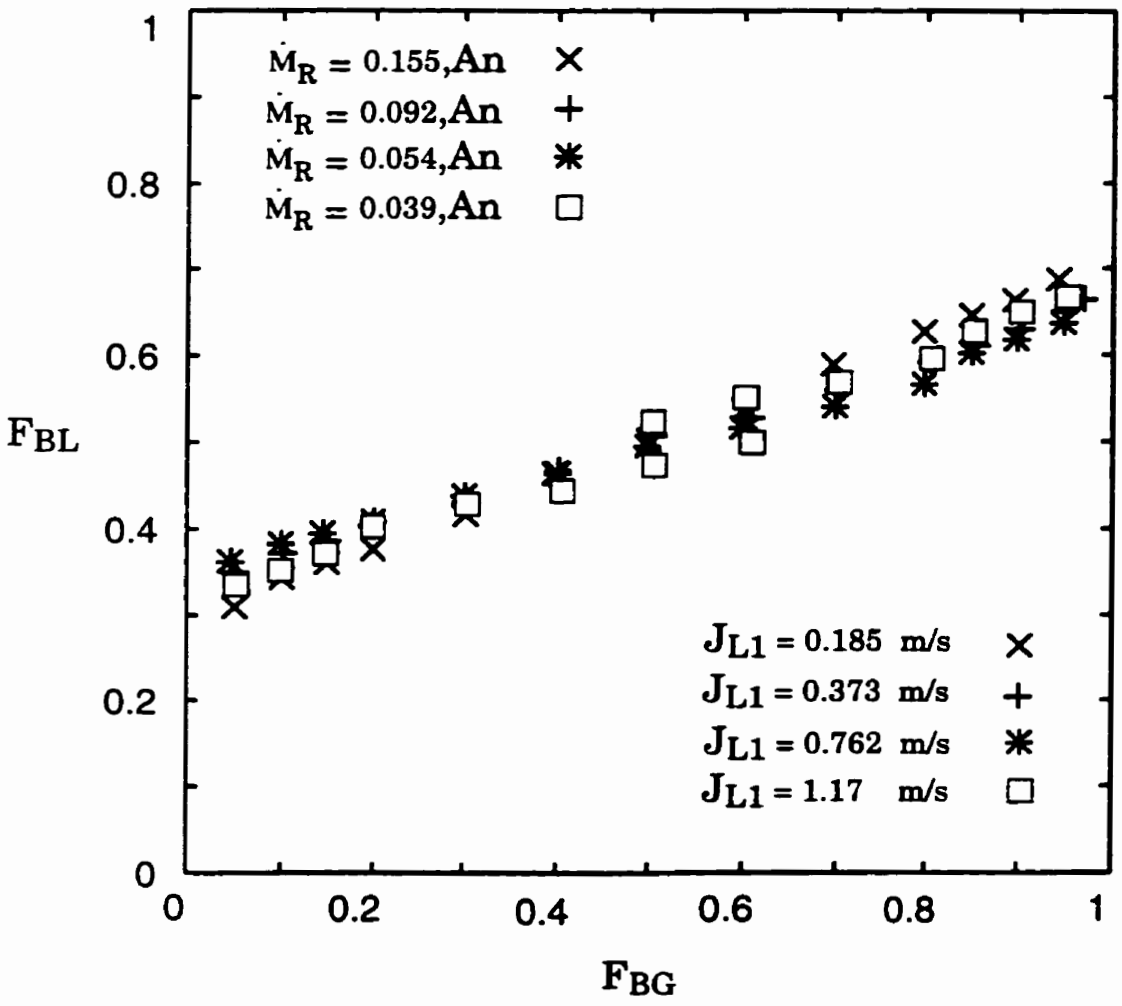

Figure 2.49 Effect of inlet momentum-flux ratio on the phase distribution in the data of Hong and Griston (1995) for J_{G1} = 18.3 m/s, (An:Annular).

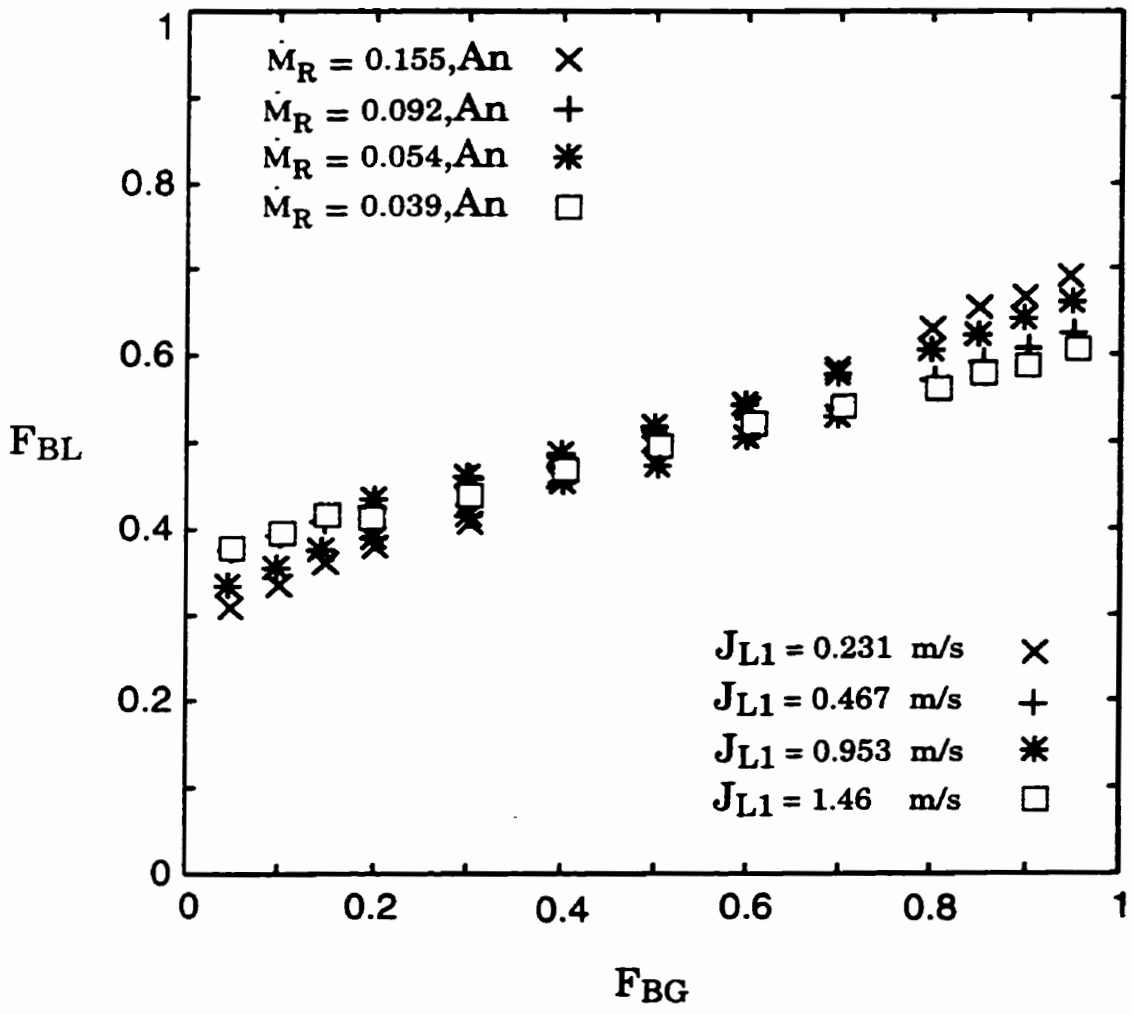

Figure 2.50 **Effect of inlet momentum-flux ratio on the phase distribution in the data of Hong and Griston (1995) for J_{G1} = 22.9 m/s, (An:Annular).**

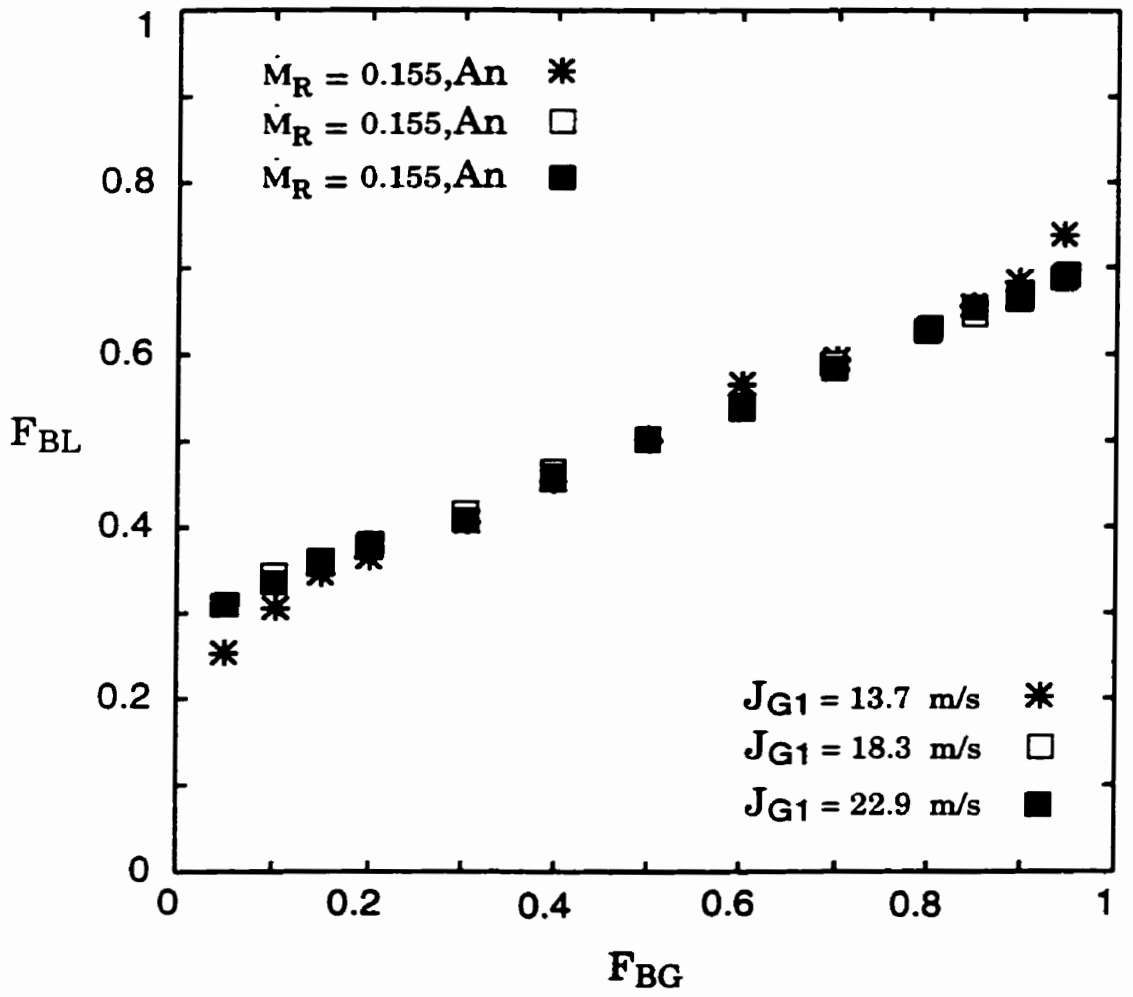

Figure 2.51 **Effect of inlet momentum-flux ratio on the phase distribution in the data of Hong and Griston (1995) for x_1= 0.105, (An:Annular).**

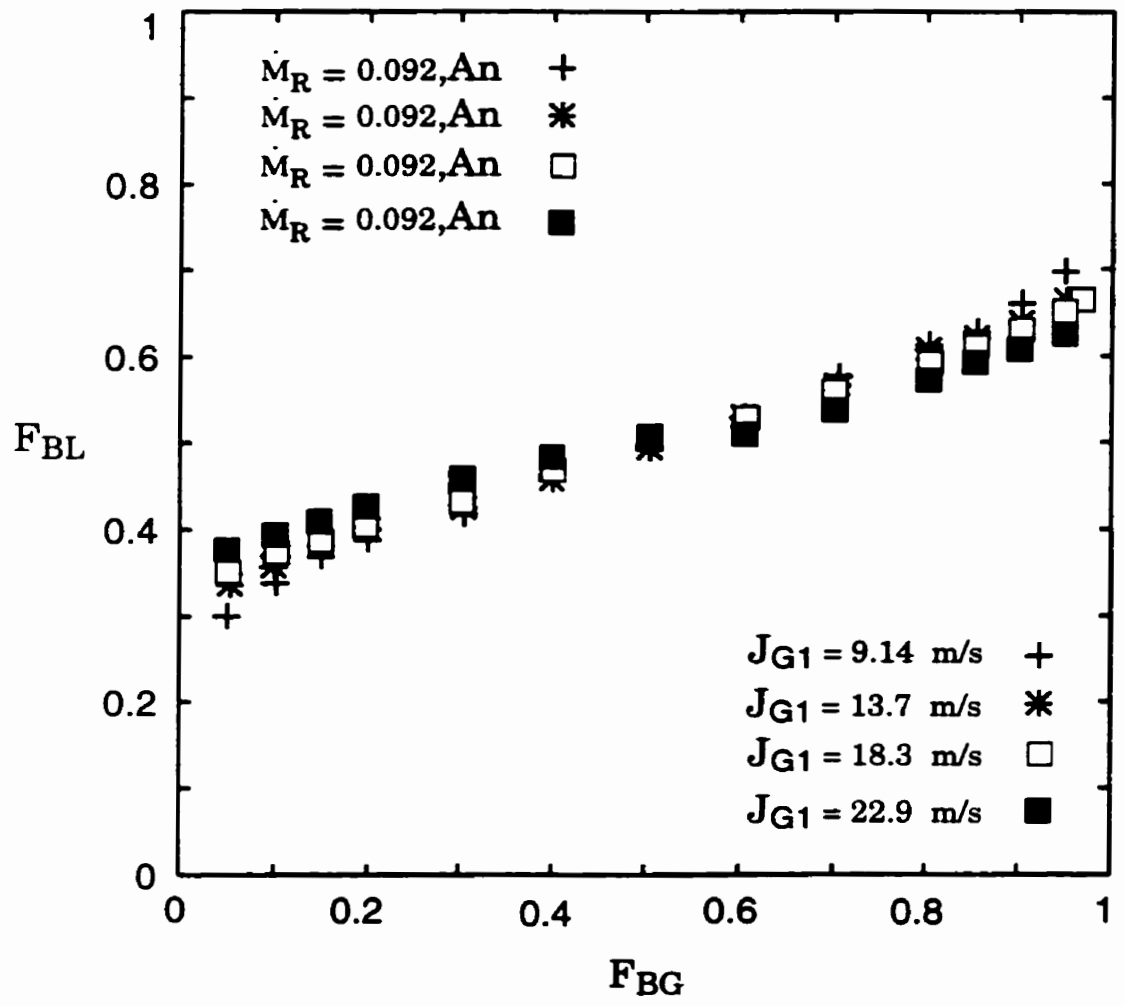

Figure 2.52 Effect of inlet momentum-flux ratio on the phase distribution in the data of Hong and Griston (1995) for x_1= 0.055, (An:Annular).

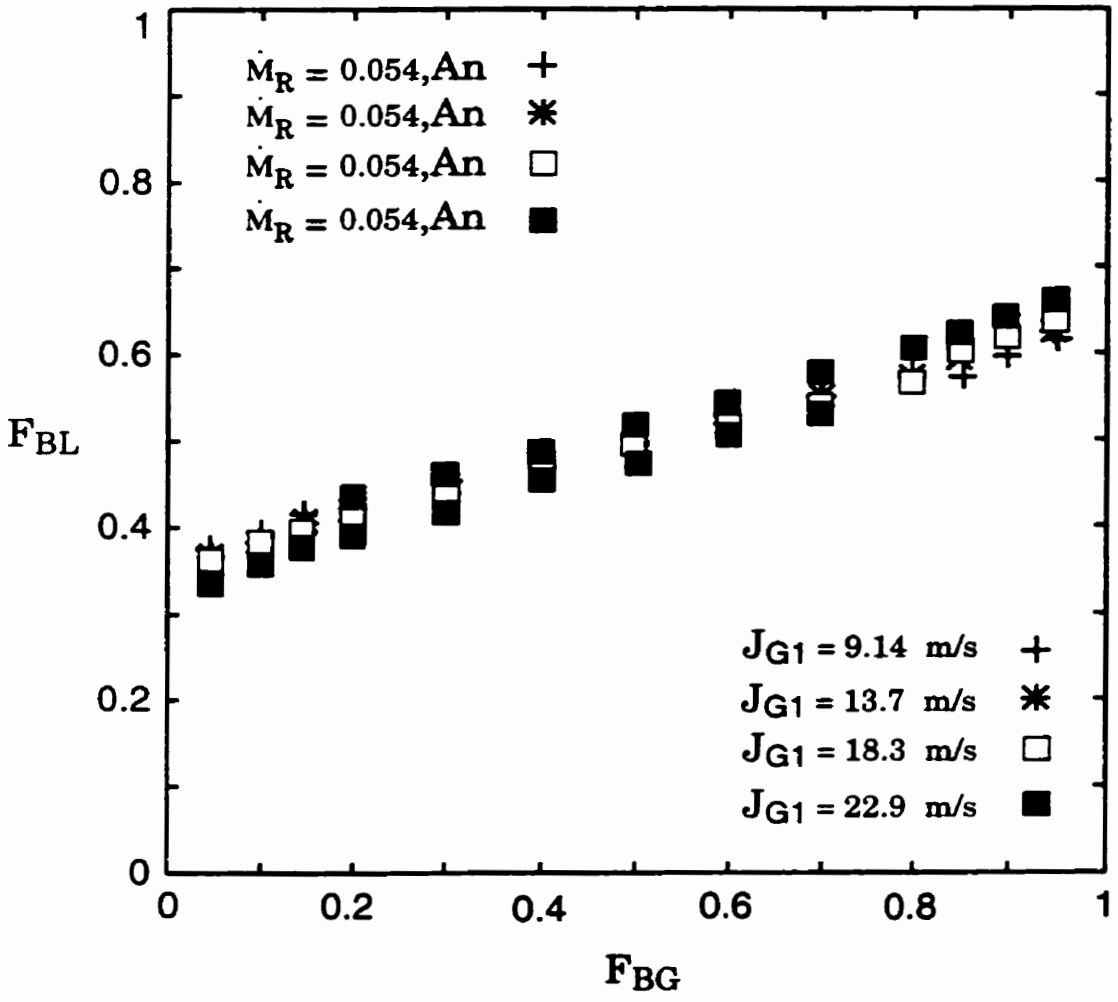

Figure 2.53 Effect of inlet momentum-flux ratio on the phase distribution in the data of Hong and Griston (1995) for x_1= 0.028, (An:Annular).

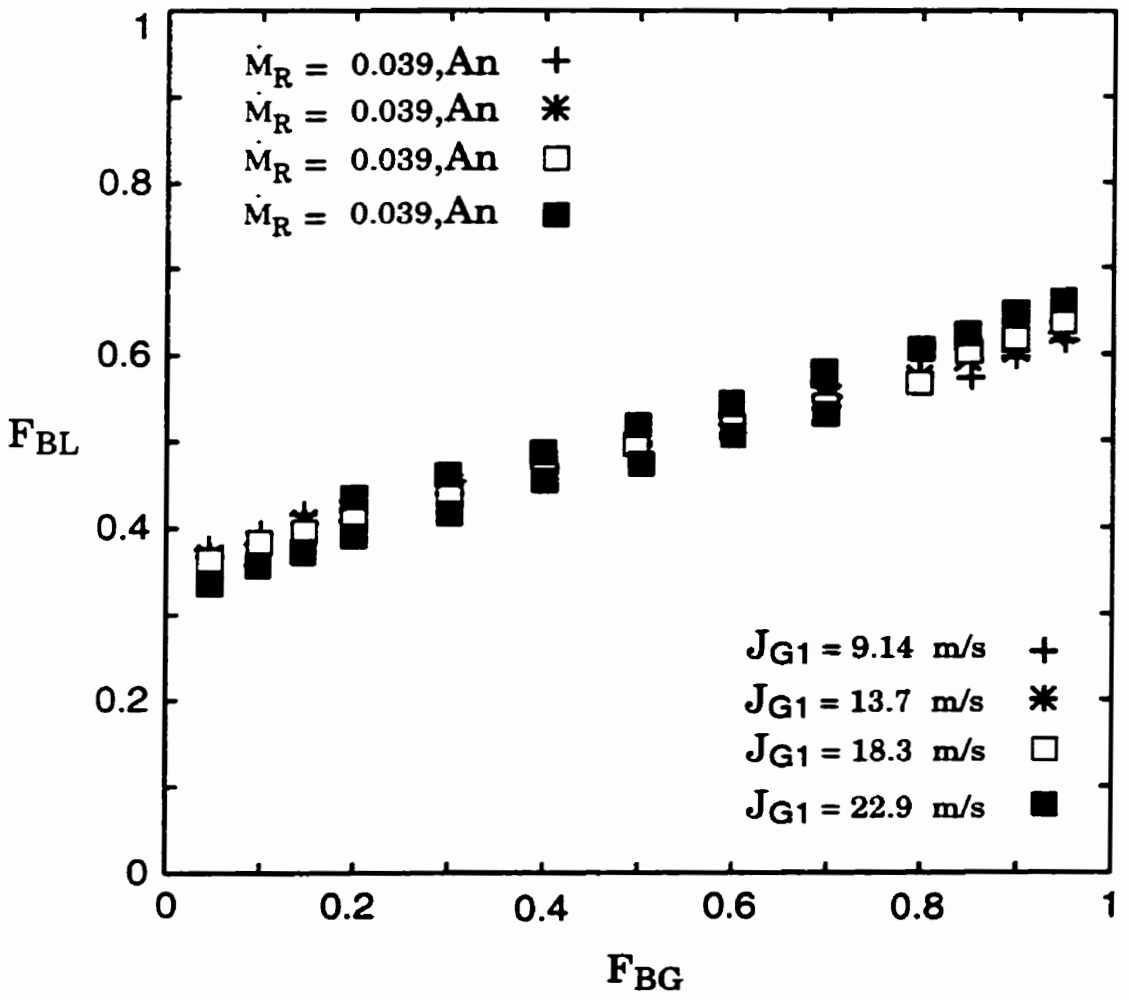

Figure 2.54 **Effect of inlet momentum-flux ratio on the phase distribution in the data of Hong and Griston (1995) for x_1= 0.018, (An:Annular).**

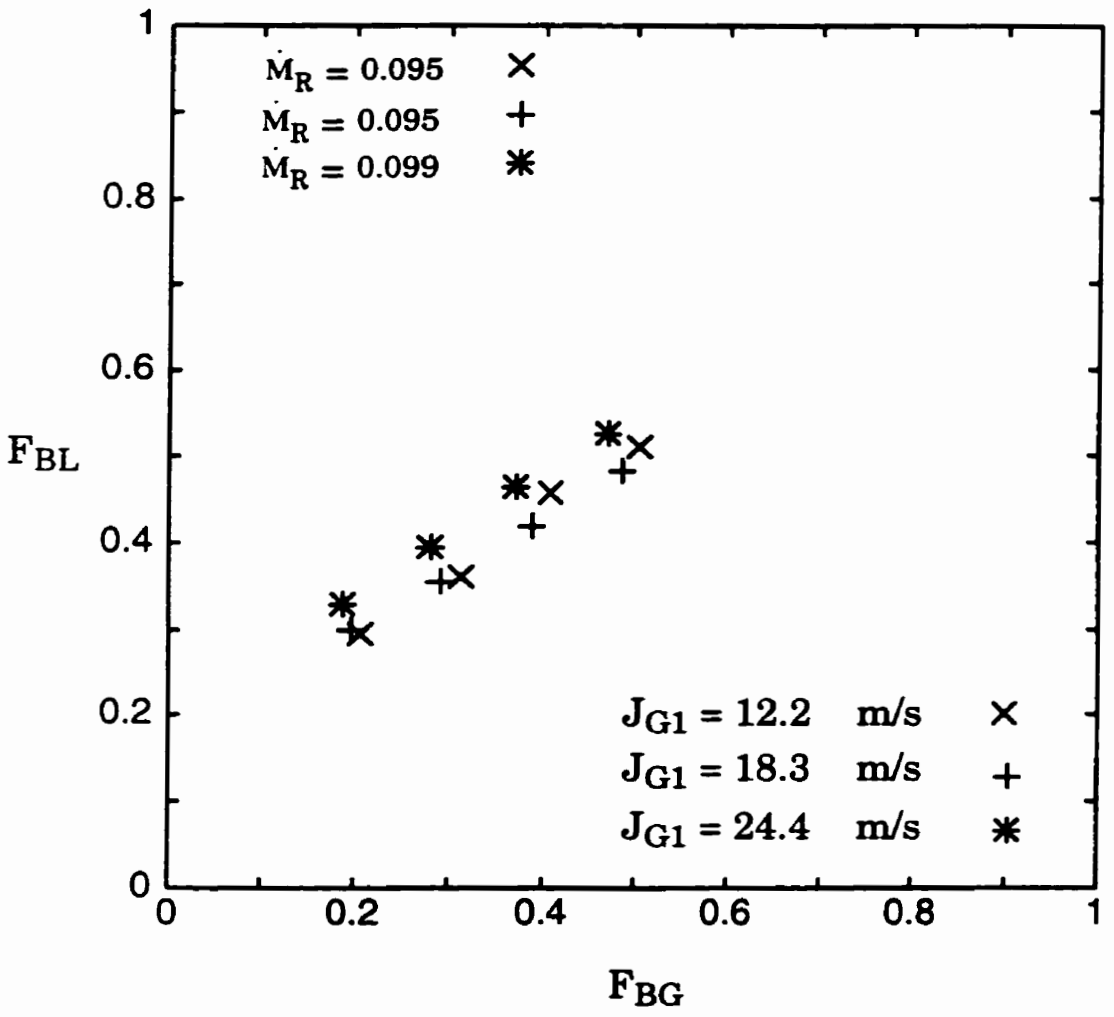

Figure 2.55 **Effect of inlet momentum-flux ratio on the phase distribution in the data of Chien and Rubel (1992) for a nominal x_1=0.2 and annular flow.**

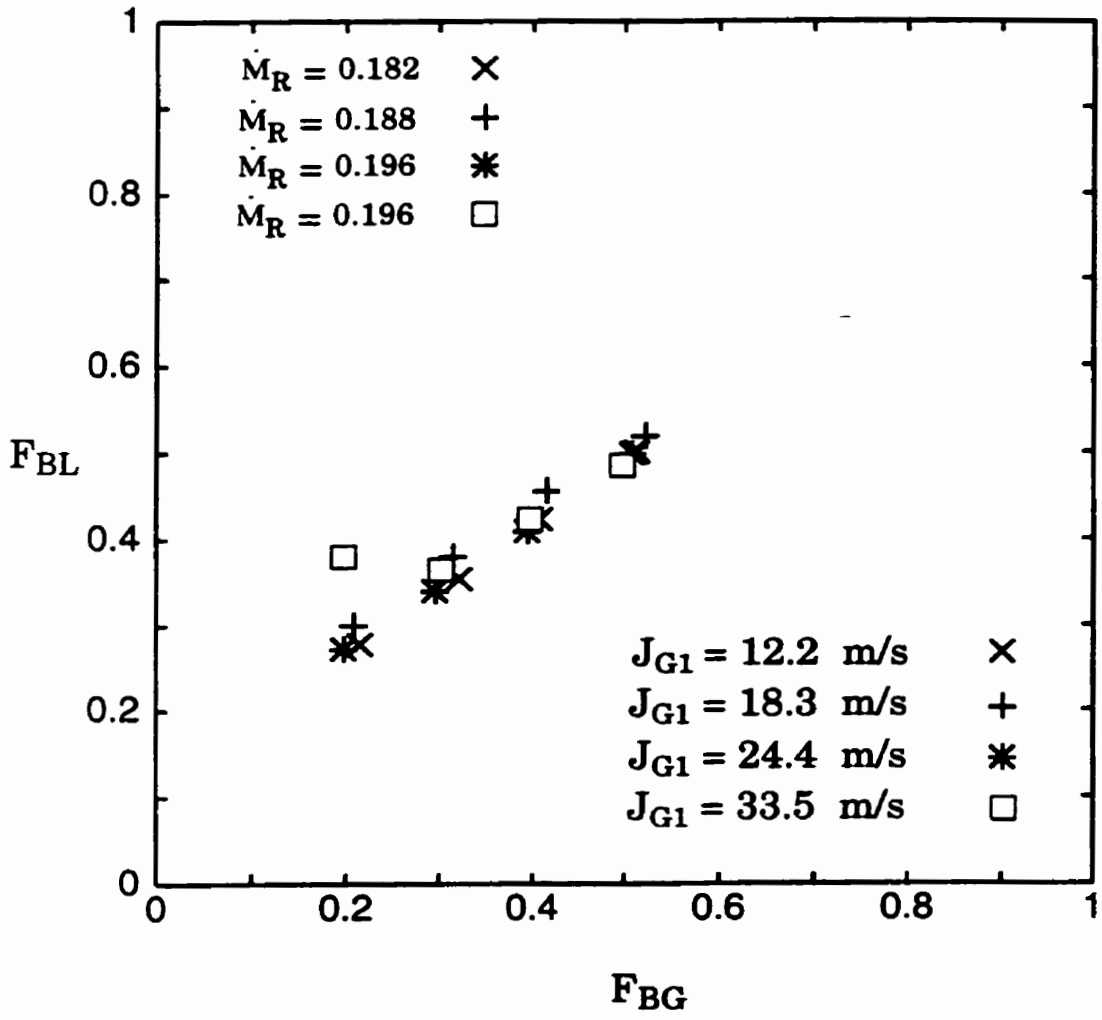

Figure 2.56 **Effect of inlet momentum-flux ratio on the phase distribution in the data of Chien and Rubel (1992) for a nominal x_1=0.4 and annular flow.**

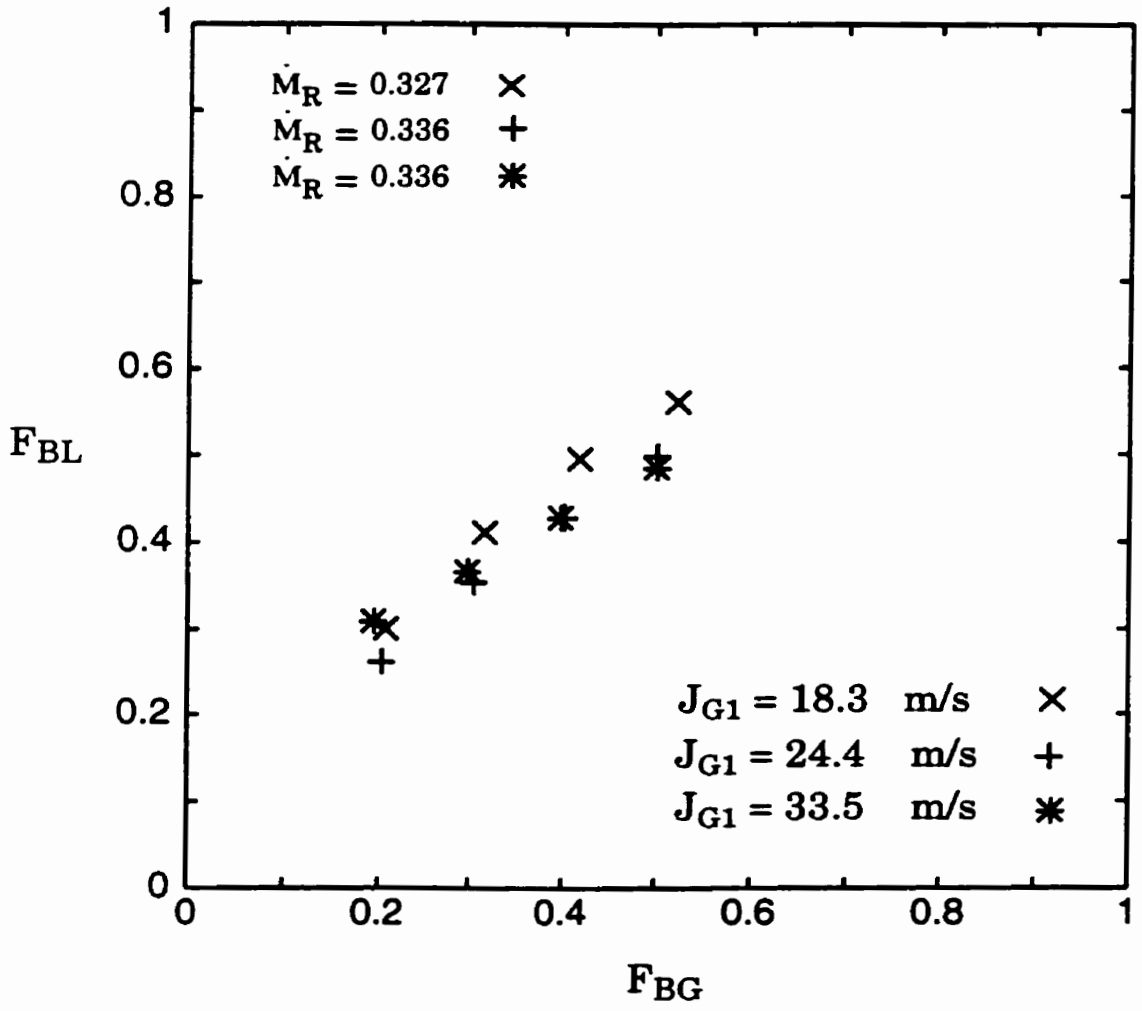

Figure 2.57 **Effect of inlet momentum-flux ratio on the phase distribution in the data of Chien and Rubel (1992) for a nominal x_1=0.6 and annular flow.**

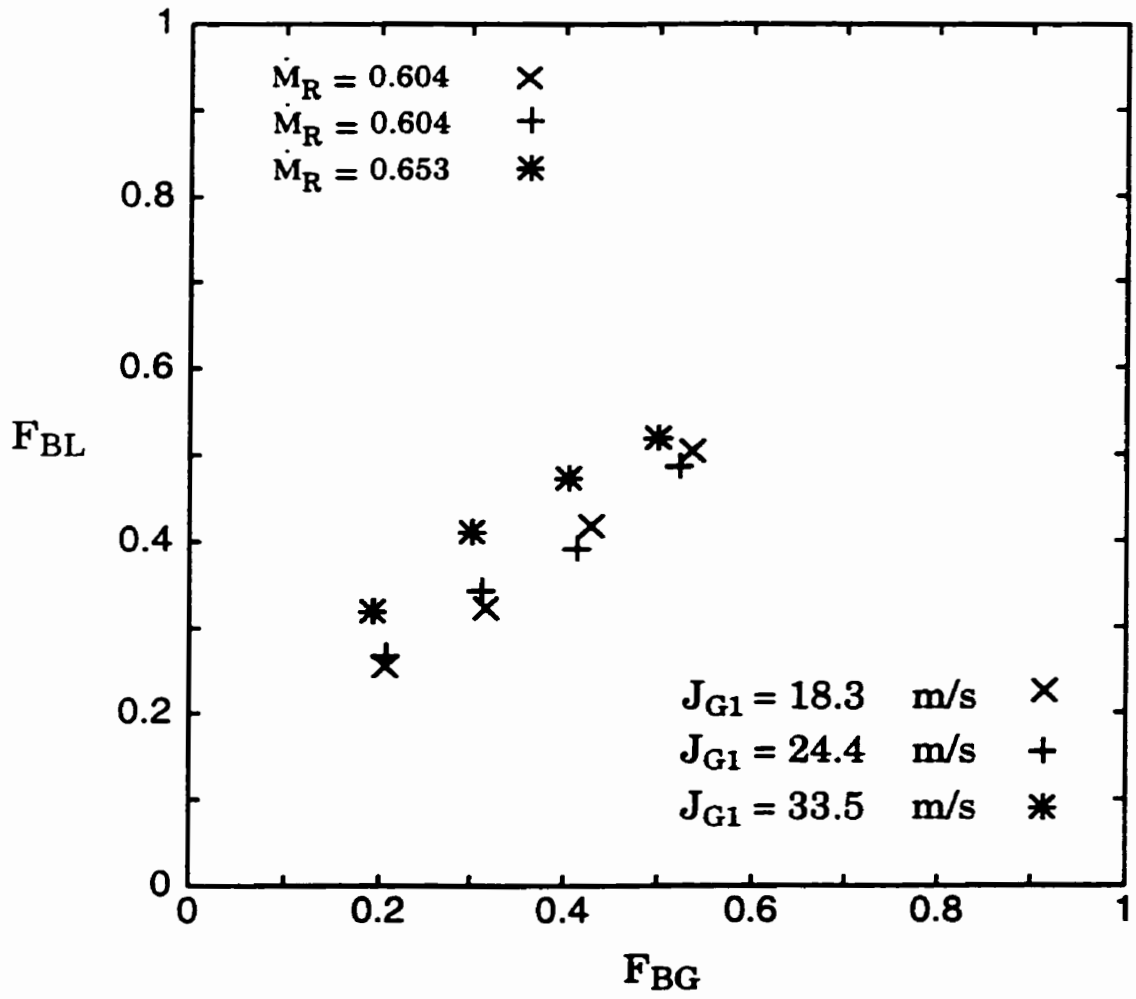

Figure 2.58 **Effect of inlet momentum-flux ratio on the phase distribution in the data of Chien and Rubel (1992) for a nominal x_1=0.8 and annular flow.**

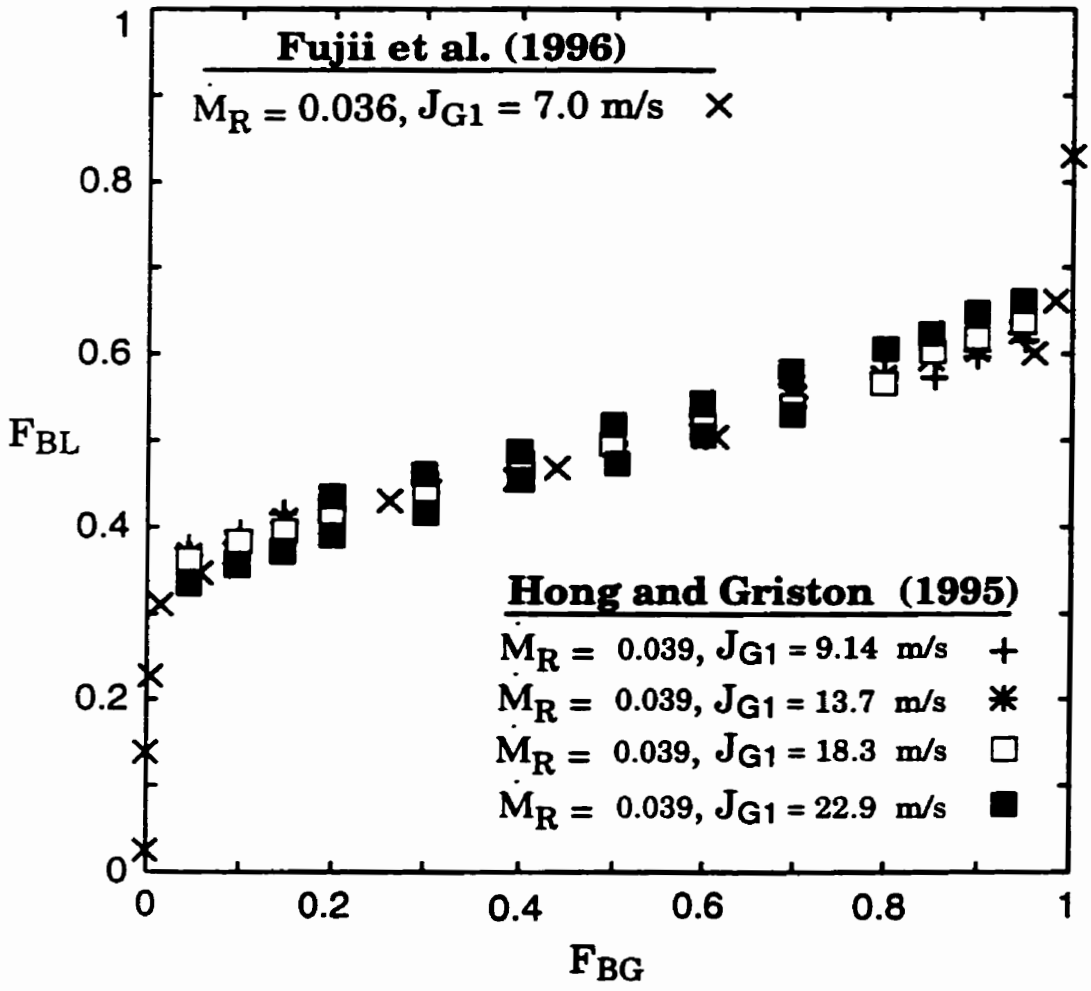

Figure 2.59 Effect of inlet momentum-flux ratio on the phase distribution in the data of Hong and Griston (1995) for x_1=0.018 and annular flow, and the data of Fujii et al. (1996) for J_{L1}=0.5 m/s and annular flow.

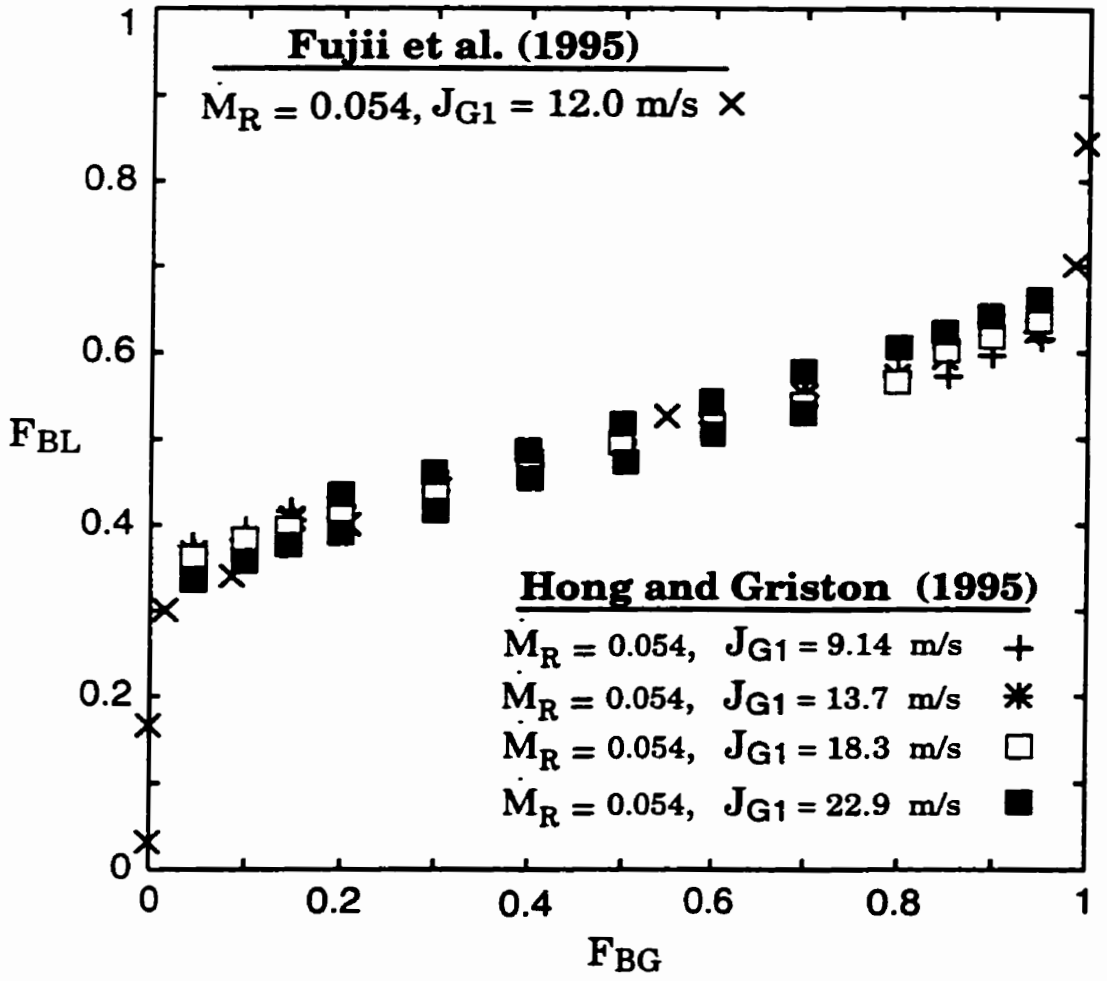

Figure 2.60 Effect of inlet momentum-flux ratio on the phase distribution in the data of Hong and Griston (1995) for x_1=0.028 and annular flow, and the data of Fujii et al. (1995) for J_{L1} = 0.5 m/s and annular flow.

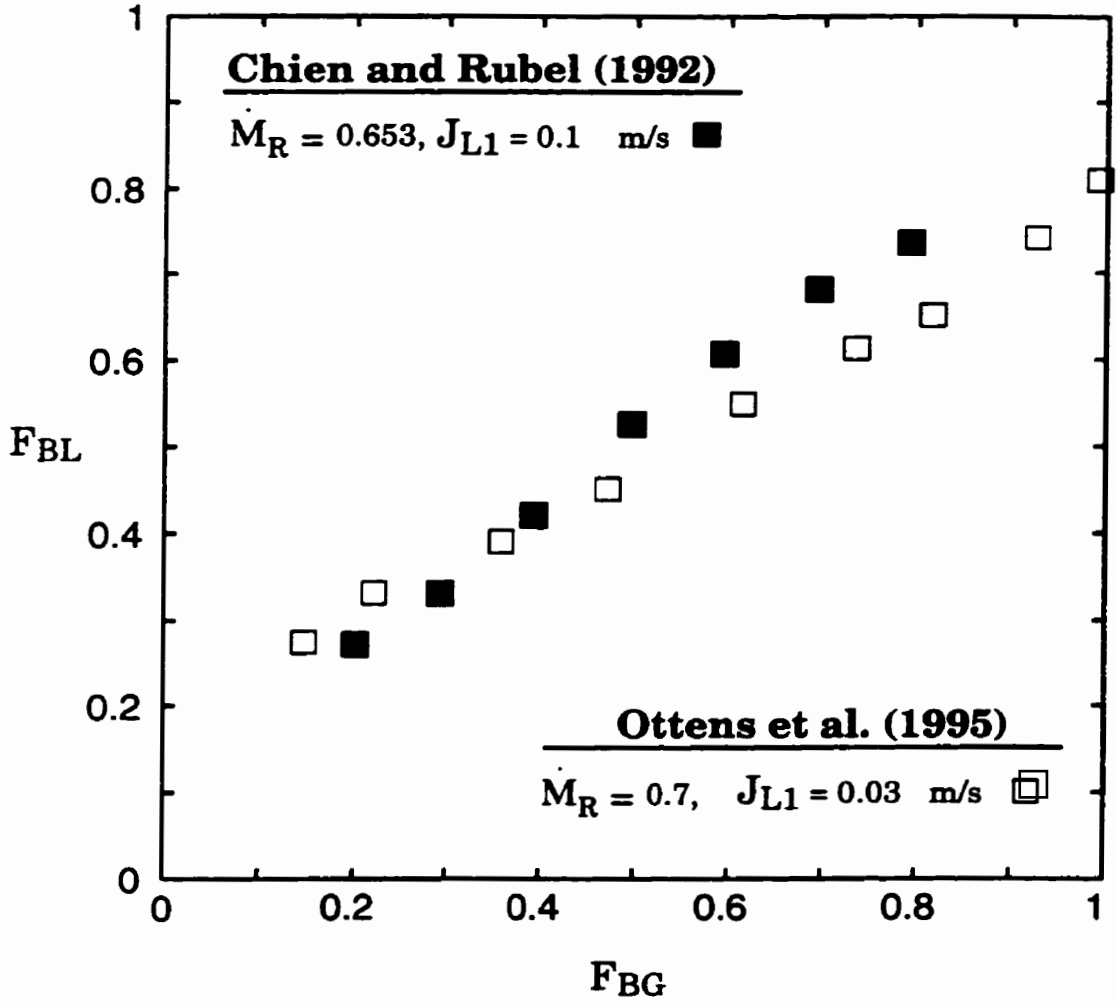

Figure 2.61 Effect of inlet momentum-flux ratio on the phase distribution in the data of Ottens et al. (1995) for J_{G1}=15.8 m/s, P_1=1 bar, and annular flow, and the data of Chien and Rubel (1992) for J_{G1} = 33.5 m/s, P_1=28.6 bar, and annular flow.

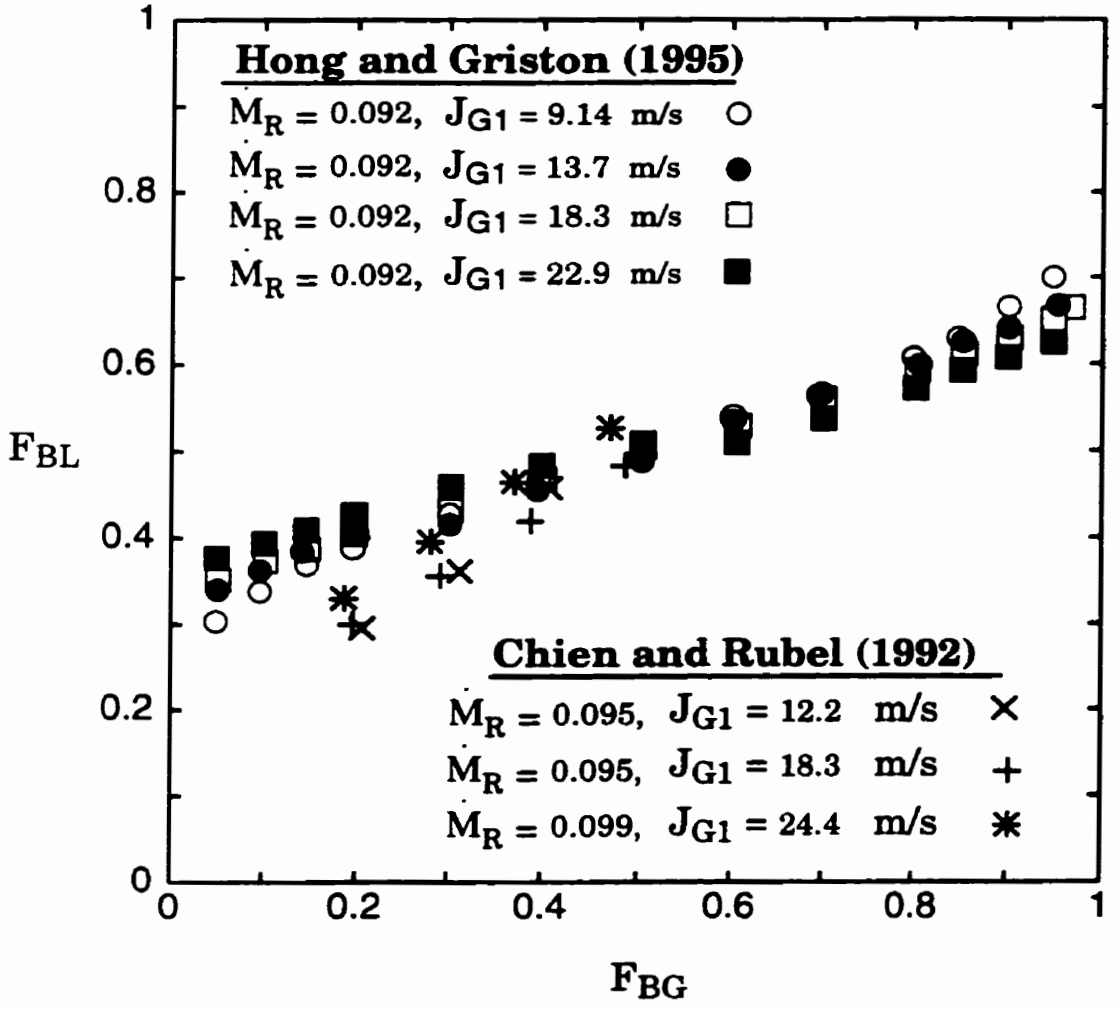

Figure 2.62 Effect of inlet momentum-flux ratio on the phase distribution in the data of Chien and Rubel (1992) for a nominal $x_1 = 0.2$, $P_1 = 28.6$ bar, and annular flow, and the data of Hong and Griston (1995) for $x_1 = 0.055$, $P_1 = 1$ bar, and annular flow.

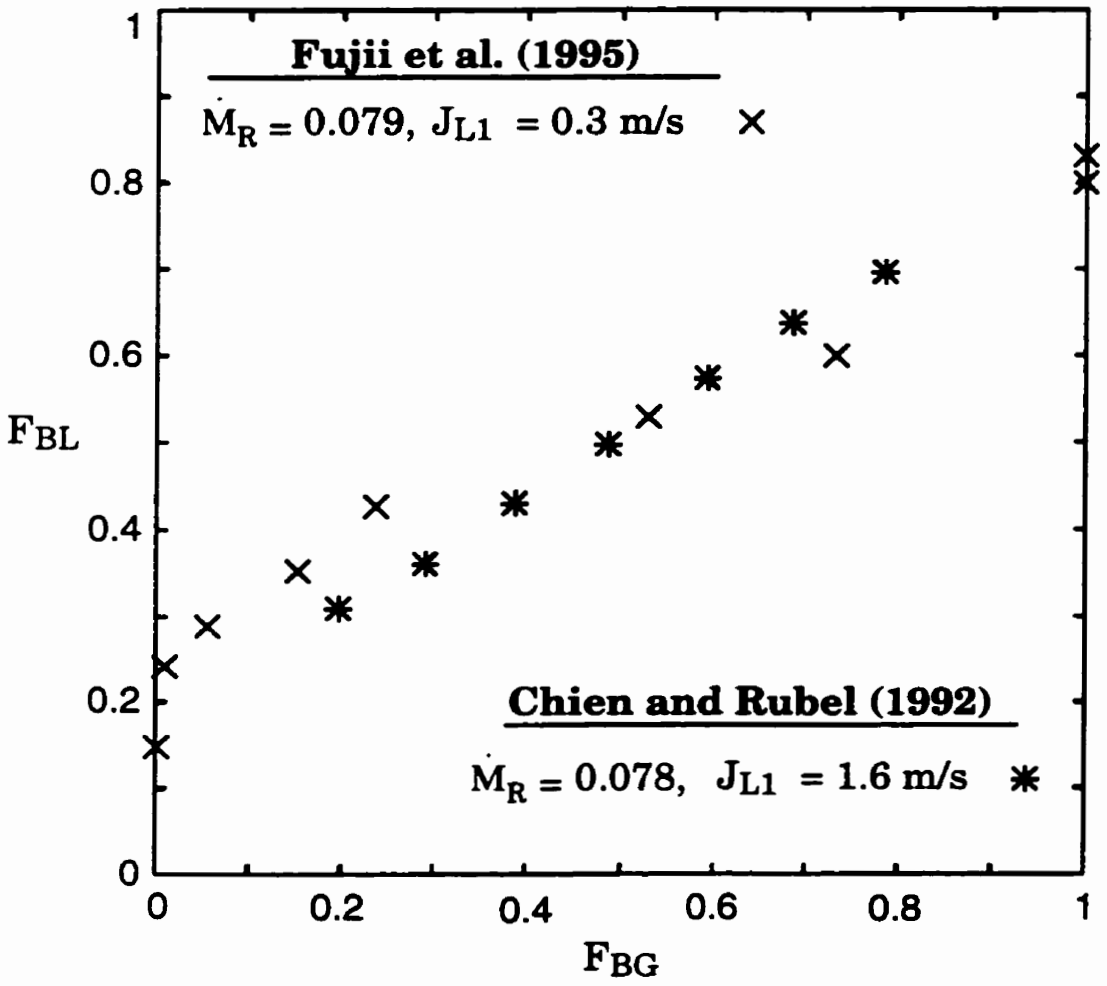

Figure 2.63 Effect of inlet momentum-flux ratio on the phase distribution in the data of Chien and Rubel (1992) for J_{G1} = 15.2 m/s, P_1 =42.4 bar, and annular flow, and the data of Fujii et al. (1995) for J_{G1}=12.0 m/s, P_1 =1 bar, and annular flow.

Chapter 3

ASSESSMENT OF EXISTING MODELS AND CORRELATIONS

3.1 Brief Description of Models and Correlations

Two empirical correlations and two analytical models have been developed for predicting the phase distribution at impacting tee junctions with horizontal inlet and outlet sides. A brief description of these predictive tools is given in the following sections.

3.1.1 Chien and Rubel (1992) Correlation

Chien and Rubel (1992) used their own experimental data to develop an empirical correlation for predicting the phase distribution at horizontal impacting tees. They compared the prediction against the data of Azzopardi et al. (1986) and they concluded that the agreement was good especially for high-inlet-quality flows. The correlation is given by

$$x_3/x_1 = a\,(F_{BG})^b \qquad \text{for } F_{BG} \le 0.5, \tag{3.1}$$

and

$$x_3/x_1 = F_{BG} / \{\, 1 - [(1 - F_{BG})^{1-b} / a\,]\} \qquad \text{for } F_{BG} \ge 0.5. \tag{3.2}$$

where, a and b are empirical coefficients given by

$a = 1.352^{(1-x_1)}$, and $b = 0.435\,(1-x_1)$.

Values of a and b were limited to the ranges $0.2 \le x_1 \le 1.0$ and $28.6 \le P_1 \le 42.4$ bar. The correlation was developed in a way that ensures "symmetry of the prediction" (see Chapter 1 for more details on the special use of the term "symmetry of prediction" where Figures 1.2(b) and 1.2(c) are discussed). For given inlet conditions (J_{G1} and J_{L1}),

fluid properties (ρ_G and ρ_L), and extraction ratio (W_3/W_1), the value of the inlet quality (x_1) can be determined. Using Equations (3.1) and (3.2), values of (x_3/x_1) can be determined over the whole range of F_{BG}. Then, the corresponding values of F_{BL} can be determined from

$$W_3/W_1 = F_{BG} (x_1/x_3), \tag{3.3}$$

$$x_3 = (x_3/x_1) x_1, \tag{3.4}$$

and

$$F_{BL} = [(1-x_3) / (1-x_1)] (W_3 /W_1). \tag{3.5}$$

It should be noted that the correlation given by Equations (3.1) to (3.5) is independent of the inlet flow regime. Also, the inlet quality (x_1) is the only parameter that has to be known in order to execute the correlation. In other words, the correlation considers the inlet quality (x_1) to be the sole factor that affects the phase distribution.

3.1.2 Hong and Griston (1995) Correlation

Hong and Griston (1995) used their own experimental data to develop an empirical correlation for predicting the phase distribution at horizontal impacting tees. They compared the correlation predictions against the data of Chien and Rubel (1992) and concluded that the agreement was good except for the cases of low gas extraction ratio and low inlet quality. The correlation is given by

$$J_{L3} / (J_{L3} + J_{G3}) = a [J_{L1} / (J_{L1} + J_{G1})] (J_{G3} / J_{G1})^b \tag{3.6}$$

where, a and b are empirical coefficients given by

$$a = a_1 + a_2 \ln (F) + a_3 (F)^{0.5}, \tag{3.7}$$

$$b = b_1 + b_2 F + b_3 \ln (F) + b_4 (F)^{0.5}, \tag{3.8}$$

$$F = J_{L1} J_{G1} / (J_{L1} + J_{G1}), \tag{3.9}$$

$a_1 = 0.2088$; $a_2 = -0.2541$; $a_3 = 0.3928$, (3.10)

and

$b_1 = -3.0662$; $b_2 = -0.4052$; $b_3 = -1.0381$; $b_4 = 2.7228$. (3.11)

Care must be taken that all the superficial velocities in Equations (3.7) to (3.9) are in ft/sec. For given inlet conditions (J_{G1} and J_{L1}), values of F, a, and b can be easily determined. Then, for each J_{G3}, Equation (3.6) can be executed to determine the corresponding J_{L3}. Values of F_{BG} and F_{BL} can then be determined from

$$F_{BG} = W_{G3} / W_{G1} = (J_{G3} / J_{G1}) (D_3 / D_1)^2, \quad (3.12)$$

and

$$F_{BL} = W_{L3} / W_{L1} = (J_{L3} / J_{L1}) (D_3 / D_1)^2. \quad (3.13)$$

It should be noted that the correlation given by Equations (3.6) to (3.11) is independent of fluid properties and system pressure. As well, Hong and Griston (1995) did not specify any particular flow regime for their correlation and therefore, it is understood to be flow-regime independent. It should also be noted that the correlation was not developed in a way that ensures "symmetry of prediction". "Symmetry of prediction" is essential for the mass balance to be satisfied (again, see Chapter 1 for more details on the special use of the term "symmetry of prediction" where Figures 1.2(b) and 1.2(c) are discussed). An examination of the correlating Equations (3.6) to (3.13) would reveal a lack of the required "symmetry of prediction". Consider the following specific case for J_{G1} = 9.14 m/s, J_{L1} = 0.03 m/s, and D_3/D_1 = 1. At F_{BG} = 0.1, Equations (3.6) to (3.13) predict F_{BL} = 0.08. At F_{BG} = 1 - 0.1 = 0.9, Equations (3.6) to (3.13) predict F_{BL} = 0.822. These predicted values of F_{BL} add up to 0.902 whereas, of course, to satisfy mass balance, they should add up to 1. Even though the correlation does not satisfy the mass

balance, its predictions were compared against the data base to see how well it works relative to the other models and correlations.

3.1.3 Ottens et al. (1995) Model

Ottens et al. (1995) developed an analytical model to predict the phase distribution at horizontal impacting tees. Their model is based on the double-stream model of Hart et al. (1991) which was developed for dividing branching junctions and for liquid hold-up less than 0.06 in the inlet. The double-stream model was derived from the steady-state macroscopic mechanical energy balance (extended Bernoulli Equation) applied to the inlet-to-run stream and the inlet-to-branch stream of both gas and liquid phases. According to the double-stream model, the value of F_{BL} is a function of the value of F_{BG}, geometry of the junction, and the ratio κ defined as the ratio of the kinetic energies of the gas and liquid per unit volume in the inlet. Ottens et al. (1995) discarded some of the assumptions assumed earlier by Hart et al. (1991) in order to develop their own model which was called the advanced double-stream model that can work over the whole range of liquid hold-up in the inlet, from 0 to 1. Ottens et al. (1995) compared the predictions of the double-stream model and the advanced double-stream model against their experimental data. Comparison revealed that there was a satisfactory agreement between the experimental data and the double-stream model predictions. Also, the advanced double-stream model did not result in a significant improvement of the agreement between the experimental data and the prediction. In the present study, we shall focus only on the double-stream model. For given inlet conditions (J_{GI} and J_{LI}), fluid properties (ρ_G, ρ_L, μ_G, and μ_L), and junction geometry (D_I), the value of F_{BG} at a certain value for F_{BL} can be determined using the following set of equations:

$$Re_{SLI} = \rho_L J_{LI} D_I / \mu_L, \tag{3.14}$$

$$\varepsilon_{LI} = ((1 / [(J_{LI} / J_{GI}){1+10.4 (Re_{SLI})^{-0.363} (\rho_L / \rho_G)^{0.5}}]) + 1)^{-1}, \tag{3.15}$$

$$\alpha_I = 1 - \varepsilon_{LI}, \tag{3.16}$$

$$V_{GI} = J_{GI} / \alpha_I, \tag{3.17}$$

$$V_{LI} = J_{LI} / \varepsilon_{LI}, \tag{3.18}$$

$$\theta_{LI} = 0.52 \ (\varepsilon_{LI})^{0.374} + 0.26 \{ J_{LI}^2 \rho_L / \varepsilon_{LI}^2 g D_I (\rho_L - \rho_G) \}^{0.58}, \tag{3.19}$$

$$Re_{LI} = Re_{SLI} / \theta_{LI}, \tag{3.20}$$

$$Re_{GI} = \rho_G D_I V_{GI} / \mu_G, \tag{3.21}$$

$$\left.\begin{array}{l} \beta_G = 1.54 \text{ if } Re_{GI} < 1500, \\ \beta_L = 1.54 \text{ if } Re_{LI} < 1500, \\ \beta_G = 1.54 - 0.54 [(Re_{GI} - 1500) / 500] \text{ if } 1500 < Re_{GI} < 2000, \\ \beta_L = 1.54 - 0.54 [(Re_{LI} - 1500) / 500] \text{ if } 1500 < Re_{LI} < 2000, \\ \beta_G = 1.0 \text{ if } Re_{GI} > 2000, \\ \beta_L = 1.0 \text{ if } Re_{LI} > 2000, \end{array}\right\} \tag{3.22}$$

$$\kappa = \beta_G \rho_G V_{GI}^2 / (\beta_L \rho_L V_{LI}^2), \tag{3.23}$$

$$\lambda_0 = 0.5 (1 + k_{12} - k_{13}) = 0.5 \text{ (on average)}, \tag{3.24}$$

and

$$F_{BL} = \lambda_0 + \kappa (F_{BG} - \lambda_0), \tag{3.25}$$

where,

Re_{SLI} is the superficial Reynolds number of the liquid in the inlet,

ε_{LI} is the liquid hold-up in the inlet,

α_I is the void fraction in the inlet,

V_{GI} and V_{LI} are the average inlet velocities of the gas and liquid, respectively,

θ_{LI} is the fraction of the pipe wall wetted by the liquid in the inlet,

Re_{GI} and Re_{LI} are the inlet Reynolds numbers for the gas and liquid, respectively,

β_G and β_L are constants dependent on the velocity distribution of the corresponding phase,

λ_0 is the junction energy dissipation factor, and

k_{12} and k_{13} are frictional loss coefficients between the inlet and outlets 2 and 3, respectively.

It should be noted that the Ottens et al. (1995) model is independent of the inlet flow regime. Also, with a value of 0.5 for λ_0 Equation (3.25) would be a straight-line equation.

3.1.4 Hwang (1986) Model

Hwang (1986) developed an analytical model for predicting the phase distribution at horizontal impacting tees (the model is also reported in Hwang et al., 1989). The model is claimed to work for all the flow regimes and is based on the dividing-streamline approach. That is, a " zone of influence" exists for each phase and that each "zone of influence" is bounded by a dividing streamline, as shown in Figure 3.1. In Figure 3.1, all liquid entering the inlet of the junction on the R.H.S. of the liquid dividing streamline, line (**b**) in Figure 3.1, will exit through outlet 3 of the junction and the remaining liquid will exit through outlet 2. The gas phase behaves in a similar manner with its split between outlets 2 and 3 defined by the gas dividing streamline, line (**a**) in Figure 3.1. Figure 3.2 shows the dominant forces acting on the gas and liquid for a typical junction with streamlines crossing with an angle β. In Figure 3.2, V_{GI} and V_{LI} are the average

velocities of the gas and liquid phases, respectively, F_{DG} and F_{DL} are the drag forces generated due to the phasic slip and acting on the gas and liquid, respectively, R_G and R_L are the radii of curvature of the gas and liquid streamlines, respectively, ρ_G and ρ_L are the gas and liquid densities, respectively, and

($\rho_G V_{GI}^2 / R_G$) and ($\rho_L V_{LI}^2 / R_L$) are the centrifugal forces acting on the gas and liquid, respectively, in normal directions to their streamlines. The procedure for executing the model can be divided up into three distinct parts:

1- To calculate the value of the slip ratio, $S = V_{GI} / V_{LI}$.

2- To solve for δ_G and the corresponding δ_L, with reference to Figure 3.1.

3- To convert values of δ_G and δ_L to values of F_{BG} and F_{BL}.

Hwang (1986) compared the model predictions against his experimental data and the data of Azzopardi et al. (1986). Comparisons revealed that model predictions are quite satisfactory. It should be mentioned that, the first and the third parts of the procedure are dependent on the flow regime, while the second one is common for all the flow regimes. In the present study, the drift-flux model was used for the first part of the procedure for bubbly and plug flow regimes while the seventh law was used for the third part for the same flow regimes. For wavy and annular flow regimes, the physical and geometrical models given in Shoham et al. (1987) were used for the first and third parts of the procedure. The models used for annular and bubbly flow regimes were also used for annular-mist and bubbly-stratified flow regimes, respectively. These models are given in details in Appendix A. As there are no available geometrical or physical models for the slug flow regime, the Hwang (1986) model was not compared against the data that correspond to the slug flow regime. The inlet conditions (J_{GI} and J_{LI}), fluid properties

(ρ_G, ρ_L, μ_G, and μ_L), junction geometry (D_1 and D_3), and the inlet flow regime, are required as input data for the model. The following steps demonstrate how the model was executed:

(1) Using models given in Appendix A, the value of the slip ratio, S, can be determined.

(2) Initiate a value for (b_G/D_1) that may be from 0 to 1; usually a value of 0.05 is recommended as a start.

(3) Calculate (R_G/D_3)$_{min}$, (R_L/D_3)$_{min}$, and R_G/D_3 from

$$(R_G/D_3)_{min} = [1+ (2 D_1/D_3)^2]^{3/2} / (2 D_1/D_3) = (R_L/D_3)_{min}, \quad (3.26)$$

$$R_G/D_3 = (R_G/D_3)_{min} / (b_G/D_1)^N, \quad (3.27)$$

where, N is an empirical coefficient and is equal to 5.

(4) Solve for the value of m_G iteratively from

$$R_G/D_3 = [1+ (m_G b_G / D_3)^2]^{3/2} / [m_G (m_G-1) b_G / D_3] \quad (3.28)$$

where, m_G is a coefficient that has a value between 1 and 2 and is related to the shape of the gas dividing streamline.

(5) Calculate γ_{min} and γ_{max} from

$$\gamma_{min} = \cos^{-1}(1/S), \quad (3.29)$$

and

$$\gamma_{max} = \pi = 3.14159. \quad (3.30)$$

(6) Assume a value for γ between γ_{min} and γ_{max}.

(7) Calculate β, R_L/R_G, R_L/D_3, and b_L/D_1 from

$$\beta = \gamma - \cos^{-1}(S \cos (\gamma)), \quad (3.31)$$

$$R_L/R_G = \{ [\cos (\beta) - \sin (\beta) / \tan(\gamma)] / [\rho_G S^2/\rho_L] \}, \quad (3.32)$$

$$R_L/D_3 = (R_L/R_G) (R_G/D_3), \quad (3.33)$$

and

$$b_L/D_1 = [\ (\ R_L/D_3\ )_{min} / (\ R_L/D_3\ )\ ]^{1/N}. \tag{3.34}$$

(8) Solve for the value of m_L iteratively from

$$R_L/D_3 = [\ 1 + (\ m_L\ b_L/D_3\ )^2\ ]^{3/2} / [m_L\ (\ m_L\text{-}1\ )\ b_L/D_3]. \tag{3.35}$$

where, m_L is a coefficient that has a value between 1 and 2 and is related to the shape of the liquid dividing streamline.

(9) Calculate b_L/D_1 from

$$b_L/D_1 = \tan [\ \tan^{-1}(\ m_G\ b_G/D_3\ ) - \beta\ ]\ ((\ D_3/D_1\ )/m_L\ )\ ]. \tag{3.36}$$

(10) Compare b_L/D_1 calculated from step (9) with the one calculated from step (7). If agreement within acceptable tolerance is not achieved, the assumed value for γ in step (6) should be modified and steps (7) to (10) repeated until convergence is achieved.

(11) From the converged value of b_L/D_1 and the initiated value of b_G/D_1, calculate δ_L and δ_G from

$$\delta_L = (\ D_1/2\ )\ (\ (\ b_L/D_1\ ) + 1\ ), \tag{3.37}$$

and

$$\delta_G = [\ 1 + (\ b_G/D_1\ ) - (\ \delta_L/D_1\ )\ ]\ D_1. \tag{3.38}$$

(12) Using models given in Appendix A, and with the calculated values of δ_L and δ_G, values of F_{BG} and the corresponding F_{BL} can be determined.

(13) The value of b_G/D_1 initiated in step (2) was increased and the steps from (3) to (12) were repeated. The stopping criterion was that neither F_{BG} nor F_{BL} should exceed 1.0.

It should be mentioned that the Hwang (1986) model as described above generates

values of F_{BG} and F_{BL} within the range from 0.5 to 1. "Symmetry of prediction" was used in order to complete the curve.

3.2 Qualitative Assessment of Predicted Trends

The effects of J_{Ll}, J_{Gl}, and P_l on the prediction of each model/correlation were investigated in order to compare with the experimental trends seen in Chapter 2. This will help in judging whether a model or a correlation obeys the correct physics behind the phase distribution at horizontal impacting tees.

3.2.1 Chien and Rubel (1992) Correlation

Figure 3.3 shows the prediction of the Chien and Rubel (1992) correlation for air and water with constant J_{Gl} of 10 m/s, P_l of 1.0 bar, and J_{Ll} from 0.001 to 1.0 m/s. As can be seen from the figure, the correlation predictions rotate around the "point of 0.5" in a clockwise direction as J_{Ll} increases. This is consistent with what was found in Chapter 2. However, it would be expected that with a very wide range of J_{Ll} such as the one covered in Figure 3.3, the effect of J_{Ll} on the prediction would be more significant than what it is seen in Figure 3.3, especially as J_{Ll} has a strong effect on the phase distribution, as seen in Chapter 2. Figure 3.4 shows the prediction of the Chien and Rubel (1992) correlation for air and water with constant J_{Ll} of 0.05 m/s, P_l of 1.0 bar, and J_{Gl} from 0.1 to 100 m/s. As J_{Gl} increases, the prediction rotates around the "point of 0.5" in an anti-clockwise direction. This is consistent with the trend seen in Chapter 2. However, the predicted effect of J_{Gl} is not significant in spite of the wide range of J_{Gl} covered. Chien and Rubel (1992) formulated their correlation such that it is sensitive only to the inlet quality, x_l. However, in Figures 3.3 and 3.4, the predictions barely change even with the very high ranges of the inlet quality covered in these two figures.

Figure 3.5 shows the prediction of the Chien and Rubel (1992) correlation for air and water with constant J_{GI} of 10 m/s, constant J_{LI} of 0.05 m/s, and P_I ranging from 1.0 to 100 bar. It can be seen that as P_I increases, the predictions rotate around the "point of 0.5" in an anti-clockwise direction which is consistent with the trend seen in Chapter 2. However, the predictions do not change significantly with the inlet pressure. According to their experimental data, Chien and Rubel (1992) concluded that, the inlet pressure has a minor effect on the phase distribution (keeping in mind that their inlet pressure range was very small). That is why the correlation considers the inlet quality to be the only factor that effects the phase distribution, as discussed in Section 3.1.1 and therefore, the prediction does not change with the inlet pressure. It should be mentioned that, in Figures 3.3 to 3.5, values of J_{LI}, J_{GI}, and P_I tested correspond to values of the inlet quality and inlet pressure, that are outside the ranges recommended by the authors, namely 0.2 to 1.0 and 28.6 to 42.4 bar, respectively. This was done to fix the tested values of J_{GI}, J_{LI}, and P_I for all the models and correlations as will be seen in the following sections.

From Figures 3.3 to 3.5, the following trend can be seen in the prediction of the Chien and Rubel (1992) correlation for the tested values of J_{GI}, J_{LI}, and P_I:

- The effects of J_{LI}, J_{GI}, and P_I on the prediction are consistent with what was found in Chapter 2. However, J_{LI}, J_{GI}, and P_I have very small effects on the prediction and that is not consistent with the magnitudes seen in Chapter 2.

3.2.2 Hong and Griston (1995) Correlation

Figure 3.6 shows the prediction of the Hong and Griston (1995) correlation for air and water with constant J_{GI} of 10 m/s, P_I of 1.0 bar, and J_{LI} ranging from 0.001 to 1.0

m/s. It can be seen that "symmetry of prediction" is not satisfied and thus, mass balance is not obeyed. However, in Figure 3.6, as J_{LI} increases, the prediction rotates in a clockwise direction, which is the correct direction, as seen in Chapter 2. Figure 3.7 shows the prediction of the Hong and Griston (1995) correlation for air and water with constant J_{LI} of 0.05 m/s, P_I of 1.0 bar, and J_{GI} ranging from 0.1 to 100 m/s. It can be seen that the predicted effect of J_{GI} is very small over the range 1 to 100 m/s, but the small change appears to be in the wrong sense. Figure 3.8 shows the prediction of Hong and Griston (1995) correlation for air and water with constant J_{LI} of 0.05 m/s, J_{GI} of 10 m/s, and P_I ranging from 1.0 to 100 bar. It can be noted that the prediction does not change with the inlet pressure. This is not surprising as the correlation considers J_{GI} and J_{LI} to be the only factors that affect the phase distribution, as discussed in Section 3.1.2.

From Figures 3.6 to 3.8, three trends can be seen in the prediction of the Hong and Griston (1995) correlation:

- The correlation does not satisfy mass balance.
- The effect of J_{LI} on the prediction is consistent with what was found in Chapter 2, while the effect of J_{GI} on the prediction is not consistent with the trend seen in Chapter 2.
- The prediction does not change with the inlet pressure.

3.2.3 Ottens et al. (1995) Model

Figure 3.9 shows the prediction of the Ottens et al. (1995) model for air and water with constant J_{GI} of 10 m/s, P_I of 1.0 bar, and J_{LI} ranging from 0.001 to 1.0 m/s. It is very clear that, as J_{LI} increases, the prediction rotates around the "point of 0.5" in a clockwise direction. Also, with the highest J_{LI}, the prediction converges to a nearly

horizontal line passing through the "point of 0.5", while with the lowest J_{Ll}, the prediction converges to a nearly vertical line passing through the "point of 0.5". This is consistent with the trend seen in Chapter 2. Figure 3.10 shows the prediction of Ottens et al. (1995) model for air and water with constant J_{Ll} of 0.05 m/s, P_l of 1.0 bar, and J_{Gl} ranging from 0.1 to 100 m/s. In the figure, the prediction does not change as J_{Gl} increases from 0.1 to 10 m/s. As J_{Gl} increases from 10 to 100 m/s, the prediction rotates around the "point of 0.5" in a clockwise direction which is not consistent with the trend found in Chapter 2. Figures 3.9 and 3.10 imply that the value of J_{Ll} has a much stronger effect in the model formulation than the value of J_{Gl}. Figure 3.11 shows the prediction of Ottens et al. (1995) model for air and water with constant J_{Gl} of 10 m/s, constant J_{Ll} of 0.05 m/s, and P_l ranging from 1.0 to 100 bar. It can be seen that, as P_l increases from 1.0 to 10 bar, the prediction rotates around the "point of 0.5" in a clockwise direction, which is not consistent with the trend found in Chapter 2, while, as P_l increases from 10 to 100 bar, the prediction rotates around the "point of 0.5" in an anti-clockwise direction, which is consistent with the trend found in Chapter 2.

From Figures 3.9 to 3.11, two trends can be seen in the prediction of the Ottens et al. (1995) model:

- The effect of J_{Ll} on the prediction is very significant and consistent with what was found in Chapter 2, while the effect of J_{Gl} on the prediction is very weak and not consistent with the trend seen in Chapter 2.
- At inlet pressures, from 1.0 to 10 bar, the prediction changes with the inlet pressure in a trend which is not consistent with the trend seen in Chapter 2, while, at higher

inlet pressures, from 10 to 100 bar, the prediction changes with the inlet pressure in a trend which is consistent with the trend seen in Chapter 2.

3.2.4 Hwang (1986) Model

Figure 3.12 shows the prediction of Hwang (1986) model for air and water with constant J_{GI} of 10 m/s, P_I of 1.0 bar, and J_{LI} ranging from 0.001 to 1.0 m/s. The corresponding inlet flow regimes are given in the figure as the model is dependent on the inlet flow regime. It is very clear that, as J_{LI} increases, the prediction rotates around the "point of 0.5" in a clockwise direction. This is consistent with the trend seen in Chapter 2. It should be mentioned that in Figure 3.12, when values of J_{GI} and J_{LI} corresponded to the slug flow regime according to the Mandhane et al. (1973) flow-regime map, the model was executed assuming a wavy flow regime as the model can not be executed for the slug flow regime. Figure 3.13 shows the prediction of Hwang (1986) model for air and water with constant J_{LI} of 0.05 m/s, P_I of 1.0 bar, and J_{GI} ranging from 0.1 to 100 m/s. The corresponding flow regimes are given in the figure. It can be seen that as J_{GI} increases from 0.1 to 10 m/s, the prediction rotates around the "point of 0.5" in an anti-clockwise direction. This trend is consistent with the trend found in Chapter 2. The two flow regimes encountered when J_{GI} increases from 0.1 to 10 m/s are stratified and wavy, which are close to each other in appearance. When J_{GI} increases from 10 to 100 m/s, the prediction rotates around the "point of 0.5" in a clockwise direction which is not consistent with the trend found in Chapter 2. A possible reason for this inconsistency might be that, as J_{GI} increases from 10 to 100 m/s, the flow regime changes from wavy to annular and these two flow regimes are completely different in structure from each other. In order to verify that reason, the code was executed with the

same value of J_{GI}=100 m/s without changing the flow regime, i.e. assuming that the flow regime is wavy. It can be seen from Figure 3.13 that the prediction in this case is in the correct position according to the trend found in Chapter 2. Figure 3.14 shows the prediction of the Hwang (1986) model for air and water with constant J_{LI} of 0.05 m/s, J_{GI} of 10 m/s, and P_I ranging from 1.0 to 100 bar. The corresponding flow regime is indicated in the figure. It can be seen that as P_I increases, the prediction rotates around the "point of 0.5" in an anti-clockwise direction. This is consistent with the trend seen in Chapter 2.

From Figures 3.12 to 3.14, the trend seen in the prediction of the Hwang (1986) model can be summarized as follow:

- The effects of J_{LI}, J_{GI}, and P_I on the prediction are significant and consistent with what was found in Chapter 2.

From Figures 3.3 to 3.14, it is clear that, Hwang (1986) model is the only model capable of predicting consistent effects of J_{LI}, J_{GI}, and P_I with the effects seen in Chapter 2.

3.3 Quantitative Assessment of Predicted Values

Predictions from each model/correlation were compared against a data set base covering a wide range of operating conditions. Results of these comparisons are presented later in graphical and tabulated formats.

3.3.1 Data Sets

The work of different researchers was arranged in the form of numbered data sets so that it would be easy to refer to later on. A data set consists of data points with different values of F_{BL} and F_{BG} for the same inlet conditions. These inlet conditions include J_{GI},

J_{Ll}, P_l, T_l, and D_l. Tables 3.1 to 3.6 give all the available data sets for horizontal impacting tee junctions. Chien and Rubel (1992) tested wet steam through a 49.3-mm I.D. junction at P_l = 28.6 and 42.4 bar, and T_l = saturation temperature. Fujii et al. (1995) tested nitrogen and water through a 10-mm I.D. junction at atmospheric pressure and room temperature. Fujii et al. (1996) tested air and water through a 10.5-mm I.D. junction at atmospheric pressure and room temperature. Hong and Griston (1995) tested air and water through a 19-mm I.D. junction at atmospheric pressure and room temperature. Hwang (1986) tested air and water through a 38-mm I.D. junction at P_l = 1.3 to 1.9 bar and room temperature. Ottens et al. (1995) tested air and water through a 29.5-mm I.D. junction at atmospheric pressure and room temperature. It should be mentioned that for all the given data sets, the range of F_{BL} and F_{BG} covered was from 0 to 1 except for Chien and Rubel (1992) who covered a range from 0.2 to 0.8. It should also be mentioned that the flow regimes in Tables 3.1 to 3.6 are based on either visual observation or the Mandhane et al. (1974) flow-regime map.

Data Set	Flow Regime	P_l (bar)	J_{Gl} (m/s)	J_{Ll} (m/s)
CR-1	Annular	28.6	12.2	0.788
CR-2	Annular	28.6	12.2	0.328
CR-3	Annular	28.6	12.2	0.158
CR-4	Annular	28.6	12.2	0.082
CR-5	Annular	28.6	18.3	1.18
CR-6	Annular	28.6	18.3	0.472
CR-7	Annular	28.6	18.3	0.218
CR-8	Annular	28.6	18.3	0.089
CR-9	Annular	28.6	24.4	1.49
CR-10	Annular	28.6	24.4	0.603
CR-11	Annular	28.6	24.4	0.279
CR-12	Annular	28.6	24.4	0.118
CR-13	Annular	28.6	33.5	1.73
CR-14	Annular	28.6	33.5	0.829

"continued"

CR-15	Annular	28.6	33.5	0.384
CR-16	Annular	28.6	33.5	0.144
CR-17	Annular	42.4	15.2	3.16
CR-18	Annular	42.4	15.2	1.58
CR-19	Annular	42.4	15.2	1.05
CR-20	Annular	42.4	15.2	0.790

Table 3.1 Chien and Rubel (1992) data sets for wet steam, T_l= saturation temperature, and D_l= 49.3 mm.

Data Set	Flow Regime	J_{G1} (m/s)	J_{L1} (m/s)
F1-1	Annular	2.0	0.2
F1-2	Annular	4.0	0.2
F1-3	Annular	6.0	0.2
F1-4	Annular	12.0	0.05
F1-5	Annular	12.0	0.15
F1-6	Annular	12.0	0.3
F1-7	Annular	12.0	0.5
F1-8	Plug	0.03	0.5
F1-9	Plug	0.09	0.5
F1-10	Plug	0.17	0.5
F1-11	Plug	0.46	0.5
F1-12	Plug	0.03	0.2
F1-13	Plug	0.1	0.2
F1-14	Plug	0.2	0.2
F1-15	Plug	0.4	0.2
F1-16	Slug	0.96	0.5
F1-17	Slug	1.25	0.5
F1-18	Slug	2.34	0.5

Table 3.2 Fujii et al. (1995) data sets for nitrogen and water, P_l= atmospheric pressure, T_l= room temperature, and D_l=10 mm.

Data Set	Flow Regime	J_{G1} (m/s)	J_{L1} (m/s)
F2-1	Annular	7.0	0.5
F2-2	Plug	0.1	0.5

Table 3.3 Fujii et al. (1996) data sets for air and water, P_l= atmospheric pressure, T_l= room temperature, and D_l=10.5 mm.

Data Set	Flow Regime	J_{G1} (m/s)	J_{L1} (m/s)
HG-1	Wavy	4.57	0.046
HG-2	Wavy	9.14	0.092
HG-3	Annular	13.7	0.139
HG-4	Annular	18.3	0.185
HG-5	Annular	22.9	0.231
HG-6	Wavy	4.57	0.093
HG-7	Annular	9.14	0.187
HG-8	Annular	13.7	0.280
HG-9	Annular	18.3	0.373
HG-10	Annular	22.9	0.467
HG-11	Wavy	4.57	0.191
HG-12	Annular	9.14	0.381
HG-13	Annular	13.7	0.572
HG-14	Annular	18.3	0.762
HG-15	Annular	22.9	0.953
HG-16	Wavy	4.57	0.292
HG-17	Annular	9.14	0.584
HG-18	Annular	13.7	0.875
HG-19	Annular	18.3	1.17
HG-20	Annular	22.9	1.46

Table 3.4 Hong and Griston (1995) data sets for air and water, P_1= atmospheric pressure, T_1= room temperature, and D_1=19 mm.

Data Set	Flow Regime	Nominal P_1 (bar)	J_{G1} (m/s)	J_{L1} (m/s)
H-1	Bubbly	1.4	1.51	1.35
H-2	Bubbly	1.4	2.27	1.35
H-3	Bubbly	1.4	3.03	1.35
H-4	Bubbly	1.5	2.30	2.05
H-5	Bubbly	1.5	3.45	2.04
H-6	Bubbly	1.5	4.60	2.04
H-7	Bubbly	1.6	2.67	2.54
H-8	Bubbly	1.6	3.78	2.54
H-9	Bubbly	1.6	4.95	2.49

Table 3.5 Hwang (1986) data sets for air and water, T_1= room temperature, and D_1=38 mm.

Data Set	Flow Regime	J_{GI} (m/s)	J_{LI} (m/s)
O-1	Wavy	15.8	0.00063
O-2	Wavy	15.8	0.00302
O-3	Annular	15.8	0.012
O-4	Annular	15.8	0.03

Table 3.6 Ottens et al. (1995) data sets for air and water, P_I= atmospheric pressure, T_I= room temperature, and D_I=29.5 mm.

3.3.2 Deviation Parameters

When comparing the prediction of a certain model or a correlation against a certain data set, three deviation parameters were calculated to help in judging the quantitative performance of the model and comparing the different models with each other. These parameters are: the absolute root mean square, ARMS, the root mean square, RMS, and the arithmetic mean difference, AMD. They are defined as follow:

$$ARMS = \sqrt{\frac{\sum_{i=1}^{N} \left(y_{predicted} - y_{measured}\right)_i^2}{N}}, \tag{3.39}$$

$$RMS = \sqrt{\frac{\sum_{i=1}^{N} \left(\frac{y_{predicted} - y_{measured}}{y_{measured}}\right)_i^2}{N}} * 100, \tag{3.40}$$

and

$$AMD = \frac{\sum_{i=1}^{N} \left(y_{predicted} - y_{measured}\right)_i}{N}, \tag{3.41}$$

where, $y_{predicted}$ = F_{BL} predicted at a certain F_{BG},

$y_{measured}$ = F_{BL} measured at the same F_{BG}, and

N = number of data points in the data set.

3.3.3 Chien and Rubel (1992) Correlation

Predictions of the Chien and Rubel (1992) correlation were compared against their own data only as the correlation was limited by its authors to the pressure range of 28.6 to 42.4 bar, and such high pressures were not used in other data sets. Figures 3.15 to 3.34 show the prediction of Chien and Rubel (1992) correlation against their data. It will be noticed that in these figures, the predictions of other models and correlations are shown as well and will be commented on in later sections. The agreement between the predictions and the data is very good which is expected as the correlation was developed to fit these data. It should be mentioned that, the experimental data of Chien and Rubel (1992) cover narrow ranges of F_{BG} and F_{BL}, from 0.2 to 0.5 for most of the data sets and from 0.2 to 0.8 for only four data sets.

Table 3.7 shows the deviation parameters for Chien and Rubel (1995) correlation predictions against their own data sets. In the table, the small values of all the deviation parameters support the observation of good agreement between the prediction and the data which was seen in Figures 3.15 to 3.34.

Chien and Rubel (1992) correlation			
Data Set	**ARMS**	**RMS %**	**AMD**
CR-1	0.013	3.6	+ 0.003
CR-2	0.026	7.7	+ 0.024
CR-3	0.048	17	+ 0.038
CR-4	0.063	20.9	+ 0.054
CR-5	0.012	3.1	+ 0.007
CR-6	0.004	0.8	- 0.002
CR-7	0.034	6.8	- 0.029
CR-8	0.042	12.9	+ 0.039

"continued"

CR-9	0.043	10.7	- 0.043
CR-10	0.022	6.3	+ 0.020
CR-11	0.018	6.2	+ 0.016
CR-12	0.038	10.4	+ 0.036
CR-13	0.012	3.6	- 0.011
CR-14	0.048	12.4	- 0.012
CR-15	0.016	4.6	+ 0.001
CR-16	0.034	9.1	- 0.033
CR-17	0.012	2.8	- 0.008
CR-18	0.022	4.3	- 0.007
CR-19	0.036	7.2	- 0.014
CR-20	0.031	5.8	+ 0.017
Overall	0.031	8.59	+ 0.003

Table 3.7 Deviation parameters for Chien and Rubel (1992) correlation against their own data sets.

3.3.4 Hong and Griston (1995) Correlation

Figures 3.15 to 3.34 show the prediction of the Hong and Griston (1995) correlation against the data of Chien and Rubel (1992). It can be seen that for constant J_{GI}, as the value of J_{LI} decreases, or in other words as the inlet quality increases, the agreement between the prediction and the data gets better. Also, for low-inlet-quality data sets, the correlation does not work well for small values of F_{BG}, from 0 up to a variable value that might reach 0.05 in some cases. Actually, in some cases the correlation gives unrealistic negative values of F_{BL} for small values of F_{BG}.

Table 3.8 shows the deviation parameters for the Hong and Griston (1995) correlation prediction against all data sets. It should be mentioned that, in the table, the overall value of the RMS was calculated without taking the RMS value of data set O-1 into consideration. This was done as the RMS value for that data set is very large because of the distribution of the data points.

Hong and Griston (1995) Correlation			
Data Set	**ARMS**	**RMS %**	**AMD**
CR-1	0.074	23.5	+ 0.051
CR-2	0.093	30.4	+ 0.079
CR-3	0.093	34.2	+ 0.076
CR-4	0.055	18.6	+ 0.045
CR-5	0.074	22.3	+ 0.067
CR-6	0.068	21.2	+ 0.047
CR-7	0.057	17.6	+ 0.021
CR-8	0.043	14.0	+ 0.040
CR-9	0.053	14.9	+ 0.041
CR-10	0.086	28.6	+ 0.071
CR-11	0.091	31.6	+ 0.076
CR-12	0.063	19.5	+ 0.060
CR-13	0.094	26.9	+ 0.091
CR-14	0.042	11.2	+ 0.033
CR-15	0.067	19.9	+ 0.060
CR-16	0.019	5.60	+ 0.007
CR-17	0.083	22.0	+ 0.029
CR-18	0.111	24.5	- 0.019
CR-19	0.113	27.1	- 0.013
CR-20	0.030	8.50	+ 0.005
F1-1	0.098	393.5	+ 0.263
F1-2*	0.140	47.2	- 0.093
F1-3	0.206	91.6	+ 0.027
F1-4	0.131	41.2	- 0.114
F1-5	0.042	9.4	- 0.005
F1-6	0.038	14.0	- 0.012
F1-7	0.093	56.5	- 0.021
F1-8	0.324	87.7	- 0.312
F1-9*	1.376	276	- 0.745
F1-10*	2.152	486.9	- 0.978
F1-11*	0.392	83.7	- 0.229
F1-12	0.281	80.6	- 0.266
F1-13	1.503	567	+ 0.333
F1-14*	0.496	222	- 0.130
F1-15*	0.552	174.1	- 0.131
F1-16	1.108	328.6	- 0.473
F1-17*	0.270	43.5	- 0.120
F1-18	0.341	133.1	- 0.165
F2-1*	0.516	170.2	+ 0.123
F2-2*	0.328	80.3	- 0.303

"continued"

HG-1	0.089	37.7	- 0.058
HG-2	0.061	9.08	- 0.033
HG-3	0.032	7.47	- 0.021
HG-4	0.032	7.13	- 0.018
HG-5	0.040	6.95	- 0.017
HG-6	0.070	13.6	- 0.030
HG-7	0.029	5.90	- 0.013
HG-8	0.031	5.50	- 0.013
HG-9	0.037	6.22	- 0.022
HG-10	0.030	6.52	- 0.023
HG-11	0.028	6.41	- 0.012
HG-12	0.018	3.33	- 0.012
HG-13	0.025	4.46	- 0.018
HG-14	0.028	5.71	- 0.021
HG-15	0.033	6.04	- 0.017
HG-16	0.024	4.75	- 0.002
HG-17	0.018	3.37	- 0.015
HG-18	0.017	3.97	- 0.008
HG-19	0.030	5.34	- 0.005
HG-20	0.035	7.09	- 0.019
H-1*	0.274	58.4	- 0.225
H-2*	0.259	57.6	- 0.235
H-3*	0.249	68.4	- 0.226
H-4*	0.284	69.6	- 0.202
H-5*	0.236	63.9	- 0.100
H-6*	0.205	54.8	- 0.119
H-7	0.287	77.7	- 0.235
H-8*	0.284	76.9	- 0.201
H-9*	0.242	62.6	- 0.178
O-1	0.454	43796	- 0.320
O-2*	0.225	42.7	- 0.187
O-3	0.142	42.5	- 0.042
O-4	0.107	30.0	- 0.023
Overall	0.468	139.24	- 0.088

** see text*

Table 3.8 Deviation parameters for Hong and Griston (1995) correlation against all data sets.

It can be seen from the table that for Chien and Rubel (1992) data with constant J_{GI}, the data set that has the lowest J_{LI}, or the highest inlet quality, has the lowest deviation parameters. This is consistent with the observations from Figures 3.15 to 3.34 and it

occurred for all the values of J_{GI} except for J_{GI} = 24.4 m/s, where the data set that has the highest J_{LI} has the lowest deviation parameters (CR-9). However, it can be seen from Figures 3.23 to 3.26 that the correlation works better in case of the lowest J_{LI} (0.118 m/s), while in case of the highest J_{LI} (1.49 m/s) it predicts unrealistic results for small values of F_{BG}.

Figures 3.35 to 3.52 show the correlation prediction against the data of Fujii et al. (1995). In Figures 3.35 and 3.41, it is not clear that the correlation works better for higher inlet qualities but it is very clear that the correlation does not work for small values of F_{BG} (from 0 to 0.05), which is consistent with the observation from Figures 3.15 to 3.34 in the case of Chien and Rubel (1992) data. In Figures 3.42 to 3.52, it is very clear that the correlation does not work for the flow regimes encountered. These are plug and slug flow regimes. The slug flow regime is very turbulent in nature and it would be expected to be very hard to predict its behaviour. The fact that the correlation does not work for the plug flow regime might be attributed to the reason that the correlation was developed to fit data that corresponded to wavy and annular flow regimes. Annular and wavy flow regimes have higher values for J_{GI} than the plug flow regime. In Section 3.2.2, it was demonstrated that the Hong and Griston (1995) correlation is not capable of predicting the effect of J_{GI} correctly in terms of magnitude and trend.

Figures 3.53 and 3.54 show the correlation prediction against the data of Fujii et al. (1996). It can be seen that the correlation does not work for small values of F_{BG} (from 0 to 0.05) and for the plug flow regime which is consistent with the observations from Figures 3.42 to 3.49. In Table 3.8, the high values of the deviation parameters for data

set F1-1 support the fact that the correlation does not work for small values of F_{BG}. From Table 3.8, it is clear that for plug and slug flow regimes, the values of the deviation parameters are very high compared to the annular ones, which is consistent with the fact that the correlation does not work for these flow regimes. In Table 3.8, data sets of Fujii et al. (1995) and (1996) marked with asterisks are data sets that encounter infinite values for either the three deviation parameters or the RMS only. This occurred with some plug and slug data sets when the correlation does not work well and with two annular data sets that have a value of zero for F_{BL} which when divided by gives infinity. In order to get a value for the deviation parameters in these cases, the data points that encounter the infinite values were ignored.

Figures 3.55 to 3.74 show the correlation prediction against Hong and Griston (1995) data. In these figures, it is clear that there is a very good agreement between the prediction and the data. This is expected as the correlation was developed to fit these data. However, the fact that the correlation does not work for small values of F_{BG} (from 0 to 0.05) is observed in Figures 3.66 to 3.74. The good agreement between the prediction and the data of Hong and Griston (1995) are proved by the very small values of the three deviation parameters that are shown in Table 3.8.

Figures 3.75 to 3.83 show the correlation prediction against the data of Hwang (1986) for bubbly flow regime. It can be seen that, the correlation does not work for bubbly flow regime. This may be expected as the bubbly flow regime is very similar in nature to the plug flow regime for which the correlation does not work as seen in Figures 3.42 to 3.49. The reason the correlation does not work for the plug flow regime might be the same reason it does not work for the bubbly flow regime. The fact that the

correlation does not work for the data of Hwang (1986) is proved by the very high values of the deviation parameters shown in Table 3.8. In Table 3.8, the data sets of Hwang (1986) marked with asterisks are data sets with data points that encounter infinite values for the RMS and so these data points were ignored in order to get finite values for the RMS.

Figures 3.84 to 3.87 show the correlation prediction against the data of Ottens et al. (1995). It can be seen that, as the value of J_{LI} decreases, or in other words, as the inlet quality increases, the agreement between the prediction and the data gets worse. This is not consistent with the observation from Figures 3.15 to 3.34 in case of Chien and Rubel (1992) data. This inconsistency might be attributed to the difference in the fluid properties between the data of Chien and Rubel (1992) who tested wet steam and Ottens et al. (1995) who tested air and water.

From Table 3.8, it can be seen that, the lowest values for the deviation parameters correspond to the highest J_{LI}, lowest quality, which is consistent with the observation from Figures 3.84 to 3.87. It should be mentioned that, the huge value for the RMS for data set O-1 in Table 3.8 is a result of the data points distribution as for this data set, there are many data points with zero or close to zero F_{BL} values. When RMS is calculated, the difference between F_{BL} predicted and F_{BL} measured is divided by F_{BL} measured. So, with zero or close-to-zero F_{BL} values, the value of the RMS would be very high. Also, data set O-2 is marked with an asterisk as it has a datum point that has a value of zero for F_{BL}, which would result in an infinite value for the RMS. So, this datum point was ignored in order to get a value for the RMS.

From all the above-mentioned figures, two conclusions can be drawn regarding the Hong and Griston (1995) correlation:

- The correlation does not work for bubbly, plug, and slug inlet flow regimes.
- The correlation does not work for small values of F_{BG}, usually from 0 to 0.05.

3.3.5 Ottens et al. (1995) Model

Figures 3.15 to 3.34 show the predictions of the Ottens et al. (1995) model against the data of Chien and Rubel (1992). It is clear that, the agreement between the model predictions and the data for the case of wet steam with high inlet pressure is not satisfactory. It is very likely that the effect of the inlet pressure on the data is through its effect on the fluid properties. Even though the Ottens et al. (1995) model takes into consideration the fluid properties, the agreement between the model predictions and the data in Figures 3.15 to 3.34 is not good.

Table 3.9 shows the deviation parameters of the Ottens et al. (1995) model predictions for all data sets. Similar to what was done in Table 3.8, in Table 3.9, the overall value of the RMS was calculated without taking the RMS value of data set O-1 into consideration. In case of the Chien and Rubel (1992) data sets, values of the ARMS and AMD are quite small. This might be attributed to the fact that, there are only four data points against which the model prediction is compared for most of the Chien and Rubel (1992) data sets. This small number of data points might be a reason for the small values of the ARMS and AMD. Values of the RMS are in general quite high and this is consistent with the fact that the model does not work for Chien and Rubel (1992) data sets.

Ottens et al. (1995) Model			
Data Set	**ARMS**	**RMS %**	**AMD**
CR-1	0.117	37.2	+ 0.087
CR-2	0.125	41. 5	+ 0.102
CR-3	0.142	53.5	+ 0.107
CR-4	0.117	39.8	+ 0.094
CR-5	0.121	37.3	+ 0.103
CR-6	0.107	33.4	+ 0.077
CR-7	0.098	30.6	+ 0.046
CR-8	0.133	47.6	+ 0.108
CR-9	0.094	26.9	+ 0.063
CR-10	0.135	45.2	+ 0.111
CR-11	0.129	45.7	+ 0.103
CR-12	0.130	44.0	+ 0.112
CR-13	0.110	33.8	+ 0.087
CR-14	0.090	23.7	+ 0.079
CR-15	0.109	32.8	+ 0.092
CR-16	0.082	24.8	+ 0.053
CR-17	0.120	28.6	- 0.001
CR-18	0.140	34.9	- 0.005
CR-19	0.147	37.2	- 0.013
CR-20	0.108	32.0	+ 0.015
F1-1	0.030	7.4	+ 0.003
F1-2	0.083	19.1	- 0.053
F1-3	0.047	11.0	- 0.015
F1-4	0.089	32.7	- 0.044
F1-5	0.055	23.6	+ 0.031
F1-6	0.040	15.2	+ 0.015
F1-7	0.049	12.9	+ 0.010
F1-8	0.044	13.4	+ 0.028
F1-9	0.020	4.3	+ 0.001
F1-10	0.021	5.6	+ 0.012
F1-11	0.028	5.2	+ 0.001
F1-12	0.038	9.0	+ 0.015
F1-13	0.060	27.8	+ 0.039
F1-14	0.097	66.9	+ 0.072
F1-15	0.034	11.3	+ 0.004
F1-16	0.069	14.2	- 0.006
F1-17	0.106	12.0	- 0.041
F1-18	0.055	19.0	+ 0.021

"continued"

F2-1	0.055	21.7	+ 0.027
F2-2	0.074	27.3	+ 0.032
HG-1	0.060	89.0	0.0
HG-2	0.069	27. 3	+ 0.004
HG-3	0.031	9.1	+ 0.001
HG-4	0.028	6.5	- 0.001
HG-5	0.044	10.2	0.0
HG-6	0.077	29.5	+ 0.003
HG-7	0.027	6.8	+ 0.003
HG-8	0.034	7.7	+ 0.003
HG-9	0.041	8.6	- 0.003
HG-10	0.028	5.9	+ 0.001
HG-11	0.019	4.5	+ 0.001
HG-12	0.018	4.0	+ 0.002
HG-13	0.038	8.6	+ 0.005
HG-14	0.052	11.5	+ 0.006
HG-15	0.067	15.2	+ 0.004
HG-16	0.021	4.3	+ 0.002
HG-17	0.023	4.8	+ 0.002
HG-18	0.039	9.0	+ 0.012
HG-19	0.078	17.8	+ 0.003
HG-20	0.051	11.6	+ 0.009
H-1	0.145	27.5	- 0.034
H-2	0.121	15.5	- 0.064
H-3	0.066	9.5	- 0.029
H-4	0.167	21.1	- 0.066
H-5	0.038	7.4	- 0.003
H-6	0.124	15.0	- 0.056
H-7	0.164	28.2	- 0.051
H-8	0.070	15.2	- 0.010
H-9	0.131	17.5	- 0.057
O-1	0.260	257097	+ 0.150
O-2*	0.142	58.9	+ 0.126
O-3	0.067	14.0	+ 0.049
O-4	0.065	12.0	+ 0.036
Overall	0.085	27.7	+ 0.012

* *see text*

Table 3.9 Deviation parameters for Ottens et al. (1995) model against all data sets.

Figures 3.35 to 3.52 show the predictions of the Ottens et al. (1995) model against the data of Fujii et al. (1995). It can be seen that there is a good agreement between the predictions and the data for all the data sets. Also, the model is capable of predicting the data that corresponds to a slug inlet flow regime. In Table 3.9, data sets of Fujii et al. (1995) have small values for all the deviation parameters except for data sets F1-4, F1-13, and F-14 which have quite high values for the RMS. A reason for that might be that the data are somewhat scattered for these data sets, as shown in Figures 3.38, 3.47, and 3.48.

Figures 3.53 and 3.54 show the predictions of the Ottens et al. (1995) model against the data of Fujii et al. (1996). In these figures, good agreement is achieved between the data and the prediction. This is supported by the small values of the deviation parameters in Table 3.9 for the data sets of Fujii et al. (1996).

Figures 3.55 to 3.74 show the predictions of the Ottens et al. (1995) model against the data of Hong and Griston (1995). In these figures, there is a good agreement between the prediction and the data. Also, it can be seen that the model predictions generally take some average values of the data. That is why values of the AMD in Table 3.9 for Hong and Griston (1995) data sets are very small, zero in some cases. Values of the ARMS and RMS are very small as well except for data sets HG-1, HG-2, and HG-6 which have high values for the RMS. The fact that there are two groups of data points for these data sets, as shown in Figures 3.55, 3.56, and 3.60, might be a reason that these data sets have high values for the RMS.

Figures 3.75 to 3.83 show the predictions of the Ottens et al. (1995) model against the data of Hwang (1986). The fact that the number of data points given in some of the

Hwang (1986) data sets is small and that the data points are scattered in other data sets does not allow for a reliable comparison between the predictions and the data. However, it seems that the model is capable of predicting very low-inlet-quality data such as the data of Hwang (1986). This is supported by the small values of the deviation parameters in Table 3.9 for data sets of Hwang (1986).

Figures 3.84 to 3.87 show the predictions of the Ottens et al. (1995) model against the data of Ottens et al. (1995). In these figures, there is a good agreement between the predictions and the data in general. In Table 3.9, the huge value of the RMS for data set O-1 is due to the distribution of the data points. Also, data set O-2 is marked with an asterisk as it has a datum point that has a value of zero for F_{BL} (see Section 3.3.4 where data sets O-1 and O-2 are discussed).

From all the above-mentioned figures, two conclusions can be drawn regarding the Ottens et al. (1995) model:

- For low inlet pressures, at or near atmospheric, the model works for all types of inlet flow regimes with good agreement between the predictions and the data.
- The model does not work for high inlet pressures, much higher than atmospheric.

3.3.6 Hwang (1986) Model

Figures 3.15 to 3.34 show the predictions of the Hwang (1986) model against the data of Chien and Rubel (1992). In general, the agreement between the predictions and the data could not be termed good. However, the agreement is reasonably satisfactory for some data sets, Figures 3.25 and 3.26 as an example. In Figures 3.15 to 3.34, it can be seen that, the predictions of the Hwang (1986) model is in a better agreement with the data than the predictions of the Ottens et al. (1995) model. It should be mentioned that

both models take into consideration the fluid properties. Thus, both models are expected to predict the effect of the inlet pressure on the data correctly. However, both models, those of Hwang (1986) and Ottens et al. (1995), do not predict the high-inlet-pressure data with a satisfactory agreement.

Table 3.10 shows the deviation parameters of the Hwang (1986) model for all data sets. Similar to what was done in Tables 3.8 and 3.9, in Table 3.10, the overall value of the RMS was calculated without taking the RMS value of data set O-1 into consideration.

Hwang (1986) model			
Data Set	**ARMS**	**RMS %**	**AMD**
CR-1	0.086	27.4	+ 0.063
CR-2	0.090	29.7	+ 0.074
CR-3	0.103	38.7	+ 0.078
CR-4	0.090	30.5	+ 0.074
CR-5	0.086	19.6	+ 0.075
CR-6	0.069	21.5	+ 0.048
CR-7	0.059	17.7	+ 0.013
CR-8	0.083	28.8	+ 0.071
CR-9	0.059	16.7	+ 0.032
CR-10	0.092	30.7	+ 0.077
CR-11	0.081	28.5	+ 0.064
CR-12	0.076	24.9	+ 0.070
CR-13	0.072	22.1	+ 0.056
CR-14	0.051	13.5	+ 0.045
CR-15	0.057	17.0	+ 0.051
CR-16	0.025	7.2	+ 0.003
CR-17	0.090	21.1	- 0.002
CR-18	0.101	24.7	- 0.006
CR-19	0.102	25.1	- 0.013
CR-20	0.055	17.5	+ 0.015

"continued"

F1-1	0.031	6.9	- 0.012
F1-2	0.040	8.5	- 0.026
F1-3	0.017	5.0	+ 0.005
F1-4	0.204	145.0	+ 0.135
F1-5	0.129	52.9	+ 0.059
F1-6	0.075	27.1	+ 0.034
F1-7	0.052	13.8	+ 0.012
F1-8	0.031	8.5	+ 0.023
F1-9	0.013	2.9	0.0
F1-10	0.029	7.3	+ 0.016
F1-11	0.034	6.7	0.0
F1-12	0.065	17.5	+ 0.053
F1-13	0.109	49.6	+ 0.055
F1-14	0.147	105.1	+ 0.092
F1-15	0.080	30.9	+ 0.057
F1-16	NA	NA	NA
F1-17	NA	NA	NA
F1-18	NA	NA	NA
F2-1	0.066	25.2	+ 0.030
F2-2	0.060	21.9	+ 0.026
HG-1	0.049	24.3	0.0
HG-2	0.119	39.6	- 0.005
HG-3	0.064	17.6	+ 0.001
HG-4	0.041	9.4	- 0.001
HG-5	0.043	9.8	0.0
HG-6	0.062	23.1	- 0.004
HG-7	0.165	38.2	+ 0.005
HG-8	0.036	8.1	+ 0.003
HG-9	0.028	5.9	- 0.001
HG-10	0.009	1.9	+ 0.001
HG-11	0.042	10.1	+ 0.001
HG-12	0.017	3.8	+ 0.002
HG-13	0.023	5.3	+ 0.005
HG-14	0.029	6.5	+ 0.005
HG-15	0.043	9.8	+ 0.003
HG-16	0.021	4.7	+ 0.002
HG-17	0.014	3.0	+ 0.002
HG-18	0.021	5.1	+ 0.013
HG-19	0.054	12.4	+ 0.004
HG-20	0.022	5.3	+ 0.010

"continued"

H-1	0.112	14.9	- 0.041
H-2	0.072	9.1	- 0.037
H-3	0.035	5.3	- 0.017
H-4	0.111	12.0	- 0.048
H-5	0.019	3.7	+ 0.007
H-6	0.089	10.3	- 0.029
H-7	0.092	12. 2	- 0.035
H-8	0.026	5.2	- 0.013
H-9	0.082	10.0	- 0.035
O-1	0.270	234105.6	+ 0.144
O-2*	0.179	39.4	+ 0.108
O-3	0.085	19.1	+ 0.062
O-4	0.032	9.6	+ 0.018
Overall	0.085	30.96	+ 0.017

** see text*

Table 3.10 Deviation parameters for Hwang (1986) model against all data sets.

In Table 3.10, for Chien and Rubel (1992) data sets, the values of the deviation parameters are quite small except for some data sets for which the value of the RMS was around 30 %.

Figures 3.35 to 3.49 show the predictions of the Hwang (1986) model against the data of Fujii et al. (1995). In these figures, very good agreement is achieved between the predictions and the data. As discussed in Section 3.1.4, the model was not compared against slug-flow-regime data sets. In Table 3.10, values of the deviation parameters for Fujii et al. (1995) data sets are small which is consistent with the good agreement shown in the figures. Only two data sets, F1-4 and F1-14, have quite high values for the deviation parameters, especially for the RMS. This might be attributed to the fact that the data points are somewhat scattered in these data sets.

Figures 3.53 and 3.54 show the predictions of the Hwang (1986) model against the data of Fujii et al. (1996). Very good agreement is achieved between the data and the predictions which is supported by the small values of the deviation parameters for Fujii et al. (1996) data sets in Table 3.10.

Figures 3.55 to 3.74 show the predictions of the Hwang (1986) model against the data of Hong and Griston (1995). In these figures, the predictions of the Hwang (1986) model are in very good agreement with the data. Also, it can be seen that for most of the data sets of Hong and Griston (1995), the predictions of the Hwang (1986) model, the Ottens et al. (1995) model, and the Hong and Griston (1995) correlation collapse over most of the F_{BG} range. In Table 3.10, for Hong and Griston (1995) data sets, values of the deviation parameters are very small, which support observations from Figures 3.55 to 3.74.

Figures 3.75 to 3.83 show the predictions of the Hwang (1986) model against the data of Hwang (1986). These figures show a very good agreement between the predictions and the data which is supported by the very small values of the deviation parameters for Hwang (1986) data sets in Table 3.10.

Figures 3.84 to 3.87 show the predictions of the Hwang (1986) model against the data of Ottens et al. (1995). It can be seen that good agreement is achieved between the predictions and the data. Also, it can be seen that the predictions of the Hwang (1986) model and the Ottens et al. (1995) model are very close in Figures 3.84 to 3.86 while in Figure 3.87 the prediction of Hwang (1986) model predict the data somewhat more effectively.

From all the above-mentioned figures, two conclusions can be drawn regarding Hwang (1986) model:

- For low inlet pressures, at or near atmospheric, the model works for all types of inlet flow regimes, excepting the slug flow regime, with very good agreement between the predictions and the data.
- The model may work for high inlet pressures, much higher than atmospheric, with quite satisfactory agreement between the predictions and the data.

3.4 Recommended Models/Correlations

Based on the assessment of the models and correlations given in Sections 3.2 and 3.3, it is possible to recommend a model or a correlation that can best predict the phase distribution in horizontal impacting tees for certain inlet conditions. The independent parameters that affect phase distribution include D_1, D_2, D_3, J_{GI}, J_{LI}, and fluid properties. The recommendations are given in terms of only two parameters. They are the fluid properties and the inlet flow regime. It should be mentioned that the inlet flow regime is dependent on values of J_{GI} and J_{LI}. Values of D_1, D_2, D_3, J_{GI} and J_{LI} were not considered in giving the recommendations because of lack of the available data that cover wide ranges of these parameters. All the available data sets were classified according to the two parameters mentioned before into different categories. So, according to the fluid properties, the data base was classified into two categories, steam-water and air-water data. It should be mentioned that the data of Fujii et al. (1995) that were taken for nitrogen and water were included in the air-water-data category. This was done because air and nitrogen have very close properties. Under these two categories, the data were classified according to the inlet flow regime into sub-categories. For

steam-water data, there is only one available inlet flow regime, which is the annular flow regime while for air-water data, there are five inlet flow regimes available. These are the annular, bubbly, plug, slug, and wavy flow regimes. For each sub-category, the deviation parameters of all the models and correlations were calculated. The model or the correlation that has the lowest values of the deviation parameters is recommended for the corresponding sub-category.

Tables 3.11 and 3.12 show the deviation parameters of all the models and correlations for the sub-categories mentioned above. It should be mentioned that the Chien and Rubel (1992) correlation was not compared against the air-water data because of the low inlet pressures encountered, which are below the limits given by the authors of the correlation. It should also be mentioned that the stratified flow regime does not appear in Table 3.11 as there is no available data for that flow regime according to either

Flow Regime	Hong and Griston (1995) correlation			Hwang (1986) model			Ottens et al. (1995) model		
	ARMS	RMS%	AMD	ARMS	RMS%	AMD	ARMS	RMS%	AMD
Annular	0.125	85.1	-0.008	0.078	34.0	0.011	0.051	13.8	0.003
Bubbly	0.255	65.5	-0.181	0.076	9.5	-0.025	0.118	17.8	-0.039
Plug	0.939	282.8	-0.323	0.077	43.6	0.036	0.052	27.9	0.023
Slug	0.674	204.0	-0.249	NA	NA	NA	0.077	15.7	-0.005
Wavy	0.180	23.7	-0.080	0.125	27.5	0.025	0.113	49.4	0.031

Table 3.11 Deviation parameters of all the models and correlations for air-water data tabulated according to the flow regime.

Hong and Griston (1995) correlation			Hwang (1986) model			Ottens et al. (1995) model			Chien and Rubel (1992) correlation		
ARMS	RMS%	AMD	ARMS	RMS%	AMD	ARMS	RMS%	AMD	ARMS	RMS%	AMD
0.077	22.3	0.038	0.08	23.9	0.038	0.12	36.8	0.061	0.031	8.6	0.003

Table 3.12 Deviation parameters of all the models and correlations for steam-water data.

visual observation or the Mandhane et al. (1974) flow-regime map.

From Table 3.11, it is clear that the Ottens et al. (1995) model has the lowest deviation parameters for cases of annular, plug, and slug flow regimes, while the Hwang (1986) model has the lowest deviation parameters in case of bubbly flow regime. In the case of the wavy flow regime, it is not clear which model or correlation should be recommended as the Hong and Griston (1995) correlation has the lowest RMS, the Hwang (1986) model has the lowest AMD, and the Ottens et al. (1995) model has the lowest ARMS. However, it should be taken into consideration that the Hong and Griston (1995) correlation does not satisfy mass balance and does not work for small values of F_{BG}, as shown in Sections 3.1.2, 3.2.2, and 3.3.4. Also, for the wavy flow regime values of the ARMS and AMD of Hwang (1986) and Ottens et al. (1995) models are very close, while the RMS value of the Hwang (1986) model is considerably lower than that of the Ottens et al. (1995) model. Therefore, the Hwang (1986) model may be recommended for the wavy flow regime. It should be mentioned that in case of the wavy flow regime, values of RMS were calculated without taking the RMS values of data set O-1 into consideration. This was done as the RMS values for that data set are huge due to the distribution of the data points and not due to inefficient performance of the models

and correlations. In Table 3.12, it is very clear that the Chien and Rubel (1992) correlation has the lowest deviation parameters which is expected as the correlation was developed to fit the data shown in Table 3.12. Also, in Table 3.12, values of the deviation parameters for the Hong and Griston (1995) correlation and the Hwang (1986) model are very close and considerably lower than those of the Ottens et al. (1995) model.

Based on Tables 3.11 and 3.12, Table 3.13 shows the models and correlations recommended for different inlet conditions.

Inlet conditions		**Model(s) / Correlation(s)**
High Pressure Steam and Water (28.6-42.4 bar)		Chien and Rubel (1992) correlation
Air and Water	**Annular**	Ottens et al. (1995) model
	Bubbly	Hwang (1986) model
	Slug	Ottens et al. (1995) model
	Plug	Ottens et al. (1995) model
	Wavy	Hwang (1986) model

Table 3.13 Recommended models and correlations for the prediction of phase distribution in horizontal impacting tees.

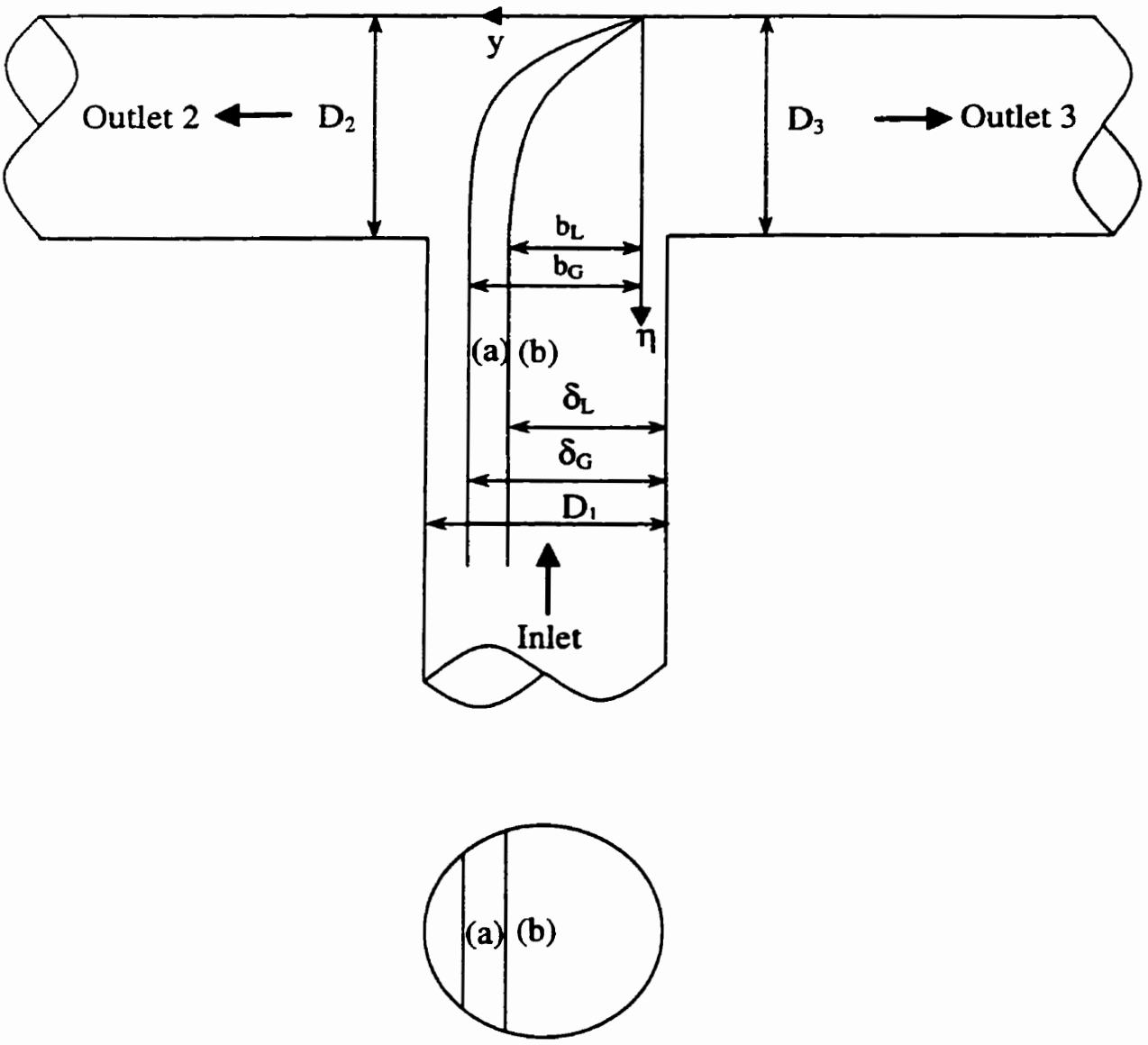

Figure 3.1 Zone of influence and the dividing streamline for the Hwang (1986) Model.

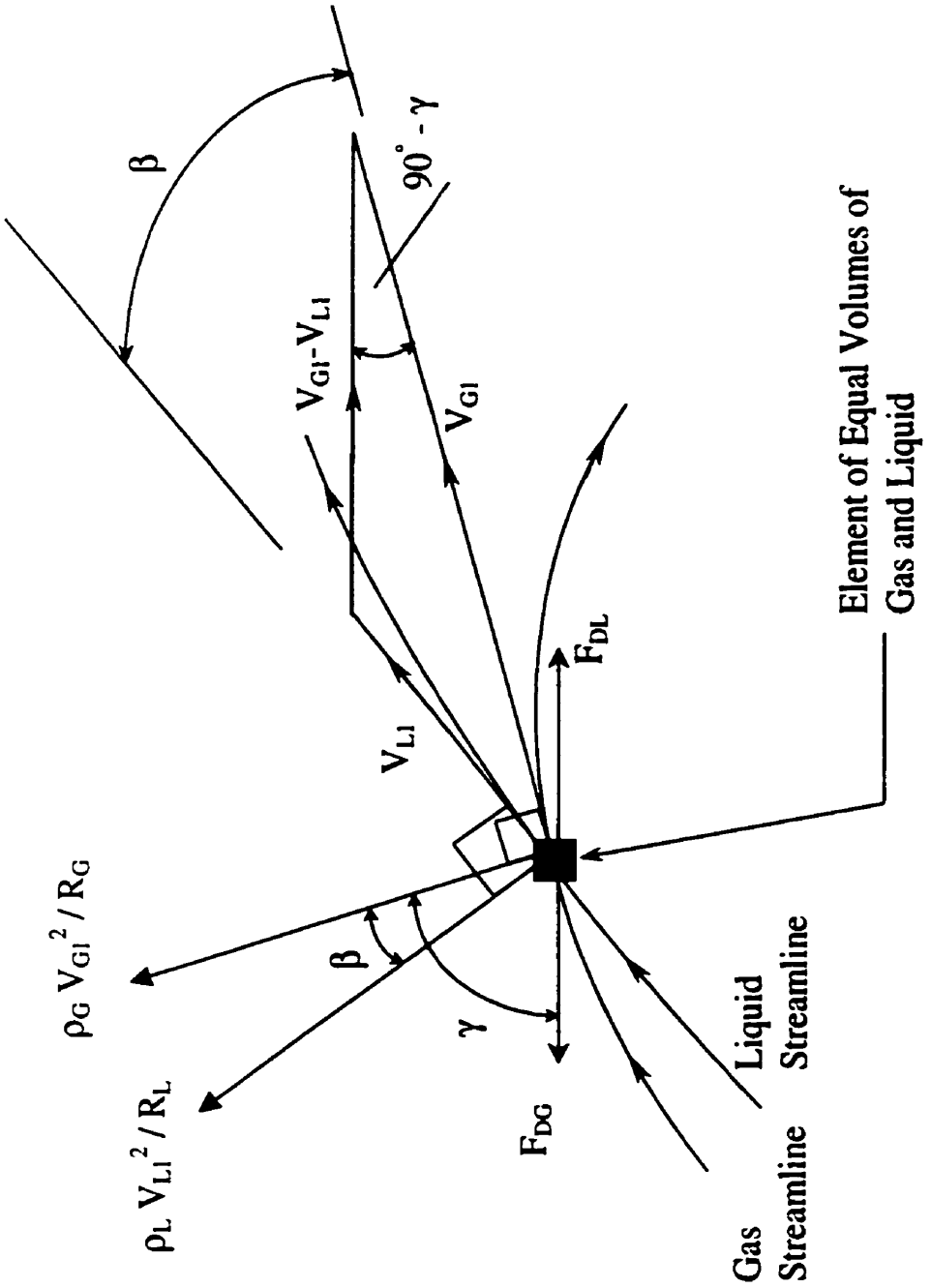

Figure 3.2 Balance of forces at a streamline crossing for the Hwang (1986) Model.

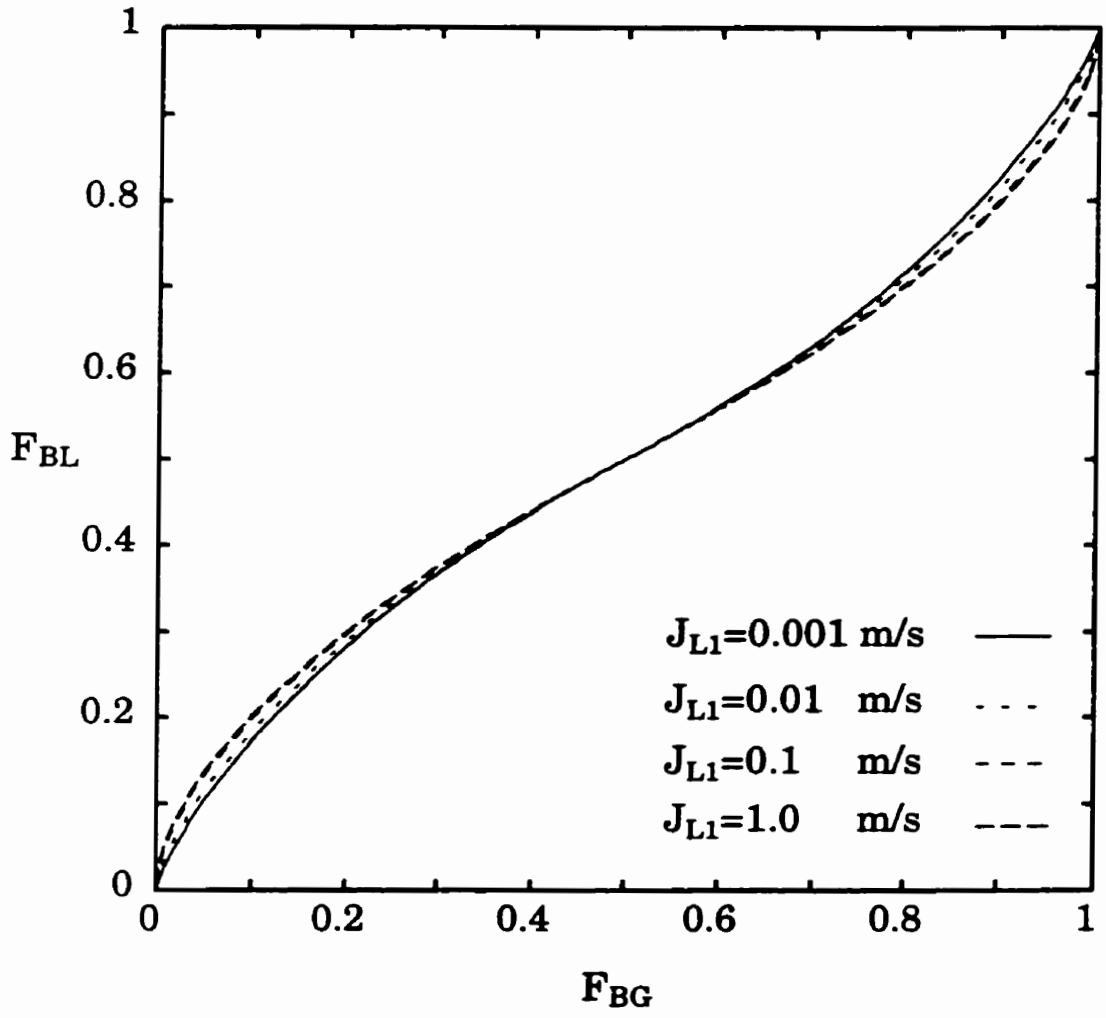

Figure 3.3 Effect of J_{L1} on the phase distribution as predicted by the Chien and Rubel (1992) correlation for J_{G1}=10 m/s and P_1= 1.0 bar.

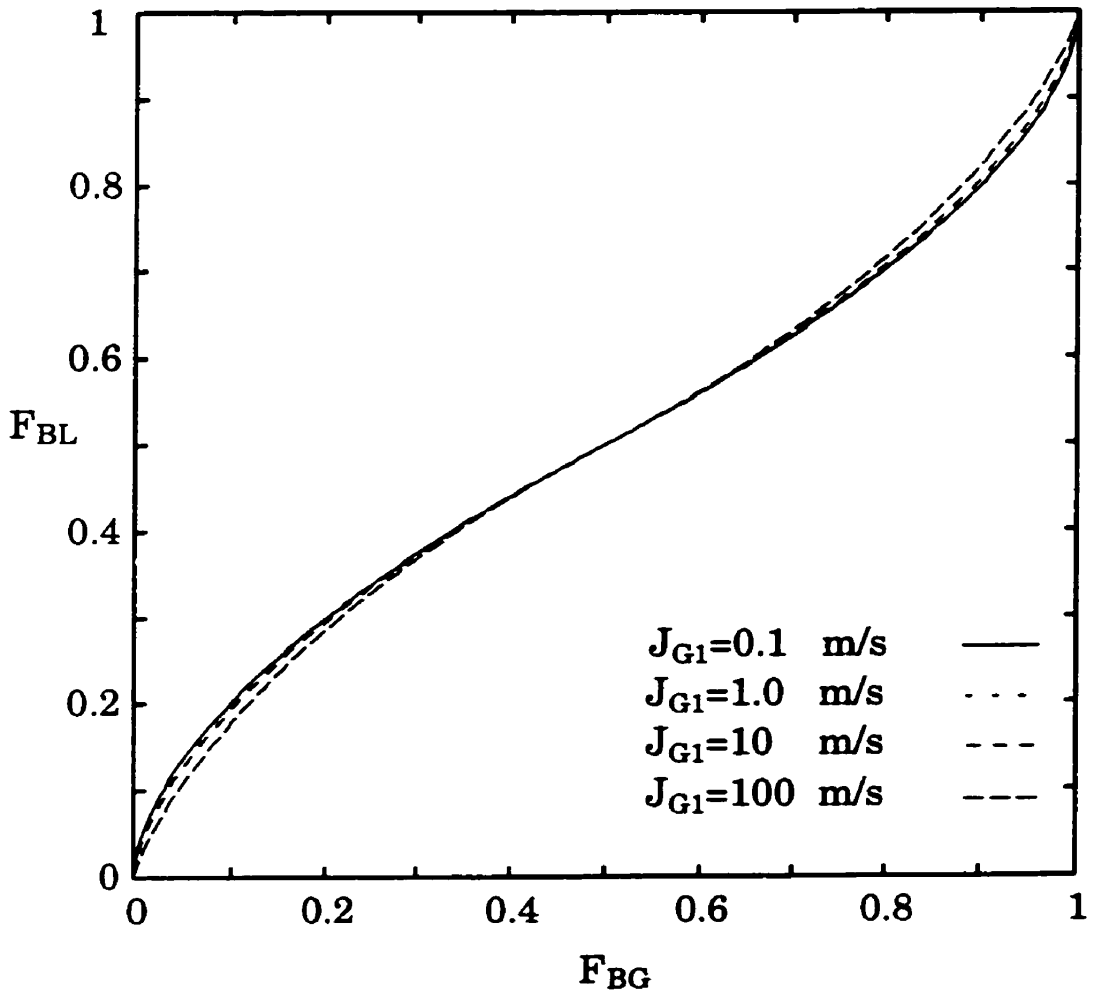

Figure 3.4 Effect of J_{G1} on the phase distribution as predicted by the Chien and Rubel (1992) correlation for J_{L1} =0.05 m/s and P_1= 1.0 bar.

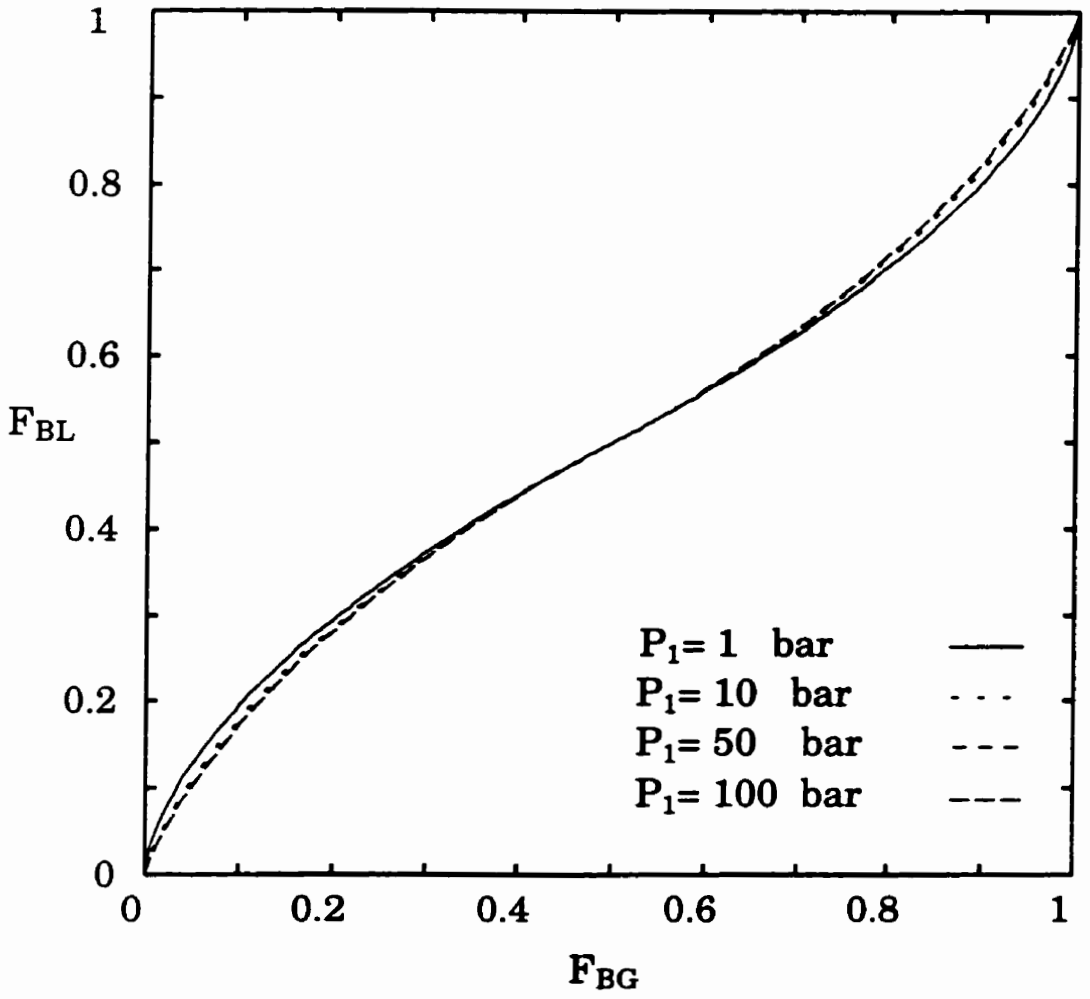

Figure 3.5 Effect of P_1 on the phase distribution as predicted by the Chien and Rubel (1992) correlation for J_{L1}= 0.05 m/s and J_{G1}=10 m/s.

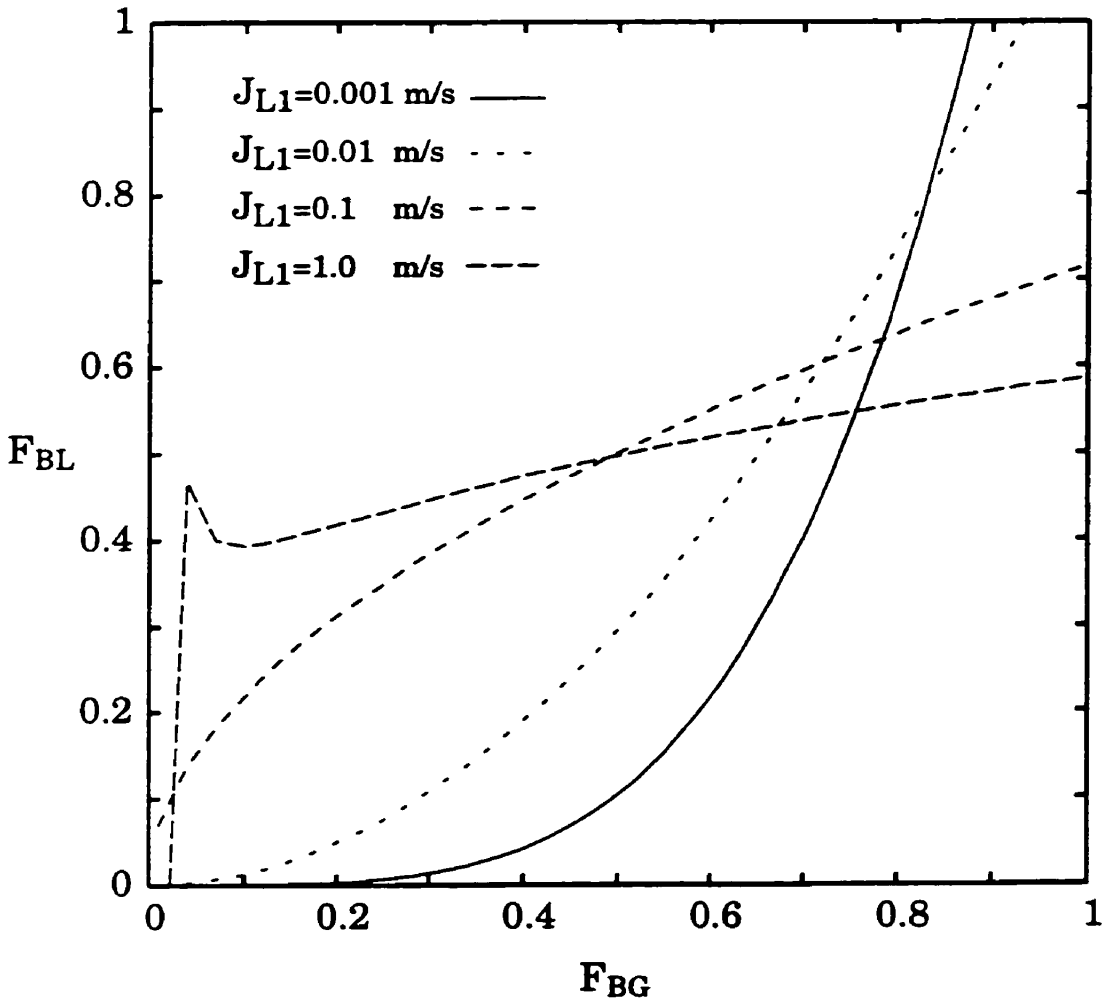

Figure 3.6 Effect of J_{L1} on the phase distribution as predicted by the Hong and Griston (1995) correlation for J_{G1} =10 m/s and P_1= 1.0 bar.

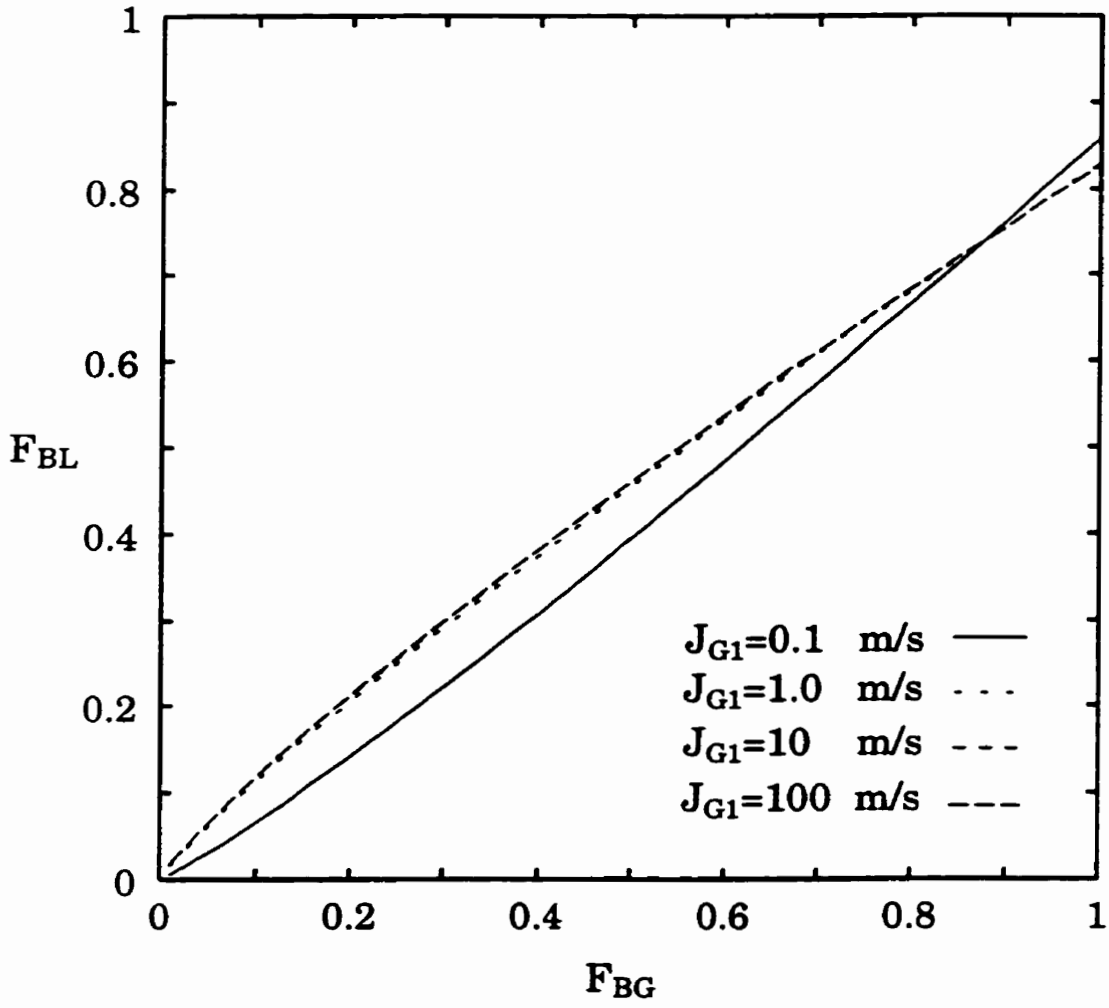

Figure 3.7 Effect of J_{G1} on the phase distribution as predicted by the Hong and Griston (1995) correlation for J_{L1}= 0.05 m/s and P_1= 1.0 bar.

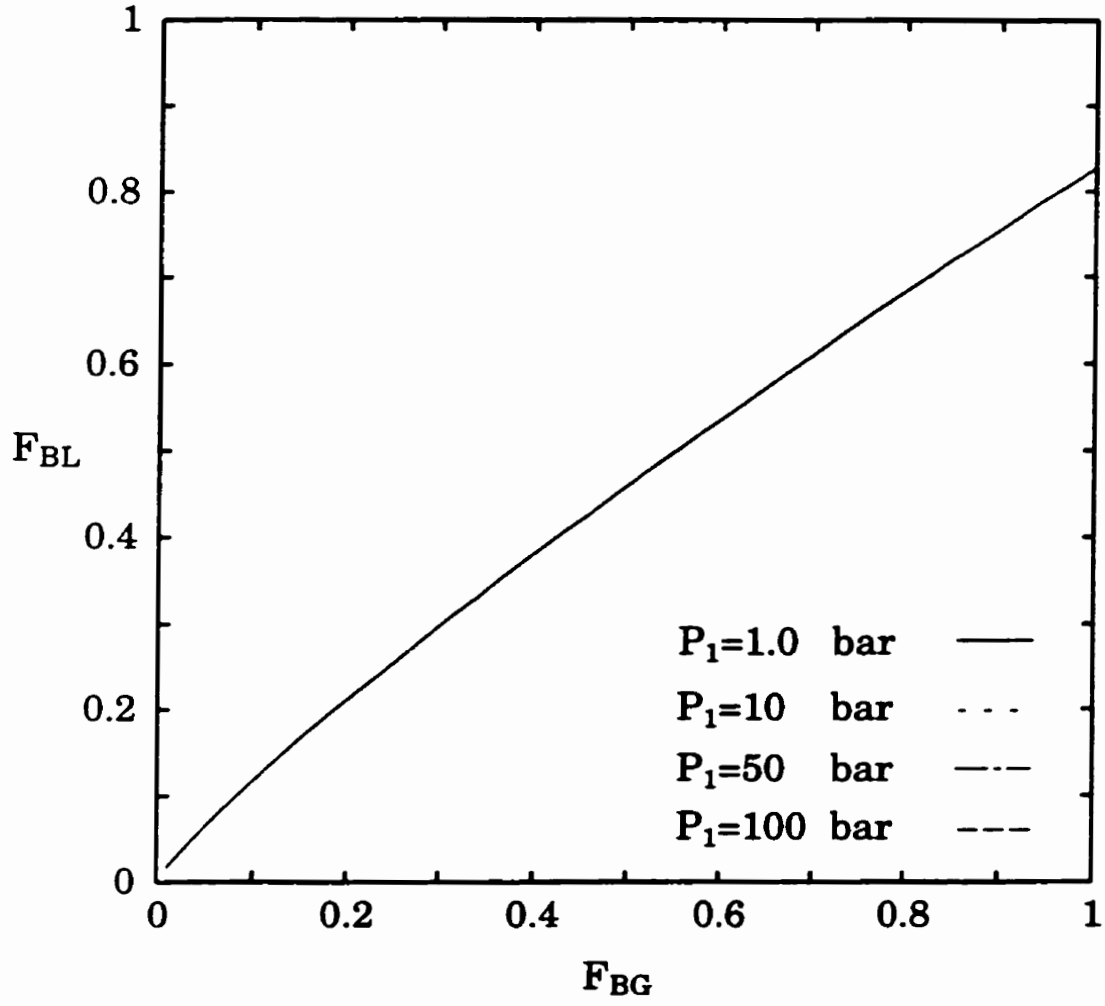

Figure 3.8 Effect of P_1 on the phase distribution as predicted by the Hong and Griston (1995) correlation for J_{L1}=0.05 m/s and J_{G1}=10 m/s.

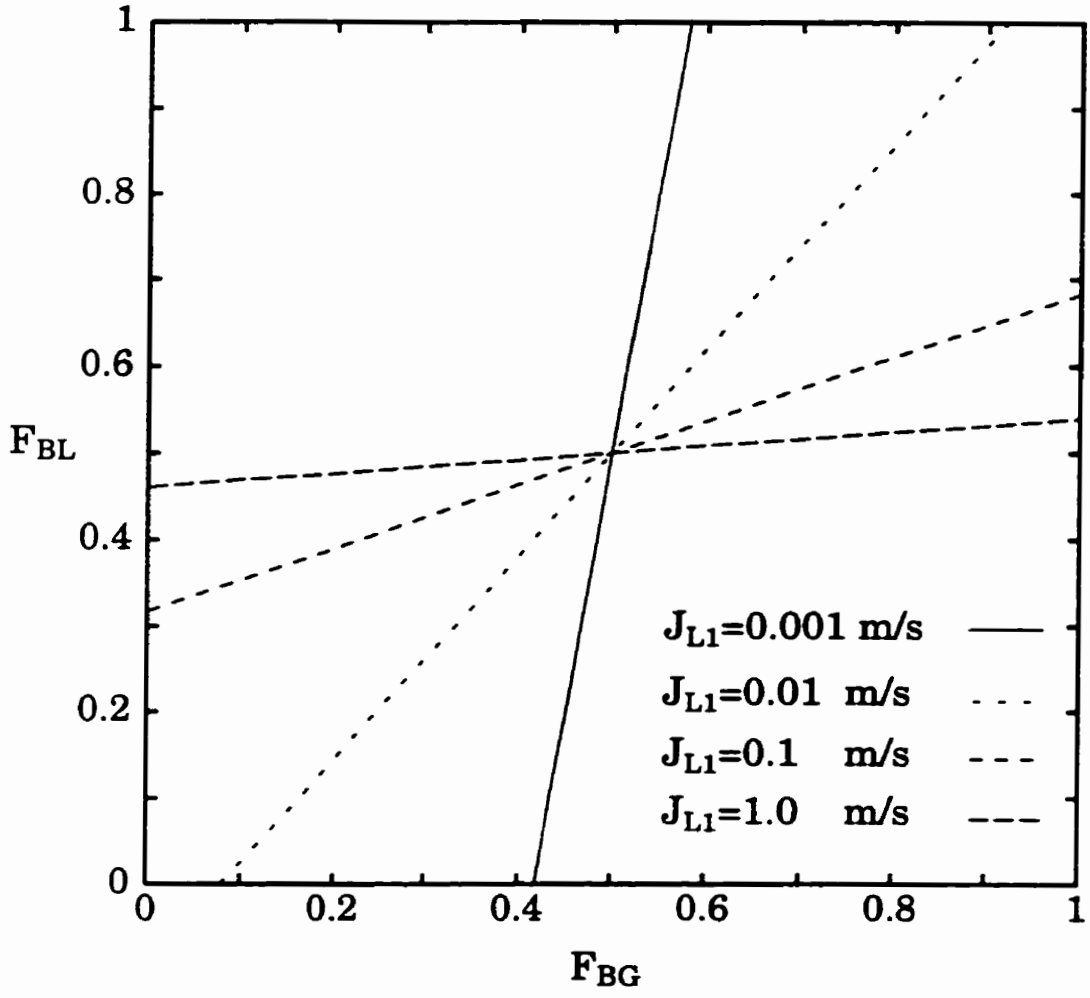

Figure 3.9 Effect of J_{L1} on the phase distribution as predicted by the Ottens et al. (1995) model for J_{G1} = 10 m/s and P_1= 1.0 bar.

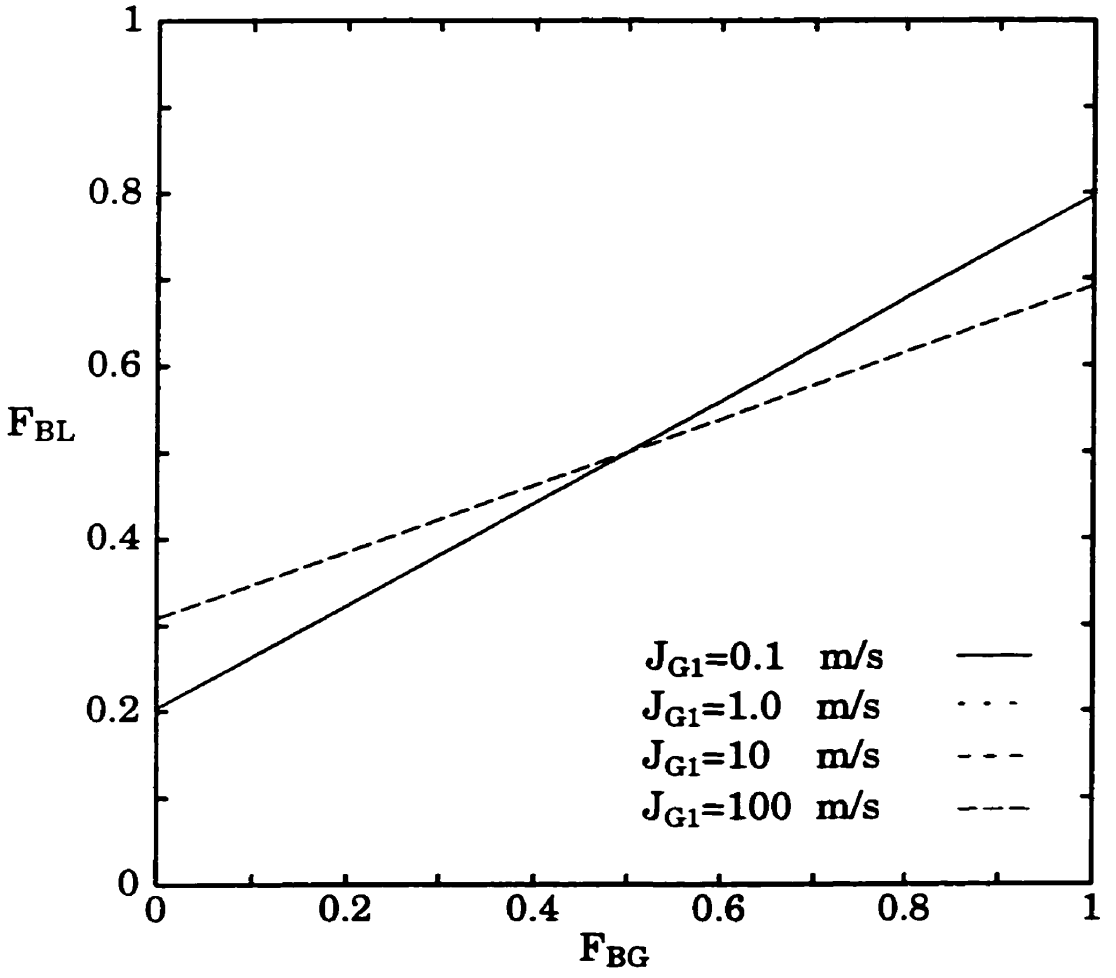

Figure 3.10 Effect of J_{G1} on the phase distribution as predicted by the Ottens et al. (1995) model for J_{L1}= 0.05 m/s and P_1= 1.0 bar.

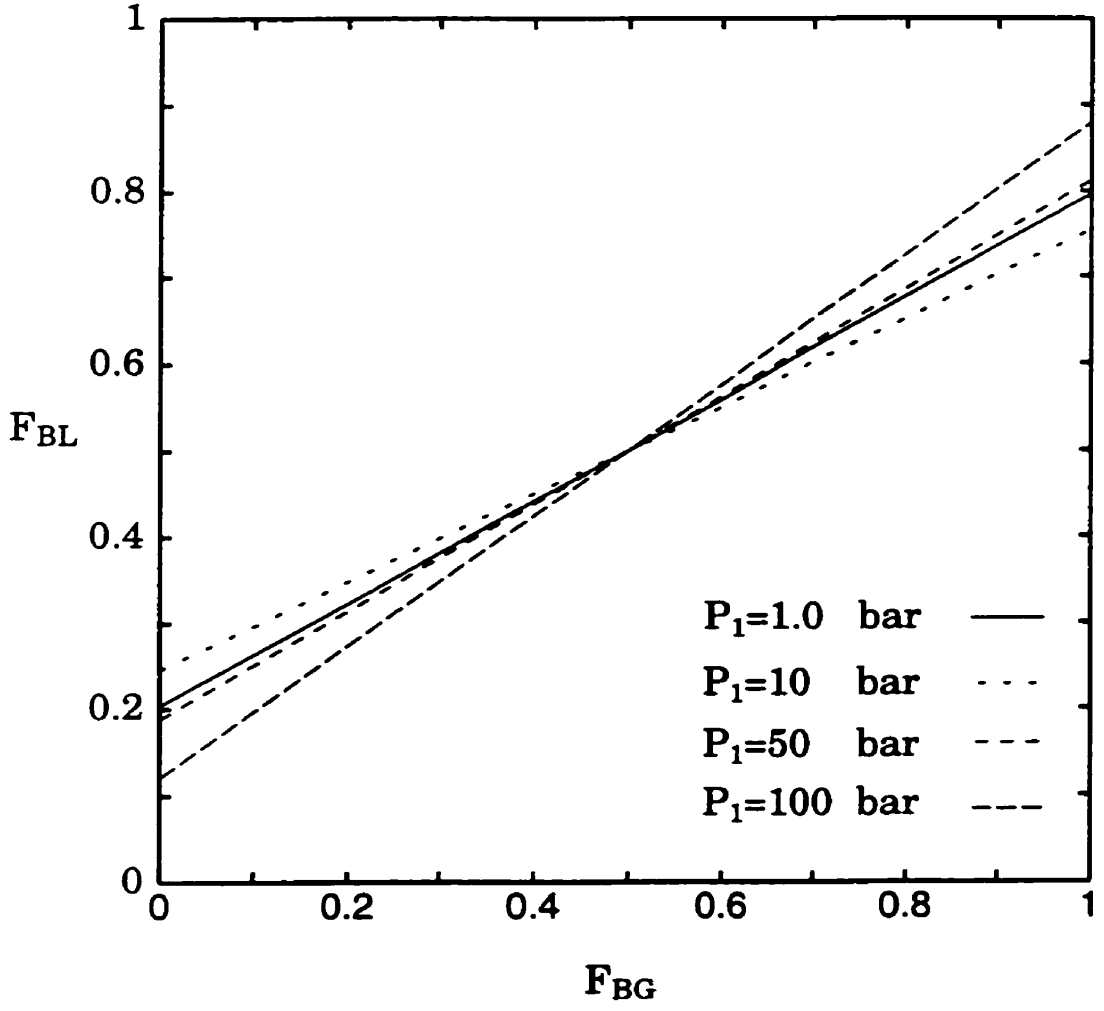

Figure 3.11 Effect of P_1 on the phase distribution as predicted by the Ottens et al. (1995) model for J_{L1} = 0.05 m/s and J_{G1} = 10 m/s.

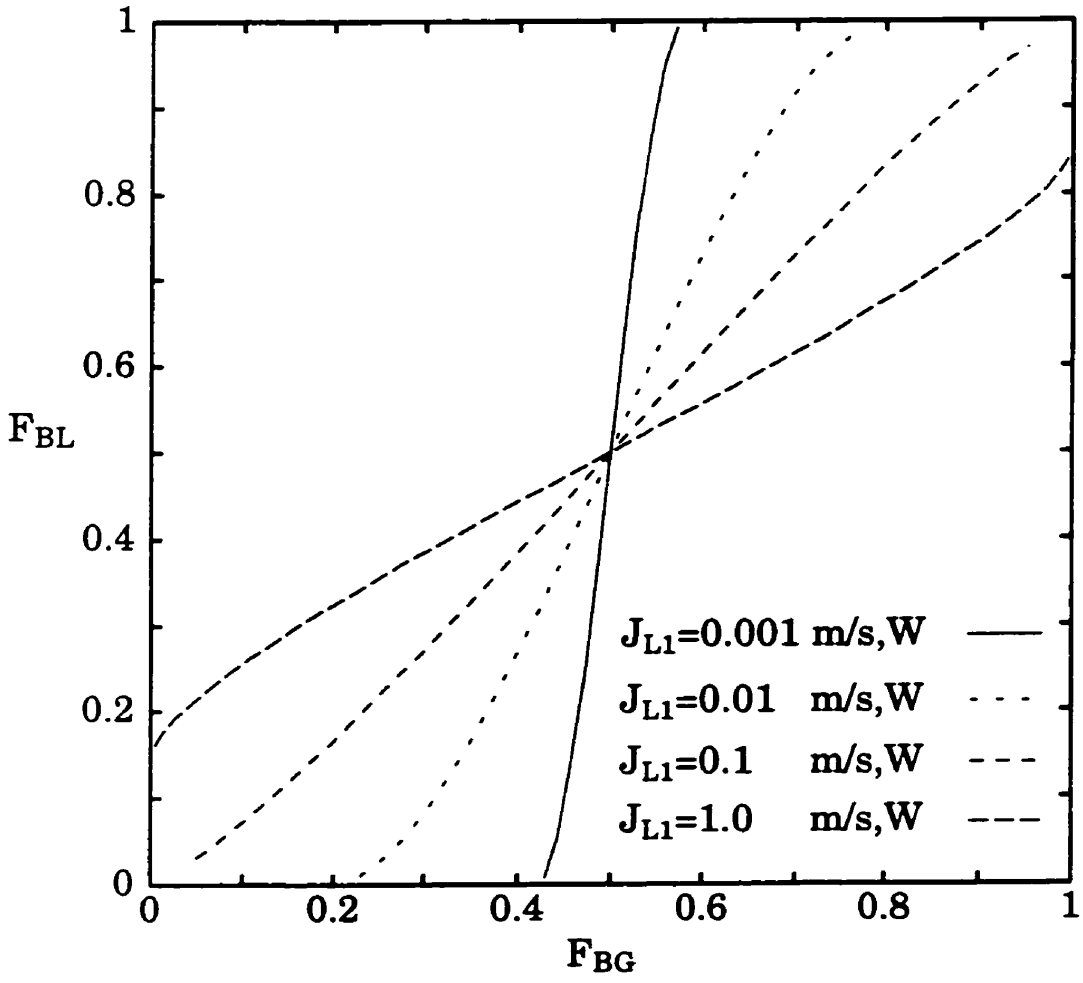

Figure 3.12 Effect of J_{L1} on the phase distribution as predicted by the Hwang (1986) model for J_{G1} = 10 m/s and P_1=1.0 bar, (W:Wavy).

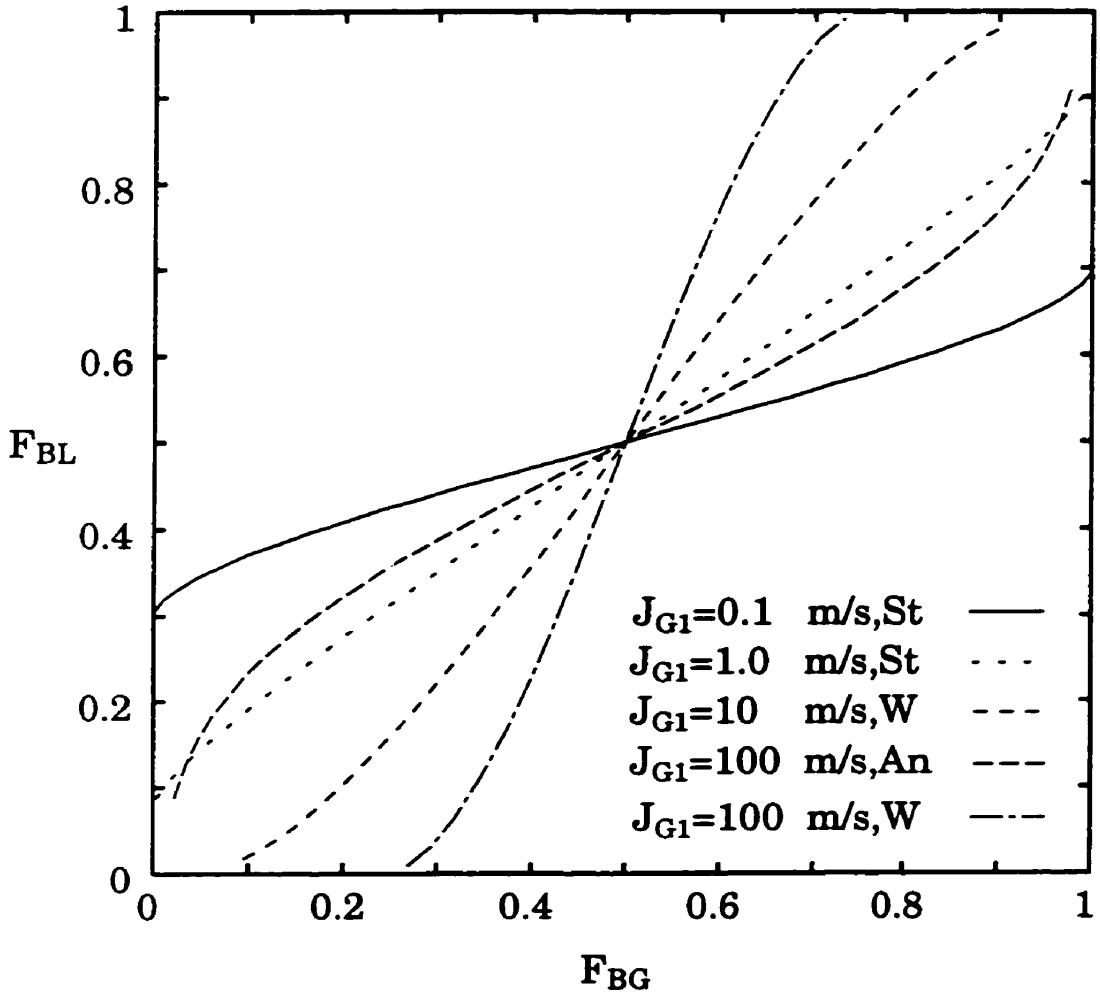

Figure 3.13 Effect of J_{G1} on the phase distribution as predicted by the Hwang (1986) model for J_{L1} = 0.05 m/s and P_1 =1.0 bar, (St:Stratified, W:Wavy, An:Annular).

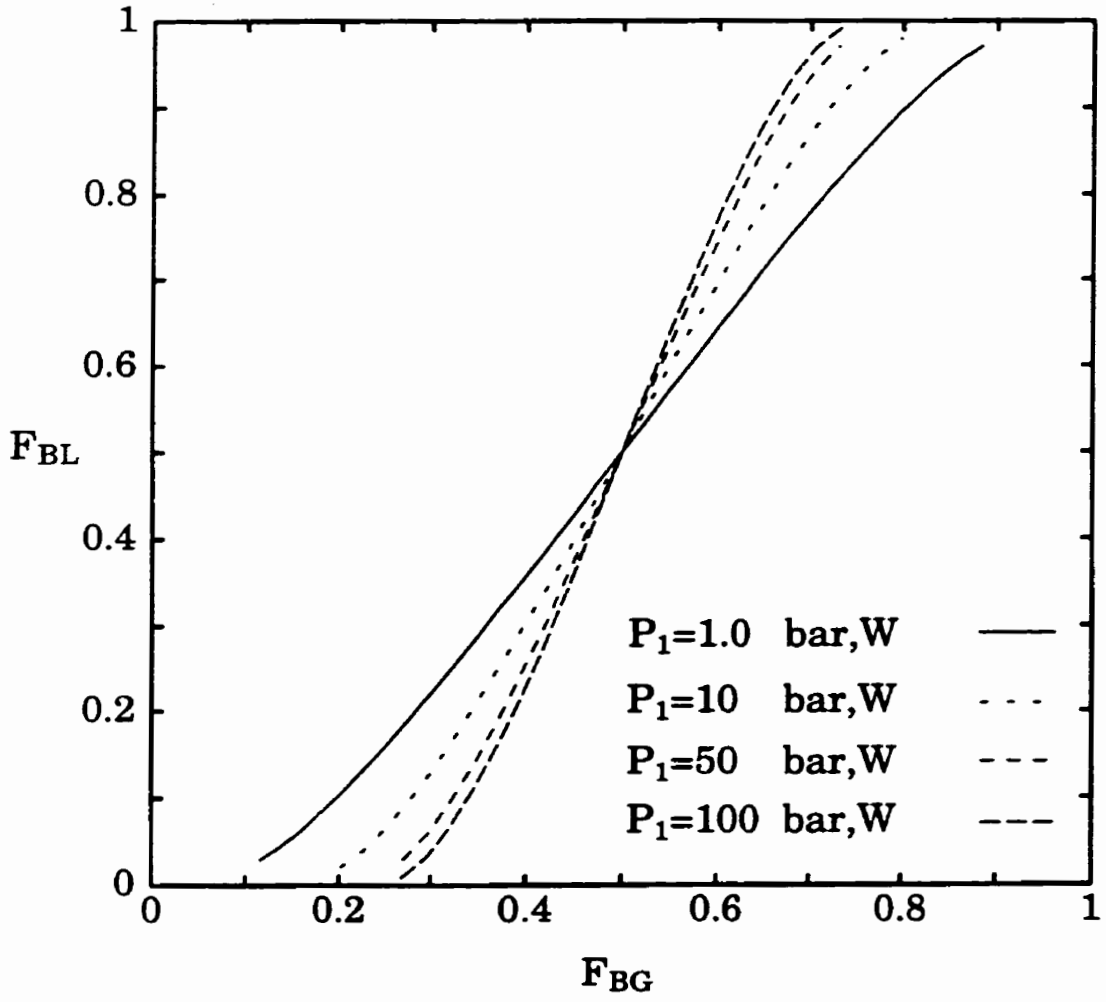

Figure 3.14 **Effect of P_1 on the phase distribution as predicted by the Hwang (1986) model for J_{L1}= 0.05 m/s and J_{G1}=10 m/s, (W:Wavy).**

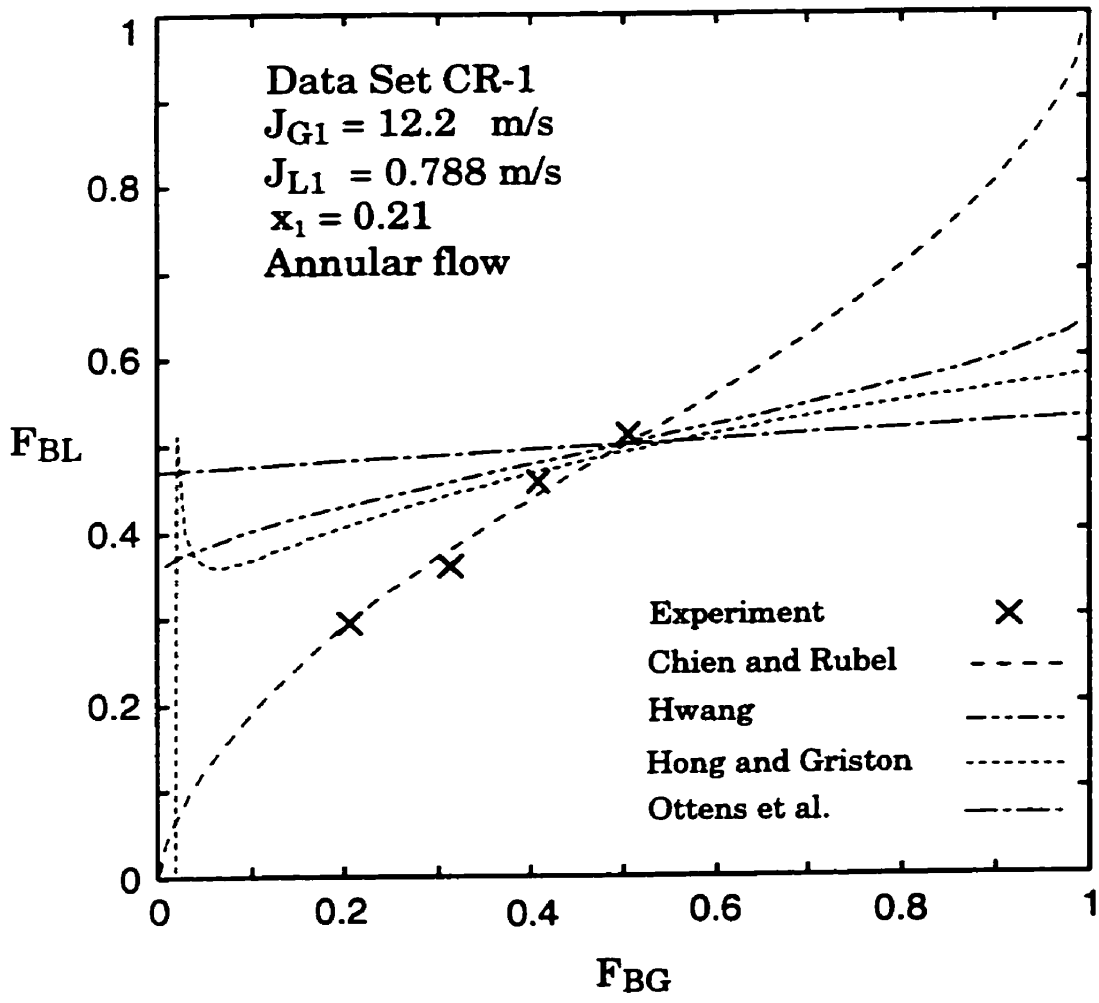

Figure 3.15 Predictions of models and correlations against data set CR-1.

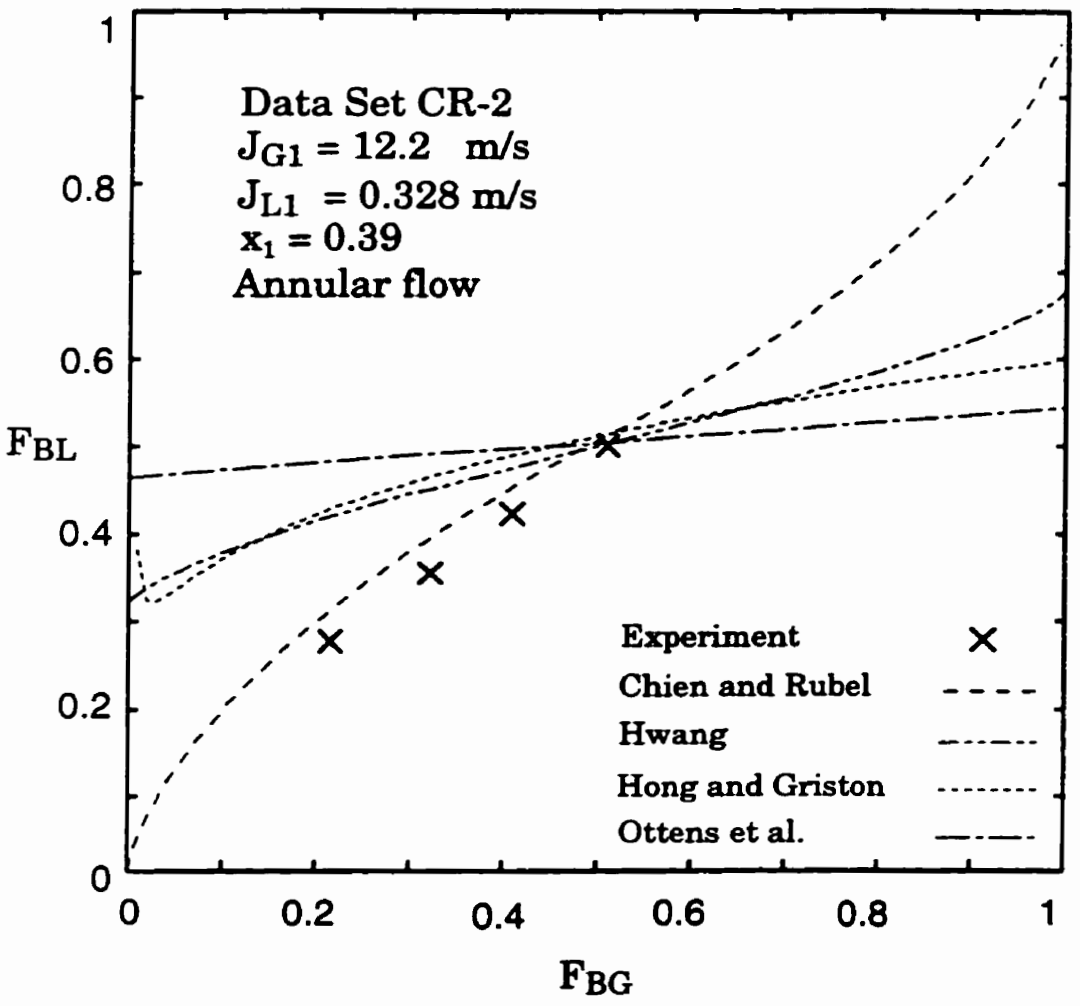

Figure 3.16 Predictions of models and correlations against data set CR-2.

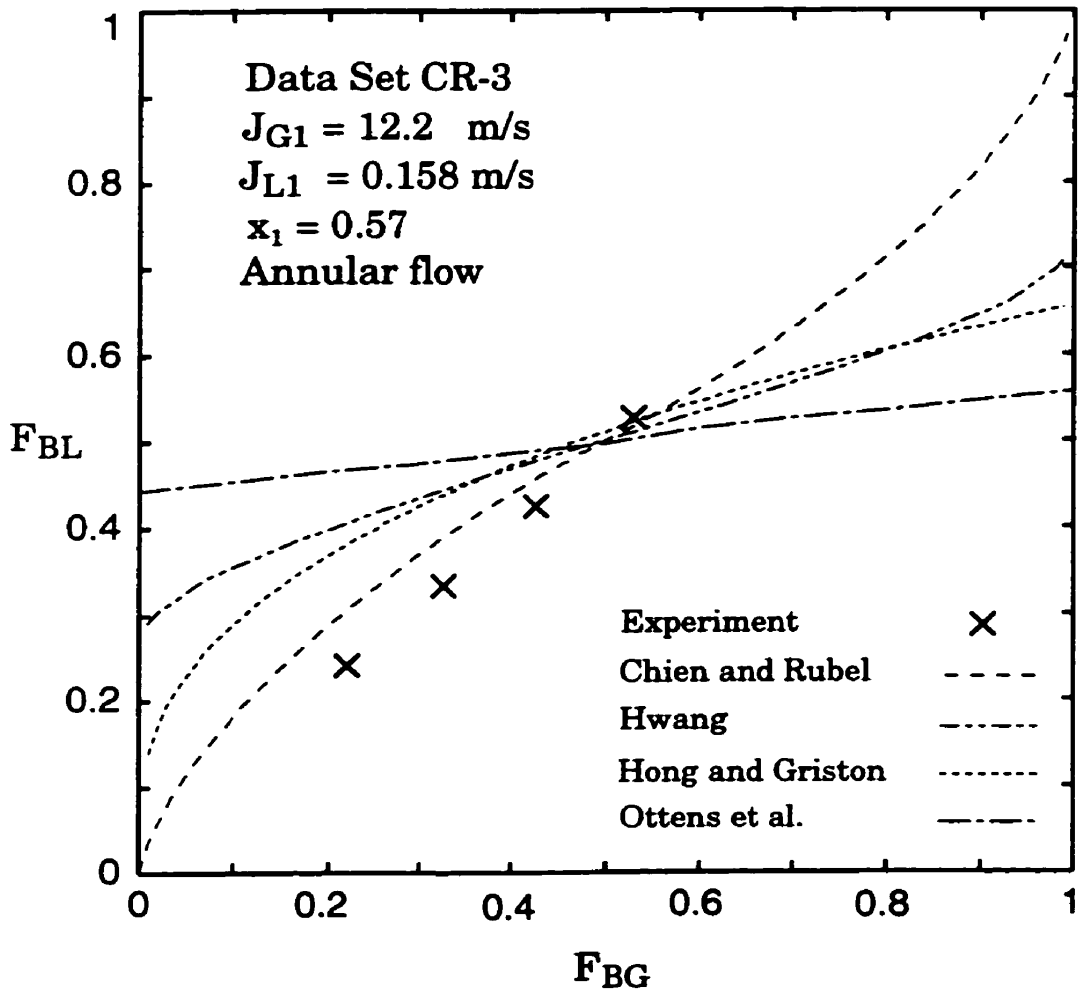

Figure 3.17 Predictions of models and correlations against data set CR-3.

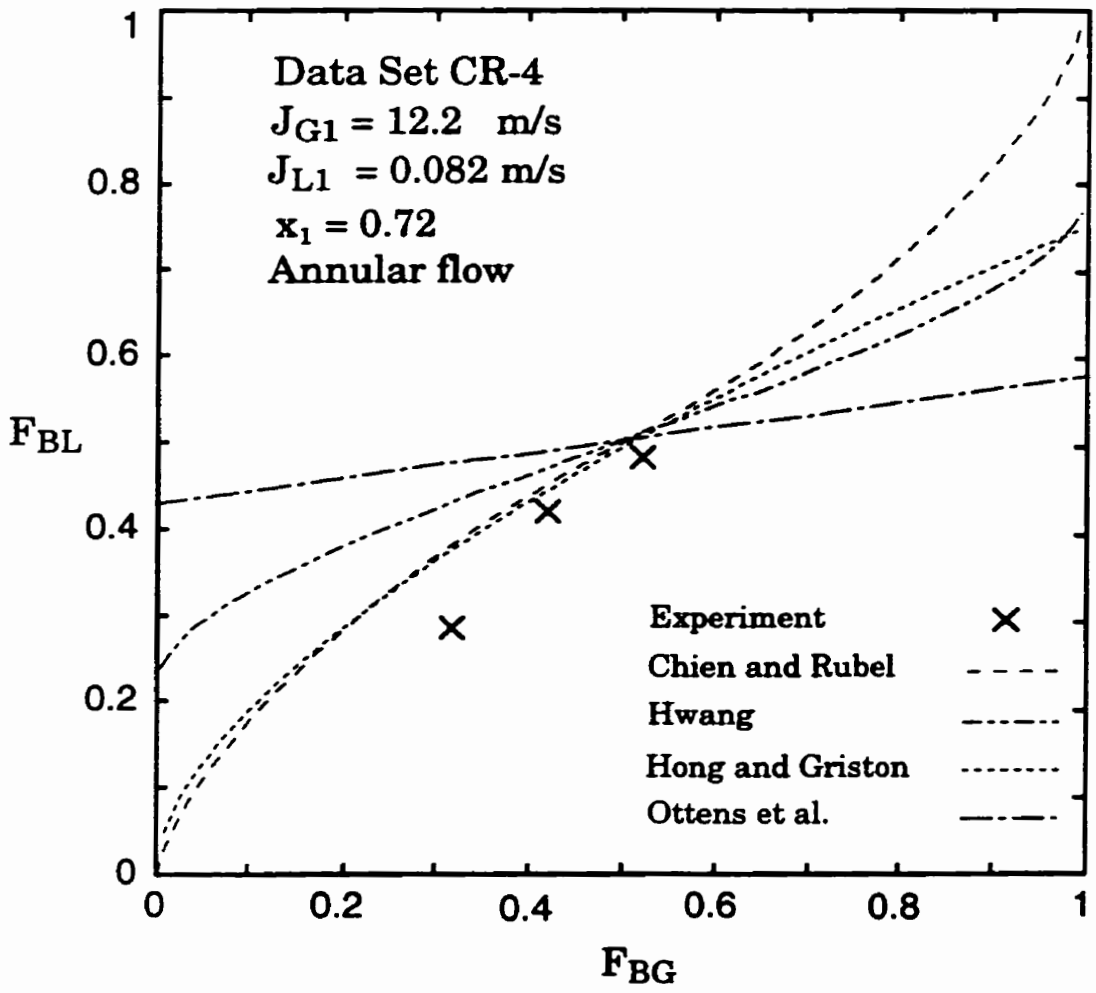

Figure 3.18 Predictions of models and correlations against data set CR-4.

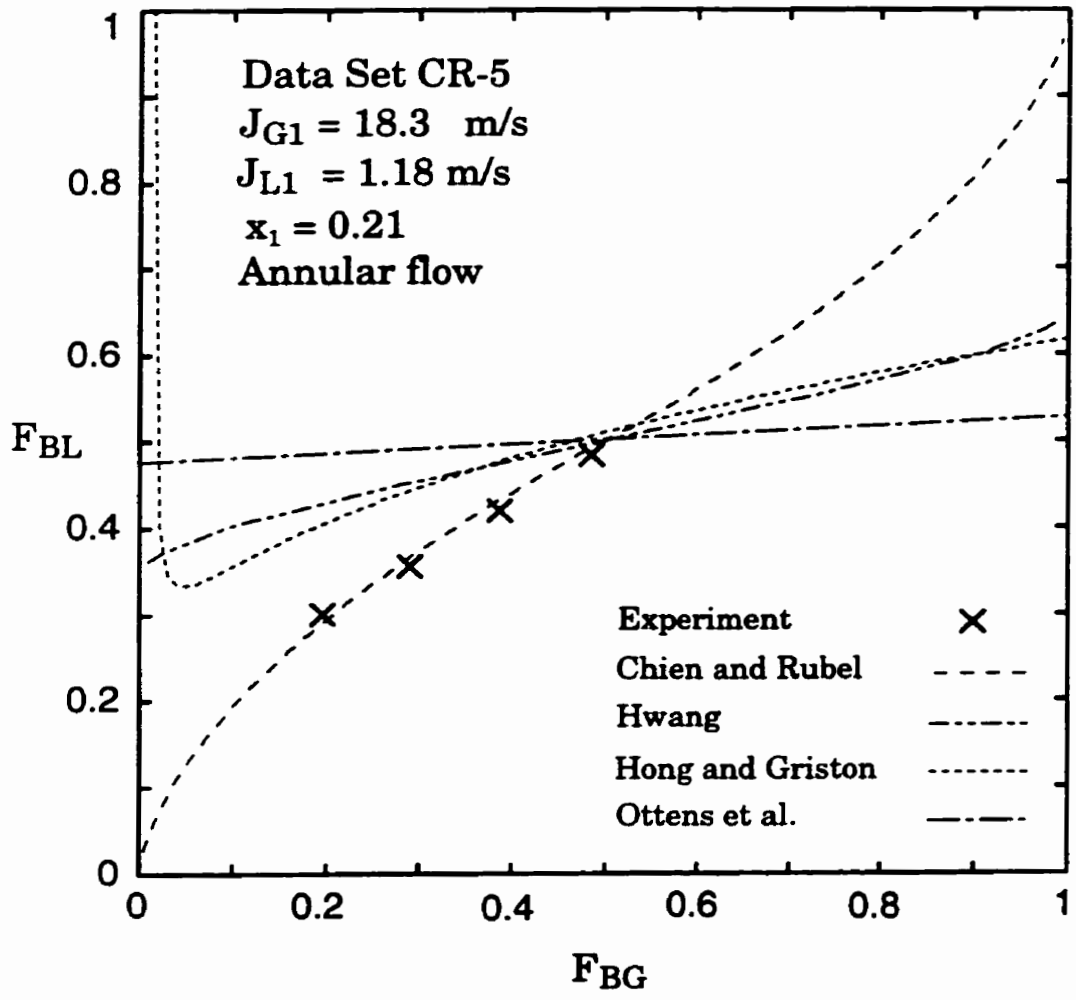

Figure 3.19 Predictions of models and correlations against data set CR-5.

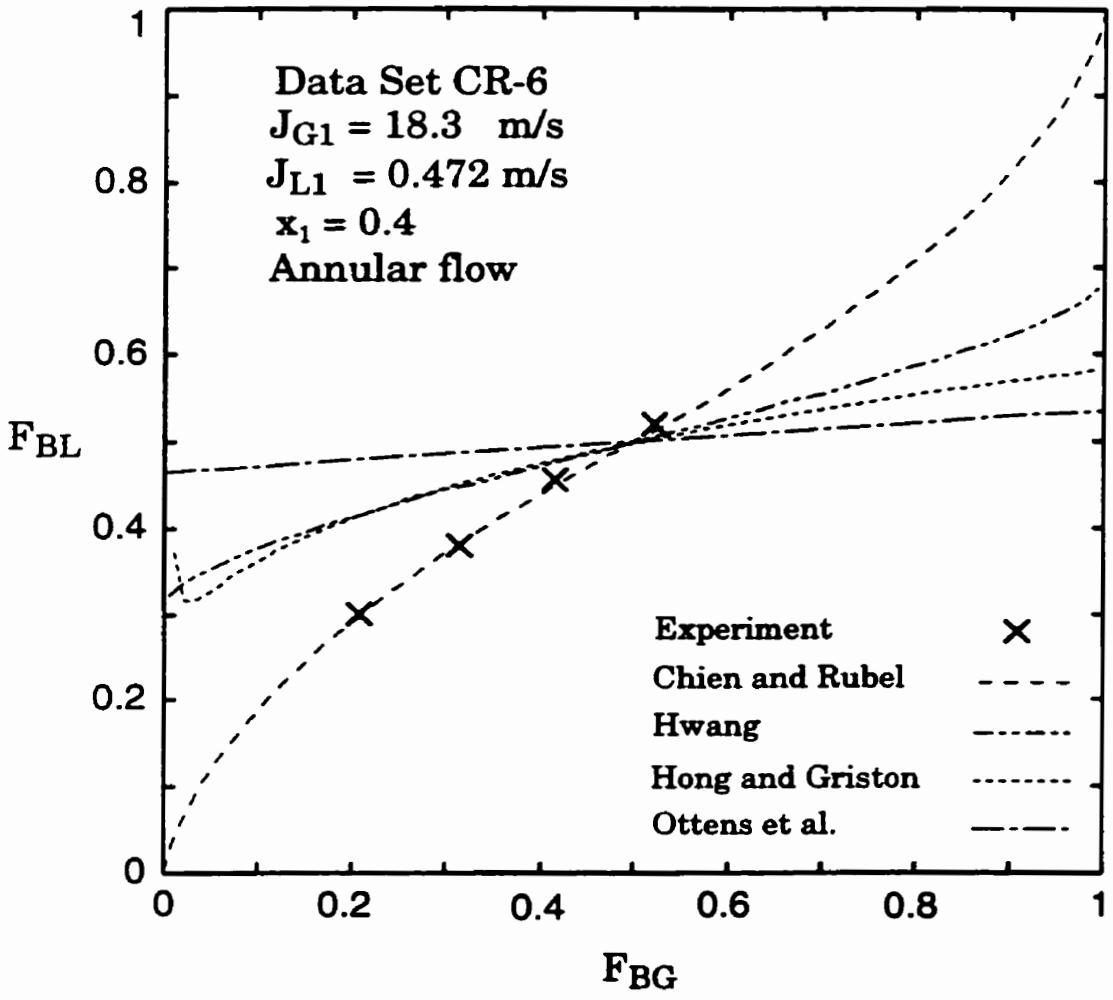

Figure 3.20 Predictions of models and correlations against data set CR-6.

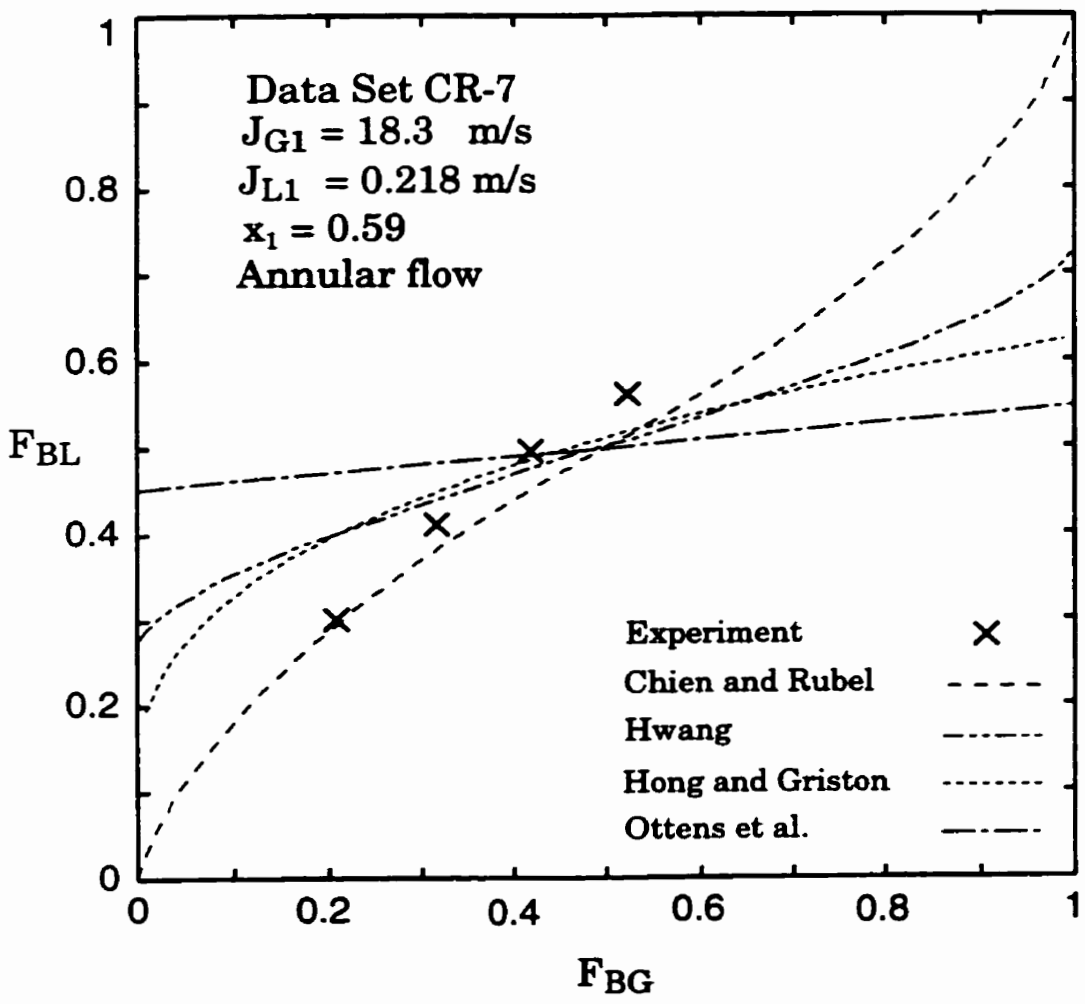

Figure 3.21 Predictions of models and correlations against data set CR-7.

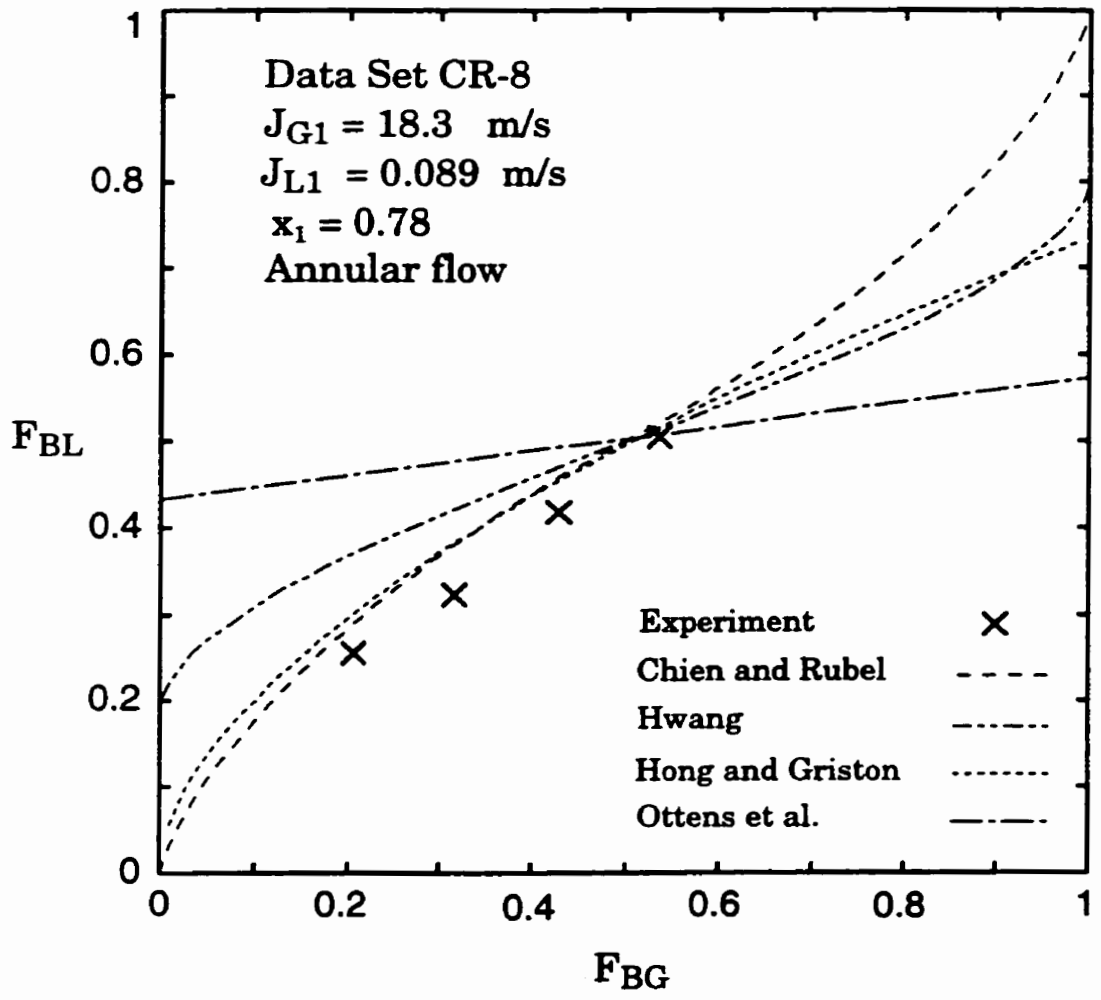

Figure 3.22 Predictions of models and correlations against data set CR-8.

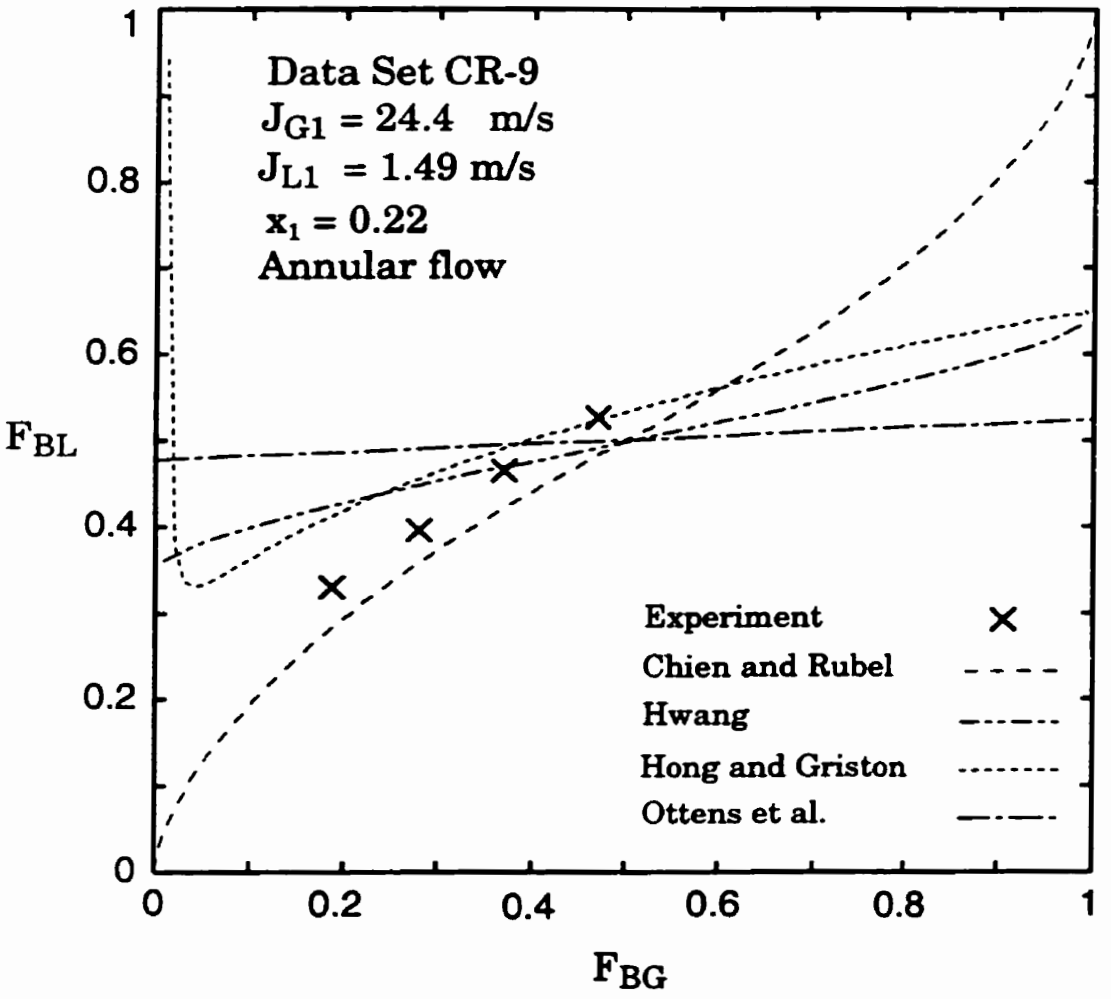

Figure 3.23 Predictions of models and correlations against data set CR-9.

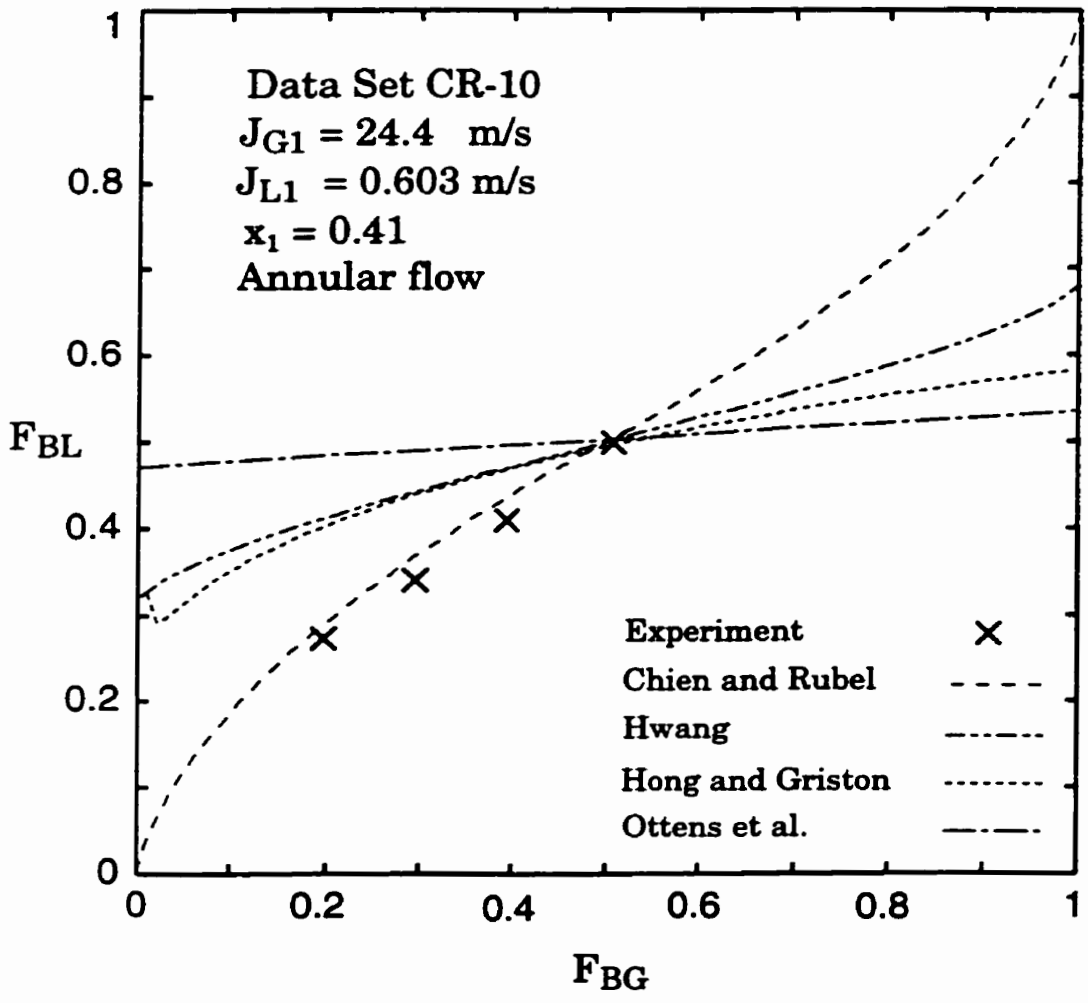

Figure 3.24 Predictions of models and correlations gainst data set CR-10.

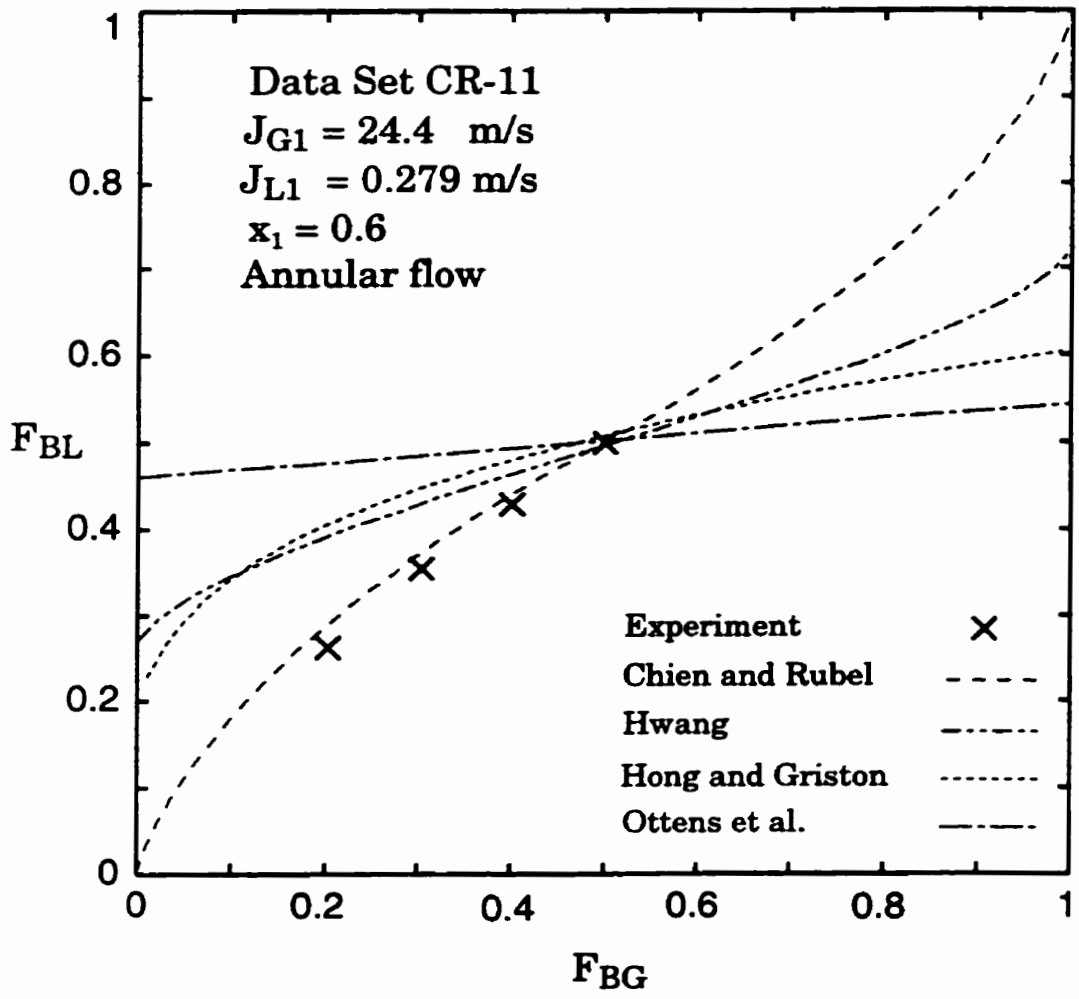

Figure 3.25 Predictions of models and correlations against data set CR-11.

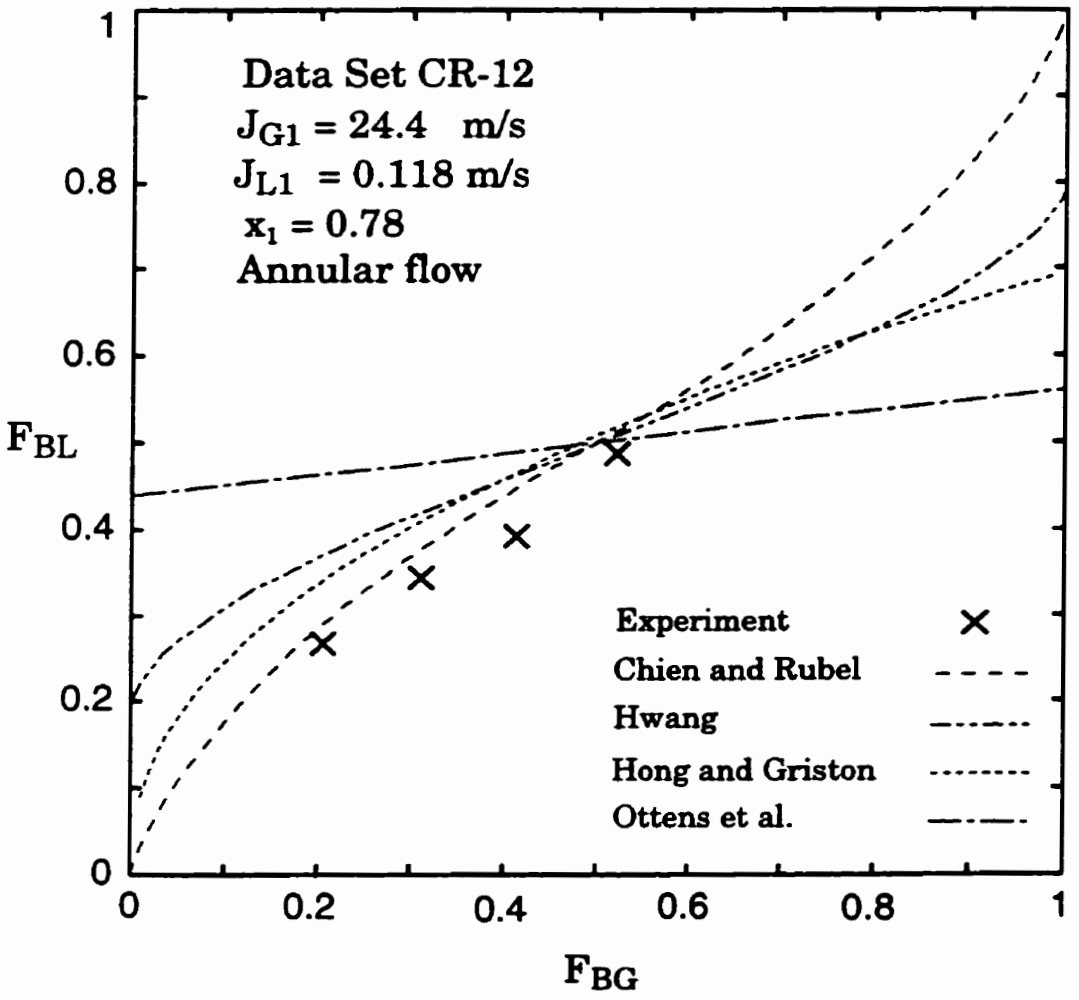

Figure 3.26 Predictions of models and correlations against data set CR-12.

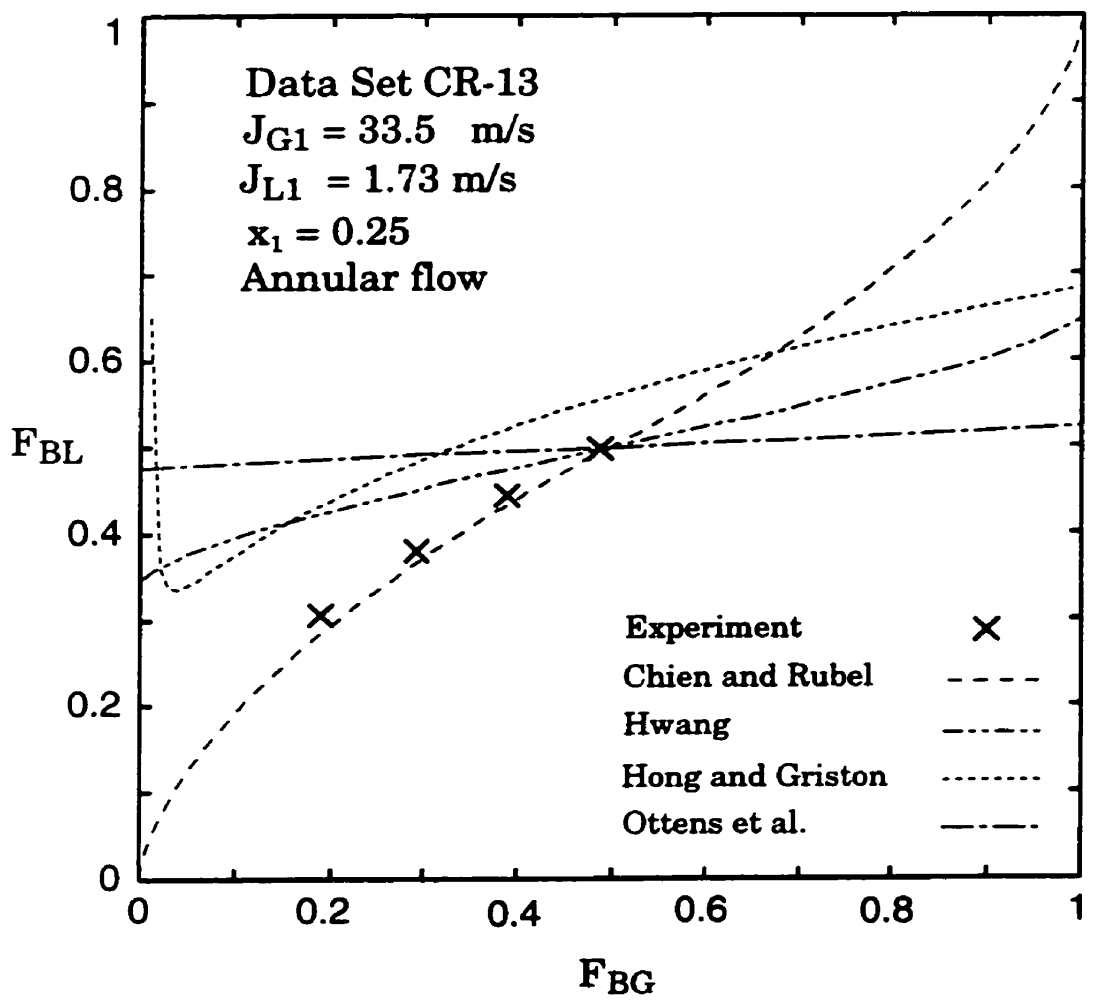

Figure 3.27 Predictions of models and correlations against data set CR-13.

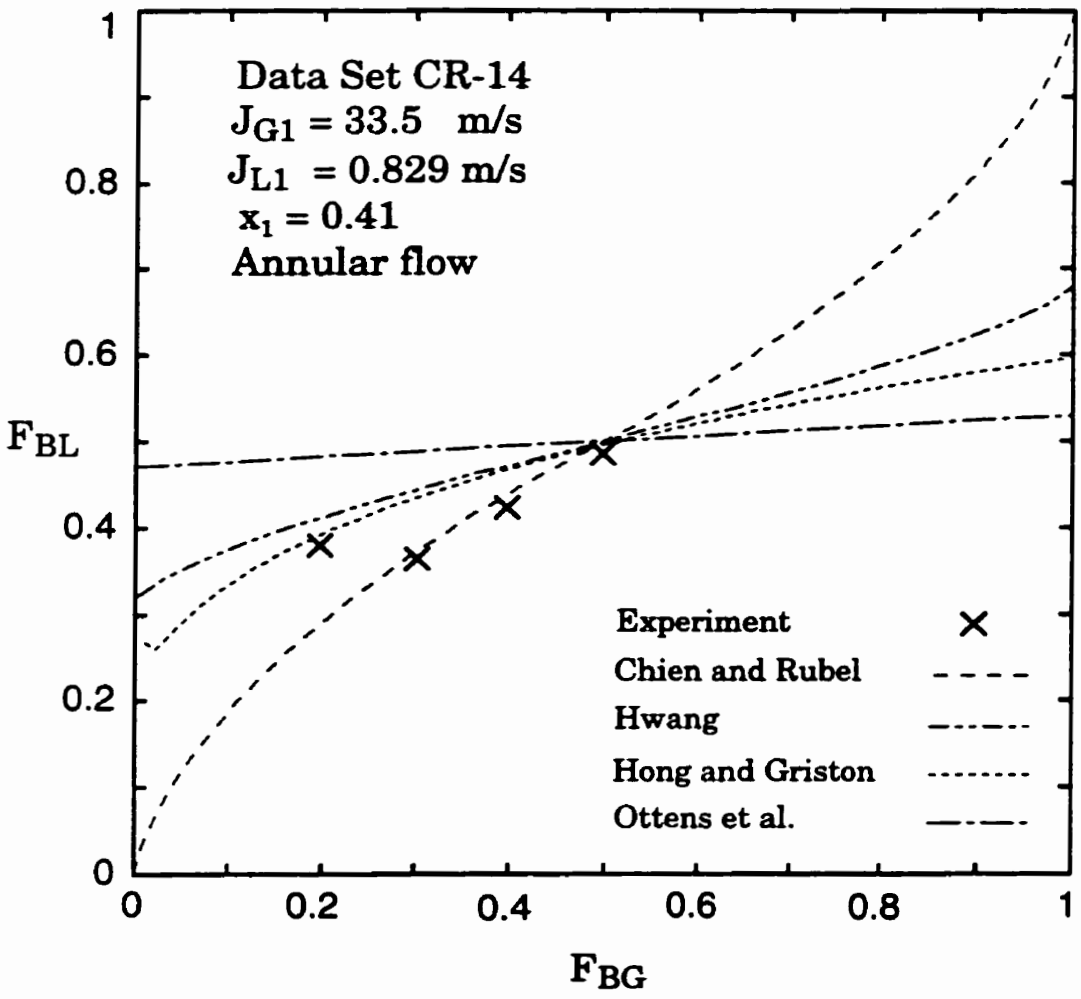

Figure 3.28 Predictions of models and correlations against data set CR-14.

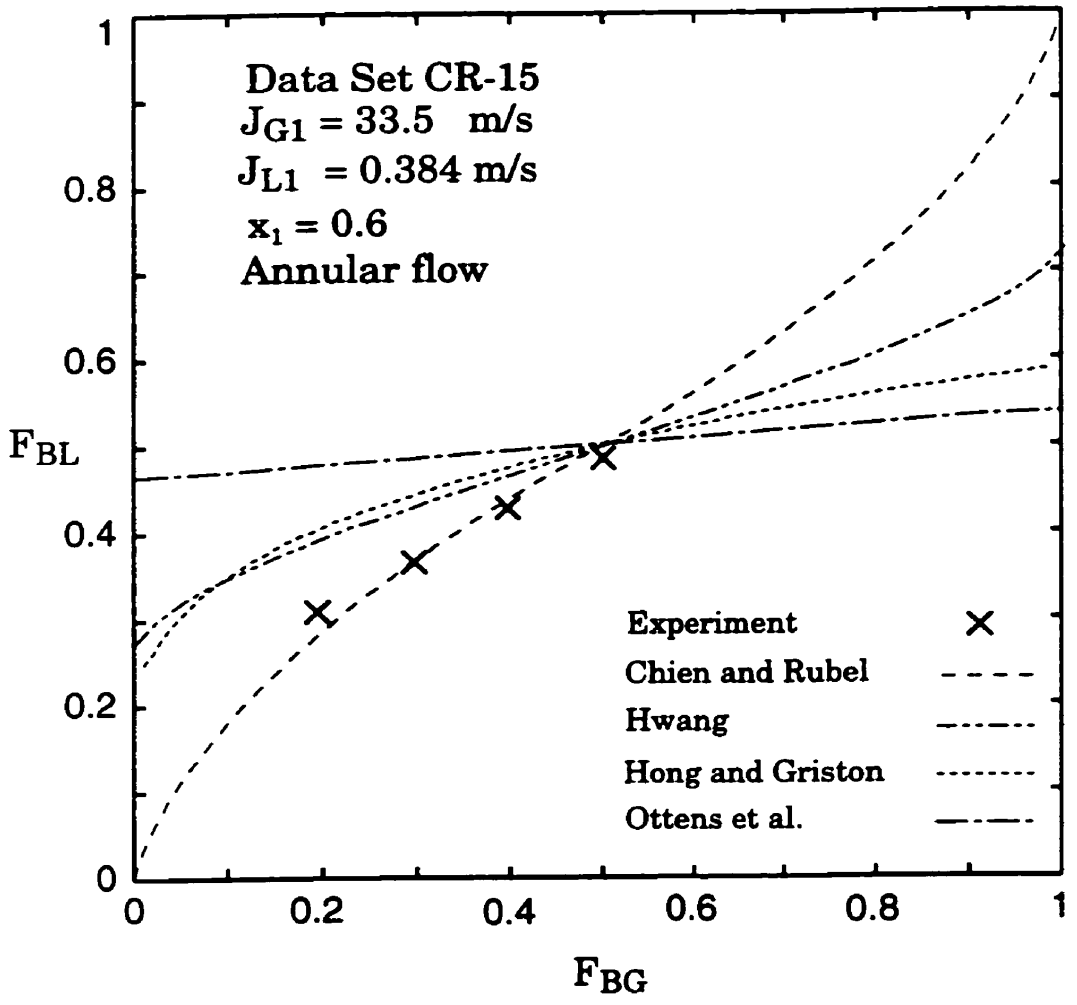

Figure 3.29 Predictions of models and correlations against data set CR-15.

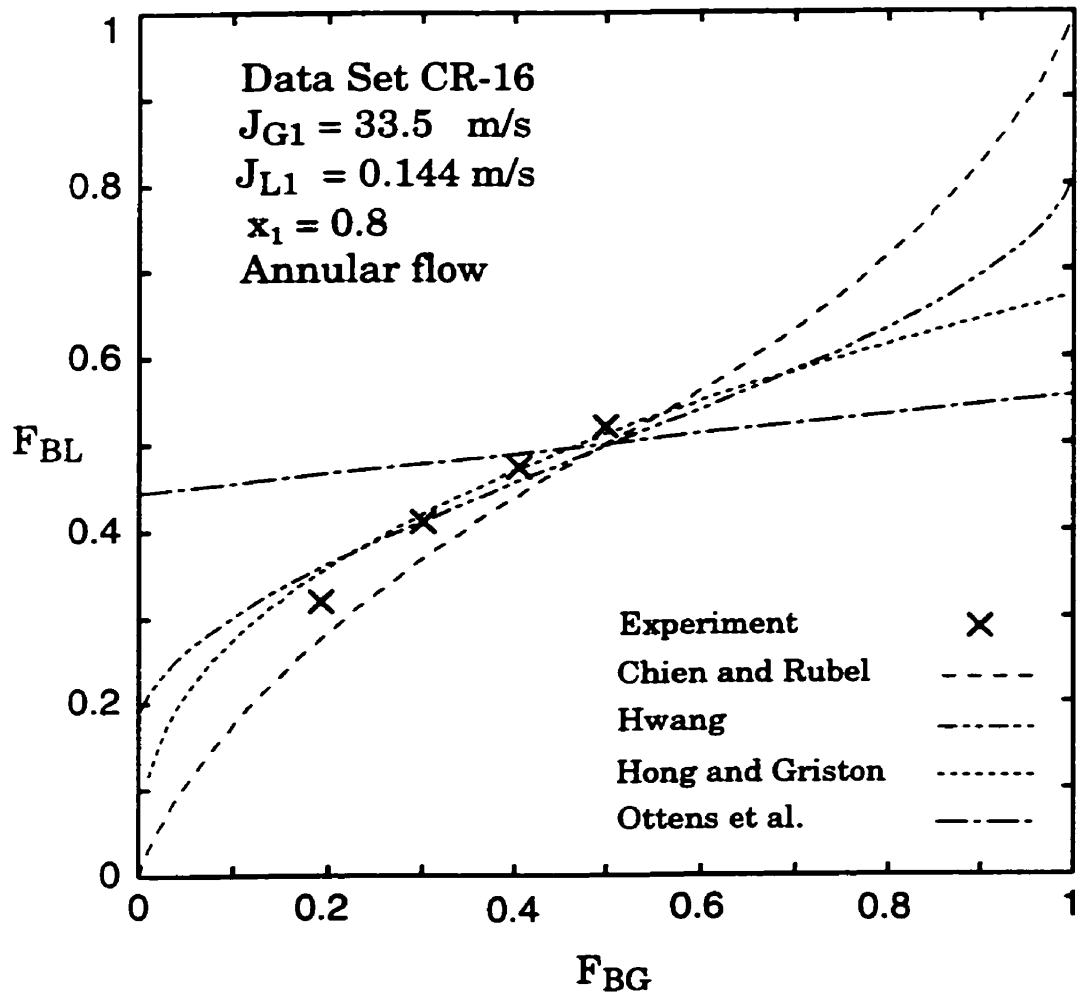

Figure 3.30 Predictions of models and correlations against data set CR-16.

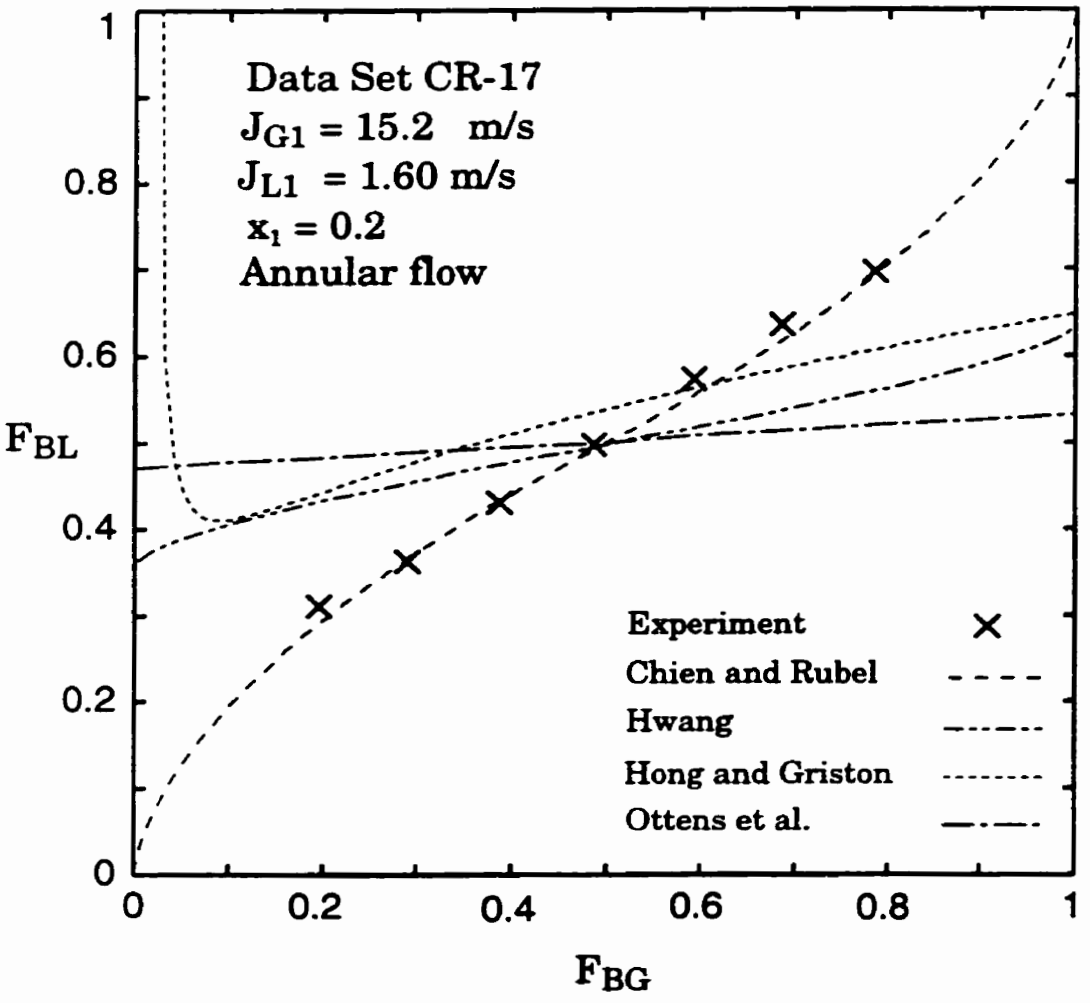

Figure 3.31 Predictions of models and correlations against data set CR-17.

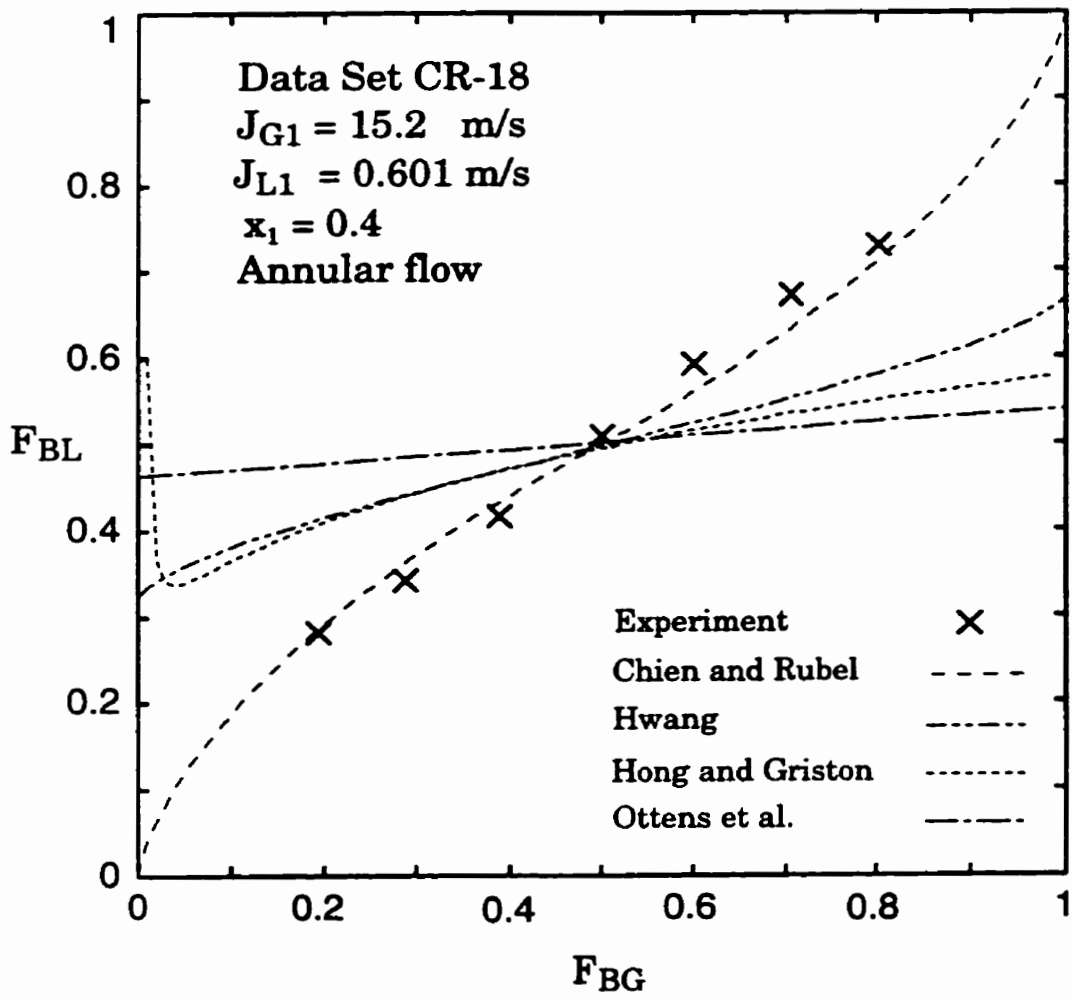

Figure 3.32 Predictions of models and correlations against data set CR-18.

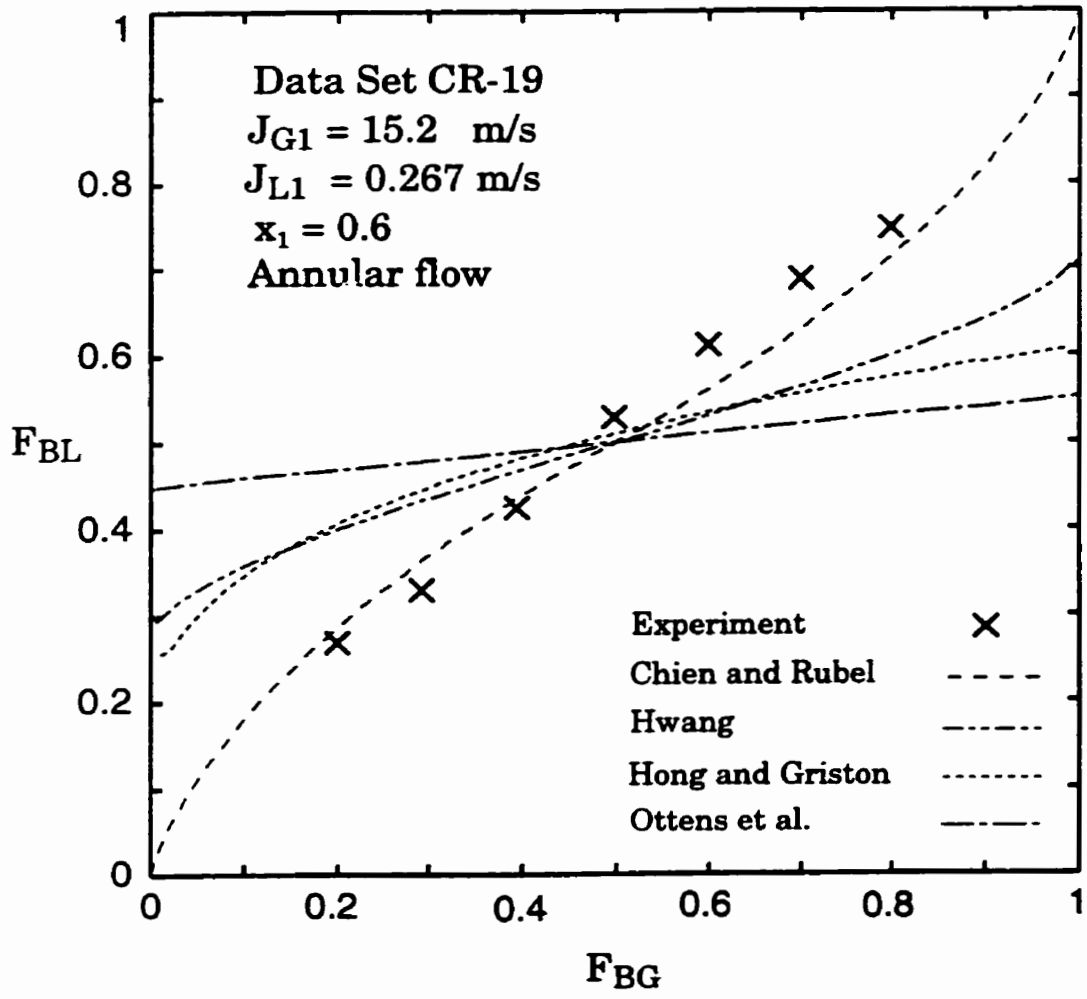

Figure 3.33 Predictions of models and correlations against data set CR-19.

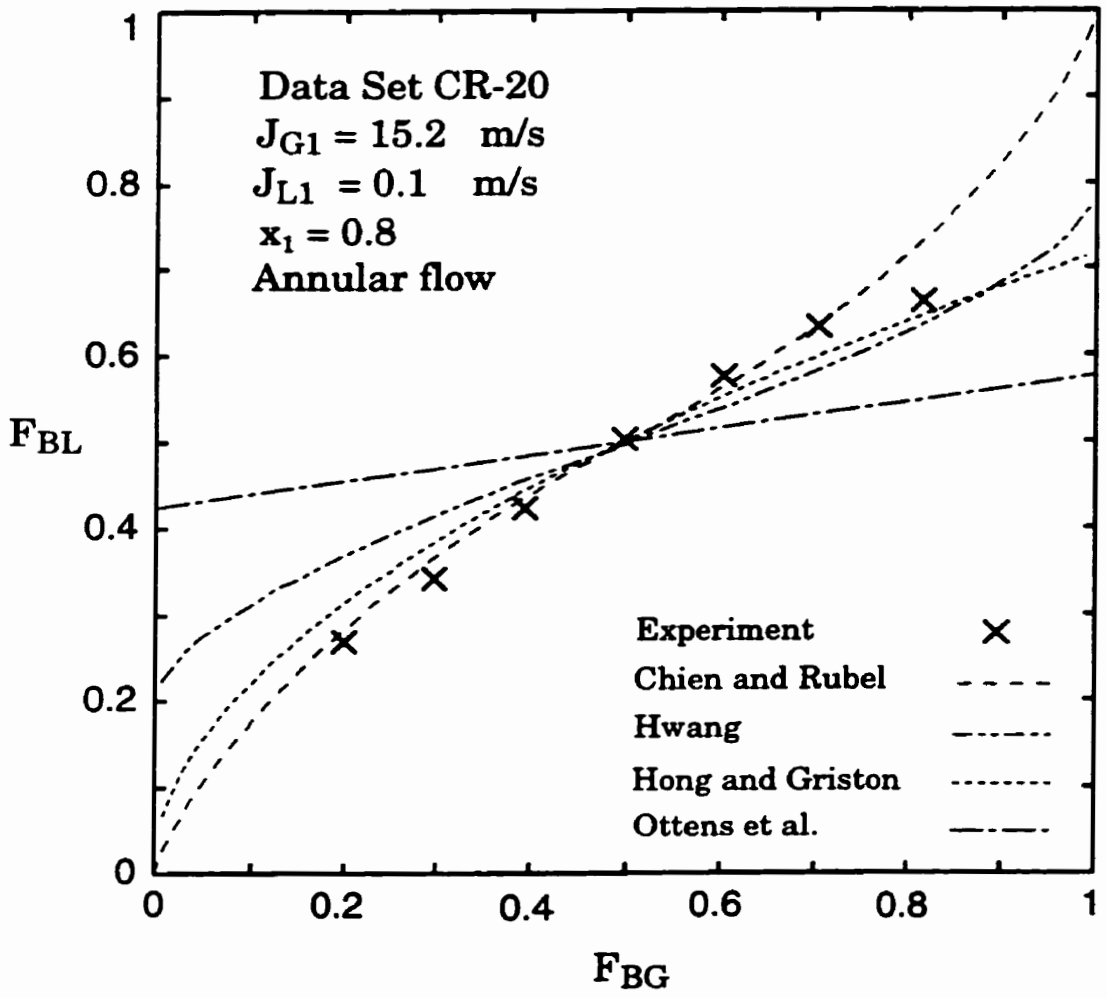

Figure 3.34 Predictions of models and correlations against data set CR-20.

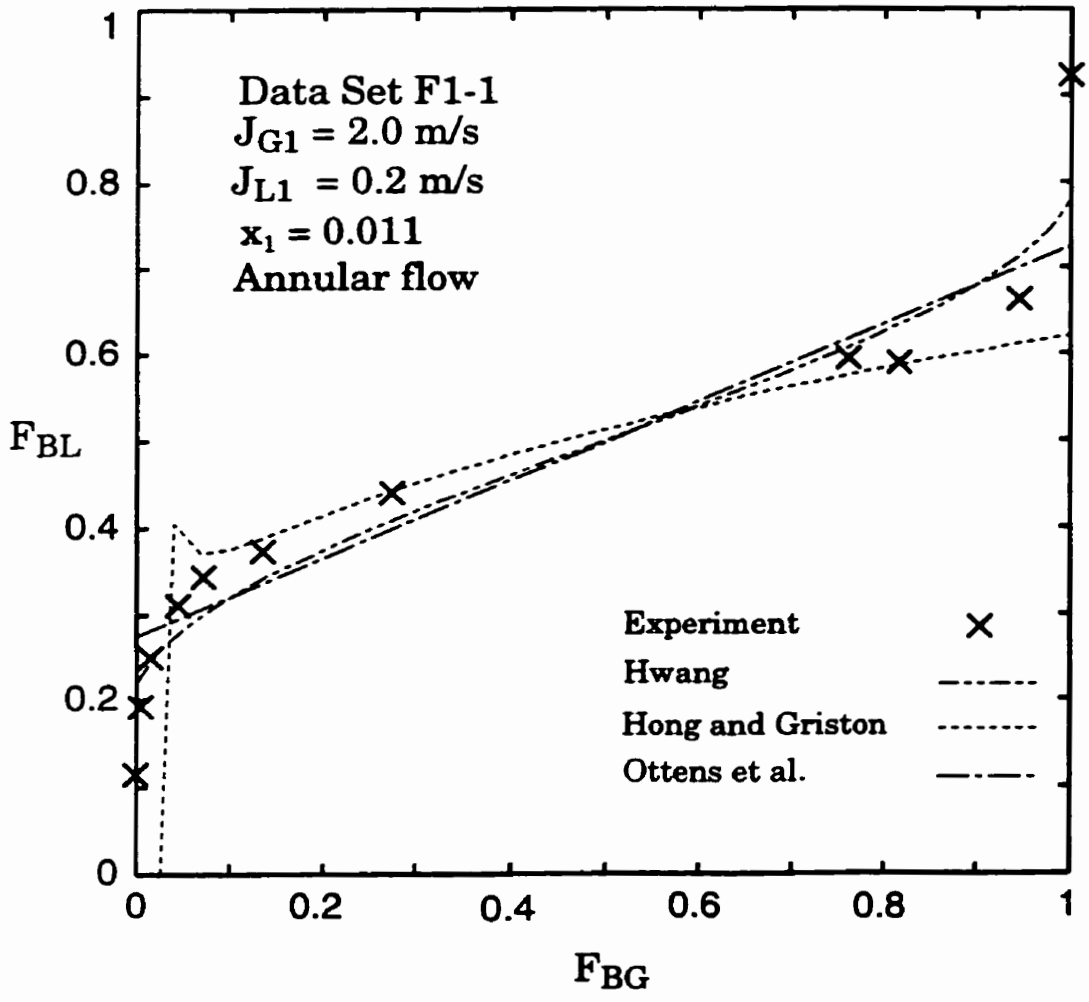

Figure 3.35 Predictions of models and correlations against data set F1-1.

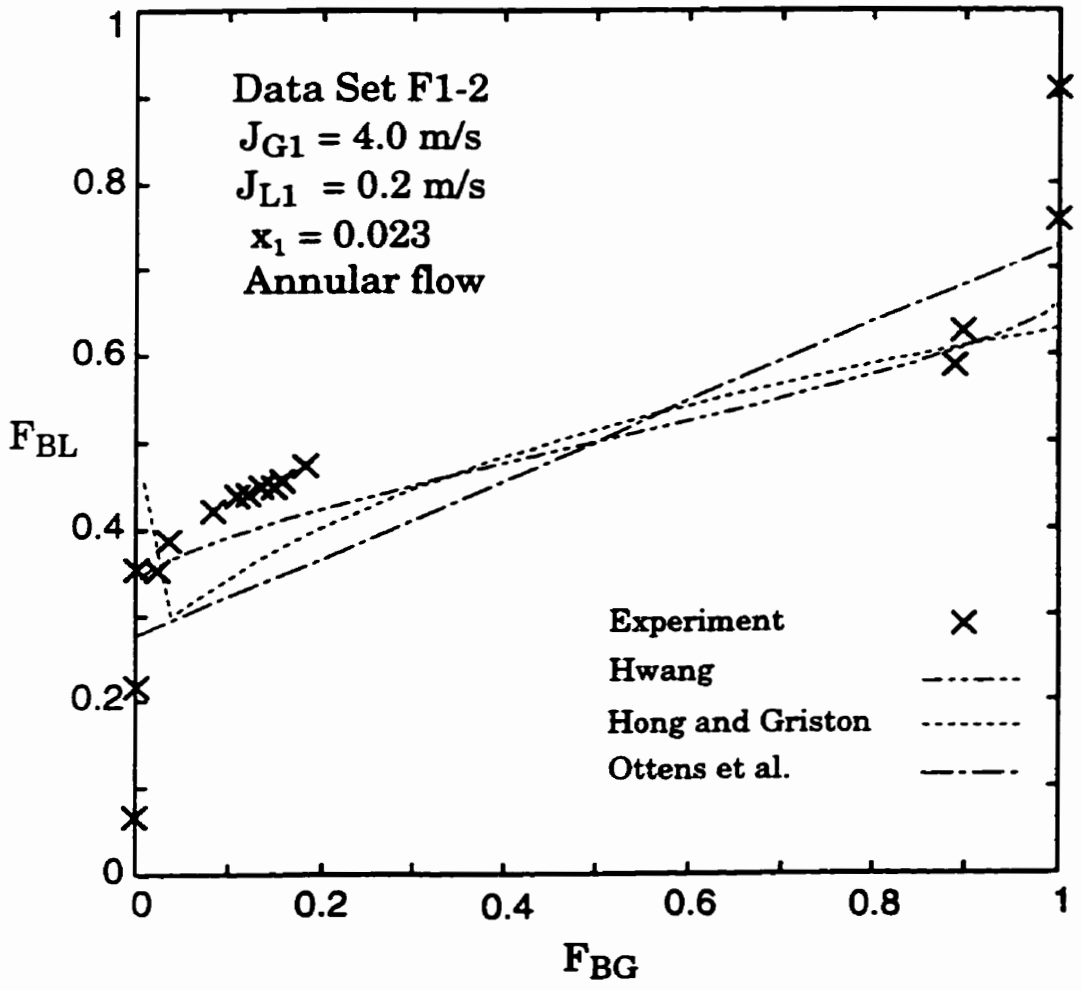

Figure 3.36 Predictions of models and correlations against data set F1-2.

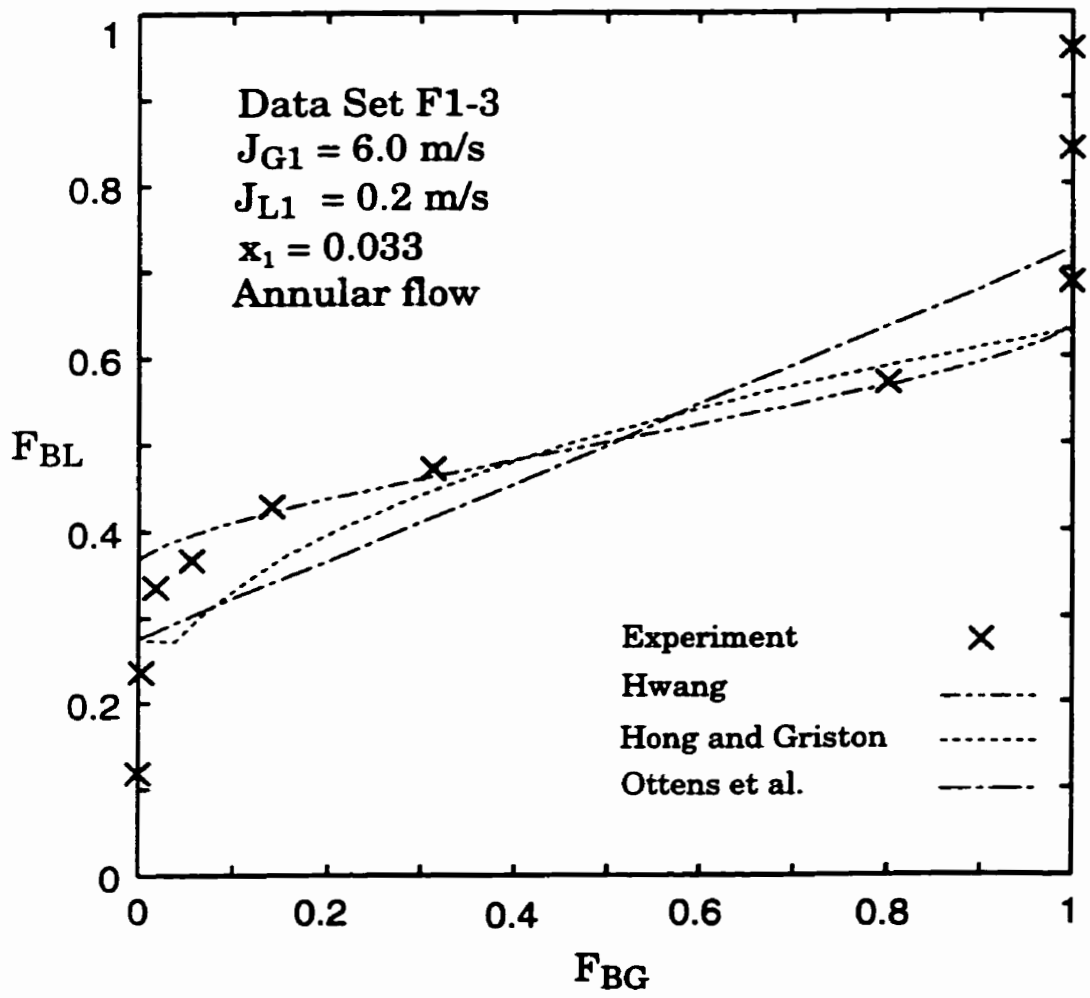

Figure 3.37 Predictions of models and correlations against data set F1-3.

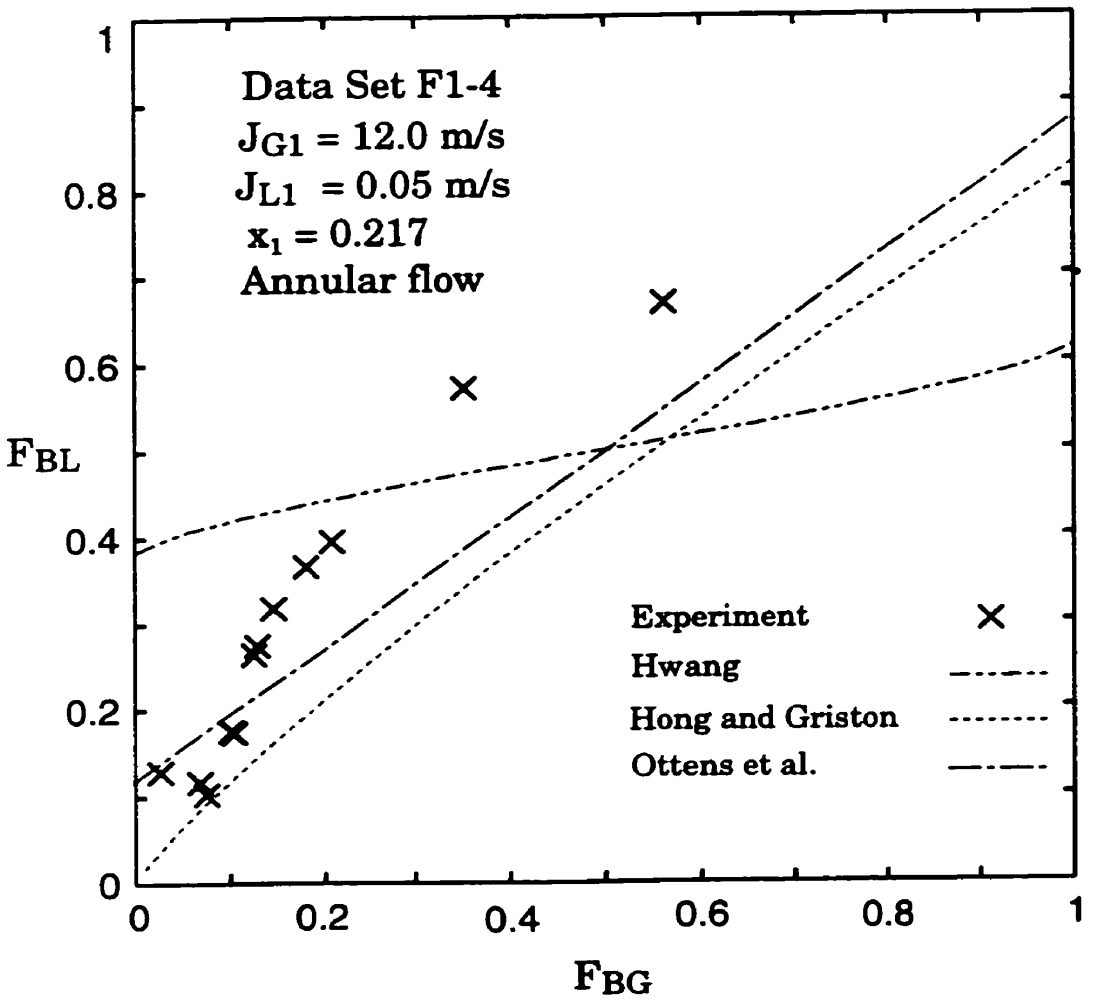

Figure 3.38 Predictions of models and correlations against data F1-4.

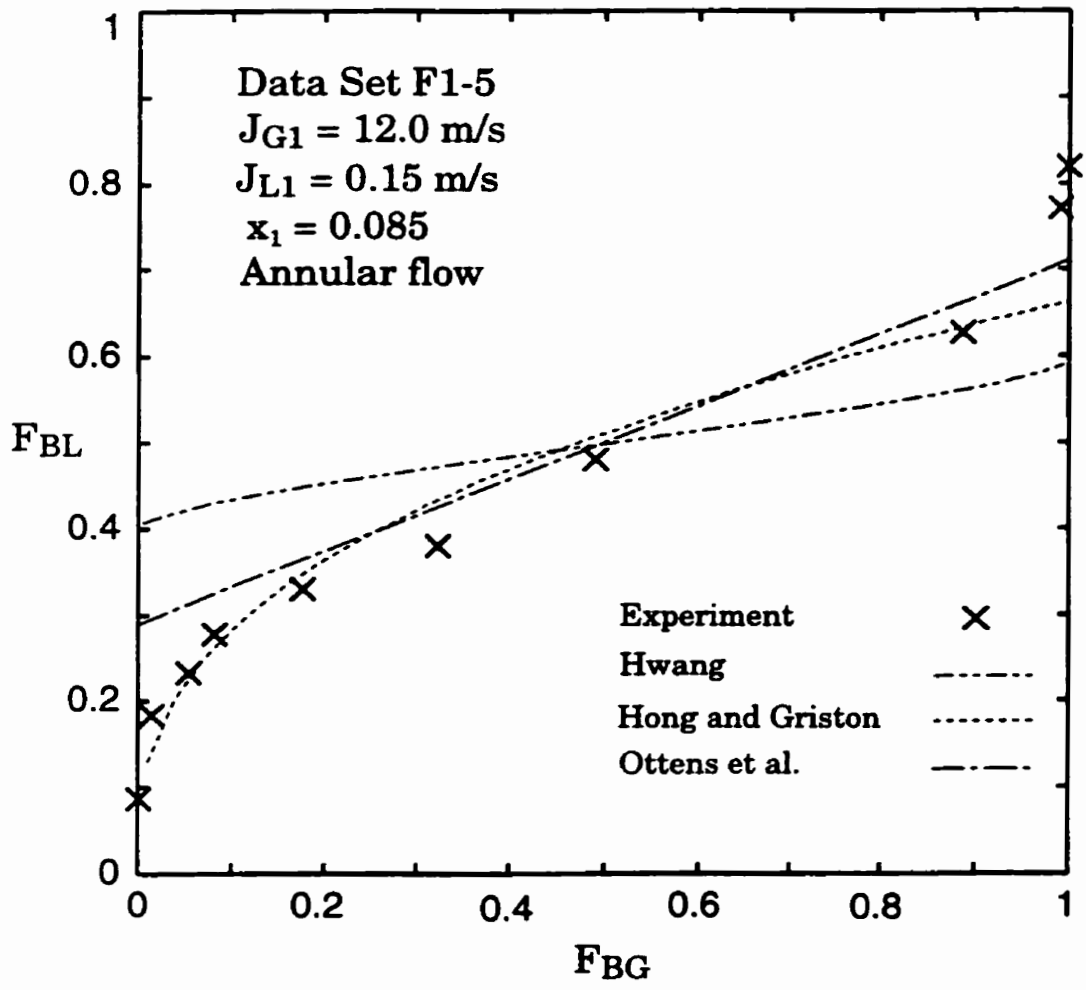

Figure 3.39 Predictions of models and correlations against data set F1-5.

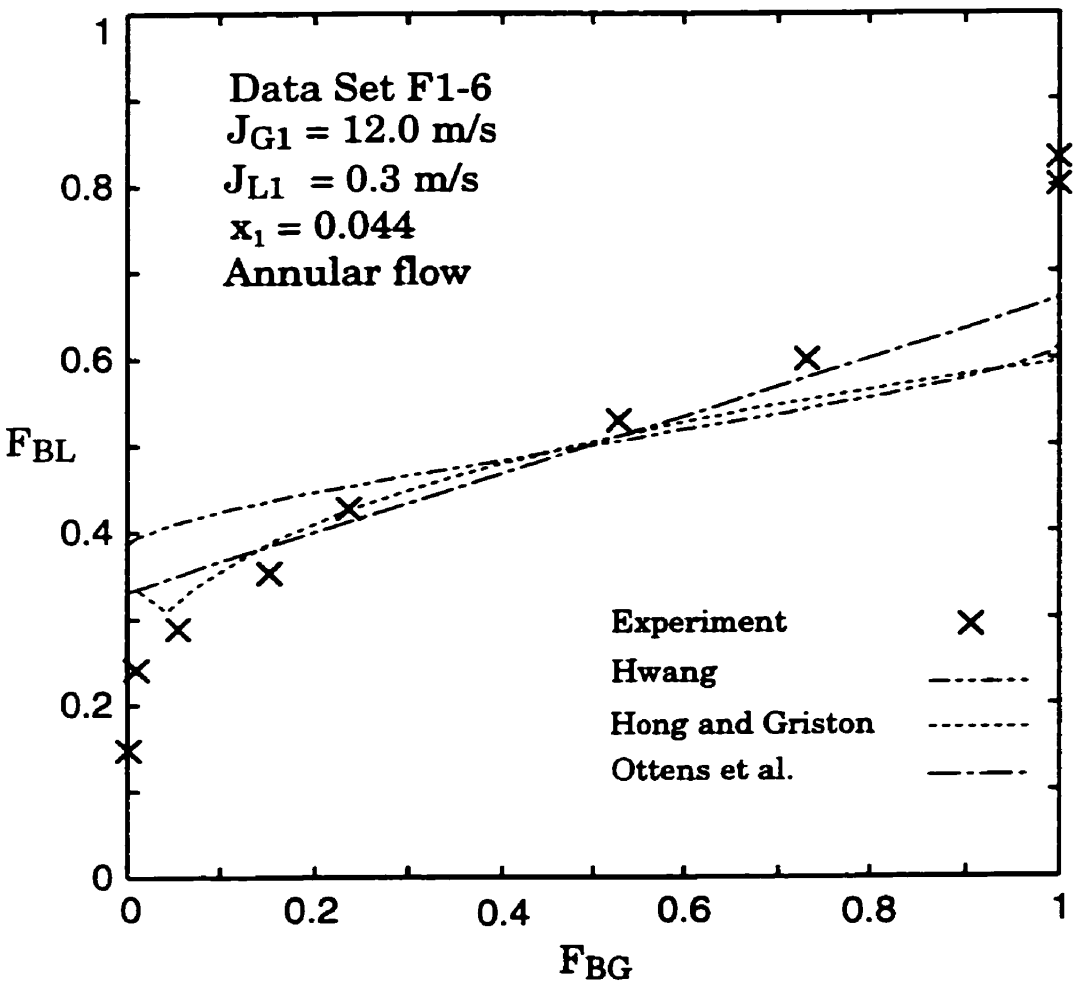

Figure 3.40 Predictions of models and correlations against data set F1-6.

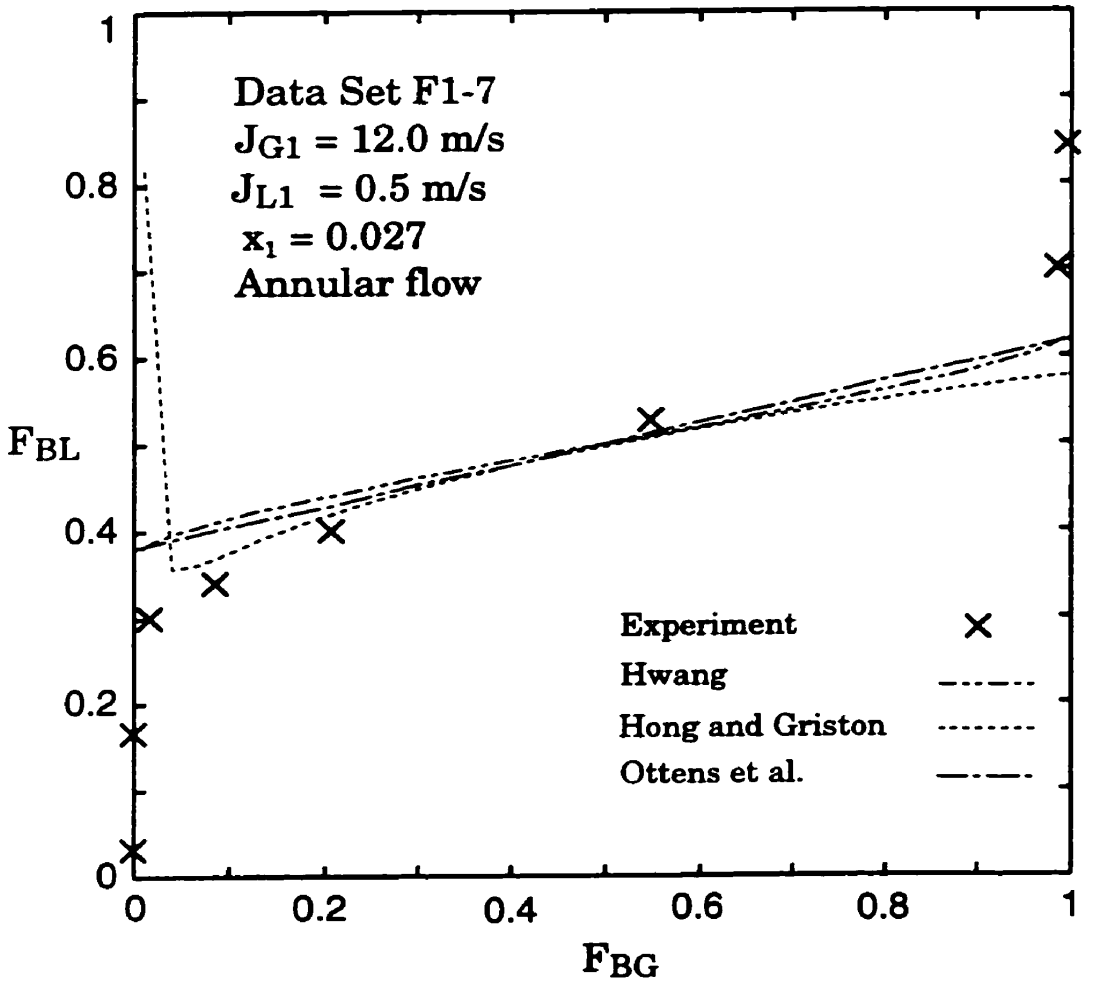

Figure 3.41 Predictions of models and correlations against data set F1-7.

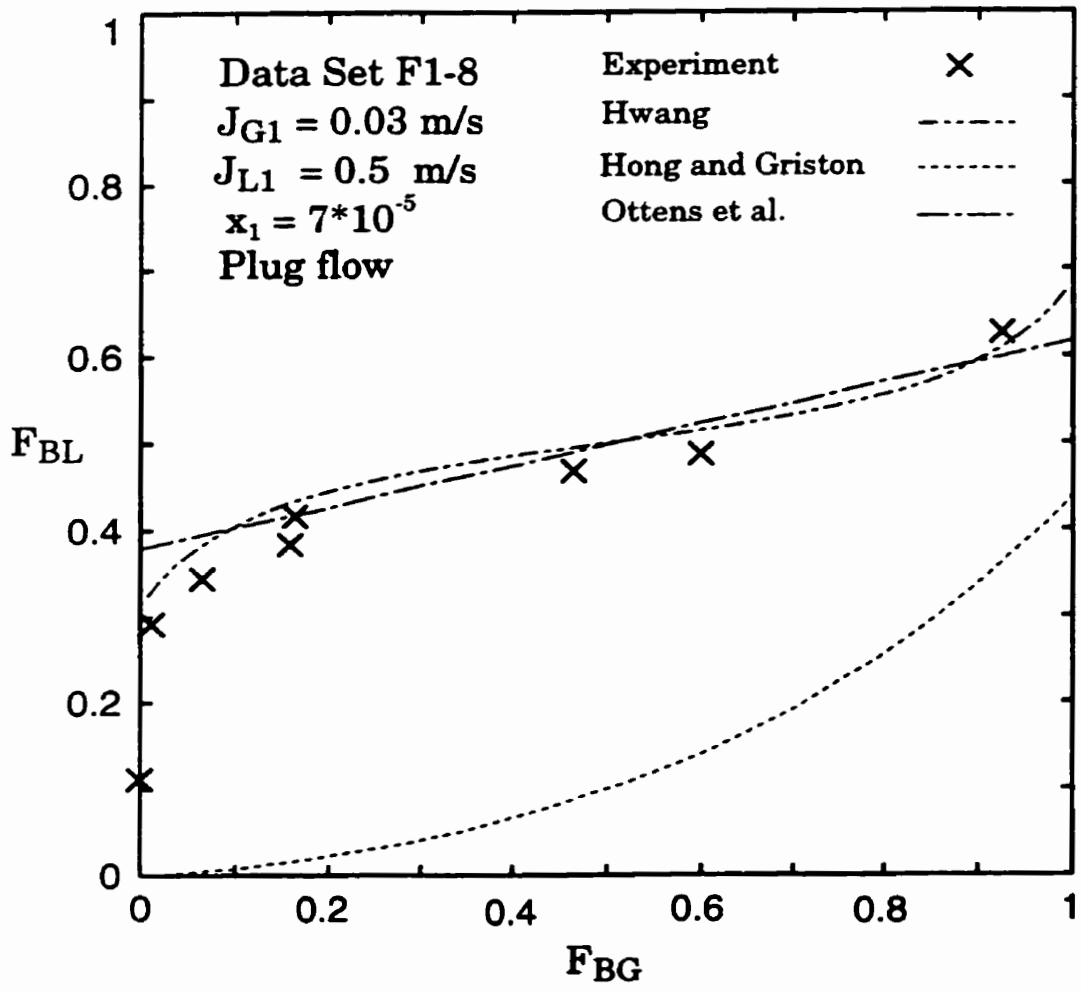

Figure 3.42 Predictions of models and correlations against data set F1-8.

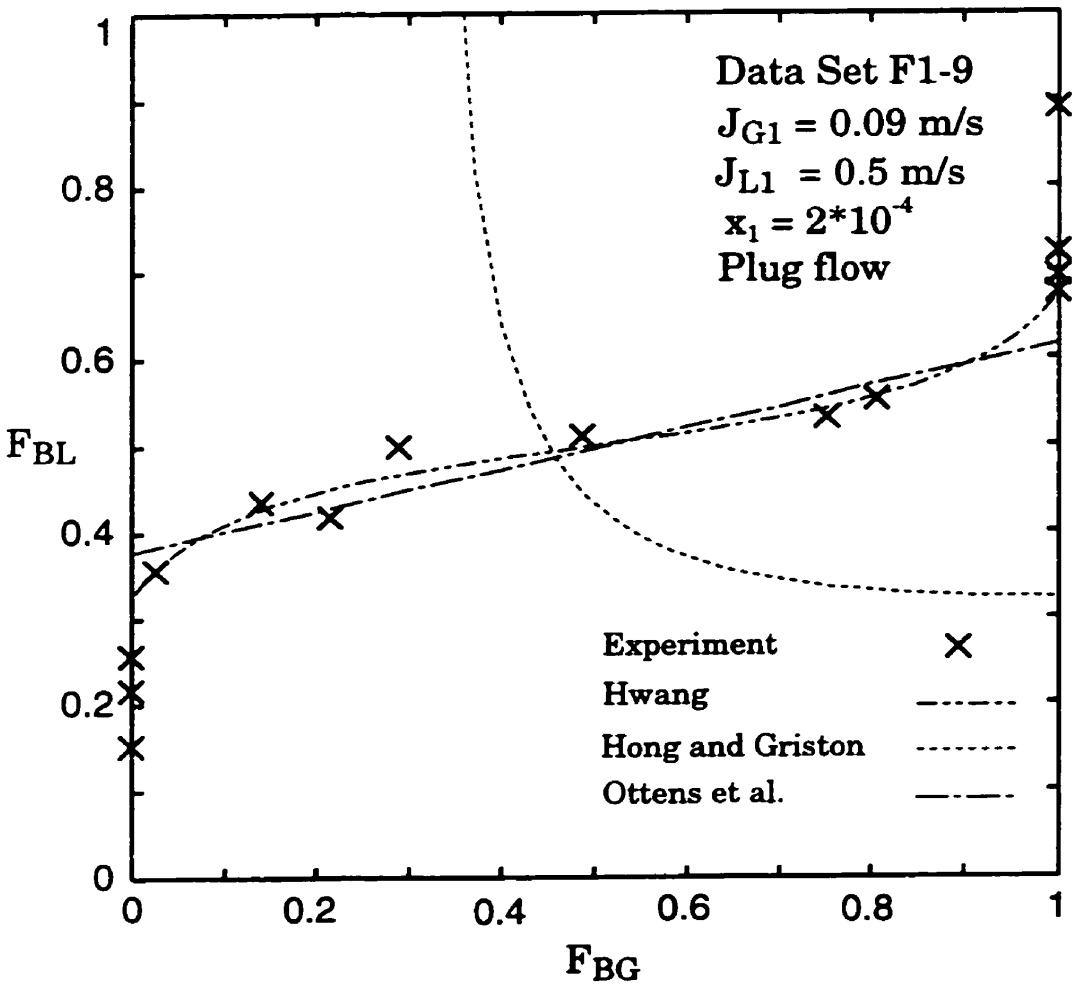

Figure 3.43 Predictions of models and correlations against data set F1-9.

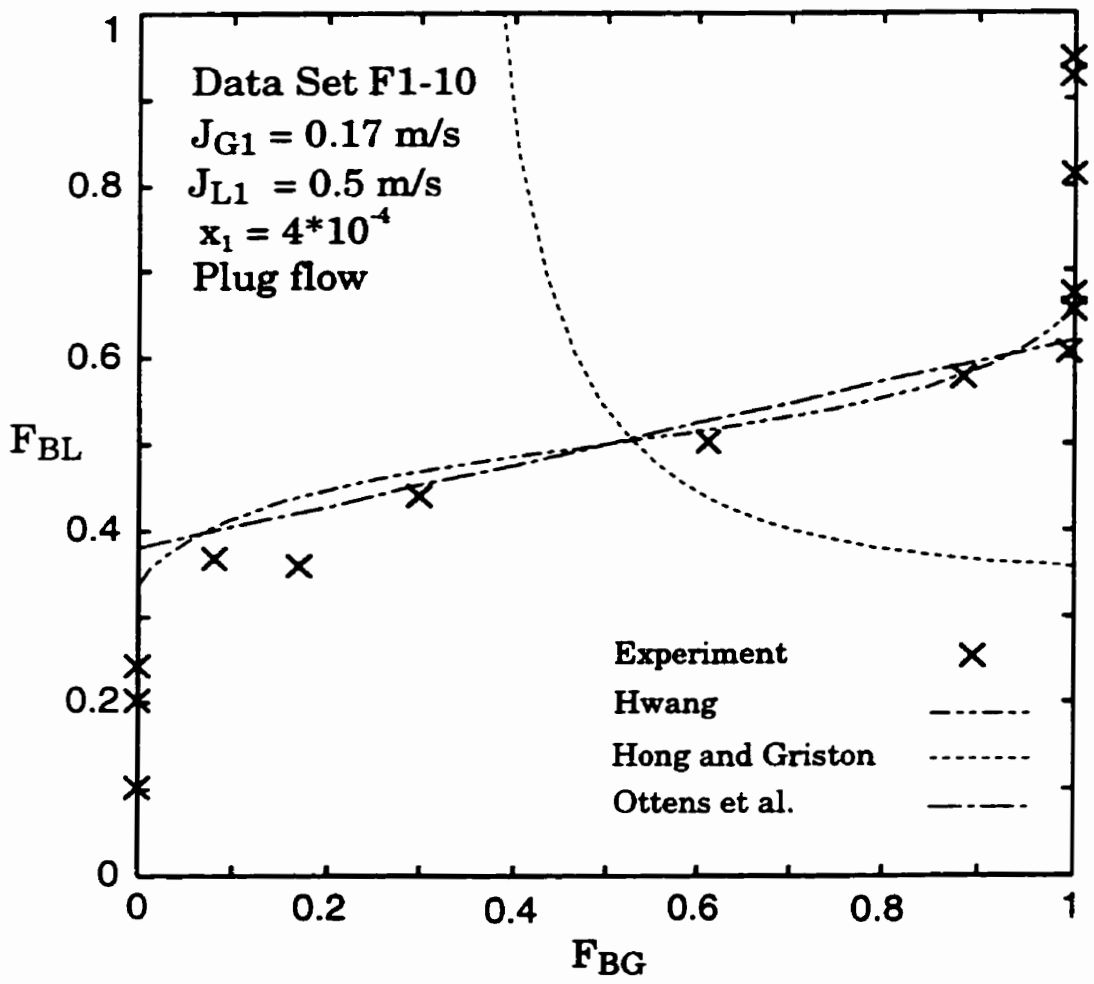

Figure 3.44 Predictions of models and correlations against data set F1-10.

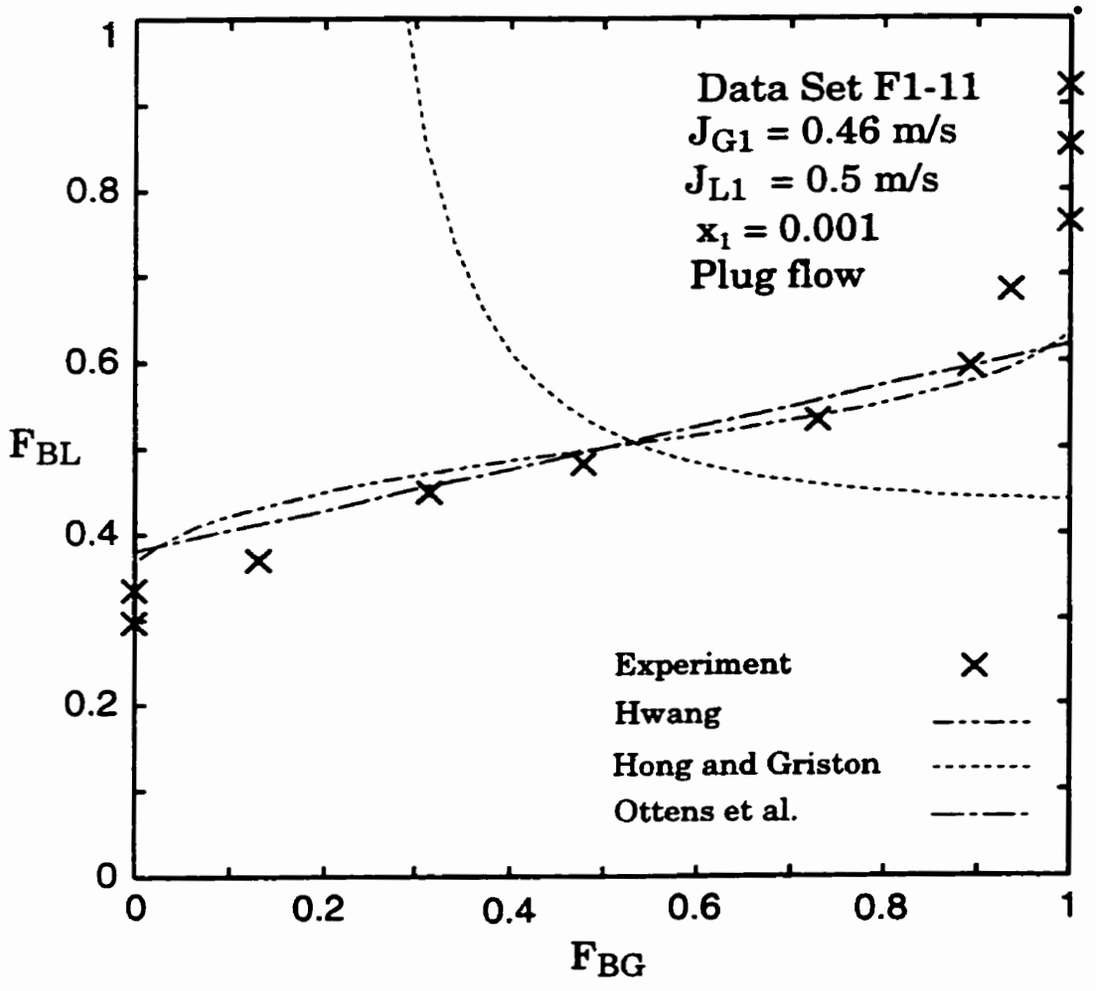

Figure 3.45 Predictions of models and correlations against data set F1-11.

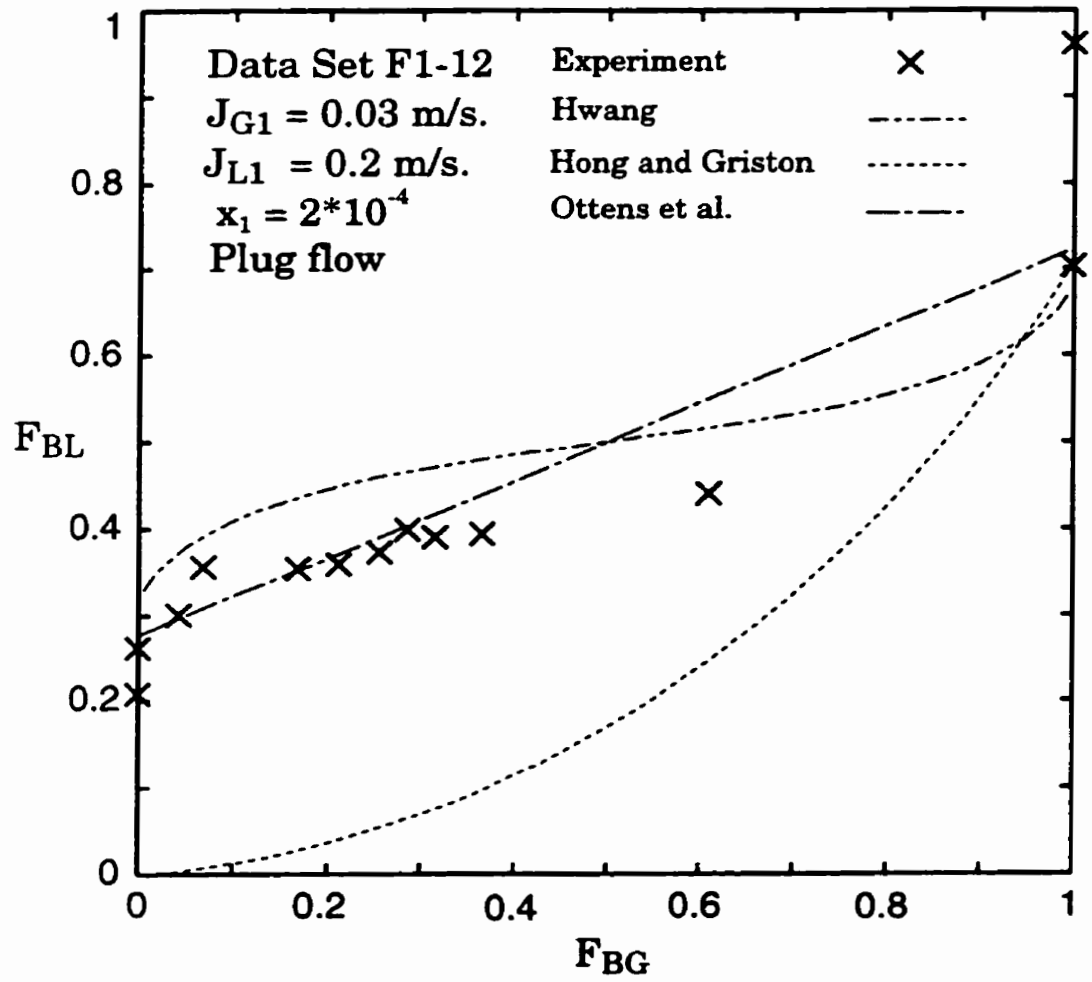

Figure 3.46 Predictions of models and correlations against data set F1-12.

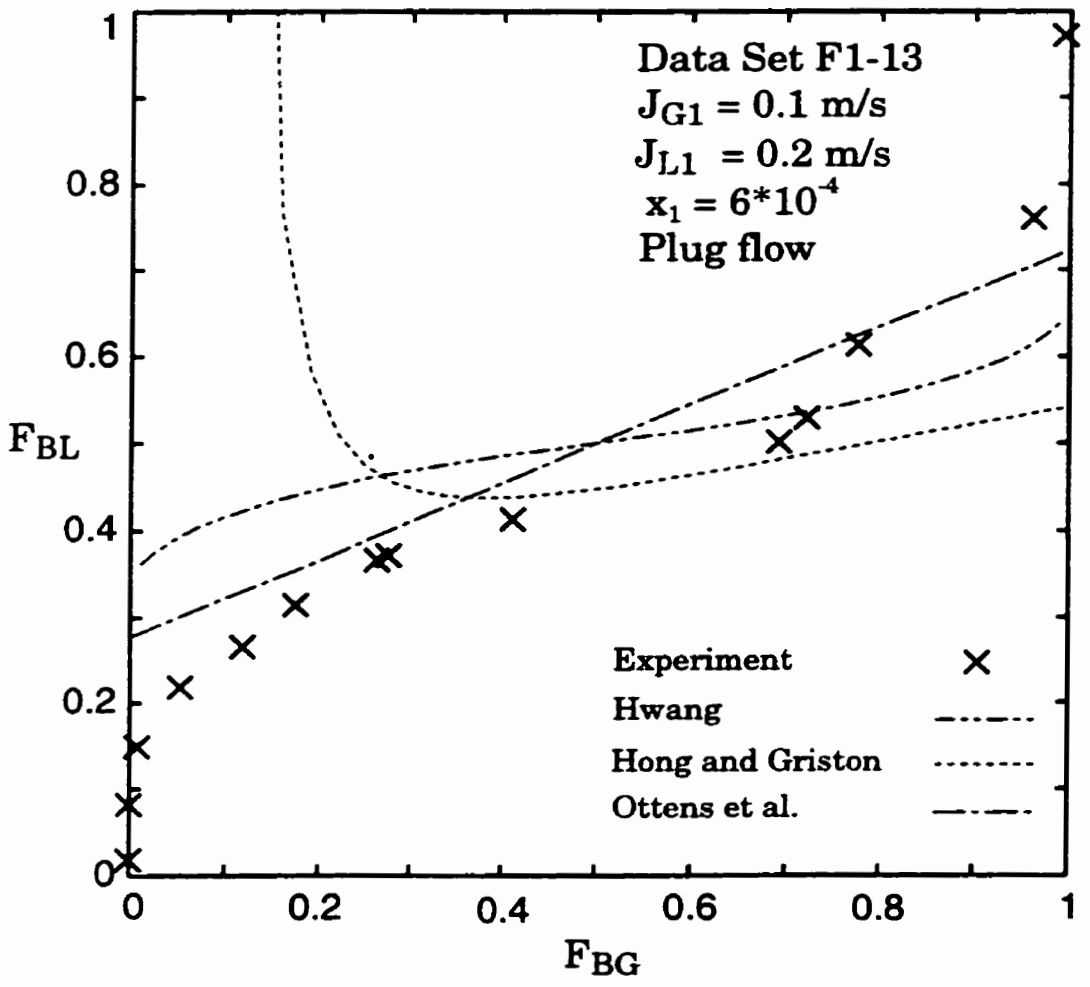

Figure 3.47 Predictions of models and correlations against data set F1-13.

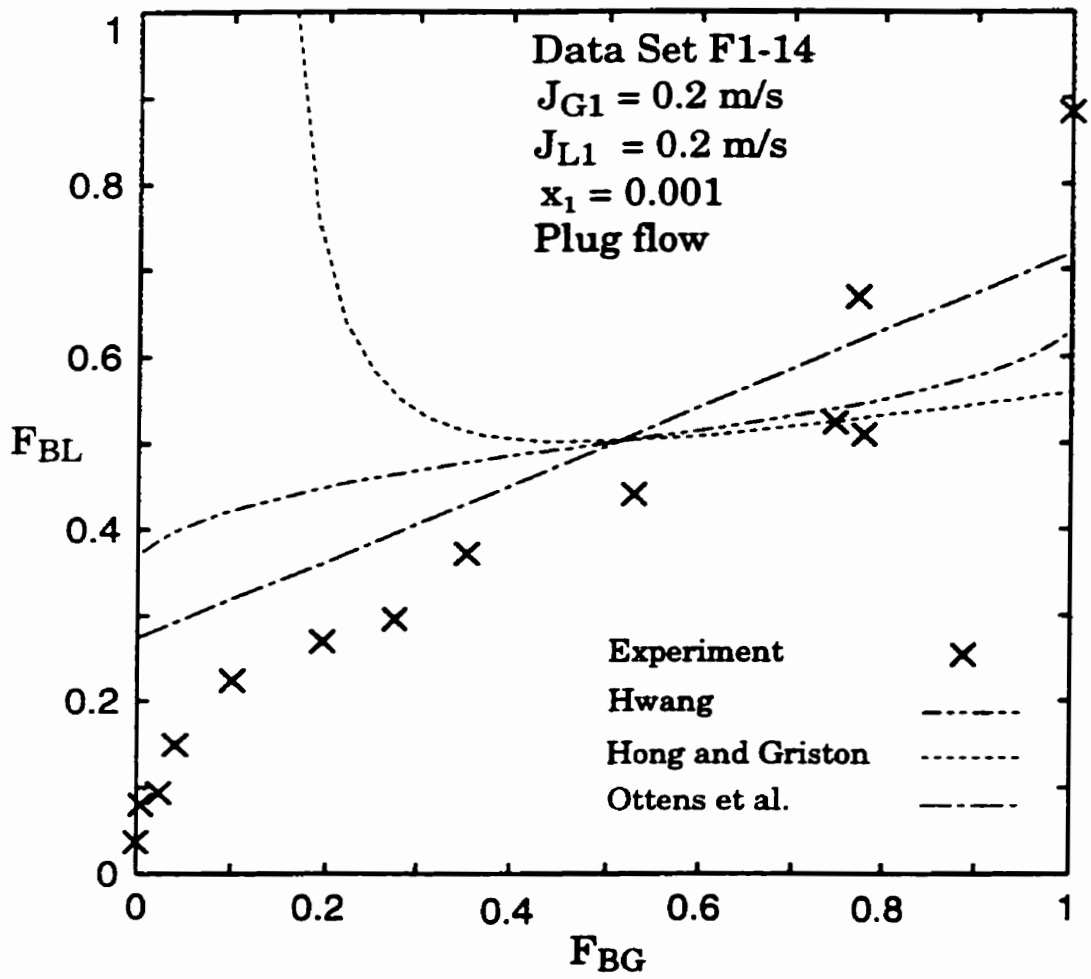

Figure 3.48 Predictions of models and correlations against data set F1-14.

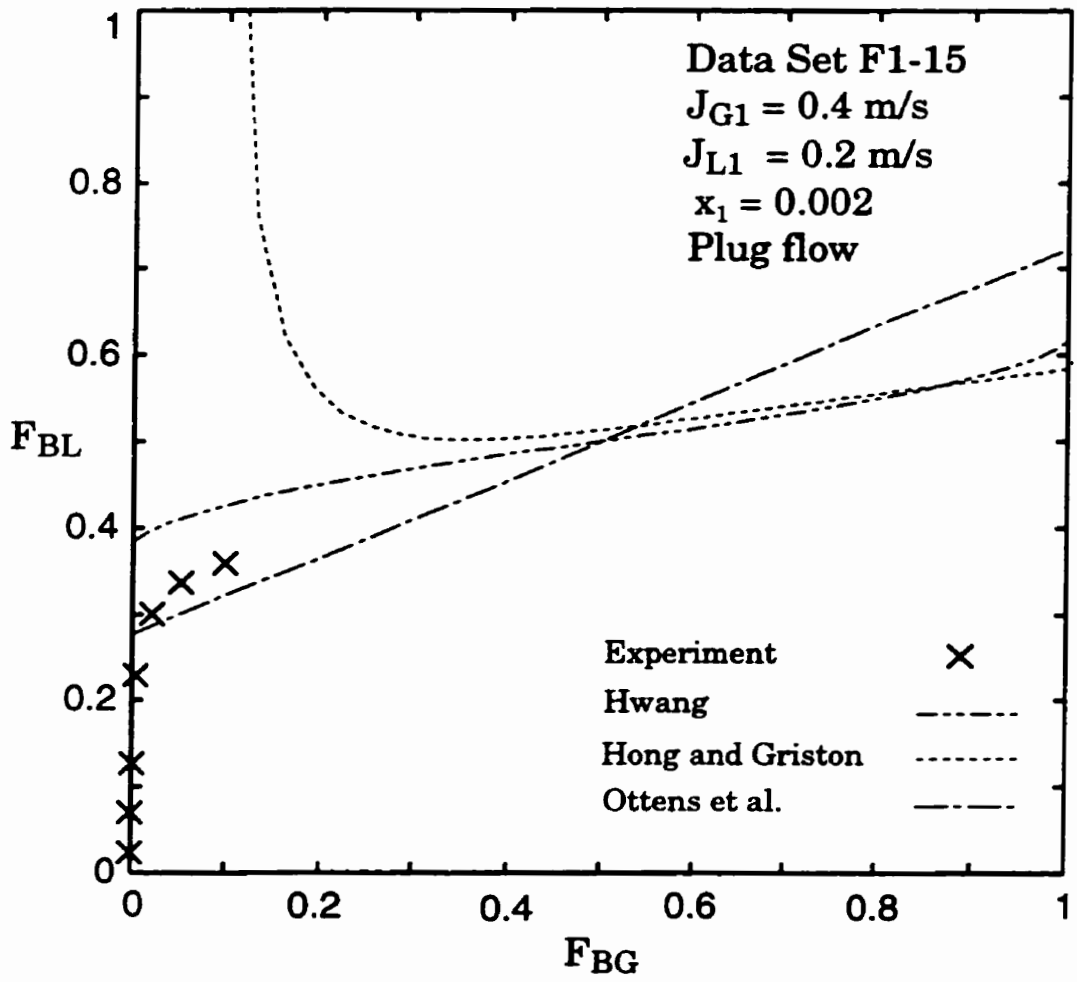

Figure 3.49 Predictions of models and correlations against data set F1-15.

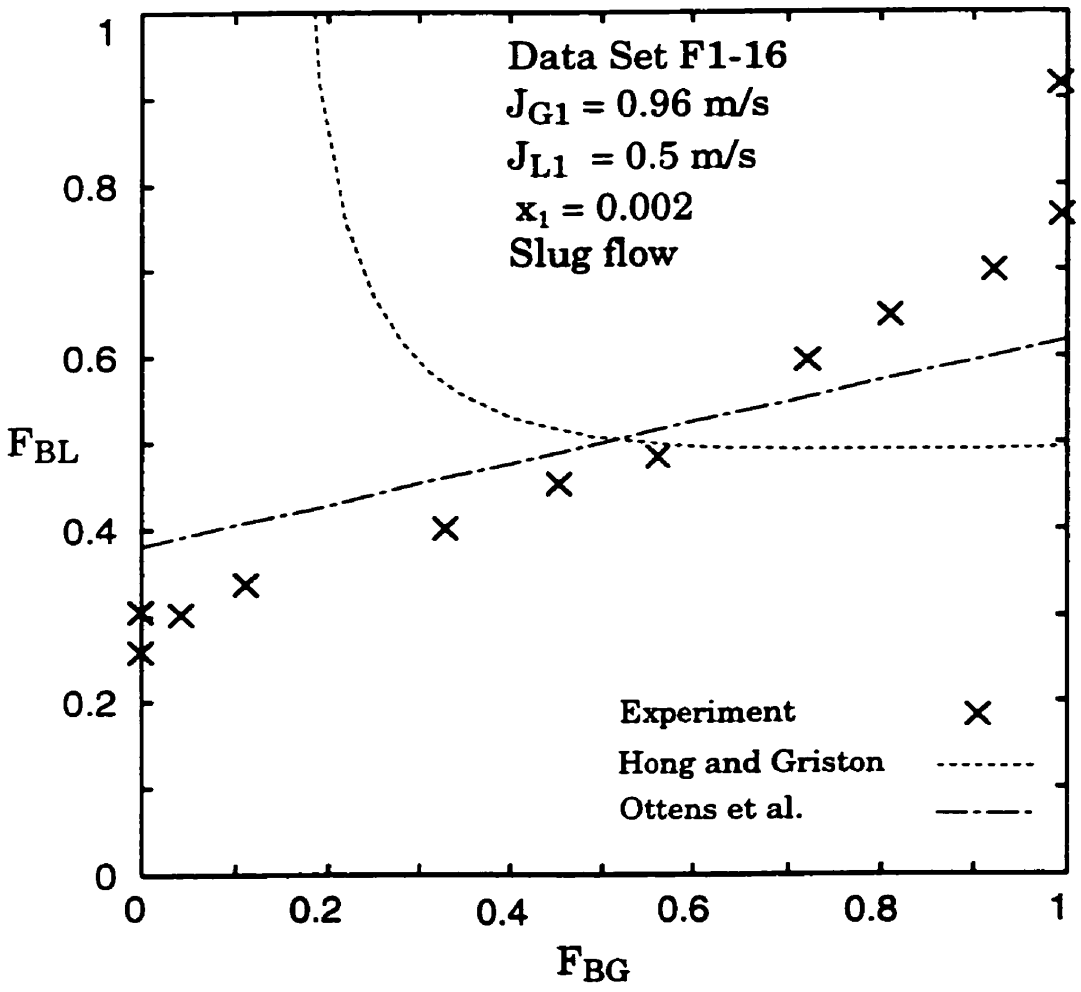

Figure 3.50 Predictions of models and correlations against data set F1-16.

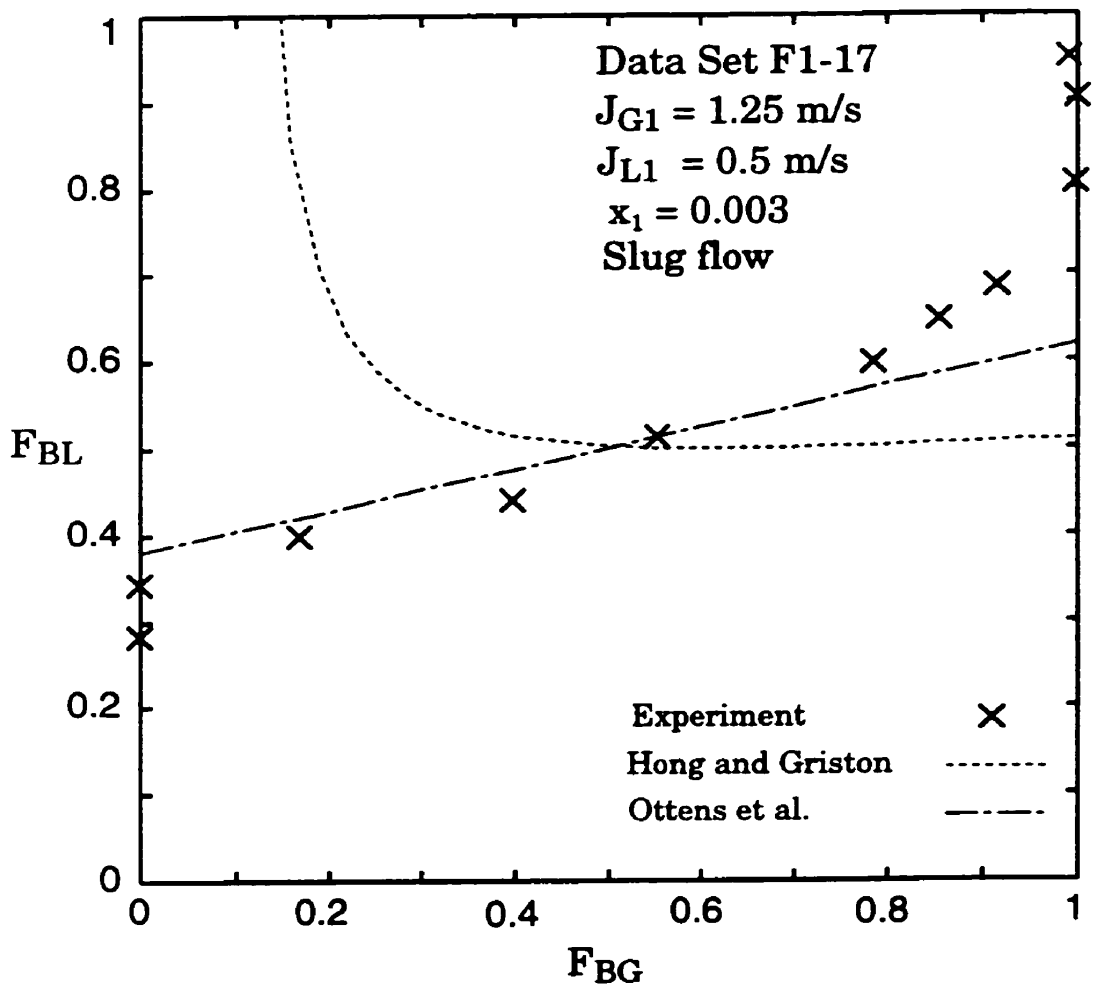

Figure 3.51 Predictions of models and correlations against data set F1-17.

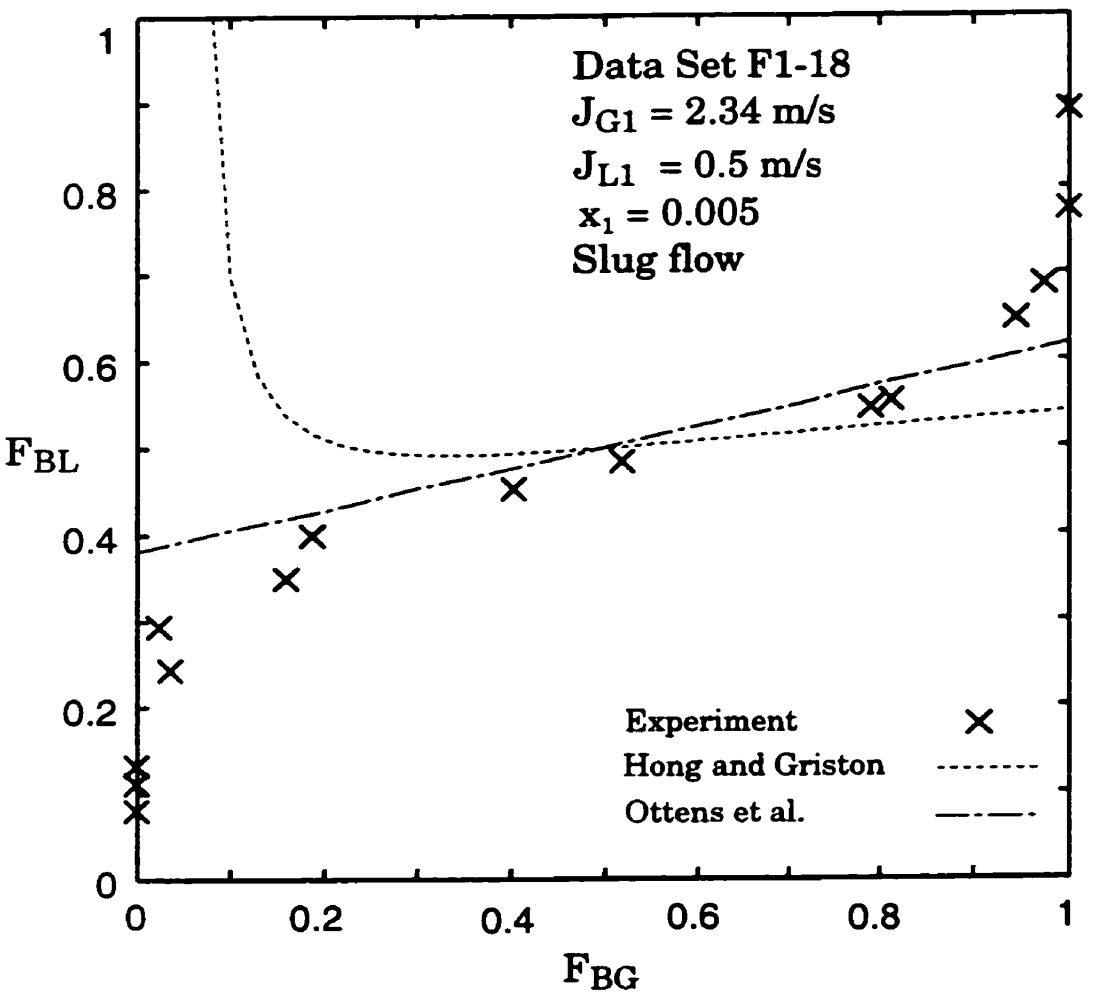

Figure 3.52 Predictions of models and correlations against data set F1-18.

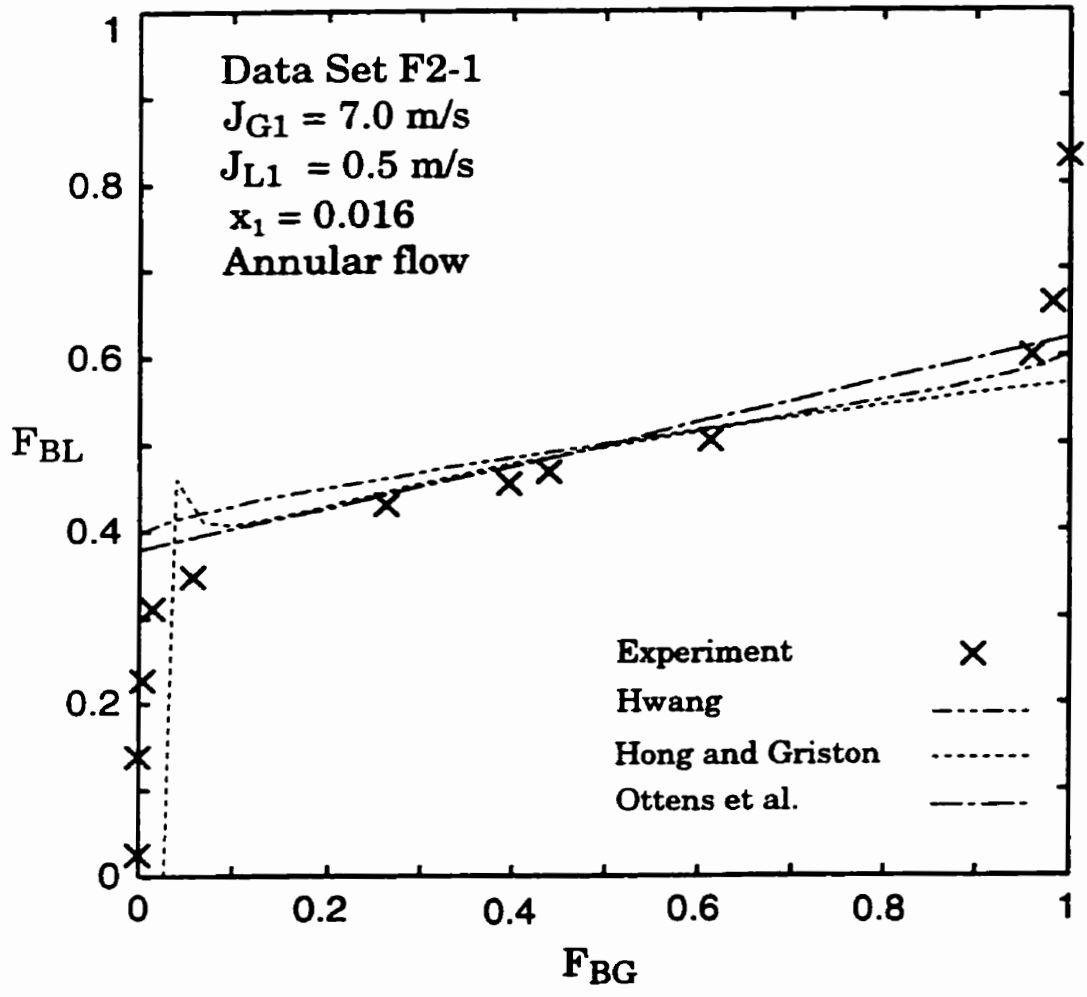

Figure 3.53 Predictions of models and correlations against data set F2-1.

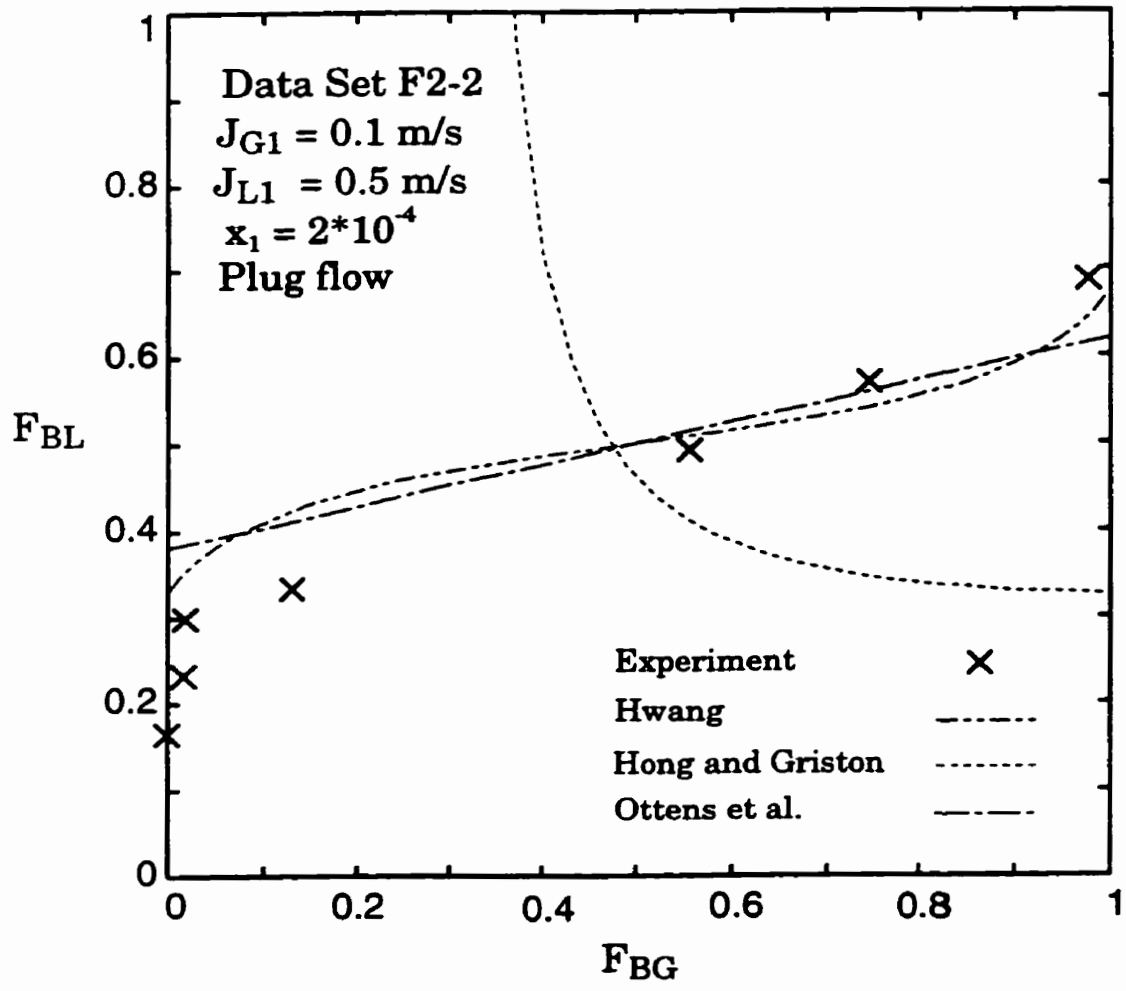

Figure 3.54 Predictions of models and correlations against data set F2-2.

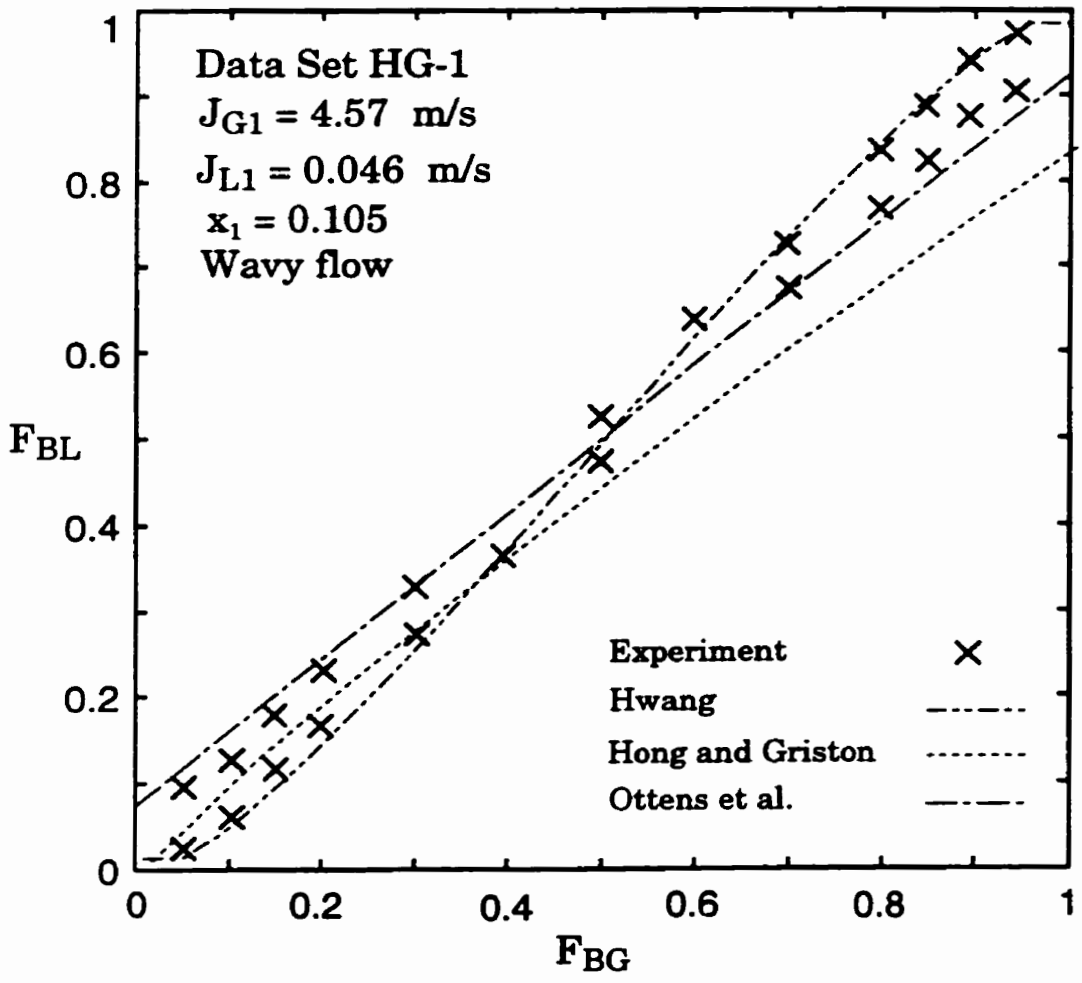

Figure 3.55 Predictions of models and correlations against data set HG-1.

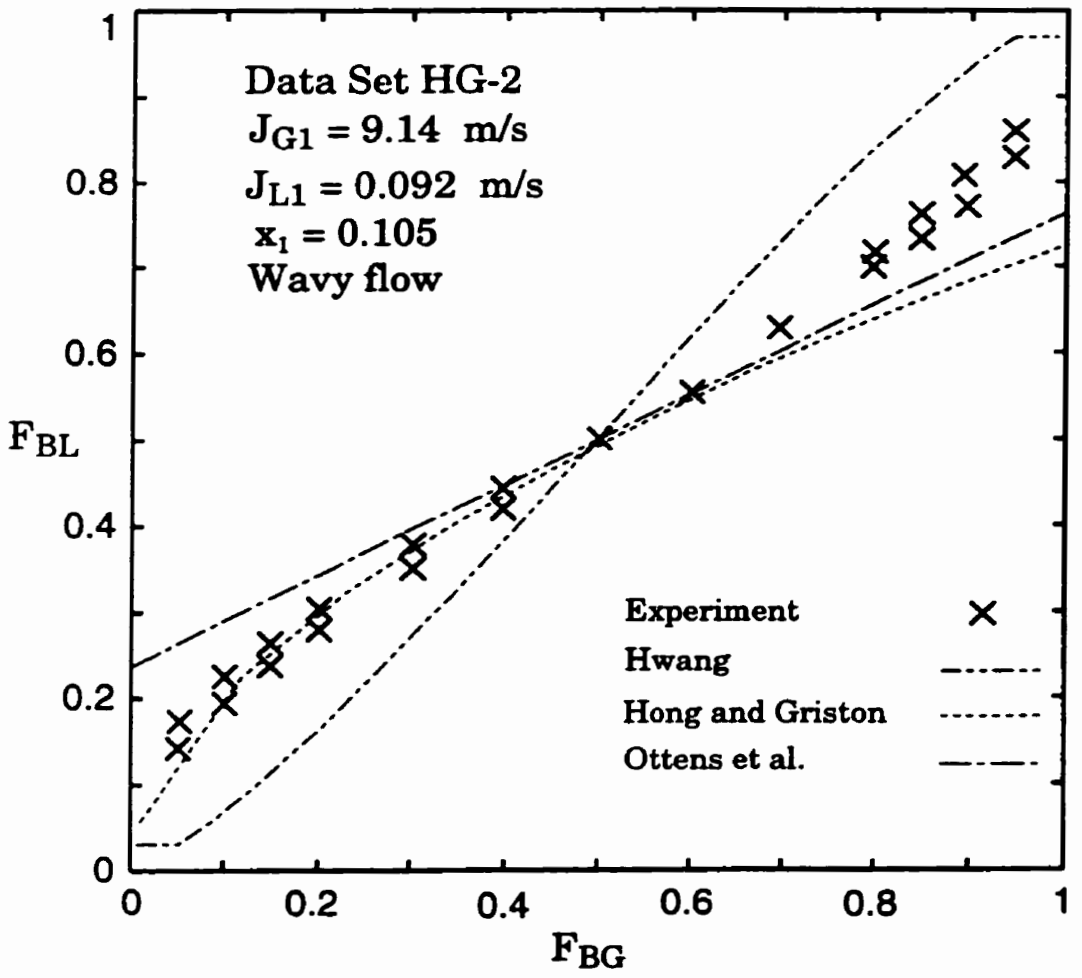

Figure 3.56 Predictions of models and correlations against data set HG-2.

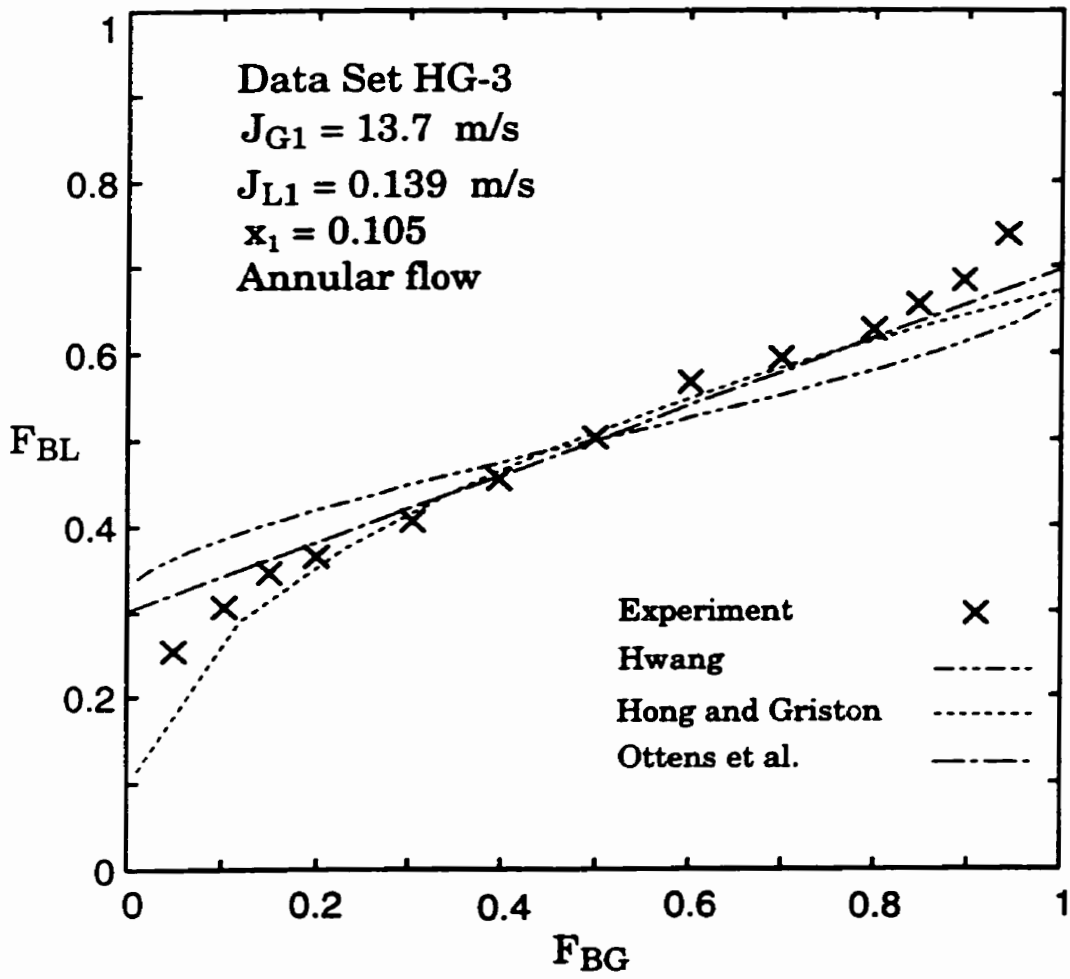

Figure 3.57 Predictions of models and correlations against data set HG-3.

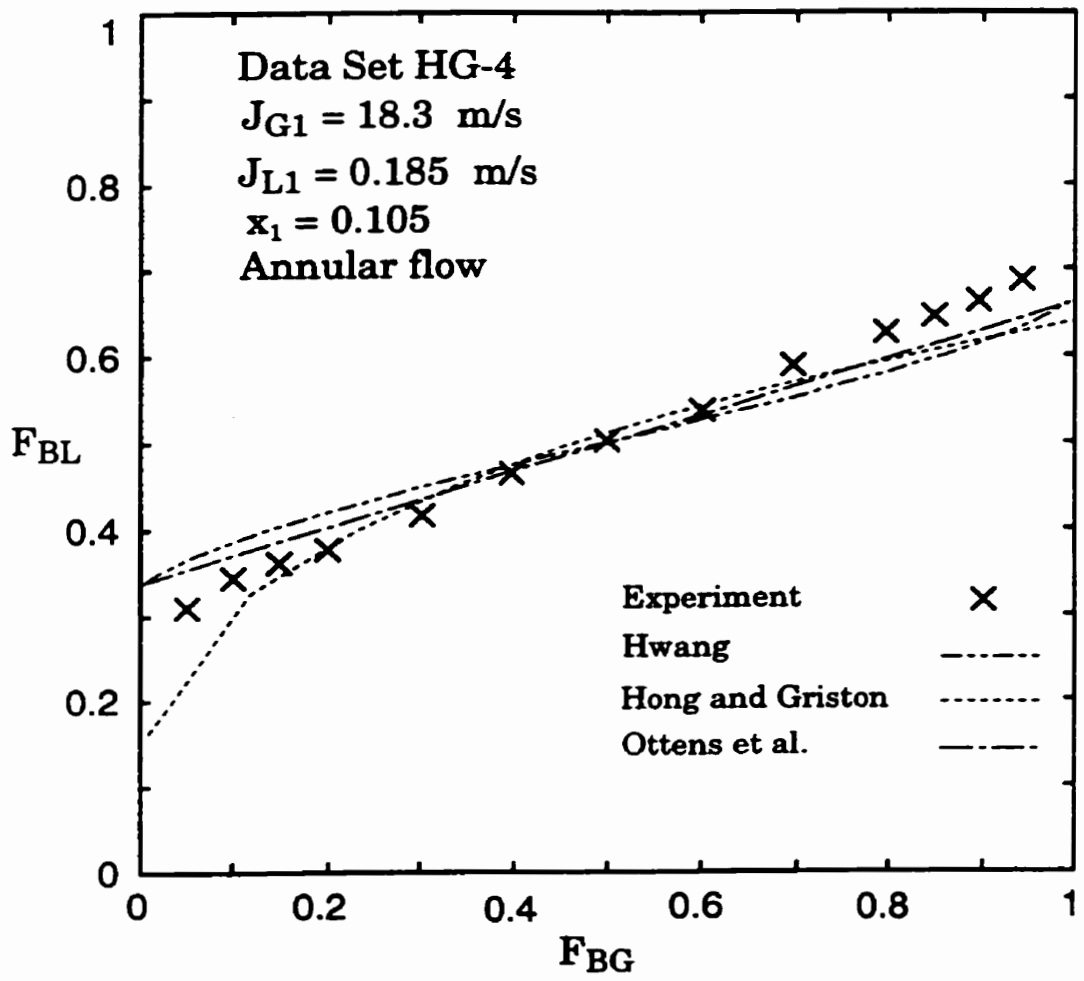

Figure 3.58 Predictions of models and correlations against data set HG-4.

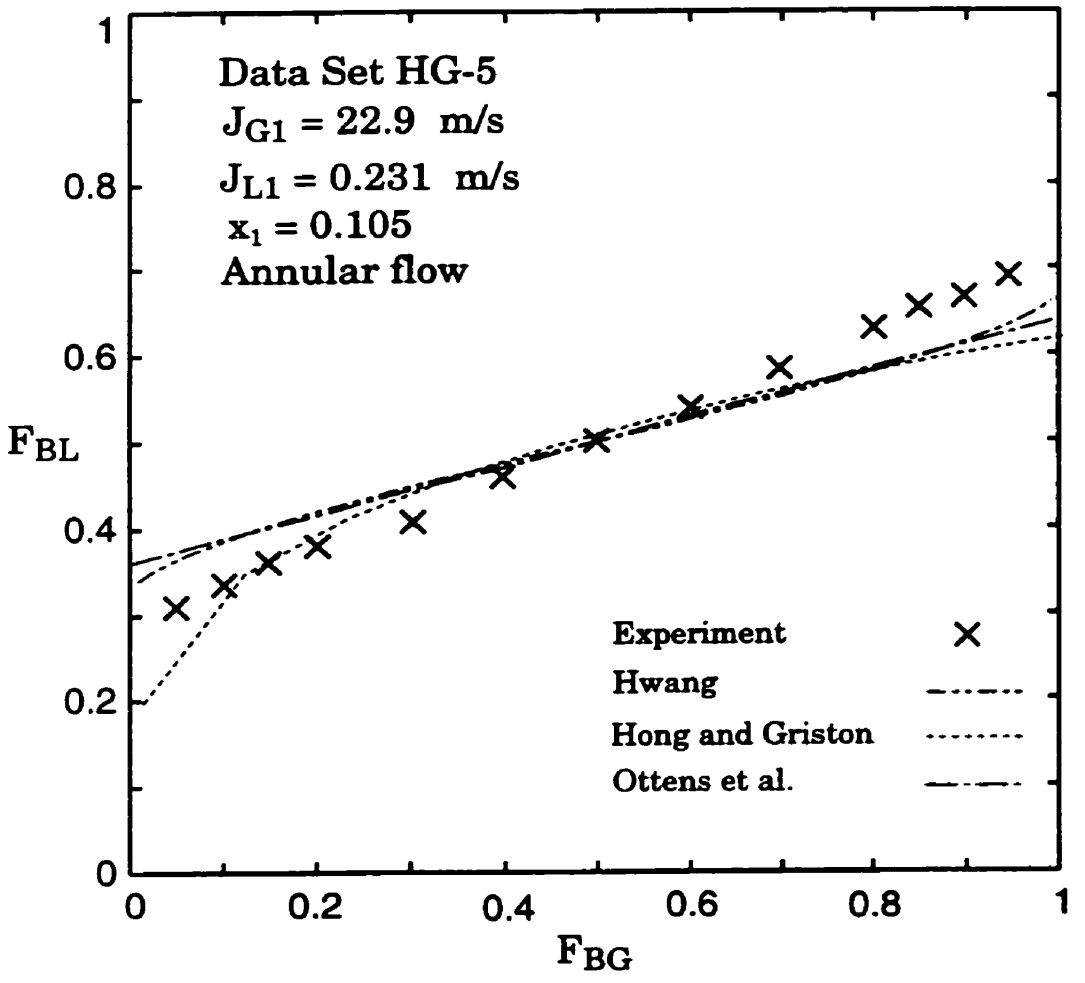

Figure 3.59 Predictions of models and correlations against data set HG-5.

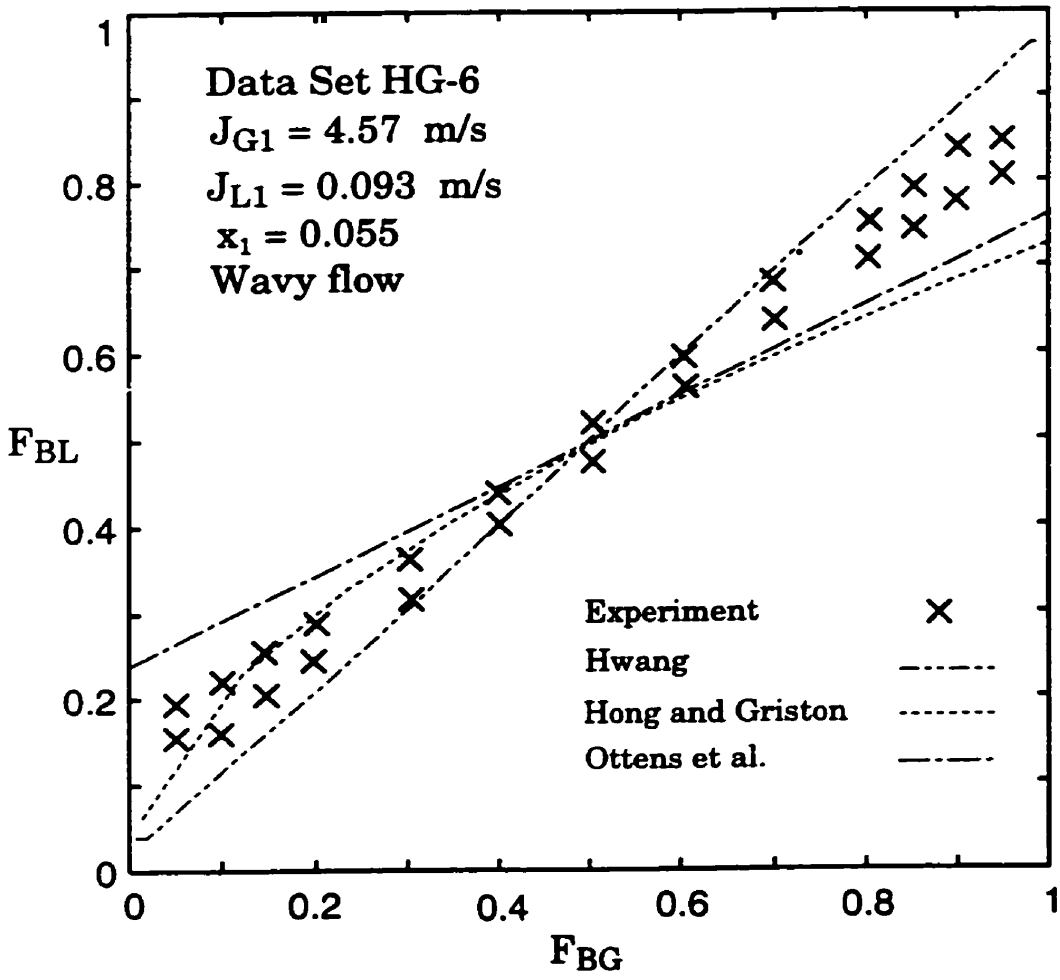

Figure 3.60 Predictions of models and correlations against data set HG-6.

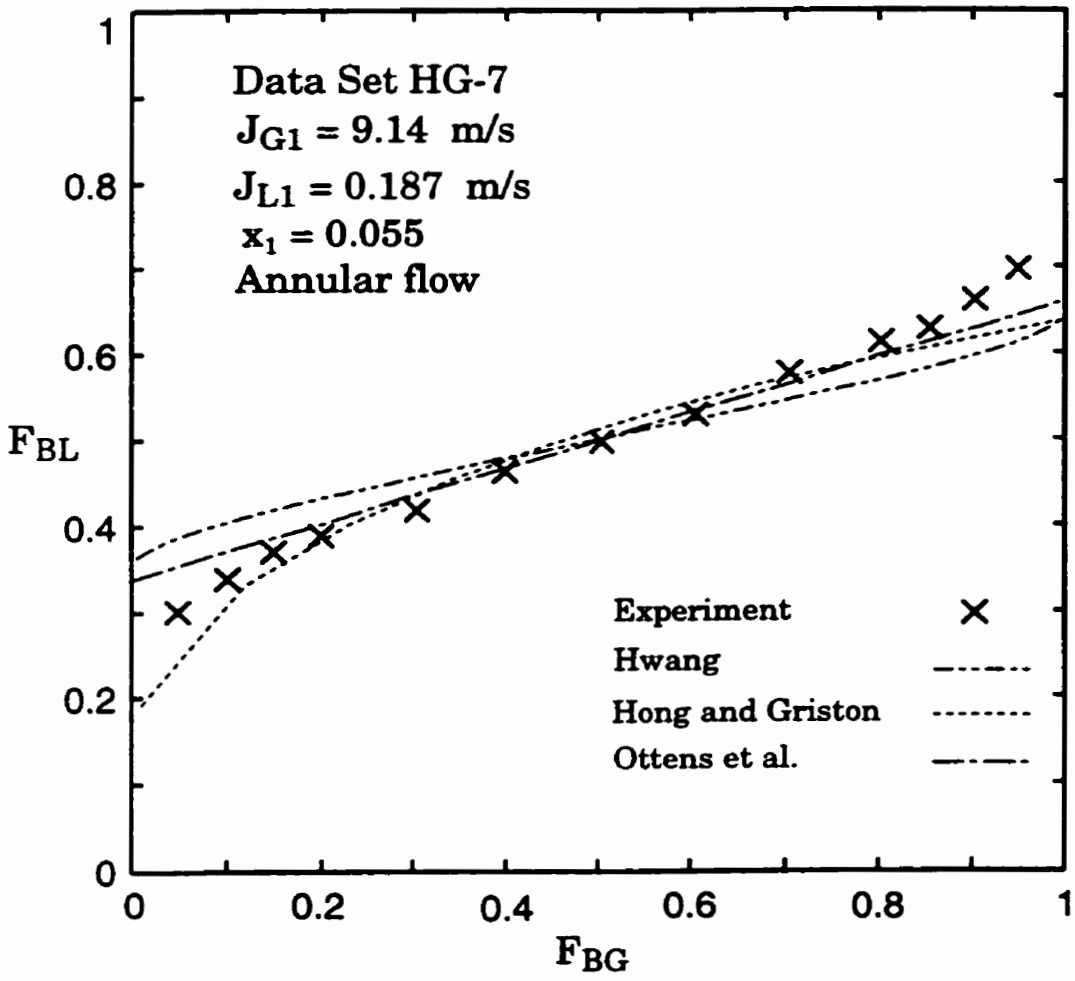

Figure 3.61 Predictions of models and correlations against data set HG-7.

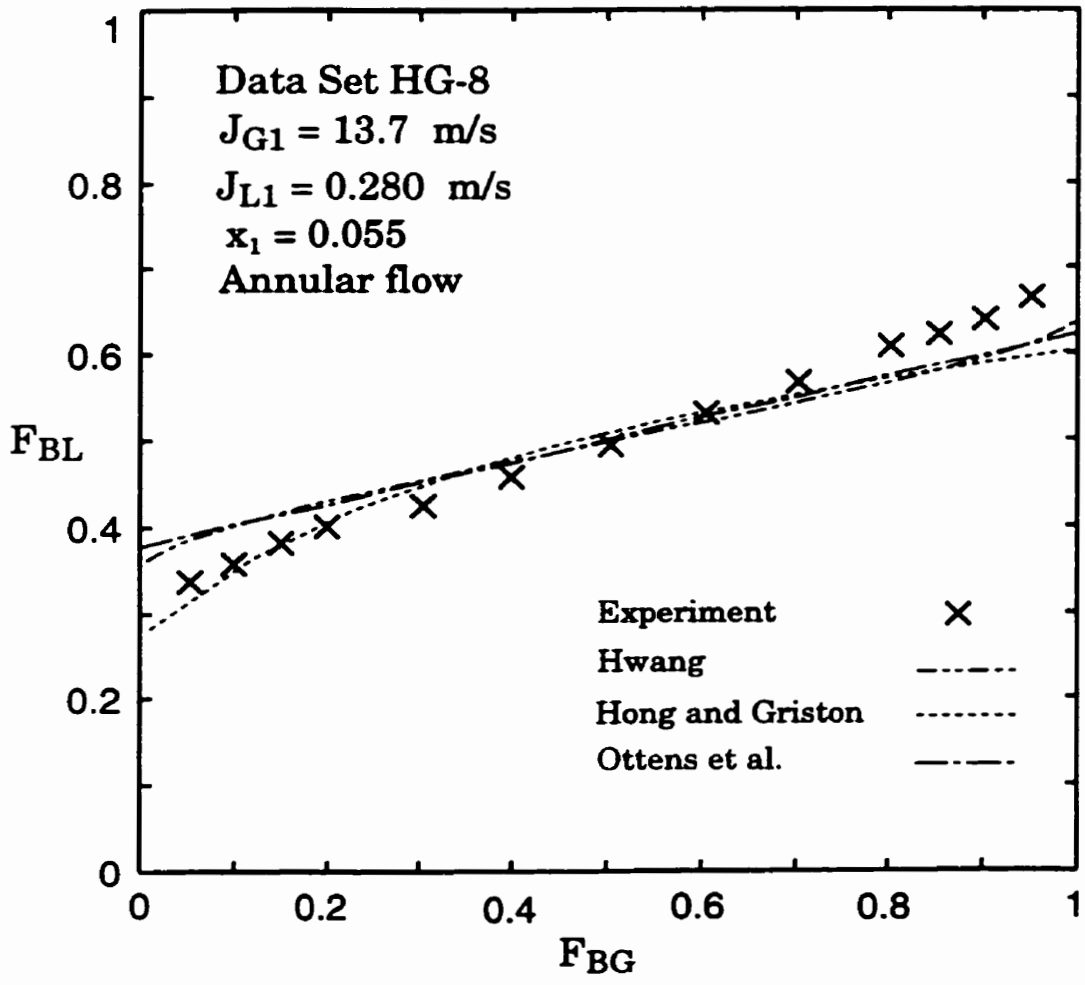

Figure 3.62 Predictions of models and correlations against data set HG-8.

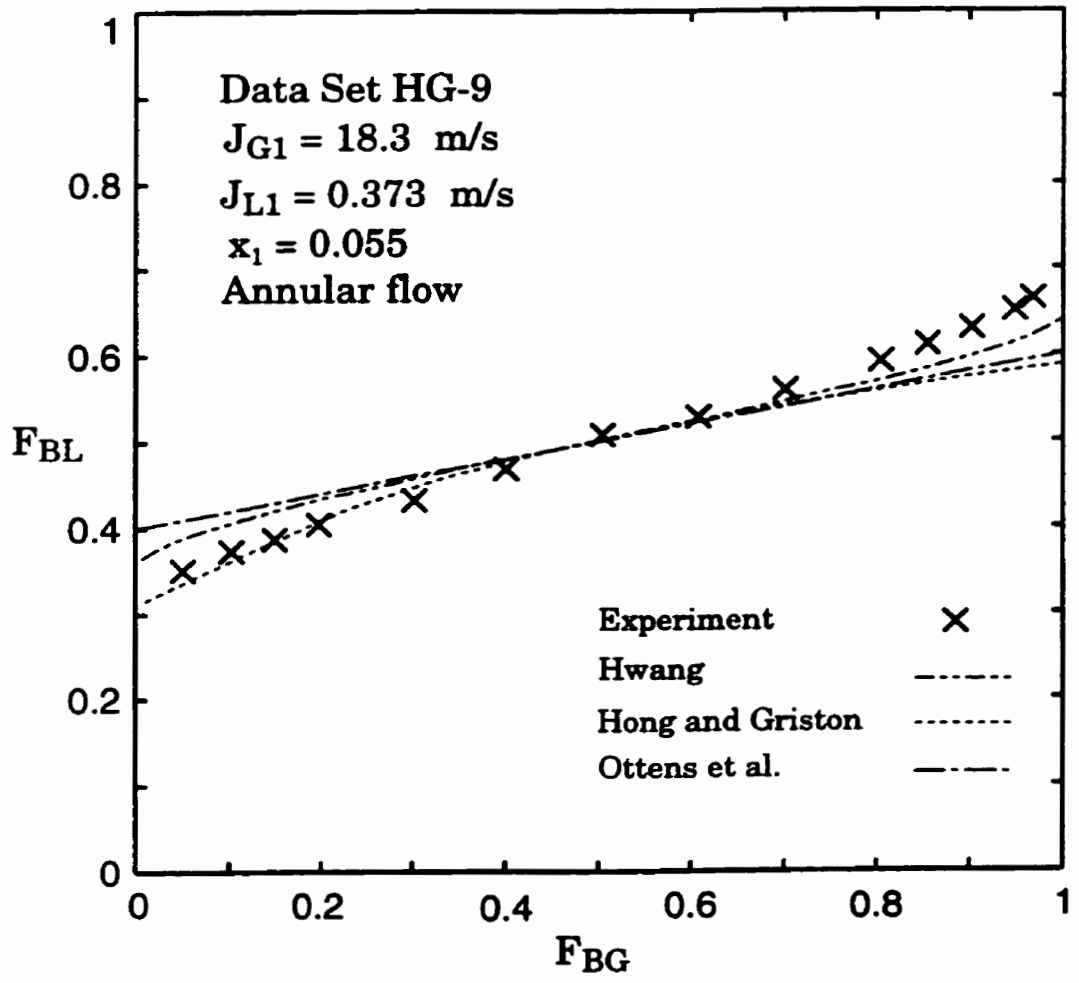

Figure 3.63 Predictions of models and correlations against data set HG-9.

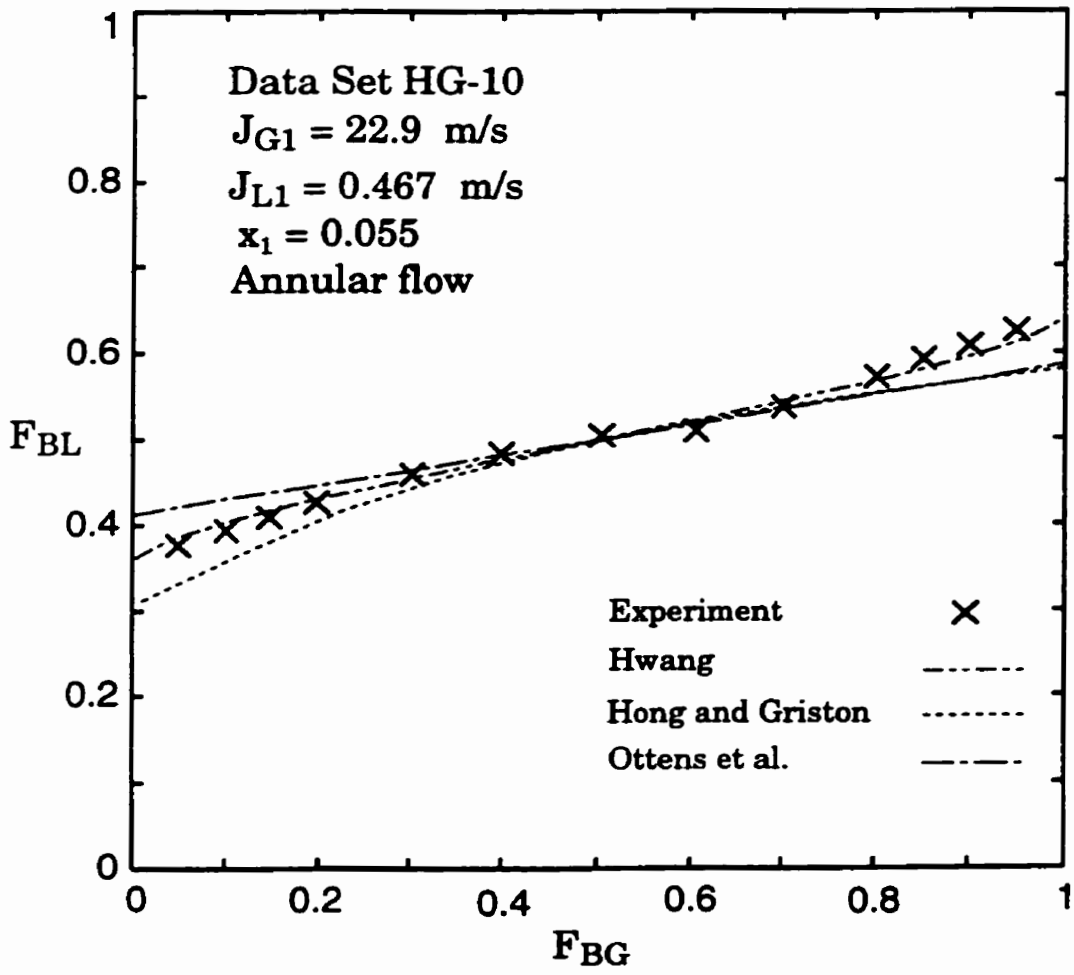

Figure 3.64 Predictions of models and correlations against data set HG-10.

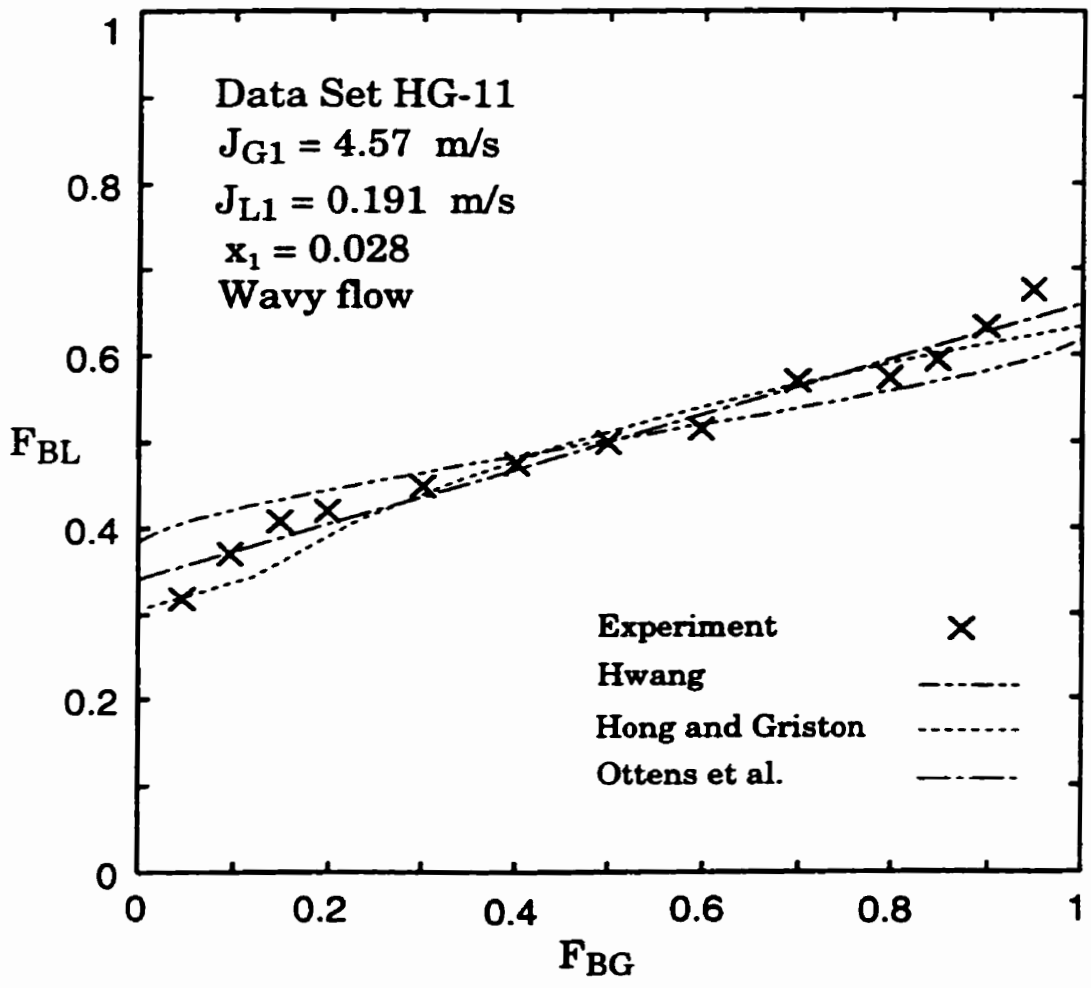

Figure 3.65 Predictions of models and correlations against data set HG-11.

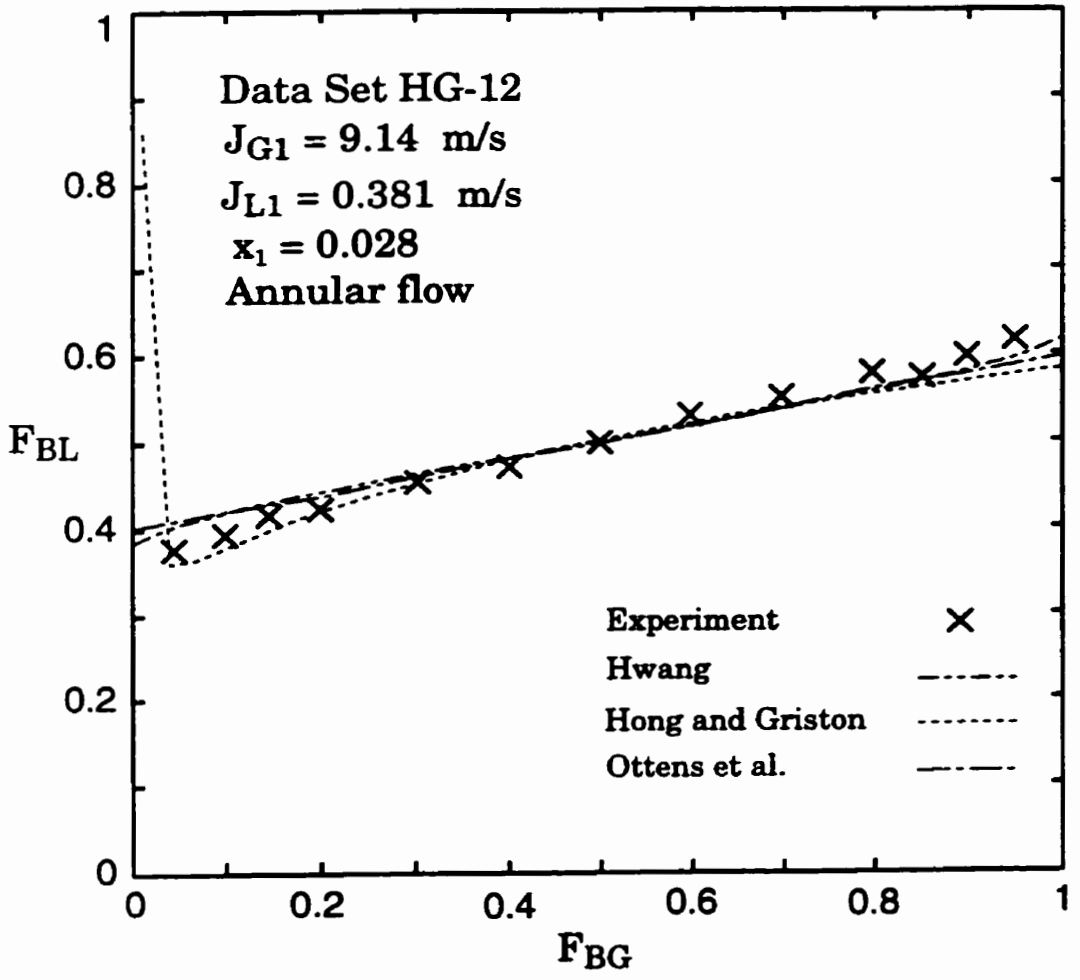

Figure 3.66 Predictions of models and correlations against data set HG-12.

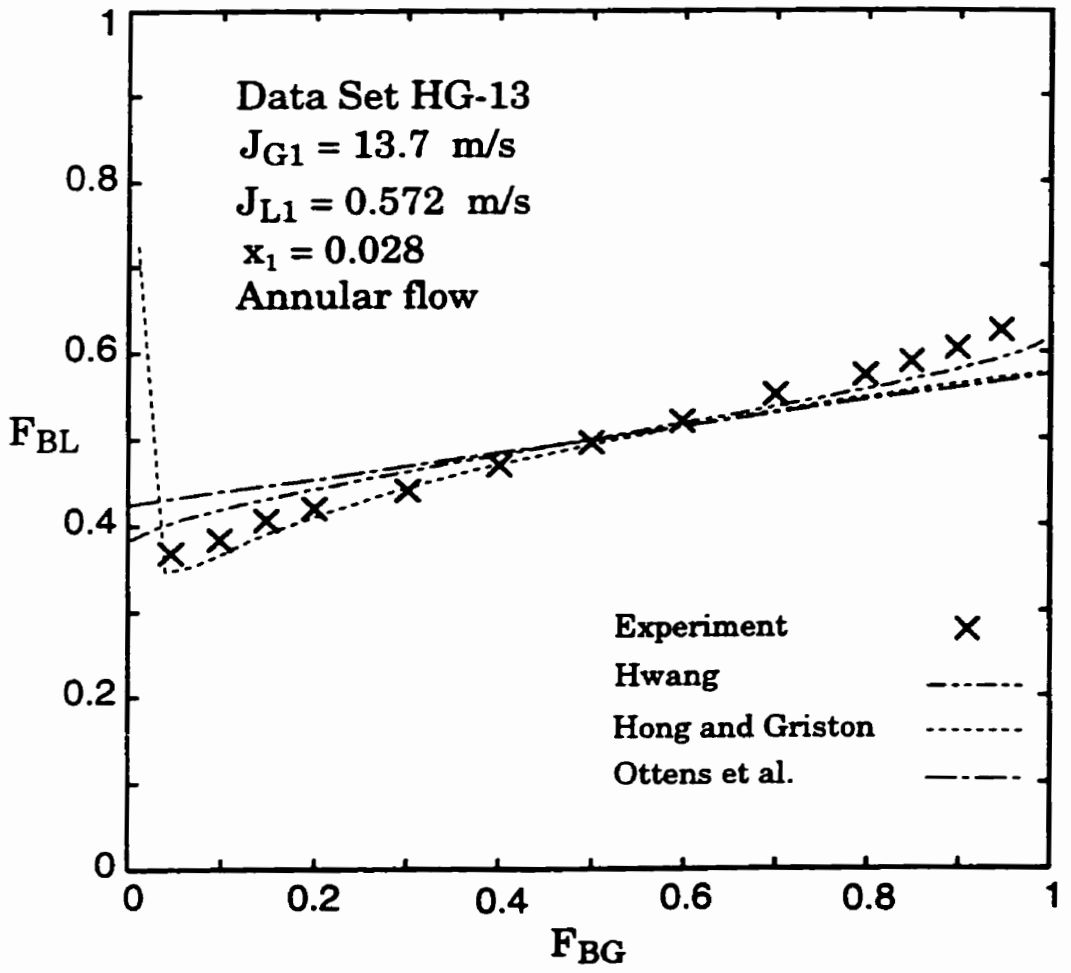

Figure 3.67 Predictions of models and correlations gainst data set HG-13.

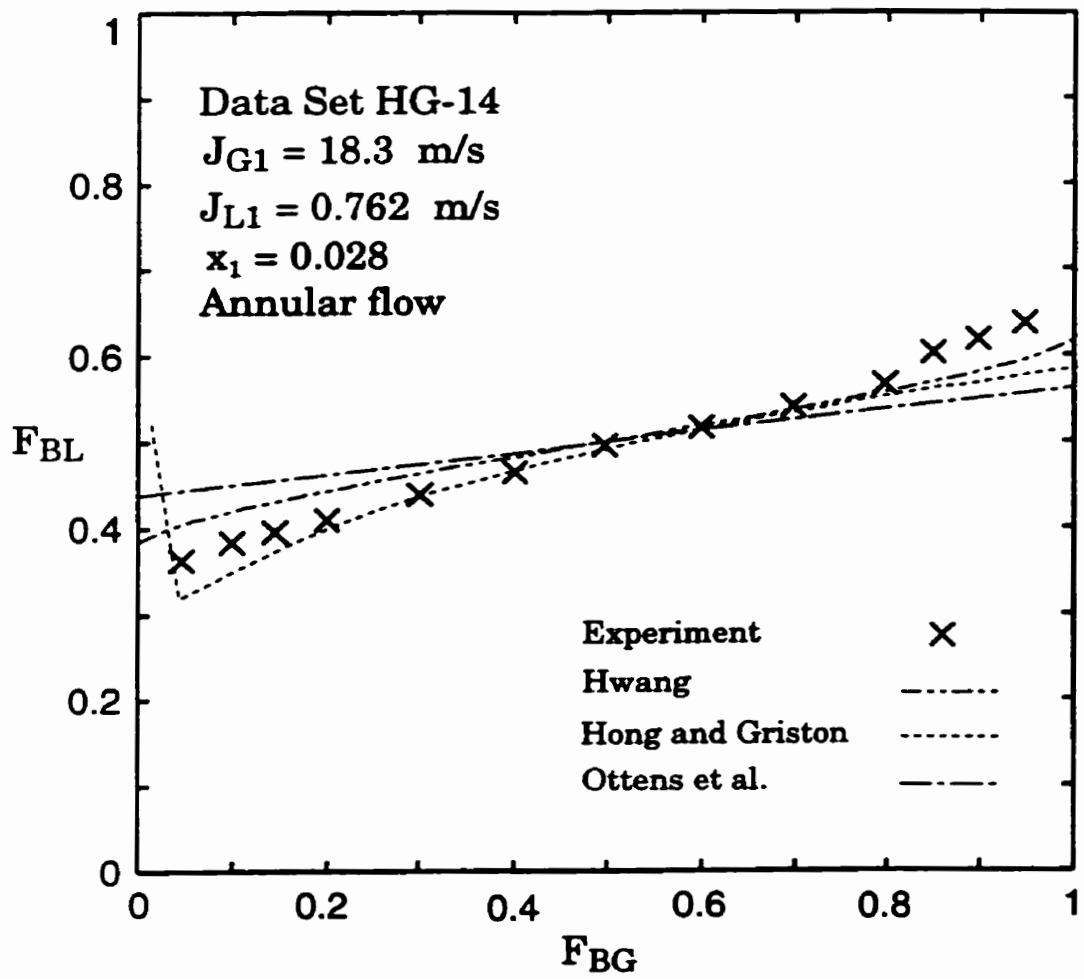

Figure 3.68 Predictions of models and correlations against data set HG-14.

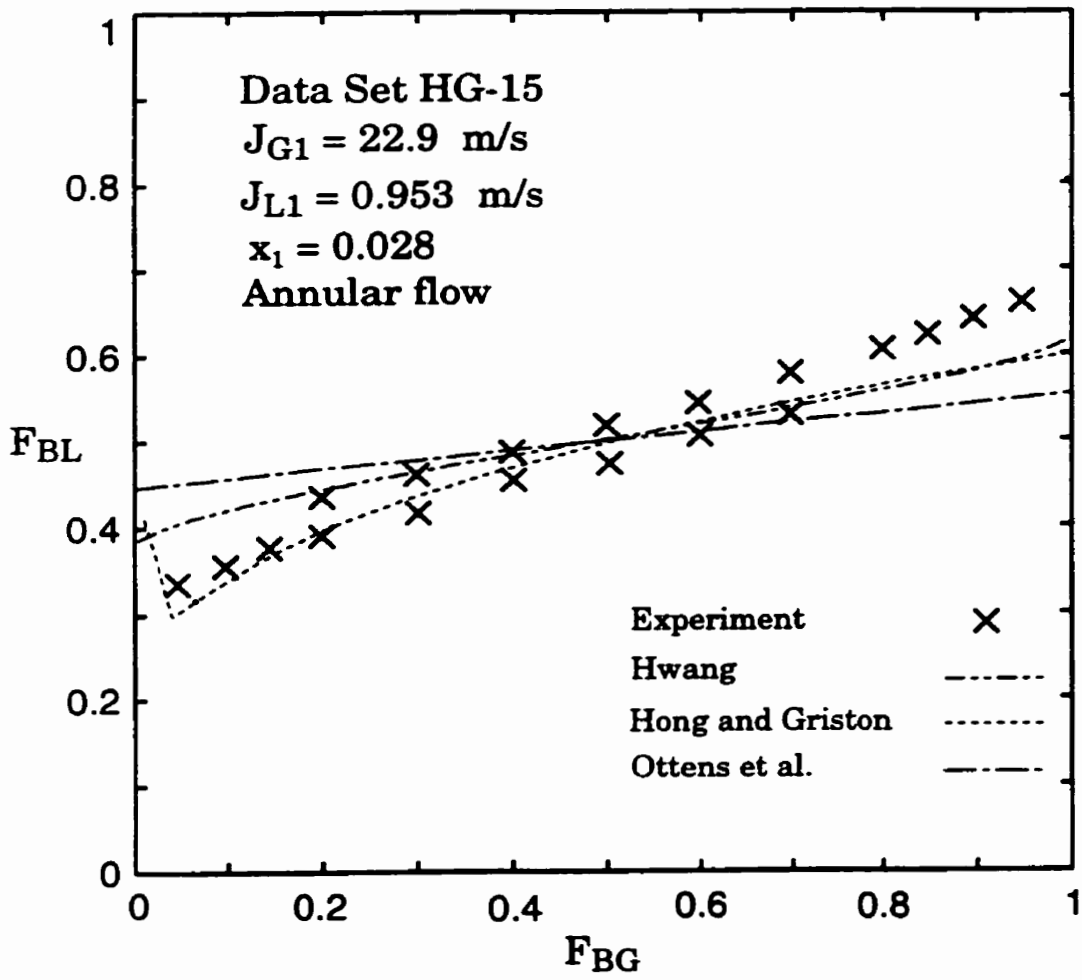

Figure 3.69 Predictions of models and correlations against data set HG-15.

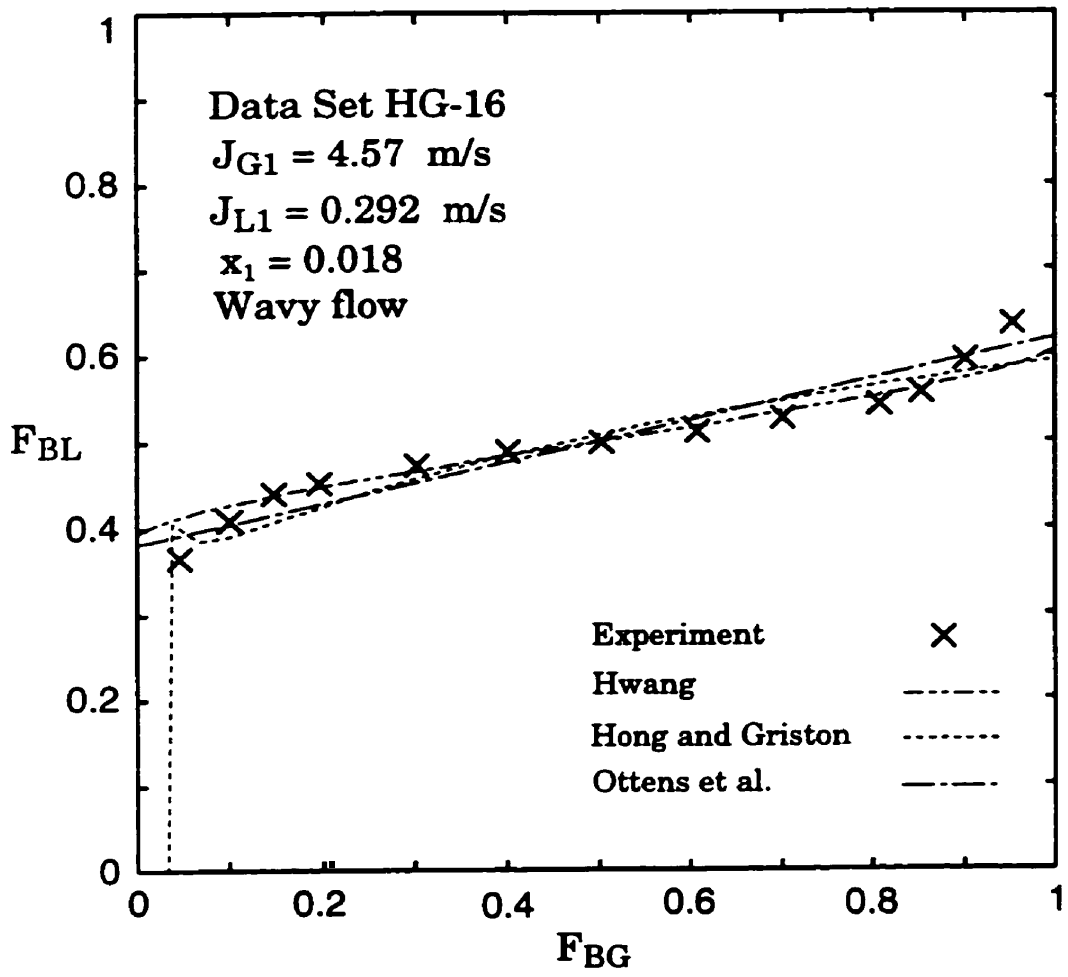

Figure 3.70 Predictions of models and correlations against data set HG-16.

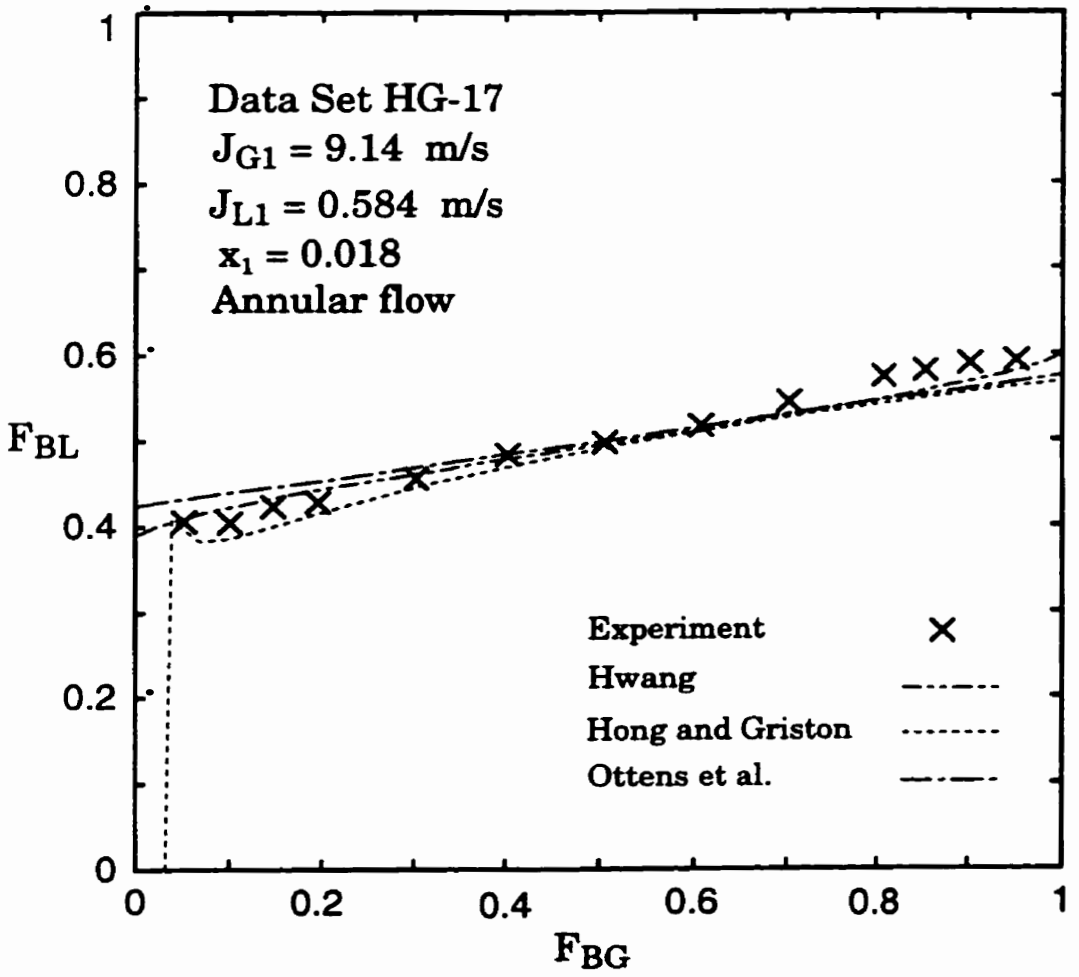

Figure 3.71 Predictions of models and correlations against data set HG-17.

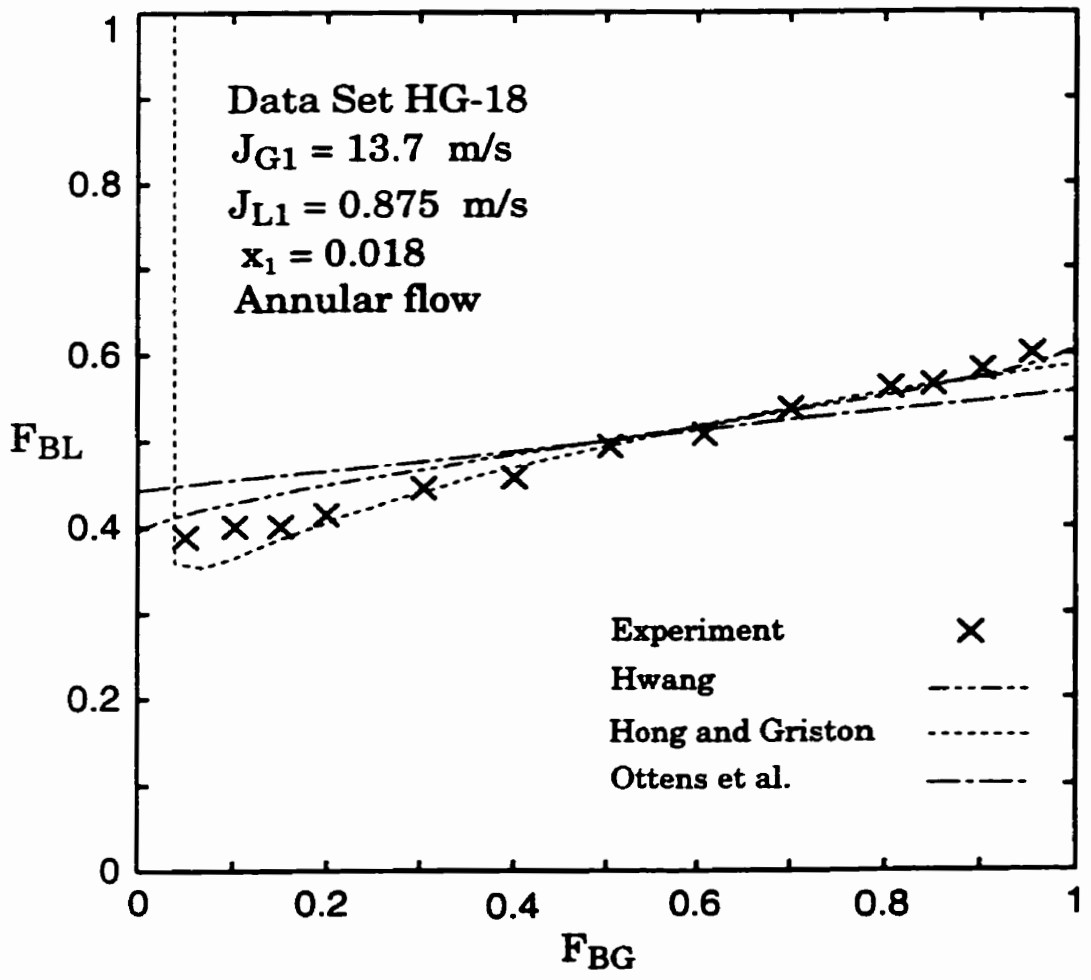

Figure 3.72 Predictions of models and correlations against data set HG-18.

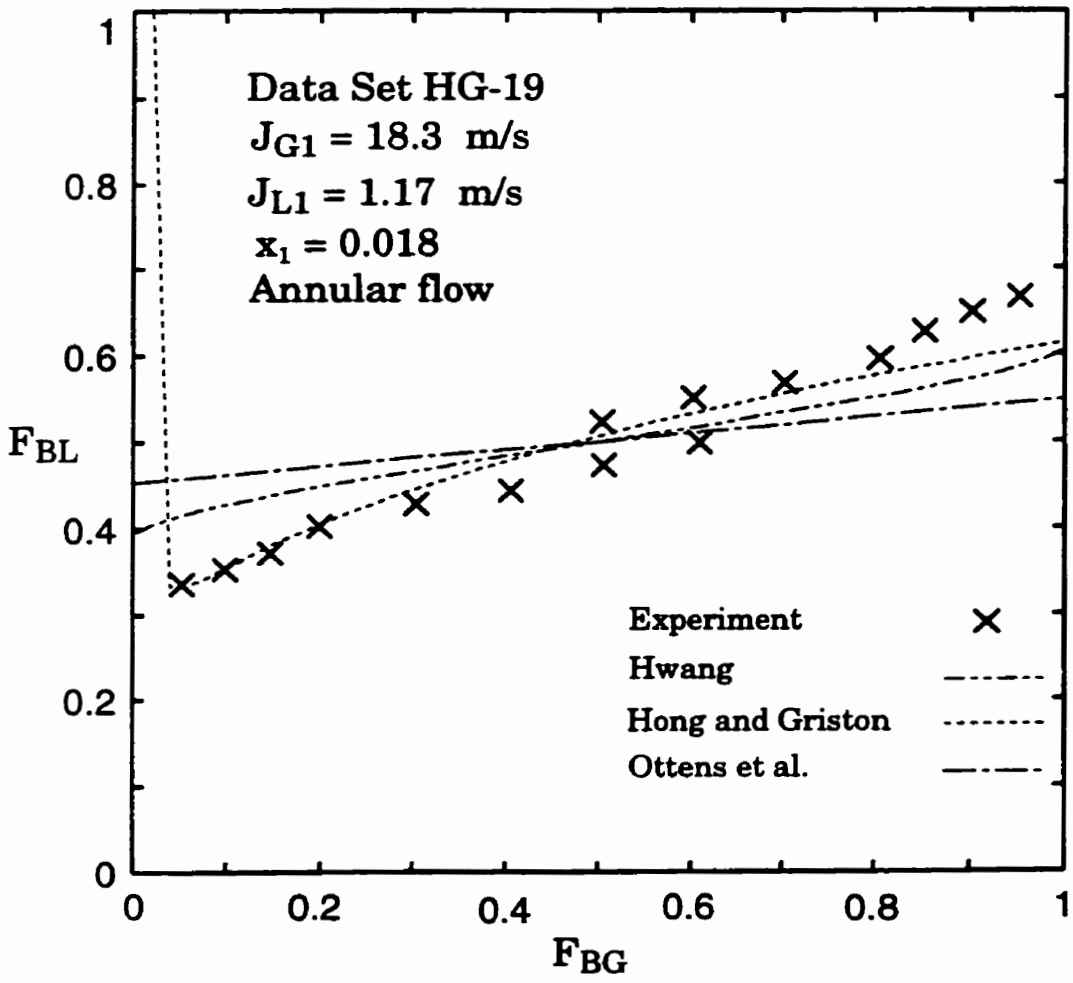

Figure 3.73 Predictions of models and correlations against data set HG-19.

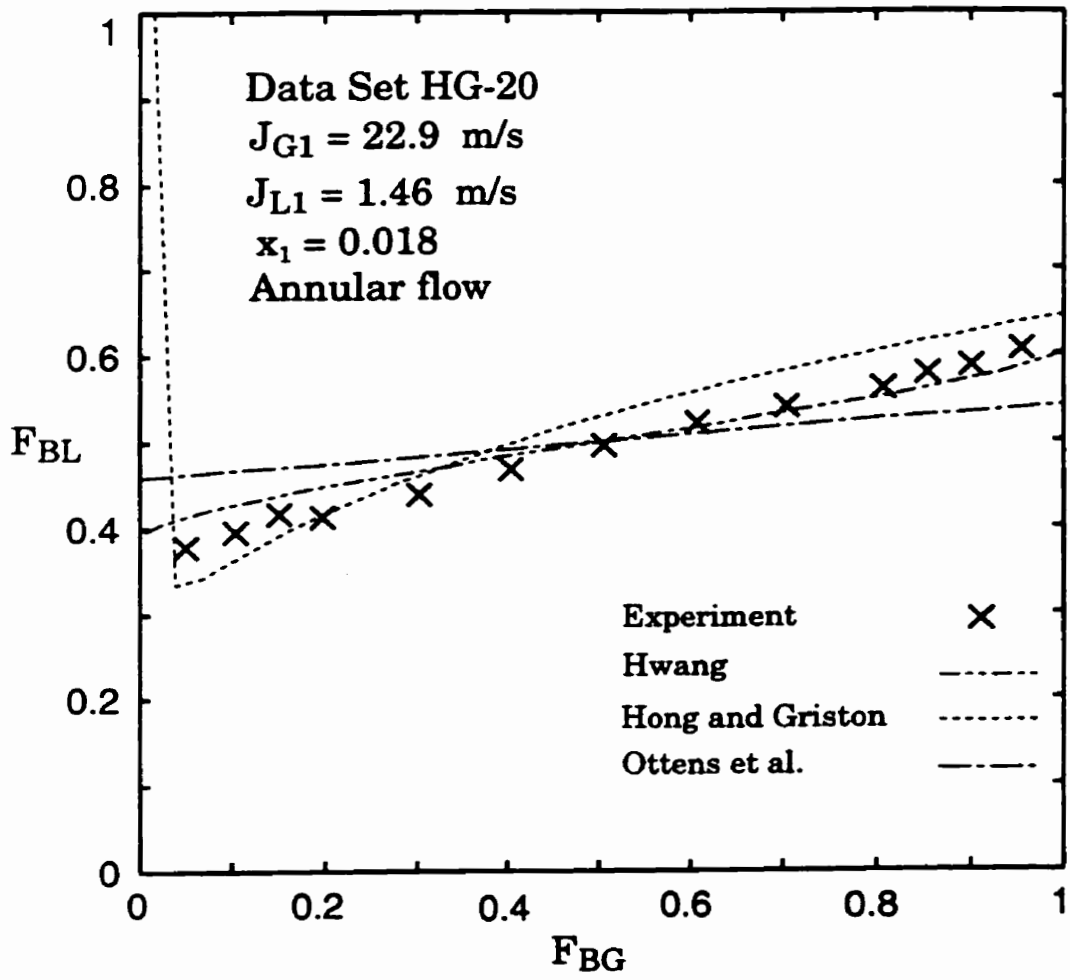

Figure 3.74 Predictions of models and correlations against data set HG-20.

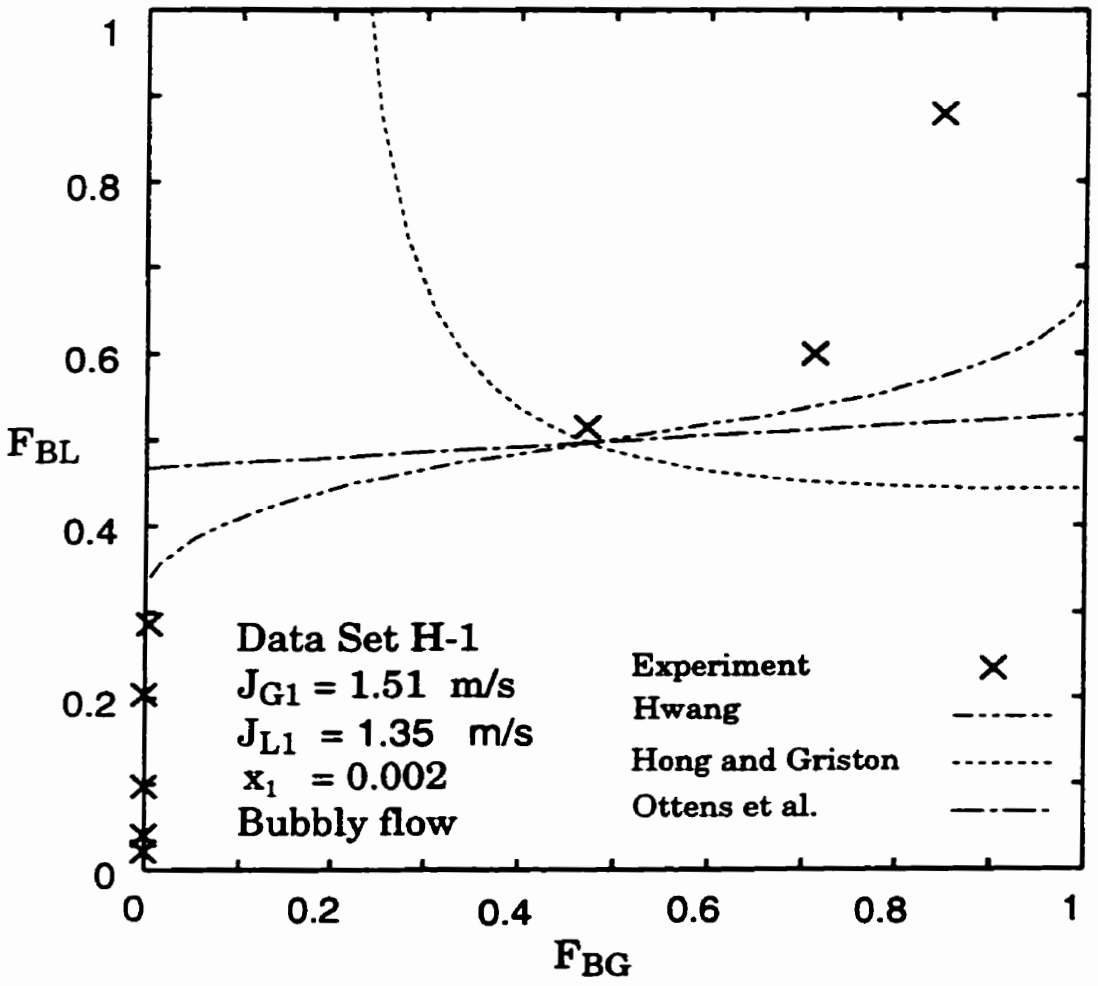

Figure 3.75 Predictions of models and correlations against data set H-1.

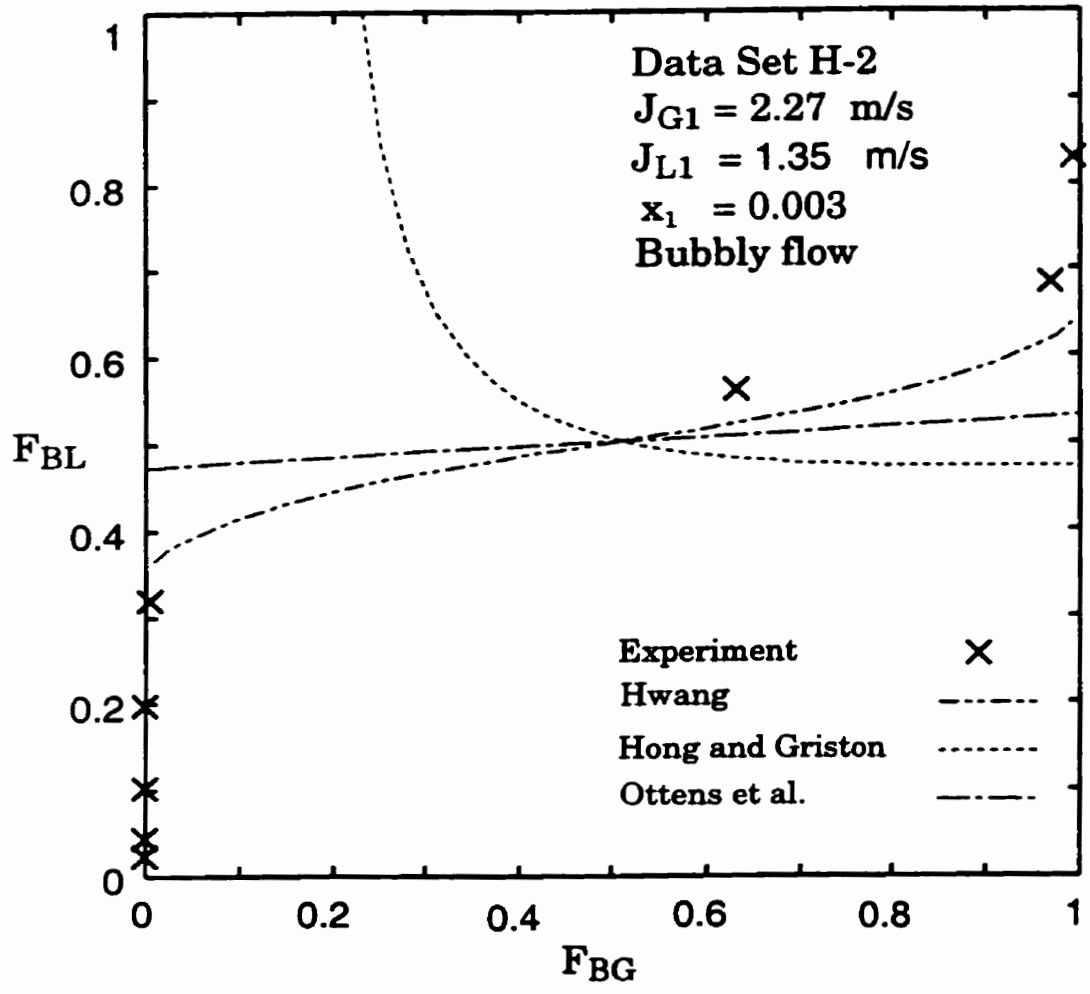

Figure 3.76 Predictions of models and correlations against data set H-2.

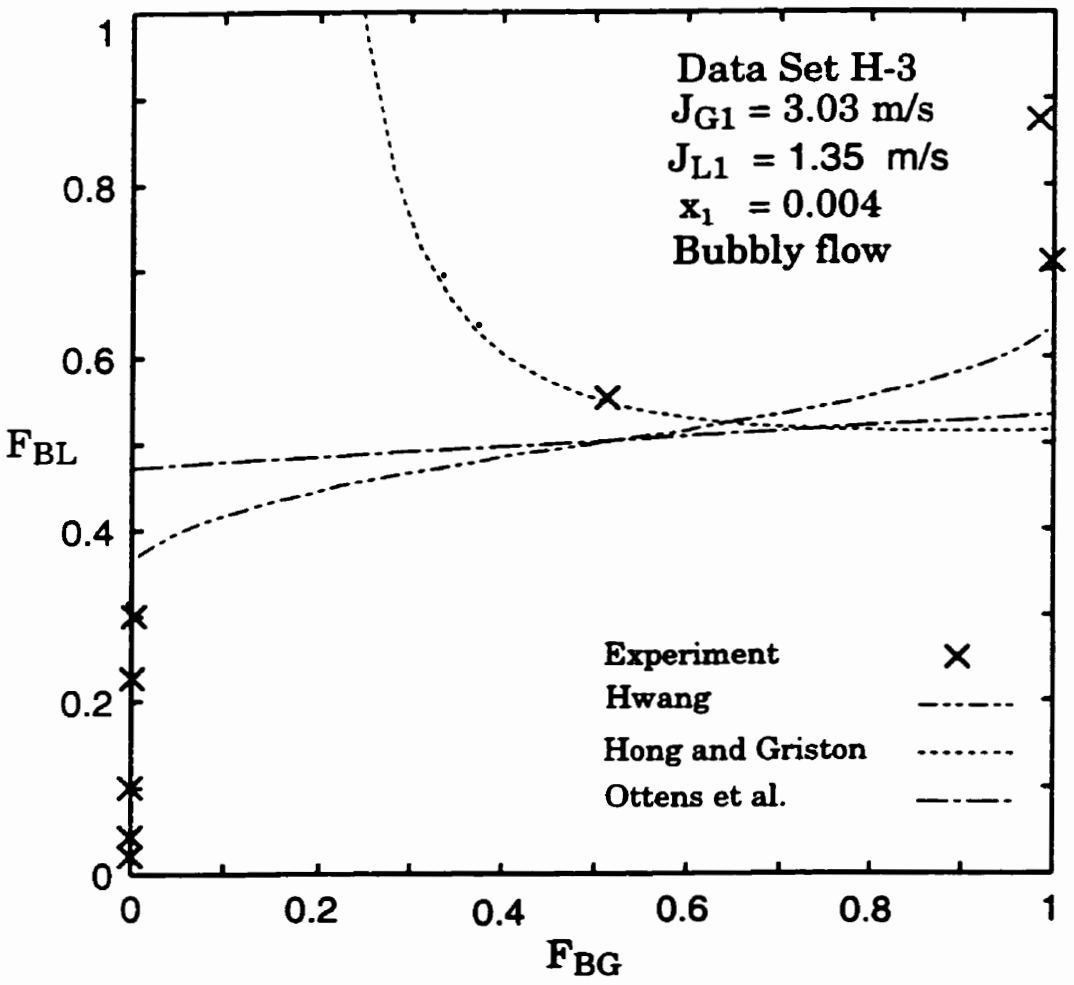

Figure 3.77 Predictions of models and correlations against data H-3.

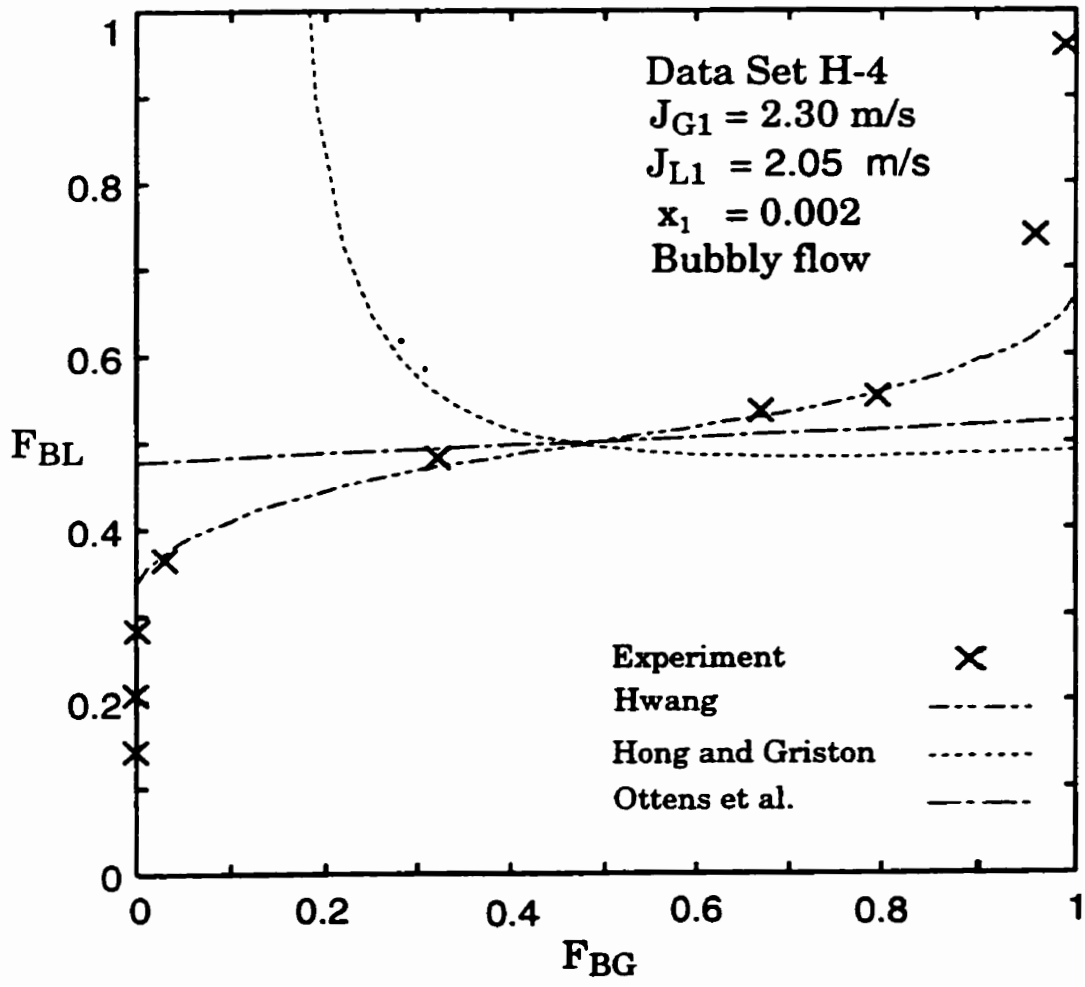

Figure 3.78 **Predictions of models and correlations against data set H-4.**

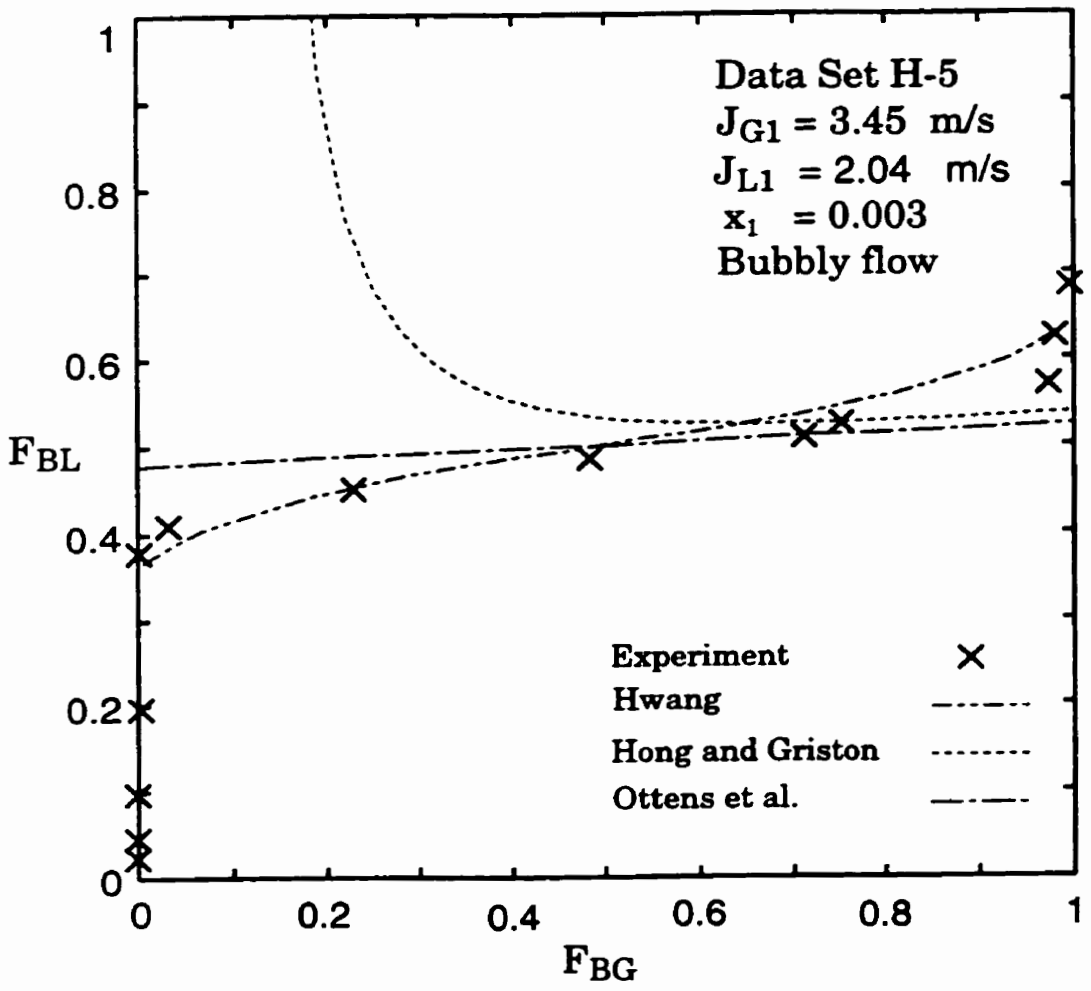

Figure 3.79 Predictions of models and correlations against data set H-5.

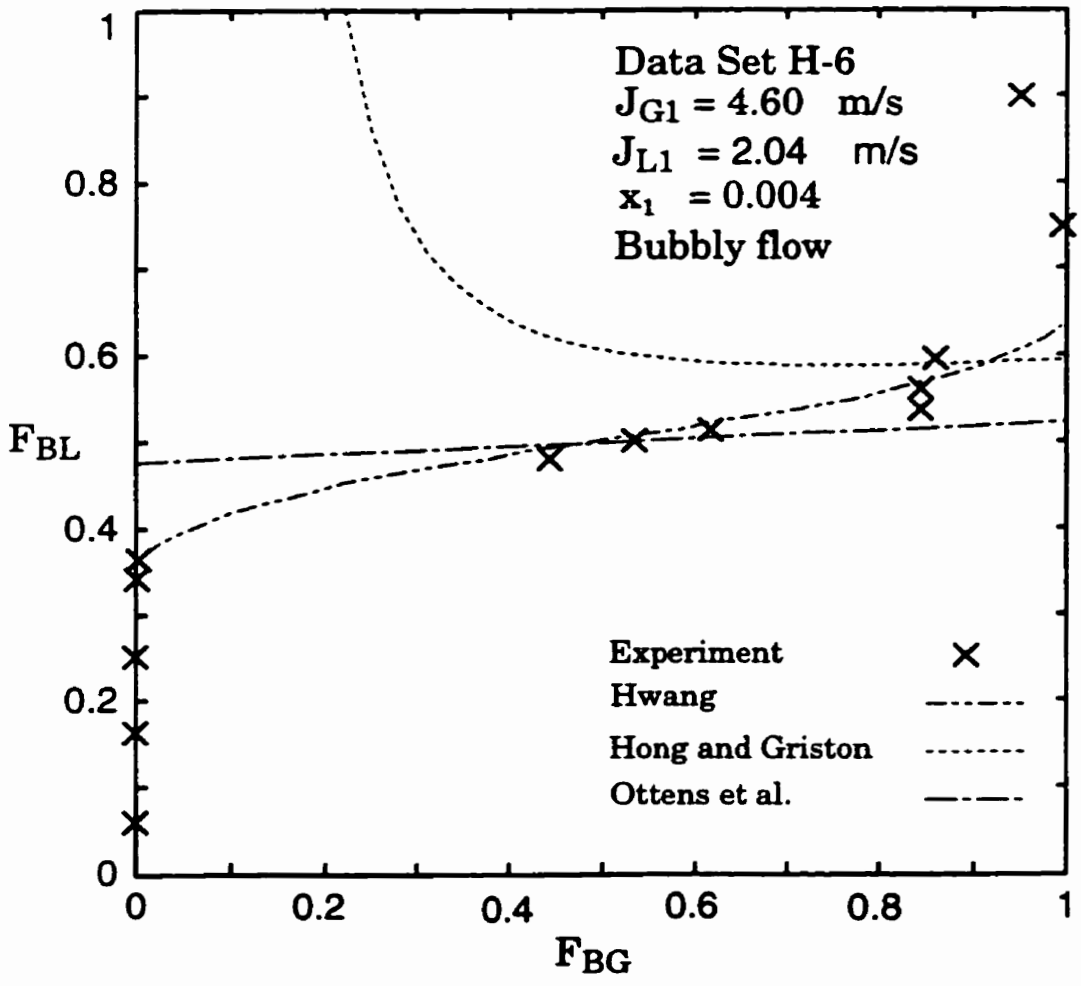

Figure 3.80 **Predictions of models and correlations against data set H-6.**

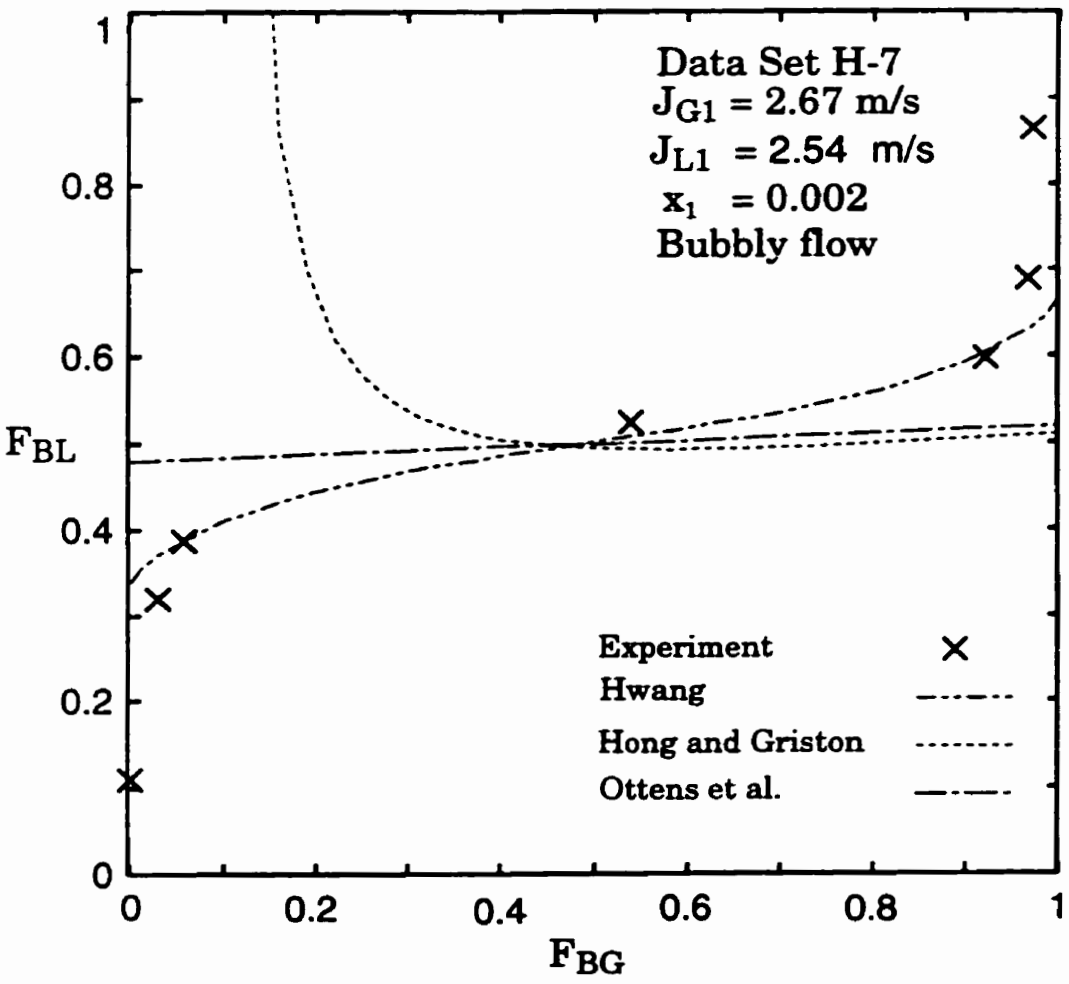

Figure 3.81 Predictions of models and correlations against data set H-7.

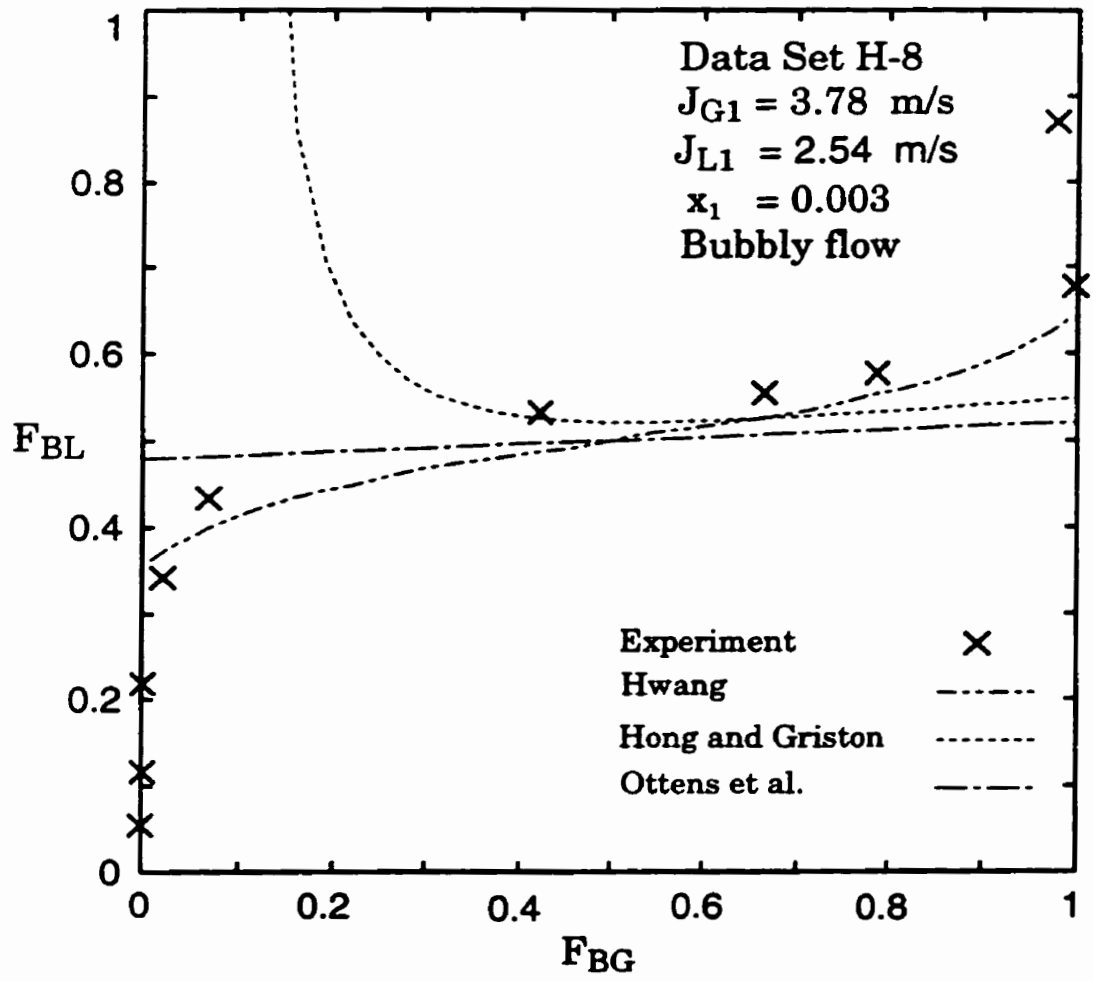

Figure 3.82 Predictions of models and correlations against data set H-8.

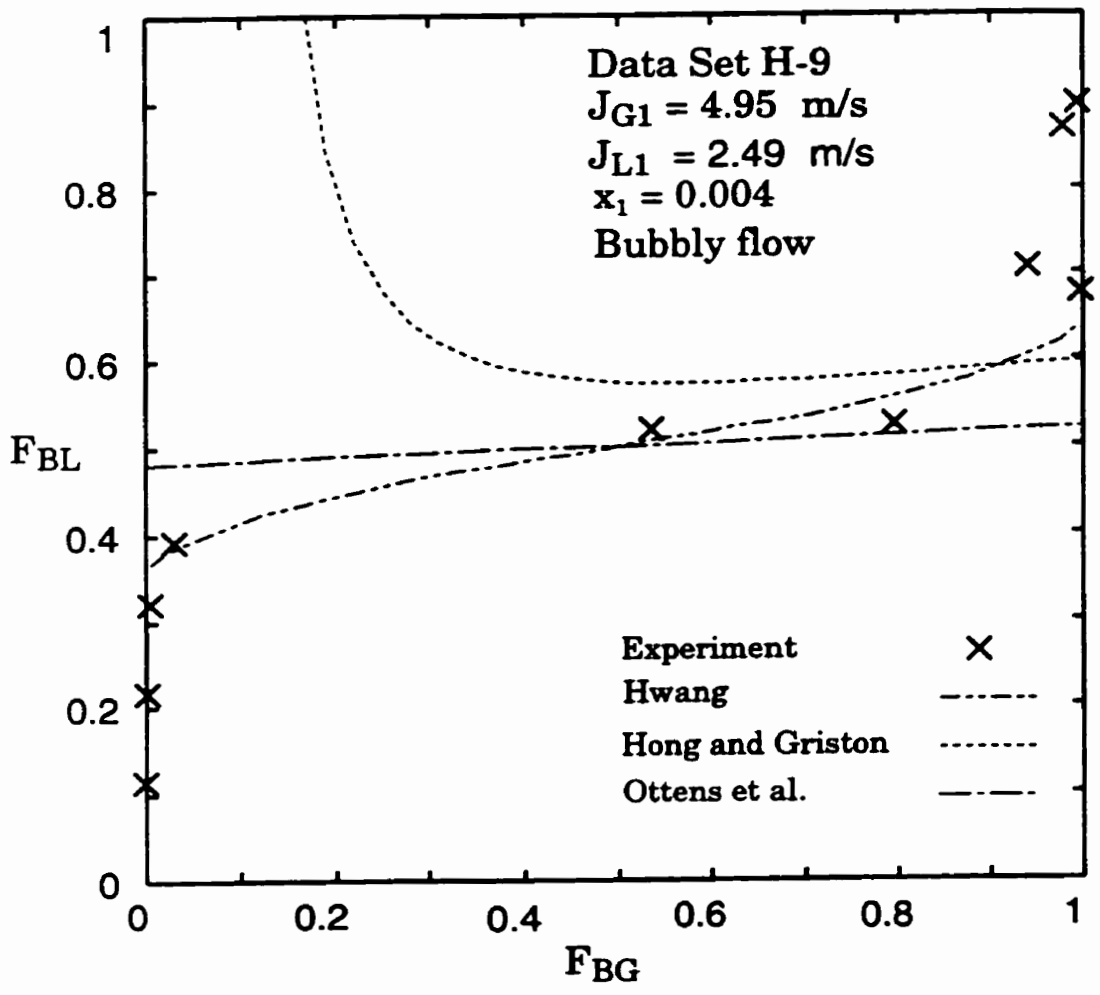

Figure 3.83 Predictions of models and correlations against data set H-9.

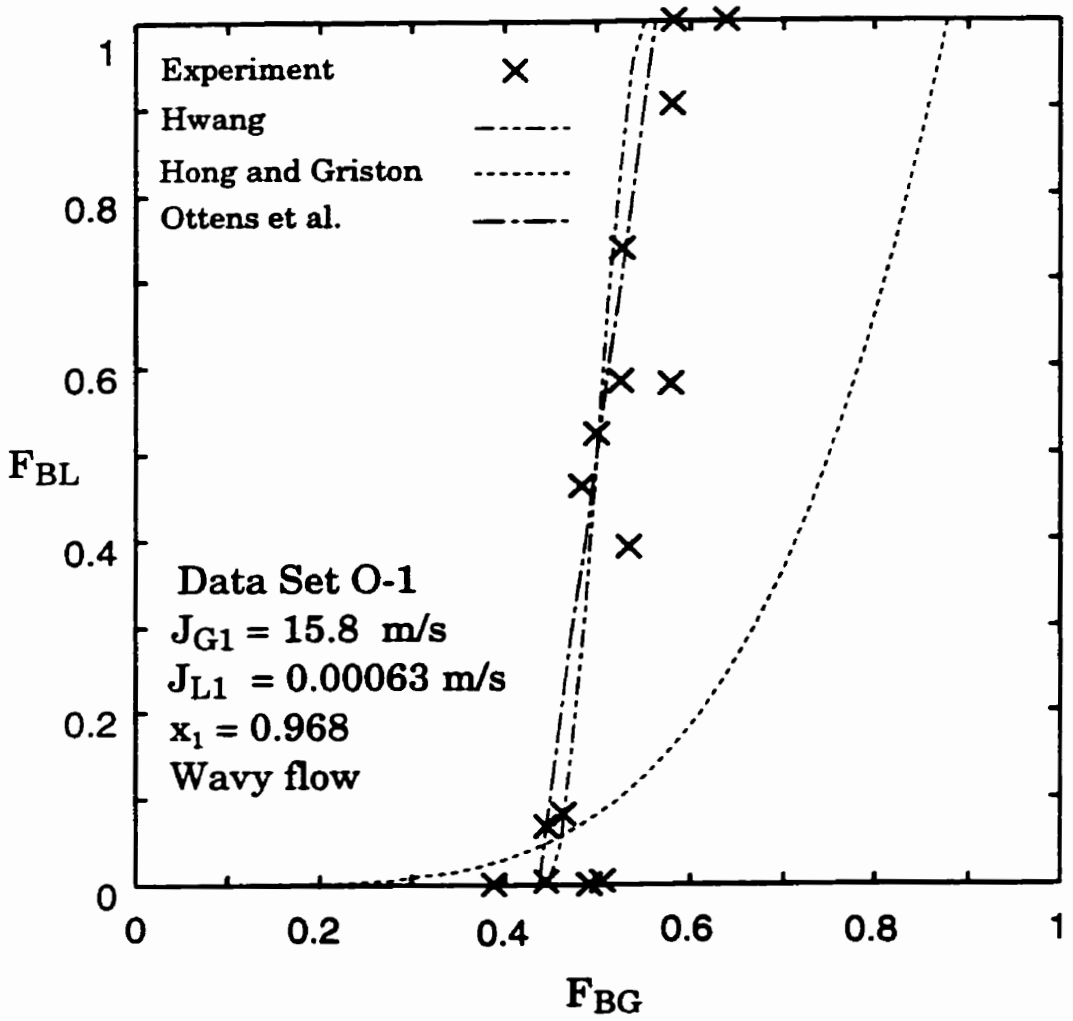

Figure 3.84 Predictions of models and correlations against data set O-1.

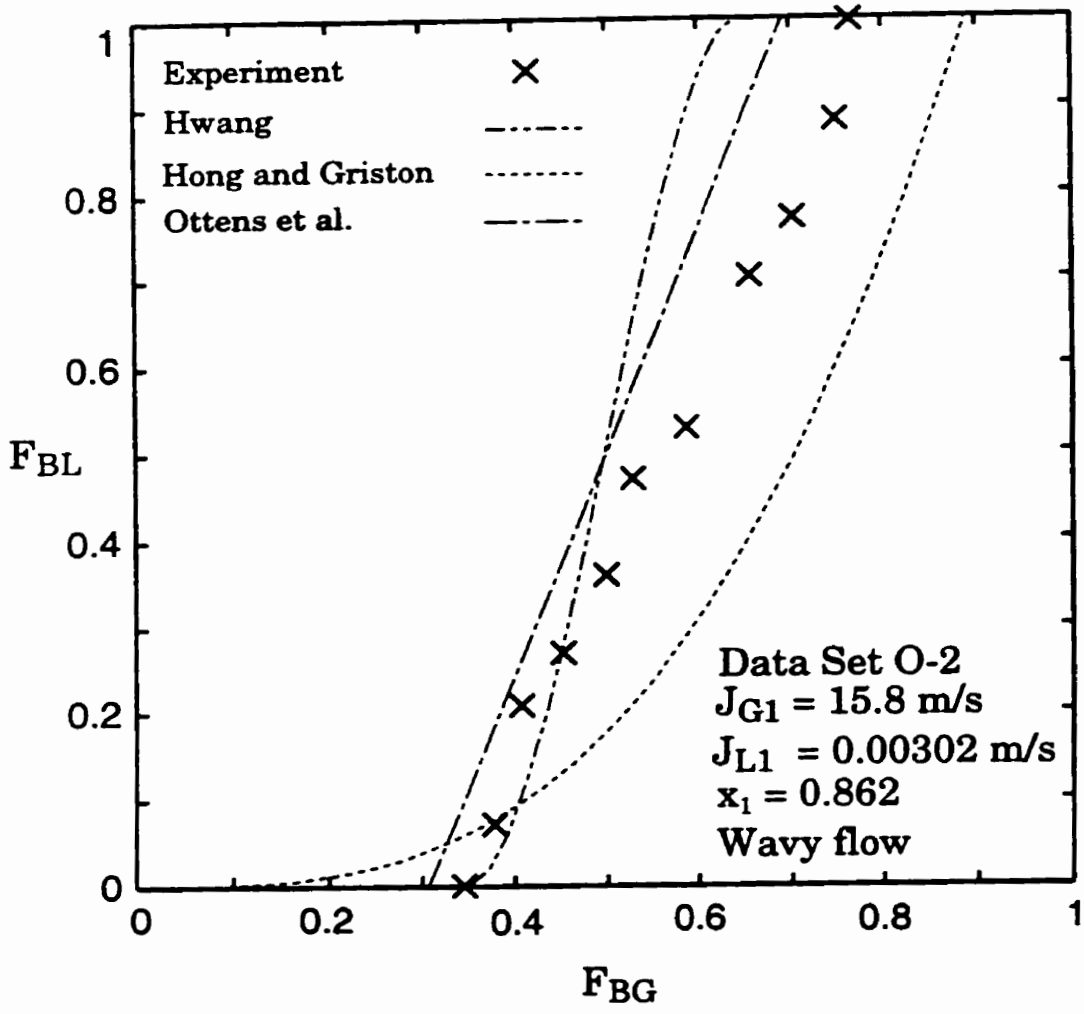

Figure 3.85 Predictions of models and correlations against data set O-2.

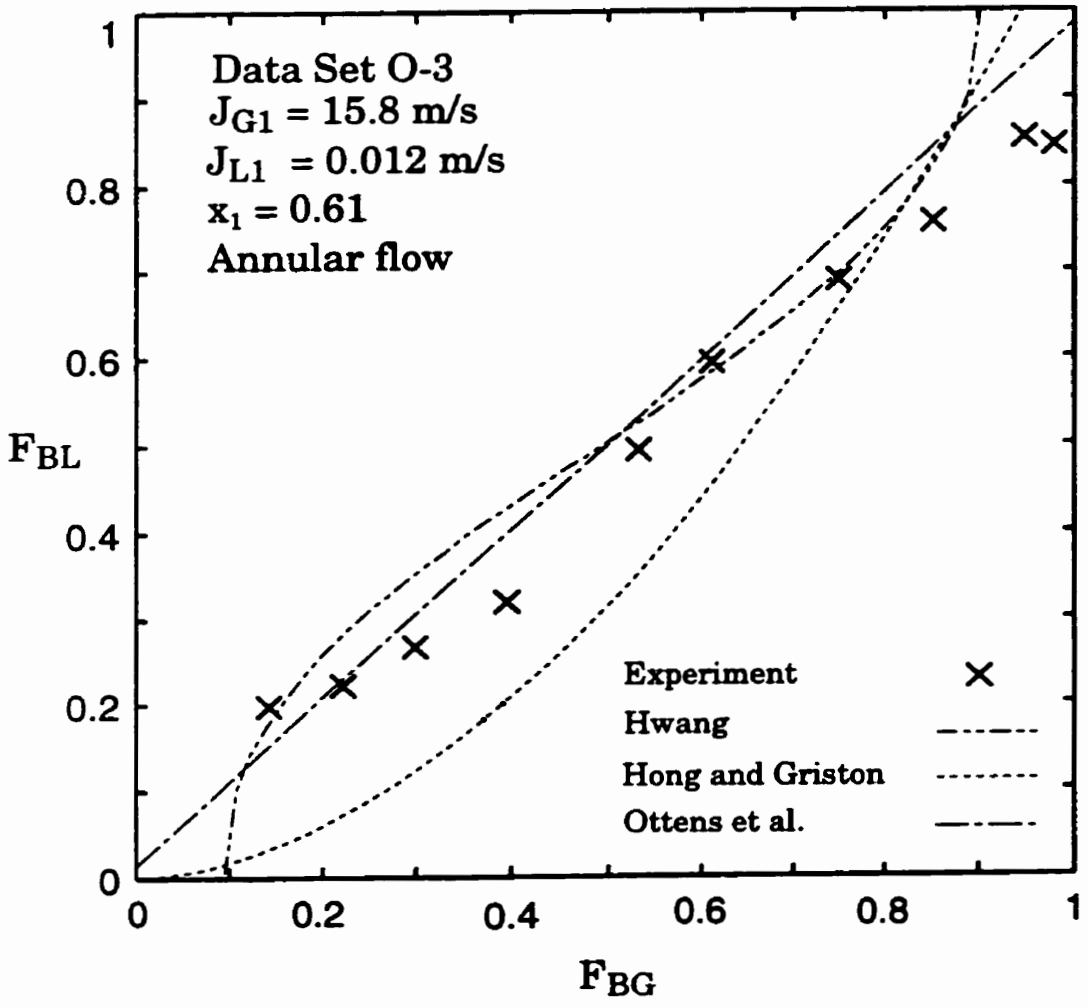

Figure 3.86 Predictions of models and correlations against data set O-3.

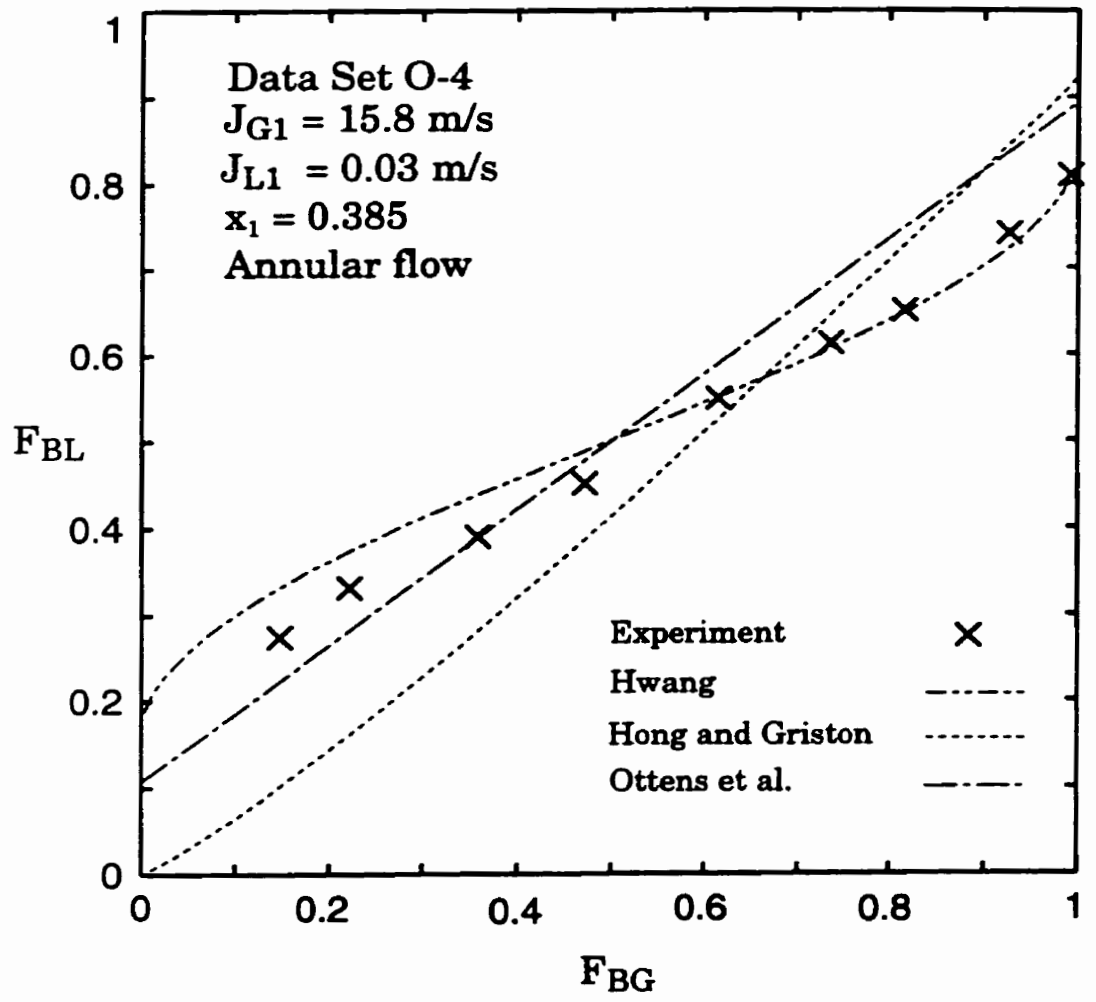

Figure 3.87 Predictions of models and correlations against data set O-4.

Chapter 4

EXPERIMENTAL TEST FACILITY

4.1 Overview

One of the objectives of the present study is to design and oversee the construction of component parts of an air-water loop to generate phase-distribution and pressure-drop data for air-water two-phase flow through horizontal impacting tee junctions. The test facility constructed to achieve this objective incorporated a horizontal impacting tee junction with the three sides having equal diameters (37.6-mm I.D.), and was designed for the following operating conditions : pressure of about 150 kPa (abs) at the junction, P_1, near ambient temperature, T_1, inlet superficial gas velocities, J_{G1}, ranging between 2.7 and 40 m/sec, inlet superficial liquid velocities, J_{L1}, ranging between 0.002 and 0.2 m/sec, and extraction ratios, W_3/W_1, between 0 and 1. These conditions were selected for the following reasons:

1- To cover ranges of J_{G1} and J_{L1} that were not covered before. Figure 3.1 shows the Mandhane et al. (1974) flow-regime map with the areas covered in previous work on phase distribution and the proposed area of study. Figure 3.2 shows the same map with the areas covered in previous work on pressure drop and the proposed area of study. It is very clear from these figures that the proposed area of study will allow four inlet flow regimes to be tested. These are: stratified, slug, wavy, and annular.

2- To test relatively high-inlet-quality flows, as most of the work done earlier on phase distribution was for very low-inlet-quality flows.

4.2 Air-Water Loop

The flow loop which was designed for this study is shown in Figure 3.3. The following paragraph describes briefly the flow through the different components of the loop. A more detailed description of the design and construction of the main components of the loop is given later.

Distilled water used in the system is to be stored in the water reservoir. Water, fed from the reservoir by a centrifugal pump, will be metered by one of two turbine meters in parallel (W_{L1}) before flowing into the two-phase mixing tee (mixer), where it will be mixed with the gas phase (air). Heat absorbed by the water due to flow through the pump and from frictional losses will be removed by a cooling coil installed inside the reservoir. Air flow from the building supply will pass through an air filter and a pressure controller for cleaning and pressure control, respectively. The air flow will be metered using one of two turbine meters in parallel (W_{G1}) before flowing into the mixer. A developing length of 67.5 tube diameters is allowed before the two-phase mixture enters the visual section, and a further 66 tube diameters is provided before entering the tee junction which is made from acrylic for visualization. Forty-one pressure taps are installed along the test-section inlet and the two outlets in order to determine the pressure distribution around the junction. Each of the two outlet two-phase mixtures will be directed to its respective separation tank. The flow rate of liquid from each separation tank will be metered using a combination of five rotameters, arranged in parallel, to give individual measurements of each outlet liquid flow rate, W_{L2} and W_{L3} . The two outlet liquid lines are then rejoined before returning to the water reservoir. The gas phase exiting

each of the two separation tanks will flow through its respective throttling valve, used to control both the extraction ratio W_3/W_1 and the test-section pressure, before being metered by either a turbine meter (for high flow rates), or a combination of four rotameters arranged in parallel (for low flow rates). This will give individual measurements of the two outlet air flow rates, W_{G2} and W_{G3} . Both air flows will then be discharged into the atmosphere.

4.2.1 Water-Flow-Rate Measurement

The inlet water flow rate W_{L1} will be metered using two turbine meters arranged in parallel. Both turbine meters were manufactured by Flow Technology Inc. The model numbers and flow ranges are as follows :

Model	Capacities
FT6-8C1YW-LED-1	3.07 – 16.1 l/min. (0.811– 4.26 USGPM)
FT0-4C1YW-LHC-1	0.382 – 4.5 l/min. (0.101 – 1.19 USGPM)

Depending on the inlet flow conditions, the turbine with the appropriate range will be selected. Output from each turbine meter will be fed into its respective signal converter (Flow Technology Inc. , RC51-1C-0000-6) which converts the turbine meter output into a 0 to 10 volt DC signal. These DC signals will be fed into two separate channels in the digital acquisition system.

Both turbine meters will be calibrated using a collection tank, scale, and timer. By collecting the water that will pass through a turbine meter over a measured period of time and weighing the collected water, the mass flow rate will be obtained and compared against the meter reading.

The water flow rates from the two separation tanks will be metered using rotameters. Each flow-measurement station consists of a bank of five rotameters arranged in parallel to give a wide measurement range, as shown below.

For outlet 2-bank of rotameters:

Model	**Capacities**
Cole-Parmer, tube number N082-03ST	2.85-47.0 ml/min.
Cole-Parmer, tube number FM102-05ST	12-260 ml/min.
Cole-Parmer, tube number N044-40C	99-1903 ml/min
Cole-Parmer, tube number N044-40C	85-1880 ml/min
Fisher Porter, 10A3555A	1250-13700 ml/min.

Thus, this flow measurement station is capable of flow-rate measurement over the range of 2.85 to 13,700 ml/min.

For outlet-3 bank of rotameters:

Model	**Capacities**
Cole-Parmer, tube number FM082-03ST	2.2-46.6 ml/min.
Cole-Parmer, tube number FM102-05ST	16-260 ml/min.
Cole-Parmer, tube number FM044-40C	70-1905 ml/min
Cole-Parmer, tube number FM044-40C	100-1880 ml/min
Fisher Porter, 10A3555A	1250-13700 ml/min.

Thus, this flow measurement station is capable of flow-rate measurement over the range of 2.2 to 13,700 ml/min.

Depending on the inlet water mass flow rate, W_{LI}, and the extraction ratio, W_3/W_1, the flows through the two outlets will be directed to the appropriate rotameter or group of rotameters. All rotameters will be calibrated using a collection tank, scale, and timer with the same method as the inlet water turbine meters.

4.2.2 Air-Flow-Rate Measurement

The inlet air flow rate, W_{G1}, will be metered using two turbine meters manufactured by Flow Technology Inc. These turbine meters are arranged in parallel with the following flow rate ranges:

Model	Capacities
FT-12C1YA-PEA-1	0.0528 – 0.638 m^3/min (1.87-22.5 ACFM)
FT-24C1YA-GEA-1	0.196 – 4.5 m^3/min (6.93-159 ACFM)

Depending on the inlet flow conditions, the turbine with the appropriate range will be selected. Output from each turbine meter is fed into a signal converter (Flow Technology Inc., RC51-1C-0000-6) which converts the turbine meter output into a 0 to 10 volt DC signal. The DC signals are then fed into individual channels in the digital acquisition system.

These two turbine meters will be calibrated using a combination of three venturi tubes of varying sizes and a large wet test meter. The venturi tubes were manufactured by Fox Valve Development Corp. and have throat diameters of 0.375, 0.625, and 1.00 inches. The wet test meter was manufactured by Elster-Handel GmbH and has a maximum flow rate of 15 m^3/hr.

The air flow rates through outlets 2 and 3, W_{G2} and W_{G3}, will each be measured by either two turbine meters (for high flow rates), or a bank of rotameters (for low flow rates). The two turbine meters are arranged in parallel, as are the banks of rotameters. The four air turbine meters were manufactured by Flow Technology Inc. The capacities of the turbine meters and the rotameters are given below.

For outlet-2 turbine meters:

Model	**Capacities**
FT-12C1YA-PEA-1	0.0537-0.637 m^3/min (1.9-22.5 ACFM)
FT-24C1YA-GEA-1	0.214-4.57 m^3/min (7.57-162 ACFM)

For outlet-2 bank of rotameters:

Model	**Capacities**
Cole-Parmer, tube number FM082-03ST	40-1670 ml/min.
Cole-Parmer, tube number FM102-05ST	670-8875 ml/min.
Cole-Parmer, tube number FM044-40C	3-64 ml/min
Cole-Parmer, tube number FM044-40C	2.8-61 ml/min
Fisher Porter, 10A3555A	162-1214 ml/min

For outlet-3 turbine meters:

Model	**Capacities**
FT-12C1YA-PEA-1	0.0534-0.637 m^3/min (1.88-22.5 ACFM)
FT-24C1YA-GEA-1	0.195-4.09 m^3/min (6.89-144 ACFM)

For outlet-3 bank of rotameters:

Model	**Capacities**
Cole-Parmer, tube number FM082-03ST	50-1700 ml/min.
Cole-Parmer, tube number FM102-05ST	620-8960 ml/min.
Cole-Parmer, tube number FM044-40C	2.8-61 ml/min
Cole-Parmer, tube number FM044-40C	2.8-62 ml/min
Brooks, 1307D10F3A1A	107-603 ml/min

The air flows through the two outlets will be directed through the appropriate turbine meter , rotameter, or bank of rotameters, depending on the inlet air mass flow rate, W_{G1}, and the extraction ratio, W_3/W_1. If a turbine meter is selected, its output is fed into its signal converter (Flow Technology Inc., RC51-1C-0000-6), which converts the turbine meter output into a 0 to 10 volt DC signal. The DC signals are then fed into individual channels in the digital acquisition system.

The outlet air turbine meters will be calibrated using the same method as that for the inlet air turbine meters. The rotameters will be calibrated using a combination of three venturi tubes, the large wet test-meter, and a small wet test-meter, which has a maximum flow rate of 0.6 m^3/hr.

4.2.3 Mixer

A schematic diagram of the two-phase mixer is shown in Figure 3.4. The entire mixer was constructed from copper tubing and fittings, which were soldered together. Air will be brought in through a 51-mm I.D. tube. Water entering the mixer through a 12.7-mm I.D. copper tube will be injected into the air flow through a large number of 1.6-mm diameter holes. The resulting two-phase mixture will then be discharged from the mixer and allowed to become fully developed over a length of 67.5 diameters before entering the visual section.

4.2.4 Test Section

A schematic diagram of the test section is shown in Figure 3.5. The piping used for the construction of the test section is commercial type K copper tubing with 37.6-mm I.D. The entire test section, including the mixer, will be supported by a rigid steel frame. A survey level was used to ensure horizontality of the test section. The following is a brief description of the major components in the test section:

Visual Section

Two visual sections are incorporated into the test section, one in the inlet and the other one in outlet 3. Because of the symmetry of the two outlets and that the extraction ratio, W_3/W_1, will be tested over the range from 0 to 1 for both outlets, one visual section in outlet 3 was considered to be sufficient to visualize all the flow

regimes encountered in both outlets. The two visual sections are identical. Each one, as shown in Figure 3.6, consists of a 254-mm long glass tube supported at both ends by special stuffing boxes. The design of the glass tube and stuffing boxes is such that the inside diameter of the glass tube and stuffing boxes are identical to the inside diameter of the copper tubing entering and exiting each visual section. This eliminates any disturbance to the flow. After assembly, a clear length of about 150 mm will be available in each visual section for the flow regime observation. Since the inside diameter of the commercial glass tubing did not match that of the copper tubing, costume-manufactured glass was used. This also allowed for the selection of a thick-wall (3.45 mm) glass tubing. In assembling each visual section, extreme care is taken to ensure alignment and coaxiality between the copper tubing, stuffing boxes, and the glass tube. The entire assembly is enclosed by a plastic protective shield to guard against injury in case of fracture of the glass tube.

Tee Junction

In order to ensure consistency with other research laboratories, a square-edged tee is used. The tee junction was machined in a 101.6 x 304.8 x 609.6 mm acrylic block. Two perpendicular holes of 37.6-mm I.D. were drilled out to construct the junction, as shown in Figure 4.7. The three sides of the tee junction were connected to the copper tubing by three copper pieces 101.6 x 101.6 mm (Figure 4.8). These copper pieces will be bolted to the acrylic block and soldered to the copper tubing. At the acrylic-copper interfaces, O-rings are used for sealing. Extreme care was taken in order to ensure that the inside diameters of the tee junction holes are exactly the same as those of the copper pieces and the copper tubing. Care will be also taken

in order to ensure that the junction holes, copper pieces holes, and the copper tubing are coaxial.

Pressure Taps

Forty-one pressure taps are installed along the whole test section, as shown in Figure 3.9. Twelve of them are drilled in the acrylic block while the others are drilled in copper tubing. For those drilled in copper tubing, a 1.6-mm hole is drilled through the tube wall. After drilling, any internal burrs are removed from the inside of the tube. Hose nipple fittings are soldered onto the outside of the copper tube to facilitate connection of the tubes to differential pressure transducers that will be used to measure the pressure distribution in the test section. Clear plastic tubing (Tygon) will be used to connect the pressure taps to the pressure transducers. The pressure taps are located along the bottom side of the test section in order to avoid air entrapment in the plastic tubing pressure lines, which are to be filled with distilled water. For those taps drilled in the acrylic block, a special arrangement is used in order to connect the pressure tap hole to the pressure transducer. The details of this arrangement are shown in Figure 3.10.

4.2.5 Separation Tanks

The two-phase mixture discharging from both outlets will flow into separation tanks located downstream of the test section. The two tanks, shown in Figure 4.11, are identical in design. They are made of type 304 stainless steel Sch. 40 pipe. All the fittings connecting the stainless steel tanks to copper tubing will be "Dielectric Unions". A 700–mm long sight glass, used to visually observe the liquid level in the

tank, is installed vertically with a scale. On the tank top blind flange, a pressure gauge and a safety valve that opens at 3.45 atm (50 psi) will be installed.

The two-phase mixture entering from the top of each separation tank will be separated using centrifugal action. This will be achieved by forcing the flow in a downward spiralling direction. Water exiting from the nozzles will flow along the tank wall where it drains downward. Air will flow out through the top of each separation tank. Baffle(1) is located above the gas-liquid interface and isolates the interface from the flow above it so that it, the interface, remains comparatively undisturbed. Baffle(1) is a circular disk made of stainless steel and perforated with many small holes (4.8-mm dia.) and has a diameter smaller than that of the inside of the separation tank. This leaves a gap of 3.2 mm for the water to flow downward through. Baffle(2) is a circular disk made of stainless steel and located 6.35 mm beneath the air intake elbow to protect the air intake from tiny water droplets expected to be formed due to the impact of the incoming two-phase flow on baffle(1). Baffle(2) diameter is 239 mm which makes its area almost half of the tank cross-sectional area. Baffle(3) is an annulus made of stainless steel and located 63.5 mm beneath baffle(2). The inside diameter of baffle(3) is 213 mm and therefore, there is an overlap between baffles (2) and (3) of 13 mm on the radius. The outside diameter of baffle(3) is 305 mm, which leaves a gap of 15 mm between baffle(3) and the inside wall of the separation tank for the water to flow downward. The function of baffle(3) is the same as baffle(2), i.e. to protect the air intake from water droplets.

The tanks incorporate two abrupt changes in the cross-sectional area. If the liquid flow rate into a particular tank is low, the gas-liquid interface in the tank will

be maintained in one of the smaller diameter sections. This procedure decreases the error in measuring the outlet liquid flow rate resulting from small changes in the height of the interface.

Provision is made for water to drain back to each separation tank (entry near the bottom) should secondary further downstream separation be necessary.

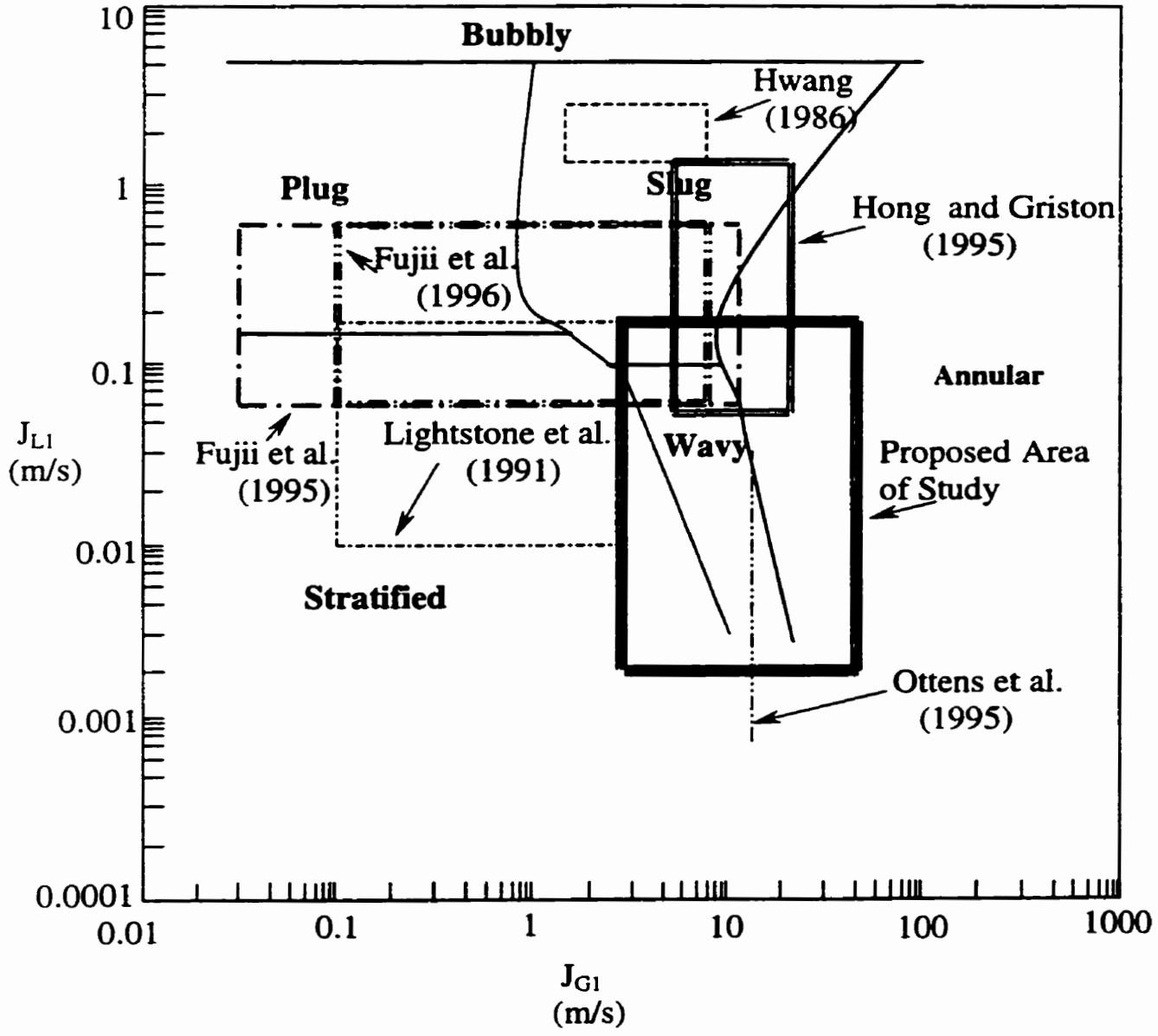

Figure 4.1 Range of inlet conditions for phase-distribution experiments conducted with horizontal impacting tee junctions plotted on the Mandhane et al. (1974) flow-regime map.

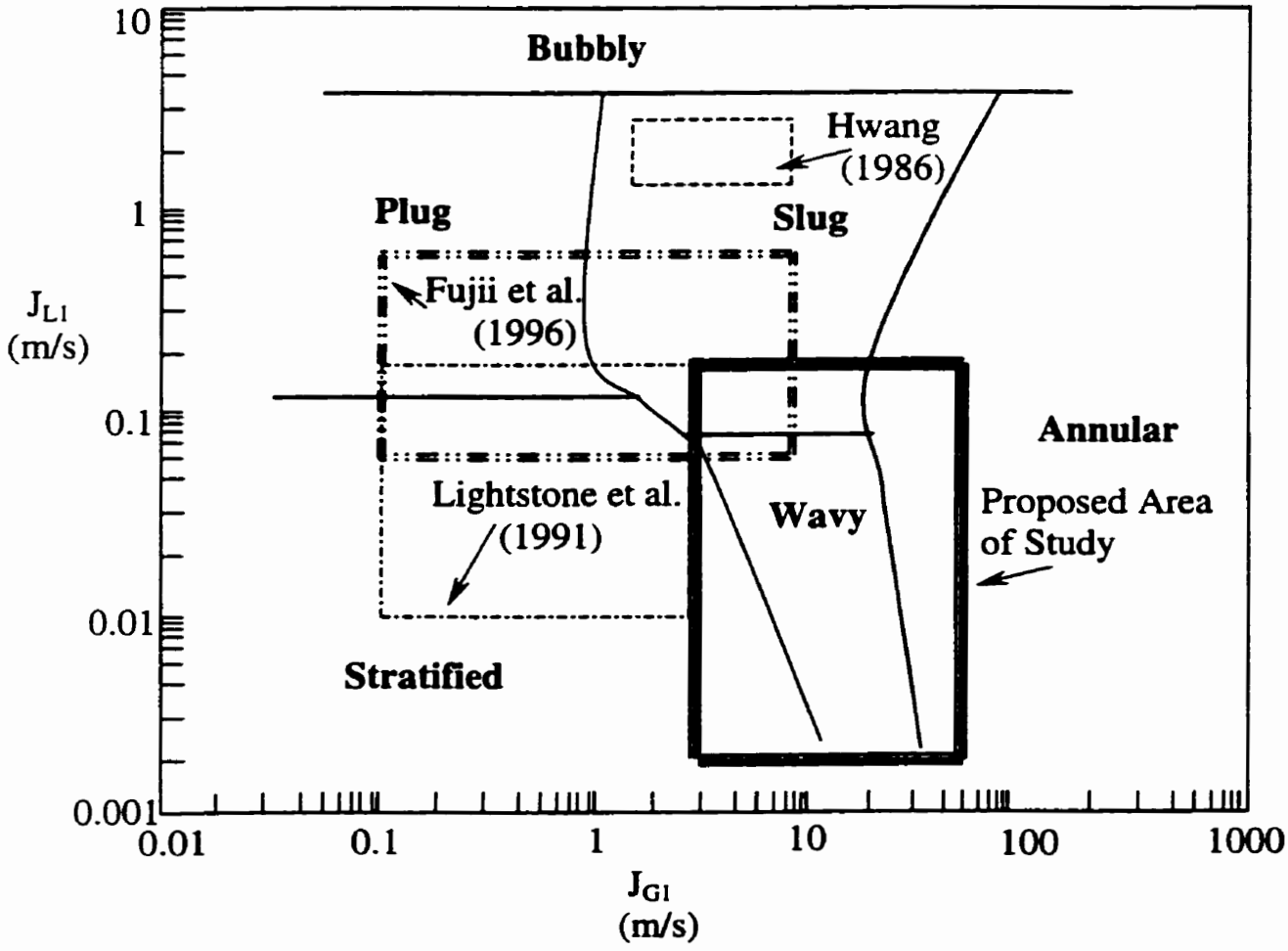

Figure 4.2 Range of inlet conditions for pressure-distribution experiments conducted with horizontal impacting tee junctions plotted on the Mandhane et al. (1974) flow-regime map.

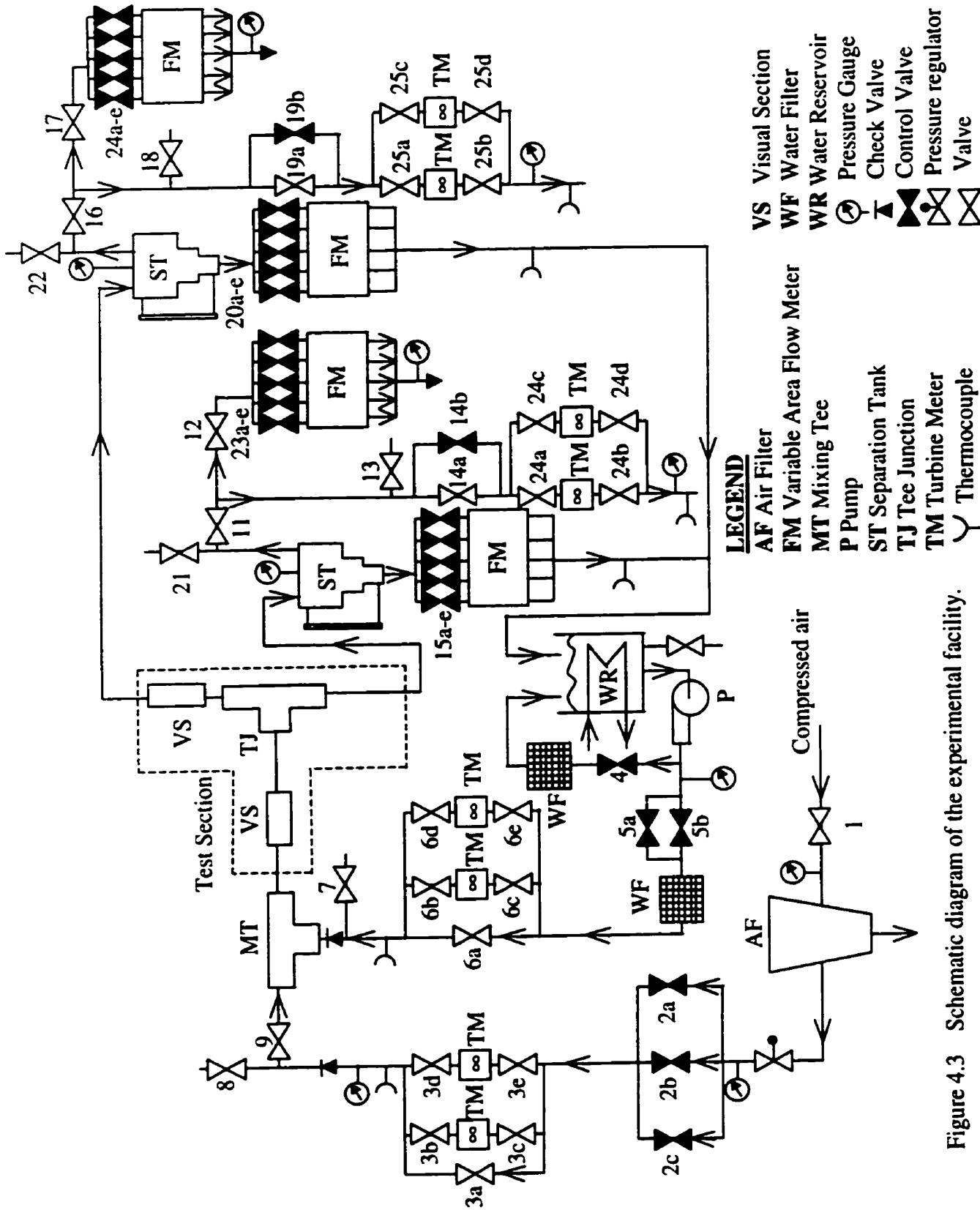

Figure 4.3 Schematic diagram of the experimental facility.

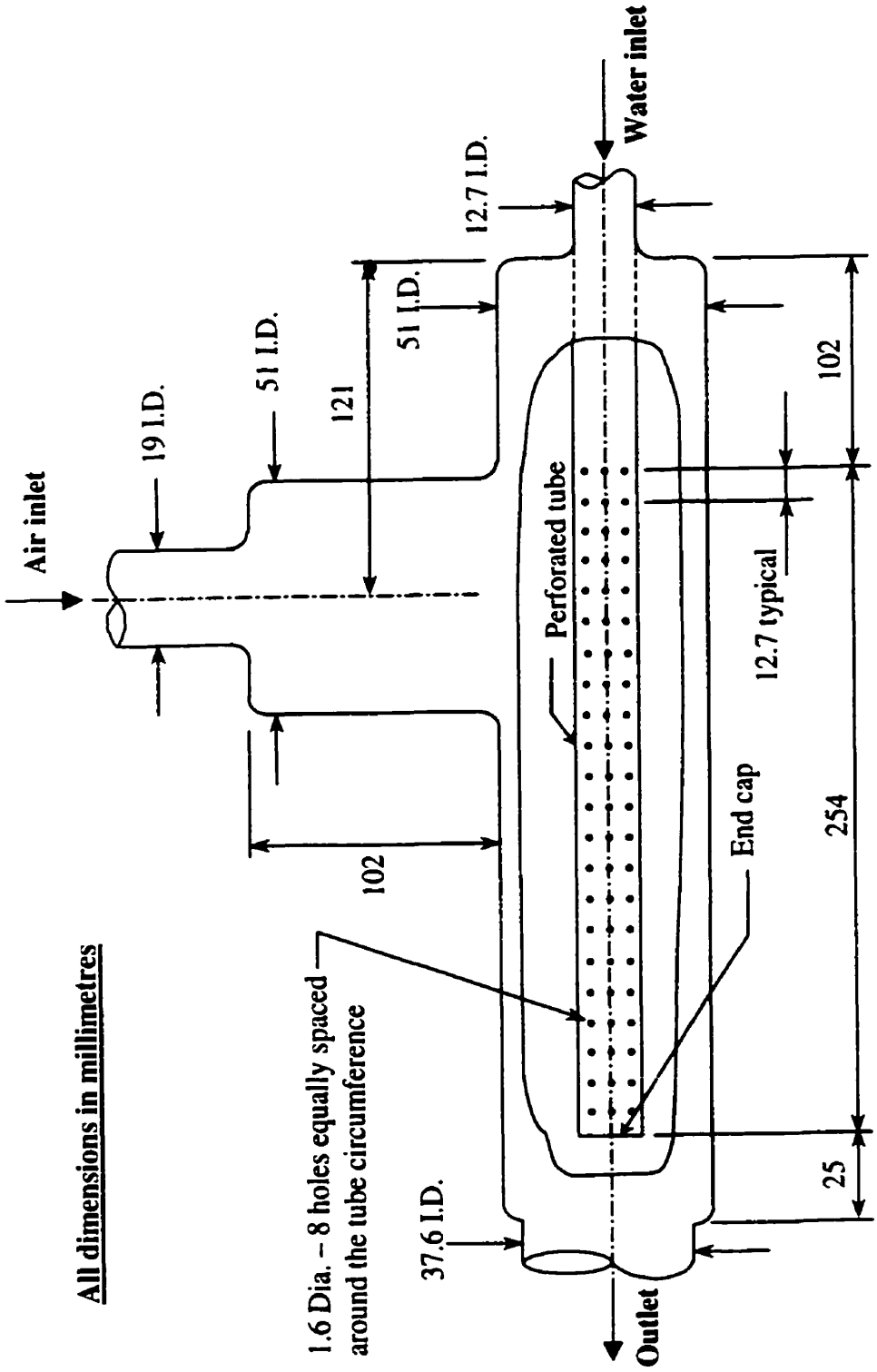

Figure 4.4 Schematic of the two-phase mixer; reproduced from Van Gorp (1998)

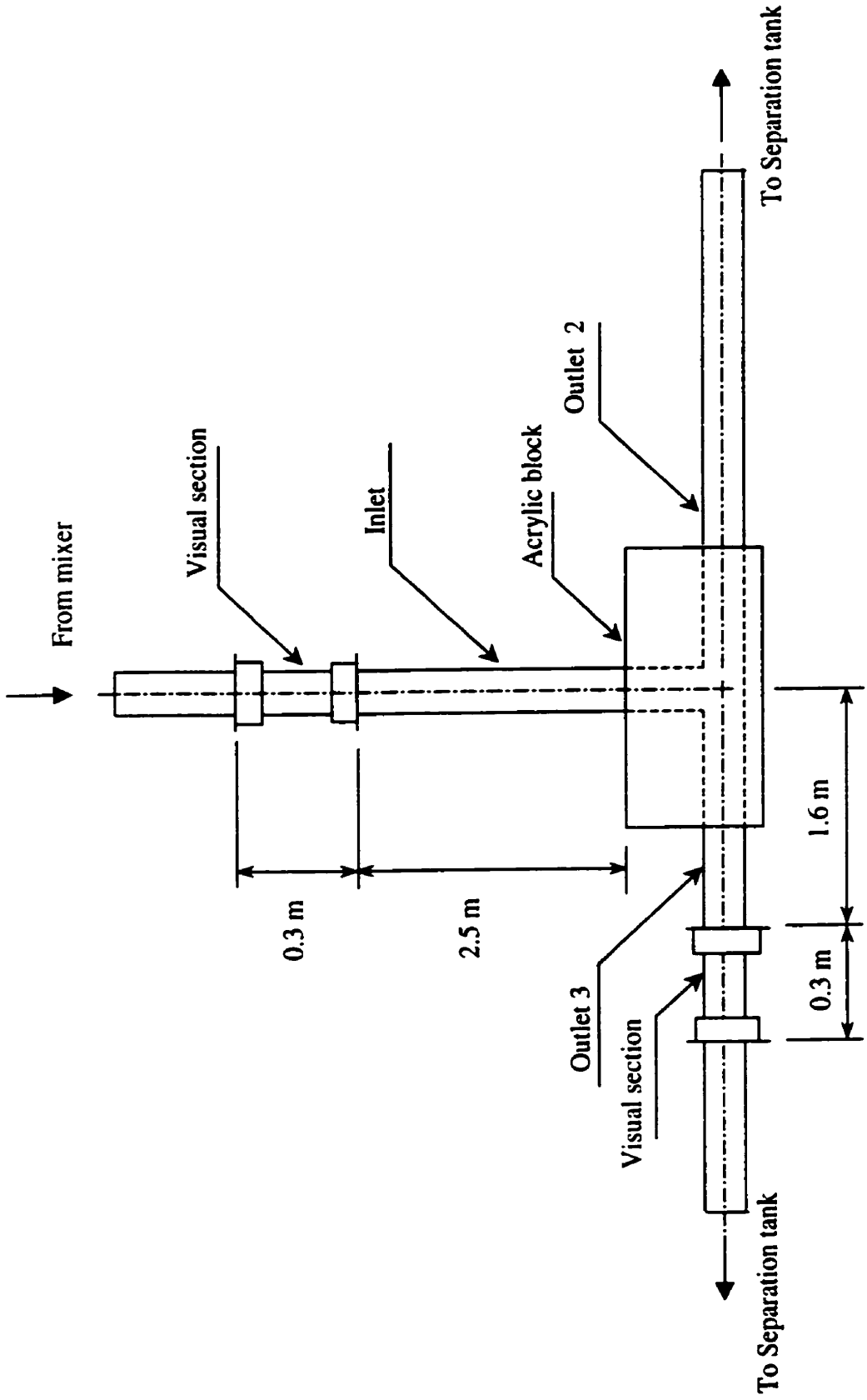

Figure 4.5 Schematic of the test section.

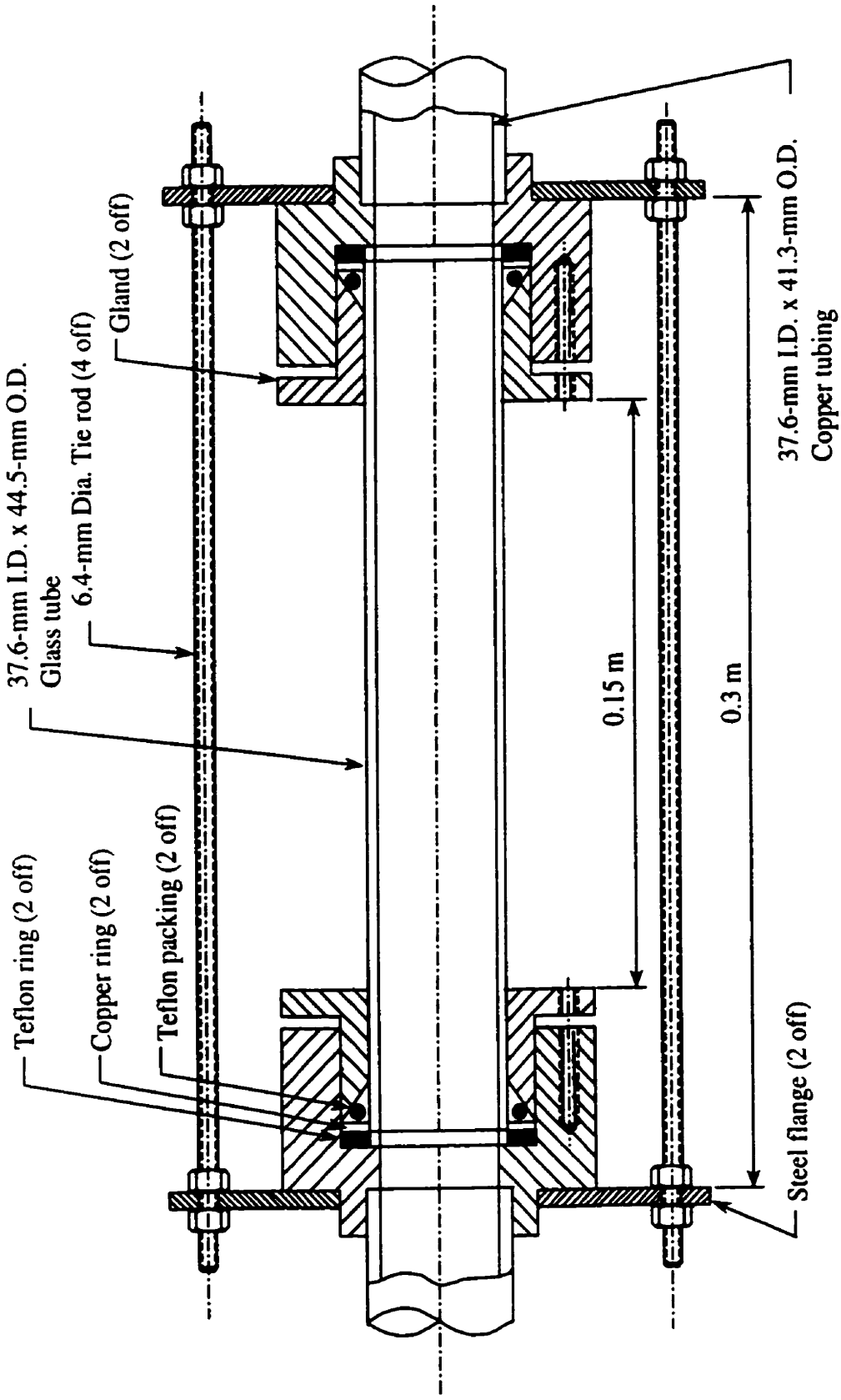

Figure 4.6 Details of the visual section.

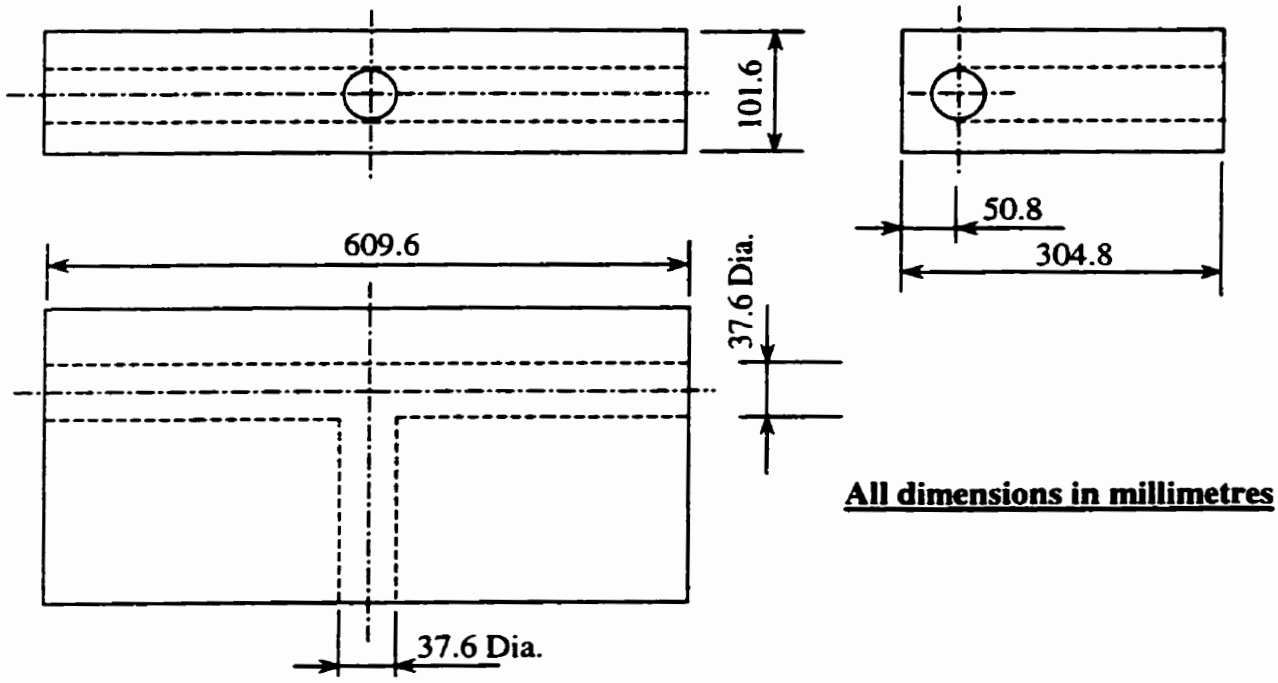

Figure 4.7 Tee junction.

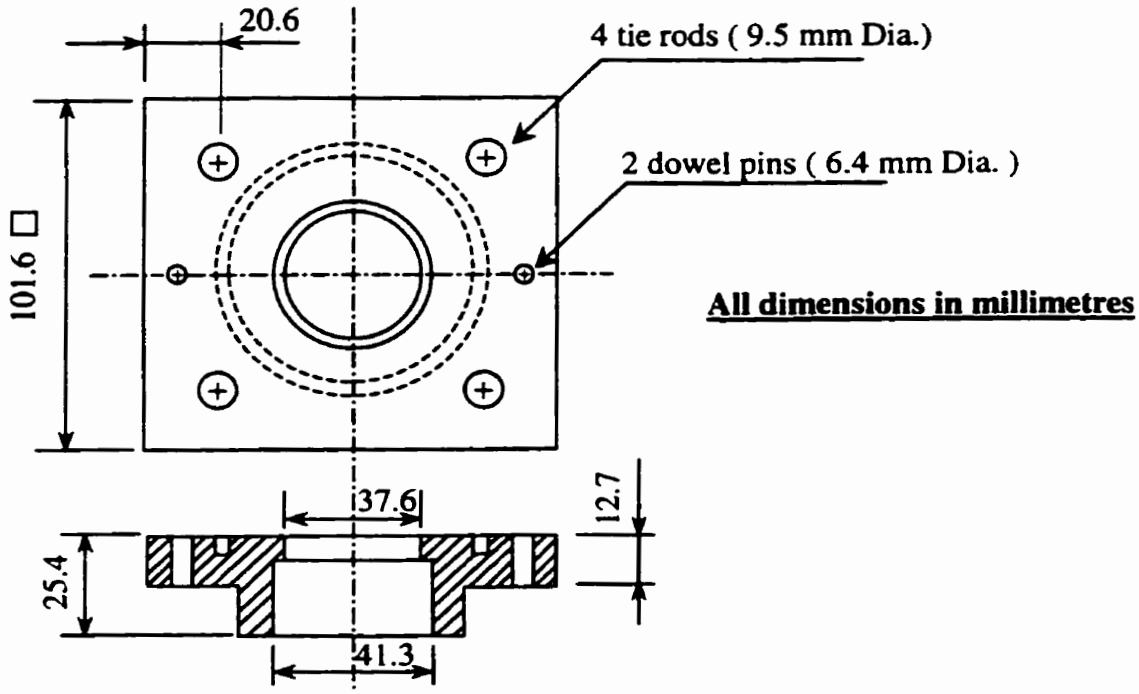

Figure 4.8 Copper piece.

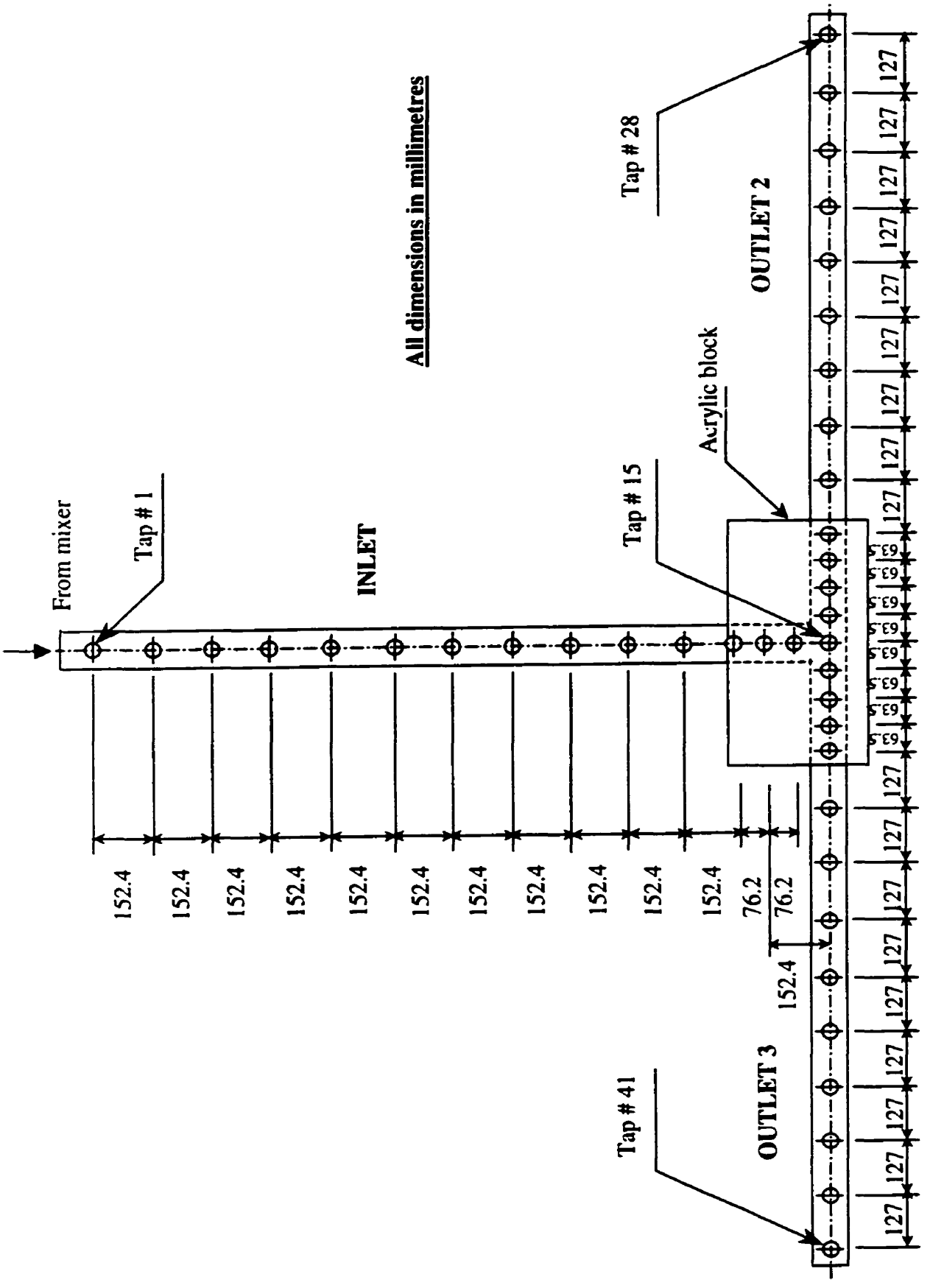

Figure 4.9 Pressure taps locations.

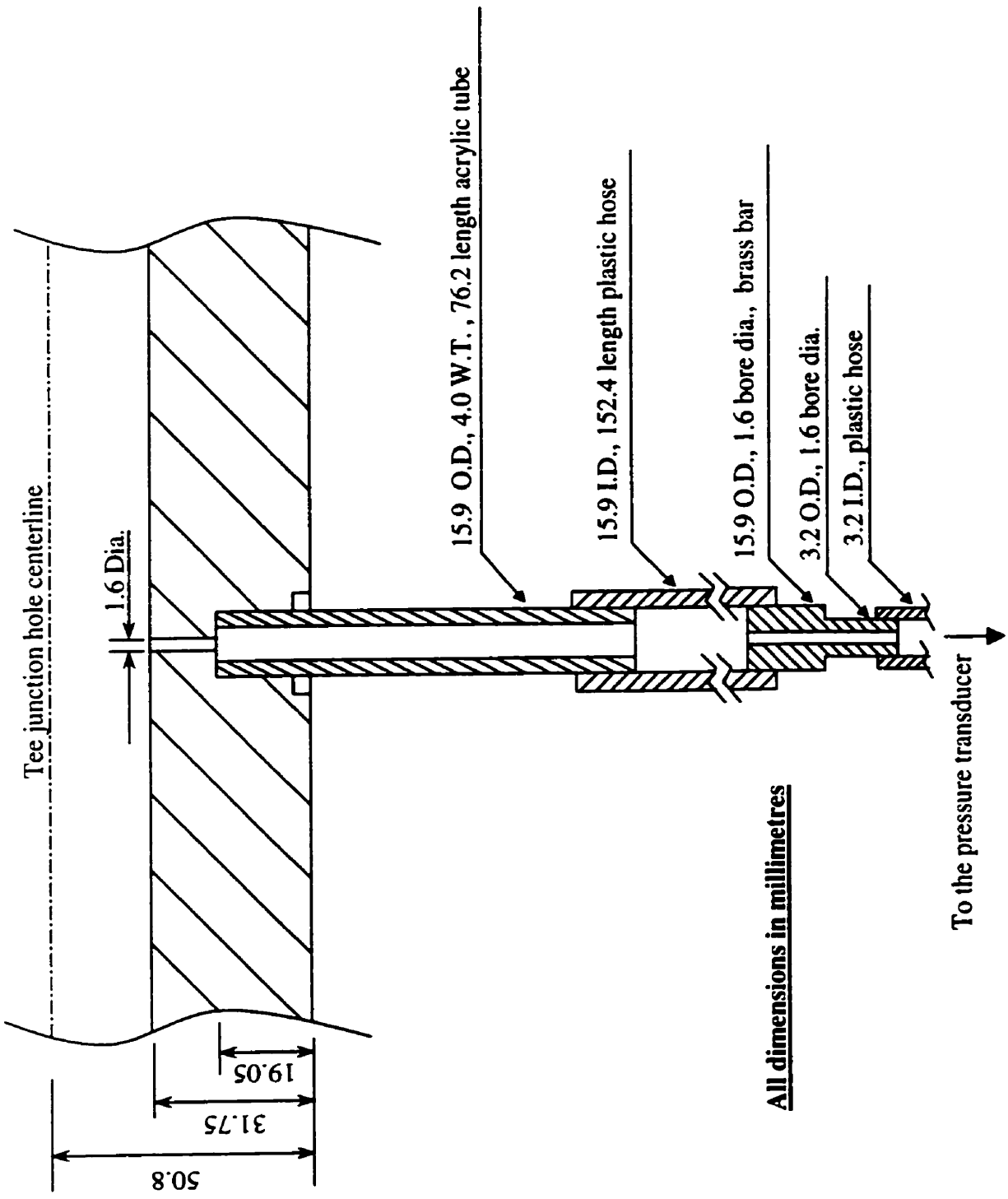

Figure 4.10 Arrangement for the tee junction pressure taps.

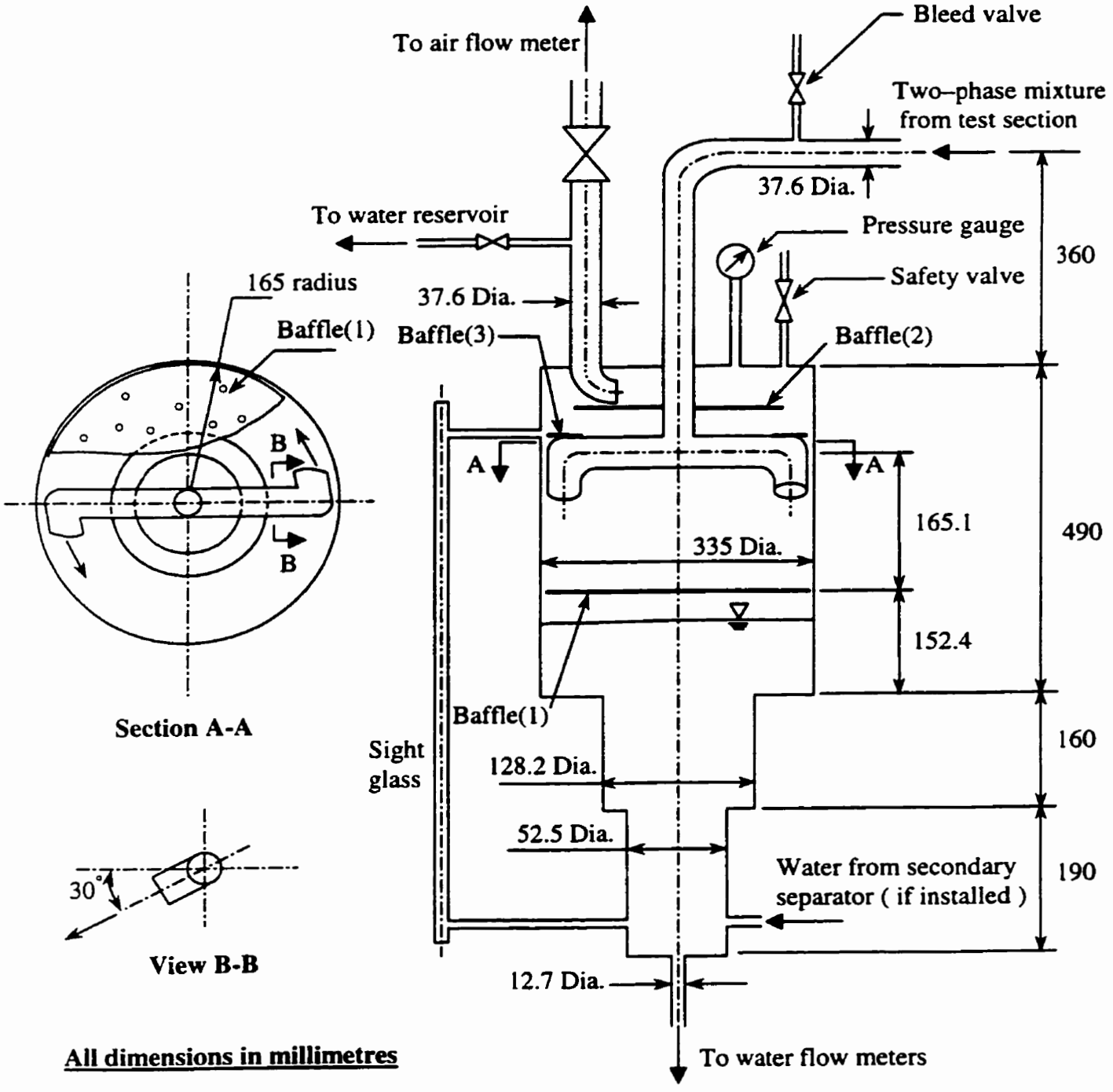

Figure 4.11 Details of a separation tank.

Chapter 5

CONCLUSIONS AND RECOMMENDATIONS

In the present study, the data base for two-phase flow in horizontal impacting tee junctions was carefully examined. The effects of different parameters on the phase distribution were investigated. Also, the analytical models and empirical correlations previously developed for predicting the phase distribution were examined. Qualitative and quantitative assessments of these models and correlations are given. The following is a list of conclusions that can be drawn from the work done:

1- There is lack of pressure-drop data, high-inlet-quality phase-distribution data, and high-inlet-pressure phase-distribution data.

2- The effect of J_{LI} on the phase distribution is such that as J_{LI} increases, the data line, or curve rotates in a clockwise direction around the "point of 0.5" on an F_{BG} vs. F_{BL} graph.

3- The effect of J_{GI} on the phase distribution is such that as J_{GI} increases, the data line, or curve rotates in an anti-clockwise direction around the "point of 0.5"on an F_{BG} vs. F_{BL} graph.

4- The effects of inlet pressure, inlet quality, and inlet momentum-flux ratio on the phase distribution are similar to the effect of J_{GI}, while the inlet flow regime (at the same x_I and P_I) has an insignificant effect on the phase distribution.

5- There is no model or correlation that can produce satisfactory predictions for all inlet conditions.

6- The Hong and Griston (1995) correlation does not satisfy mass balance. Furthermore, the correlation does not work for small values of F_{BG}. Also, it results in high errors for the slug, plug, and bubbly flow regimes.

7- The Chien and Rubel (1992) correlation is the best to predict phase distribution for high-inlet-pressure steam and water.

8- The Ottens et al. (1995) model is the best to predict phase distribution for air and water with annular, slug, and plug inlet flow regimes, while the Hwang (1986) model is the best to predict phase distribution for air and water with bubbly and wavy inlet flow regimes.

Based on the above conclusions, the following is a list of recommendations for future work:

1- To generate phase-distribution and pressure-drop data with wide ranges of inlet conditions in terms of J_{GI} and J_{LI} for air and water through a horizontal impacting tee junction.

2- To investigate (experimentally) the phase distribution and pressure drop for different fluid properties and junction orientation.

3- To develop models/correlations for predicting pressure drop for all inlet conditions

4- To develop models/correlations for predicting phase distribution that can work satisfactorily for all inlet conditions.

An experimental test facility has been designed and the components have been constructed to generate pressure-drop and phase-distribution data for low-pressure air-water mixtures over a wide range of inlet conditions.

REFERENCES

Asano, H., Fujii, T., Takenaka, N., Sakoda, K. and Arakawa, T., "Phase Separation Characteristics of Gas-Liquid Two-Phase Flow in a T-Junction (Experiments for a One-Component Two-Phase Flow)", Proceeding of the 16th Multiphase Flow Symposium, Lake Toya, Japan, pp. 103-104, 1997.

Azzopardi, B.J., Purvis, A. and Govan, A.H., "Two-Phase Flow Split at an Impacting T", UKAEA Report, AERE-R-12179, 1986.

Barnea, D., Luninski, Y. and Taitel, Y., "Flow Pattern in Horizontal and Vertical Two-Phase Flow in Small Diameter Pipes", Canadian Journal of Chemical Engineering, Vol. 61, pp. 617-620, 1983.

Chien, S.-F. and Rubel, M.T., "Phase Splitting of Wet Steam in Annular Flow Through a Horizontal Impacting Tee", SPE Production Engineering, Vol. 7, pp. 368-374, 1992.

Fujii, T., Asano, H., Takenaka, N. and Sakoda, K., "Phase Separation Characteristics of Gas-Liquid Two-Phase Flow in T-Junction (Effects of the Geometry of Junctions)", Proceeding of the 15th Multiphase Flow Symposium, Fukui, Japan, pp. 61-64, 1996.

Fujii, T., Takenaka, N., Nakazawa, T. and Asano, H., "The Phase Separation Characteristics of a Gas-Liquid Two-Phase Flow in the Impacting T-Junction", Proceeding of the 2nd International Conference on Multiphase Flow, Kyoto, Japan, pp. 6.27-6.32, 1995.

Hart, J., Hamersma, P.J. and Fortuin, J. M. H., "A Model For Predicting Liquid Route Preference During Gas-Liquid Flow Through Horizontal Branched Pipelines", Chemical Engineering Science, Vol. 46, pp. 1609-1622, 1991.

Hong, K.C., "Two-Phase Flow Splitting at a Pipe Tee", Journal of Petroleum Technology, Vol. 2, pp. 290-296, 1978.

Hong, K.C. and Griston, S., "Two-Phase Flow Splitting at an Impacting Tee", SPE Production and Facilities, Vol. 10, pp. 184-190, 1995.

Hwang, S.T., "A Study on Phase Separation Phenomena in Branching Conduits", Ph.D. Thesis, Rensselaer Polytechnic Institute, 1986.

Hwang, S.T., Soliman, H.M. and Lahey, R.T., "Phase Separation in Impacting Wyes and Tees", International Journal of Multiphase Flow, Vol. 15, pp. 965-975, 1989.

Lightstone, L., Osamusali, S.I. and Chang J.-S. " Gas-Liquid Two-Phase Flow in Symmetrically Dividing Horizontal Tubes", AIChE Journal, Vol. 37, pp. 111-121, 1991.

Ottens, M., De Swart, A., Hoefsloot, H.C.J. and Hamersma, P.J., "Gas-Liquid Flow Splitting in Regular, Reduced and Impacting Tee Junctions", Impiantistica Italiana, Vol. 8, pp. 23-33.

Shoham, O., Brill, J.P. and Taitel, Y. , "Two-Phase Flow Splitting in a Tee Junction-Experiment and Modeling", Chemical Engineering Science, Vol. 42, pp. 2667-2676, 1987.

Van Gorp, C.A., "Two-Phase Pressure Drop and Phase Distribution at a Reduced Horizontal Tee Junction: The Effect of System Pressure", M.Sc. Thesis, University of Manitoba, 1998.

APPENDIX A

GEOMETRICAL AND PHYSICAL MODELS FOR DIFFERENT FLOW REGIMES

The geometrical and physical models that were used in association with the Hwang (1986) model to calculate the slip ratio (S), F_{BG}, and F_{BL} are given in this appendix. It should be mentioned that the slip ratio (S) is calculated at the inlet side of the tee junction and so are the relevant parameters.

A.1 Bubbly and Plug Flow Regimes

The drift flux model was used to calculate the slip ratio (S) for bubbly and plug flow regimes. For given inlet quality (x_I) and fluid properties (ρ_G and ρ_L), the drift flux model, as given in Hwang (1986), calculates the slip ratio (S) using the following equations:

$$C_o = 1.1 - 0.1 \left[\left(\rho_L/\rho_G \right) ** \{ -0.0001 * \left(\rho_L/\rho_G \right) \} \right] \qquad (A.1)$$

and

$$S = C_o + \left(C_o - 1 \right) \left(\rho_L/\rho_G \right) \left(x_I / \left(1.0 - x_I \right) \right) \qquad (A.2)$$

After calculating the slip ratio (S), the second part of the Hwang (1986) model may be executed to solve for δ_G and the corresponding δ_L, see Section 3.1.4 for more details on the Hwang (1986) model. Then, values of δ_G and δ_L are converted to values of F_{BG} and F_{BL}, respectively using the seventh law. The seventh law can be stated in the form of the following equations:

$$F_{BL} = 1.104 * \left[\left(\delta_L/D_I \right)**(8/7) \right] \quad \text{if } \delta_L/D_I \le 0.5,$$

$$F_{BL} = 1.0 - \{ 1.104 * \left[\left(1.0 - \delta_L/D_I \right)**(8/7) \right] \} \quad \text{if } \delta_L/D_I > 0.5. \qquad (A.3)$$

and

$$F_{BG} = 1.219 * [(\delta_G/D_1)^{**}(9/7)] \quad \text{if } \delta_G/D_1 \leq 0.5,$$

$$F_{BG} = 1.0 - \{ 1.219 * [(1.0 - \delta_G/D_1)^{**}(9/7)] \} \quad \text{if } \delta_G/D_1 > 0.5. \qquad (A.4)$$

It should be mentioned that if the value of δ_G and/or δ_L is equal to 1.0, the value of F_{BG} and/or F_{BL} is set to 1.0, respectively.

A.2 Annular, Stratified, and Wavy Flow Regimes

In order to calculate the slip ratio (S) in case of the annular flow regime, the liquid-film thickness (δ) must be known. Also, for stratified and wavy flow regimes, the liquid level (h) must be known. The following is a physical model, given in Shoham et al. (1987), that applies a momentum balance on the two phases in order to get the previous mentioned values. The model uses the geometrical models, given also in Shoham et al. (1987), shown in Figures A.1 and A.2 for annular and stratified flow regimes, respectively.

A momentum balance on the liquid and gas phases yields

$$- A_L (dp/dx) - \tau_L S_L + \tau_i S_i = 0 \qquad (A.5)$$

and

$$- A_G (dp/dx) - \tau_G S_G + \tau_i S_i = 0 \qquad (A.6)$$

where, A_L and A_G are the cross-sectional areas occupied by the liquid and gas, respectively, τ_L, τ_G, and τ_i are the liquid, gas, and interfacial shear stresses acting on the perimeters S_L, S_G, and S_i, respectively. Equating the pressure drop (dp/dx) in Equations (A.5) and (A.6) yields the following:

$$\tau_G (S_G / A_G) - \tau_L (S_L / A_L) + \tau_i S_i [(1.0/A_L) + (1.0/A_G)] = 0. \qquad (A.7)$$

The shear stresses are evaluated as follows:

$$\tau_L = f_L (\rho_L V_{LI}^2 / 2), \quad (A.8)$$

$$\tau_G = f_G (\rho_G V_{GI}^2 / 2), \quad (A.9)$$

and

$$\tau_i = f_i (\rho_G V_{GI}^2 / 2). \quad (A.10)$$

where,

f_L, f_G, and f_i are the friction factors of the liquid, gas, and interface, respectively,

V_{LI} and V_{GI} are the average velocities of the liquid and gas, respectively.

The friction factors f_L and f_G are given by:

$$f_L = c_L (D_L V_{LI} / \nu_L)^{-n} \quad (A.11)$$

and

$$f_G = c_G (D_G V_{GI} / \nu_G)^{-m} \quad (A.12)$$

where,

D_L and D_G are the hydraulic diameters of the liquid and gas, respectively,

ν_L and ν_G are the kinematic viscosities of the liquid and gas, respectively,

and

c_L, c_G, m, and n are empirical coefficients given as follows:

for turbulent flow : $c_L = c_G = 0.046$, $m = n = 0.2$

and

for laminar flow : $c_L = c_G = 16$, $m = n = 1.0$. (A.13)

The hydraulic diameters D_L and D_G are given by:

$$D_L = 4 A_L / S_L \quad (A.14)$$

and

$$D_G = 4\,A_G / (\,S_G + S_i\,). \qquad (A.15)$$

The friction factor, f_i, is given by:

for annular flow: $f_i = f_G\,(1.0+300\delta/D_l)$,

for stratified flow: $f_i = f_G$,

and

for wavy flow: $f_i = 0.009$. (A.16)

It should be mentioned that Equations (A.5) to (A.16) are valid for annular, stratified, and wavy flow regimes with the only difference that $S_G = 0$ in case of the annular flow regime.

For given inlet conditions (J_{GI} and J_{LI}), fluid properties (ρ_G and ρ_L), and junction geometry (D_l), the inlet gas and liquid mass flow rates may be calculated by the following equations:

$$W_{GI} = (\pi/4) * D_l^2 * J_{GI} * \rho_G \qquad (A.17)$$

and

$$W_{LI} = (\pi/4) * D_l^2 * J_{LI} * \rho_L \qquad (A.18)$$

, respectively. Then the slip ratio (S) for stratified and wavy flow regimes may be calculated by executing the following steps:

(1) Assume a value for the liquid height (h), see Figure A.1.

(2) Calculate A_L using Equation (A.28).

(3) Calculate A_G from:

$$A_G = (\pi/4) * D_l^2 - A_L \qquad (A.19)$$

(4) Calculate V_{GI} and V_{LI} from:

$$V_{GI} = W_{GI} / (\,A_G * \rho_G\,) \qquad (A.20)$$

and

$$V_{LI} = W_{LI} / (A_L * \rho_L), \quad (A.21)$$

respectively.

(5) Calculate f_L, f_G, and f_i using Equations (A.11) to (A.16).

(6) Calculate τ_L, τ_G, and τ_i using Equations (A.8), (A.9), and (A.10), respectively.

(7) Calculate S_G from:

$$S_G = D_I * \cos^{-1} (2h - 1.0), \quad (A.22)$$

S_L from:

$$S_L = \pi D_I - S_G, \quad (A.23)$$

and

S_i from Equation (A.30).

(8) Check that Equation (A.7) is satisfied. If Equation (A.7) is not satisfied, change the value of h and repeat steps 2 to 8.

(9) When Equation (A.7) is satisfied, the slip ratio (S) may be calculated from:

$$S = V_{GI} / V_{LI}. \quad (A.24)$$

After calculating the slip ratio (S), the second part of the Hwang (1986) model may be executed to solve for δ_G and the corresponding δ_L, see Section 3.1.4 for more details on the Hwang (1986) model. The value of δ_G is converted to a value of F_{BG} using Equations (A.28) to (A.36) with parameter a, in the equations, replaced by δ_G. Similarly, the value of δ_L is converted to a value of F_{BL} using Equations (A.28) to (A.37), excluding Equation (A.36), with parameter a, in the equations, replaced by δ_L.

For the annular flow regime, W_{GI} and W_{LI} may be calculated using Equations (A.17) and (A.18), respectively. Then the slip ratio (S) may be calculated by executing the following steps:

(1) Assume a value for the film thickness (δ), see Figure A.2.

(2) Calculate A_L using Equations (A.39) and (A.41).

(3) Calculate A_G using Equation (A.19).

(4) Calculate V_{GI} and V_{LI} from Equations (A.20) and (A.21), respectively.

(5) Calculate f_L, f_G, and f_i using Equations (A.11) to (A.16).

(6) Calculate τ_L, τ_G, and τ_i using Equations (A.8), (A.9), and (A.10), respectively.

(7) Calculate S_G from:

$$S_G = 0.0, \tag{A.25}$$

S_L from:

$$S_L = \pi D_I, \tag{A.26}$$

and

S_i from:

$$S_i = \pi D_G. \tag{A.27}$$

(8) Check that Equation (A.7) is satisfied. If Equation (A.7) is not satisfied, change the value of δ and repeat steps 2 to 8.

(9) When Equation (A.7) is satisfied, the slip ratio (S) may be calculated from Equation (A.24).

After calculating the slip ratio (S), the second part of the Hwang (1986) model may be executed to solve for δ_G and the corresponding δ_L, see Section 3.1.4 for more details on the Hwang (1986) model. The value of δ_G is converted to a value of F_{BG} using

Equations (A.38) to (A.45) with parameter a, in the equations, replaced by δ_G. Similarly, the value of δ_L is converted to a value of F_{BL} using Equations (A.38) to (A.46), excluding Equation (A.45), with parameter a, in the equations, replaced by δ_L.

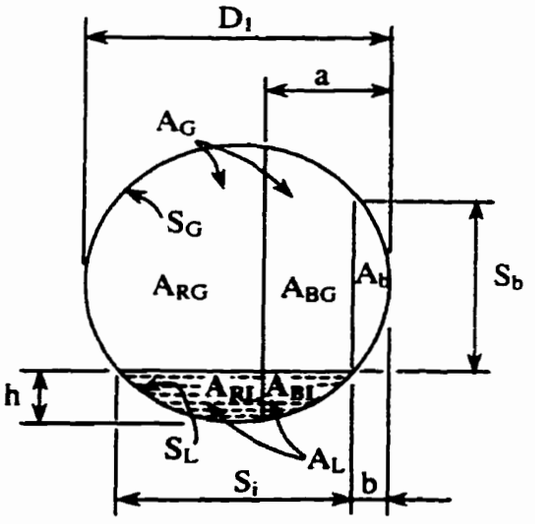

$$A_L = A_{RL}+A_{BL} = 0.25 * D_1^2 \left[\pi - \cos^{-1}((2h/D_1)-1)+((2h/D_1)-1)*\text{sqrt}\{1-((2h/D_1)-1)^2\}\right] \quad (A.28)$$

$$A_B = A_{BG}+A_{BL} = 0.25 * D_1^2 \left[\pi - \cos^{-1}((2a/D_1)-1)+((2a/D_1)-1)*\text{sqrt}\{1-((2a/D_1)-1)^2\}\right] \quad (A.29)$$

$$S_i = D_1 * \text{sqrt}\{1-((2h/D_1)-1)^2\} \quad (A.30)$$

$$b = 0.5*(D_1 - S_i) \quad (A.31)$$

$$A_b = 0.25 * D_1^2 \left[\pi - \cos^{-1}((2b/D_1)-1)+((2b/D_1)-1)*\text{sqrt}\{1-((2b/D_1)-1)^2\}\right] \quad (A.32)$$

$$S_b = D_1 * \text{sqrt}\{1-((2b/D_1)-1)^2\} \quad (A.33)$$

$$A_{BL} = 0.5(A_B-(a-b)S_b-A_b) \quad (A.34)$$

$$A_{BG} = A_B - A_{BL} \quad (A.35)$$

$$F_{BG} = A_{BG}/A_G \quad (A.36)$$

$$F_{BL} = A_{BL}/A_L \quad (A.37)$$

Figure A.1 Geometrical model for stratified and wavy flow regimes.

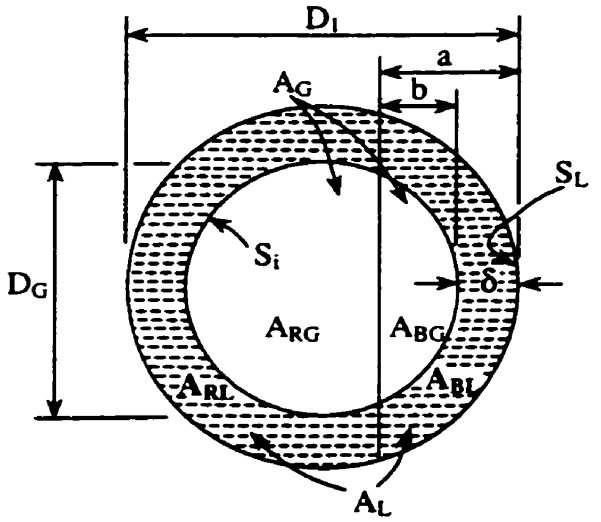

$$A_B = A_{BG}+A_{BL}= 0.25* D_I^2 [\pi-\cos^{-1}((2a/ D_I)-1)+((2a/ D_I)-1)*\text{sqrt}\{1- ((2a/ D_I)-1)^2\}] \quad (A.38)$$

$$D_G = D_I - 2\delta \quad (A.39)$$

$$A_G = A_{RG} + A_{BG} = (\pi/4) D_G^2 \quad (A.40)$$

$$A_L = A_{BL} + A_{RL} = (\pi/4) (D_I^2 - D_G^2) \quad (A.41)$$

$$b = a - \delta \quad (A.42)$$

$$A_{BG} = 0.25*D_G^2 [\pi-\cos^{-1}((2b/D_G)-1)+((2b/D_G)-1)*\text{sqrt}\{1- ((2b/D_G)-1)^2\}] \quad (A.43)$$

$$A_{BL} = A_B - A_{BG} \quad (A.44)$$

$$F_{BG} = A_{BG}/A_G \quad (A.45)$$

$$F_{BL} = A_{BL}/A_L \quad (A.46)$$

Figure A.2 Geometrical model for the annular flow regime.

Nomenclature for Appendix A

Symbol	Description	Units
a	Parameter in the geometrical models given in Figures A.1 and A.2 that is equivalent to δ_L and/or δ_G	m
A_G	Area occupied by the gas at the inlet	m^2
A_L	Area occupied by the liquid at the inlet	m^2
b	Parameter in the geometrical models given in Figures A.1 and A.2	m
c_G	Empirical coefficient; see Equation (A.13)	-
c_L	Empirical coefficient; see Equation (A.13)	-
C_o	Empirical coefficient in the drift flux model; see Equation (A.1)	-
D_I	Diameter of the inlet	m
D_G	Hydraulic diameter of the gas at the inlet	m
D_L	Hydraulic diameter of the liquid at the inlet	m
f_G	Friction factor of the gas at the inlet	-
f_i	Friction factor at the gas-liquid interface at the inlet	-
f_L	Friction factor of the liquid at the inlet	-
F_{BG}	Fraction of inlet gas exiting through outlet 3	-
F_{BL}	Fraction of inlet liquid exiting through outlet 3	-
h	Liquid level at the inlet in case of stratified and wavy flow regimes	m
J_{GI}	Superficial inlet-gas velocity	m/s
J_{LI}	Superficial inlet-liquid velocity	m/s
m	Empirical coefficient; see Equation (A.13)	-
n	Empirical coefficient; see Equation (A.13)	-

S	Slip ratio = V_{GI} / V_{LI}	-
S_G	The part of the circumference of the inlet pipe that is adjacent to gas	m
S_i	Length of the gas-liquid interface at the inlet	m
S_L	The part of the circumference of the inlet pipe that is adjacent to liquid	m
V_{GI}	Average inlet gas velocity	m/s
V_{LI}	Average inlet liquid velocity	m/s
W_{GI}	Inlet-gas mass flow rate	kg/s
W_{LI}	Inlet-liquid mass flow rate	kg/s
x_I	Inlet quality = W_{GI} / W_I	-

Greek Symbols

δ	Liquid-film thickness in the inlet pipe in case of annular flow regime	m
δ_G	Parameter defining the location of the gas dividing streamline in the inlet pipe, as in Figure 3.1	m
δ_L	Parameter defining the location of the liquid dividing streamline in the inlet pipe, as in Figure 3.1	m
ρ_G	Gas density	kg/m^3
ρ_L	Liquid density	kg/m^3
τ_G	Shear stress acting on S_G	Pa
τ_i	Shear stress acting on S_i	Pa
τ_L	Shear stress acting on S_L	Pa
ν_G	Kinematic viscosity of the gas	m^2/s
ν_L	Kinematic viscosity of the liquid	m^2/s